Antarctic Meteorites XXVI

Papers presented to the Twentysixth Symposium on Antarctic Meteorites

June 12-14, 2001

NATIONAL INSTITUTE OF POLAR RESEARCH
TOKYO

国立極地研究所

Tuesday, June 12, 2001

0900 – 1200 Registration Auditorium (6th Floor)

*Speaker

Chairs: Nakamura T. and Hiroi T. **Page**

1200 – 1300 Lunch Time

Chairs: Nakamura N. and Tsuchiyama A.

Special Session: Kobe Meteorite

Wednesday, June 13, 2001

Chairs: Nagahara H. and Kimura M. **Page**

Chairs: Mikouchi T. and Hashizume K.

1200 – 1300 Lunch Time

Thursday, June 14, 2001

ABSTRACTS

AN ATTEMPT TO PHYSICALLY SEPARATE Q

Sachiko Amari[1], Shiho Zaizen[2], and Jun-ichi Matsuda[2]

[1]Laboratory for Space Sciences and the Physics Department, Washington University, One Brookings Dr., St. Louis MO, 631230-4899 USA. [2]Department of Earth and Space Science, Osaka University, Toyonoka, Osaka 560-0014, Japan

INTRODUCTION

The discovery that planetary noble gases are carried by a very small portion of meteorites (≤0.04%) [1] eventually led to the isolation of presolar grains from meteorites [2] and this new field of astronomy has flourished during the past 10 years [3, 4]. In contrast, the carrier of planetary noble gases, dubbed Q for "quintessence", has remained elusive. There has been the consensus that the carrier is most likely carbonaceous matter. Experiments have shown that adsorption on the labylinth of the surface could explain the elemental abundance of Q [e.g., 5, 6]. Recently, Bussemann et al. [7] and Verchovsky et al. [8] examined Q-gas in various types of meteorites to better characterize Q-gas.

To shed light to the origin of planetary noble gases and the nature of the carrier, we undertook the task to isolate Q by only physical means, since Q has been known to be readily destroyed by oxidants.

EXPERIMENTAL PROCEDURE

Material which floats on the surface of water during freeze-thaw disaggregation is enriched in Q-gas and Xe-HL [9], having elemental and isotopic abundances very similar to the chemically processed residue 3C1 from Allende [1]. 2.62mg of the floating fraction was collected from 3.846g of Allende through 216 cycles of freeze-thaw disaggregation. Part of the floating fraction was named C1-8 (0.43mg) and used as the starting material in this study. The procedure to extract presolar grains from meteorites [10] was applied to this fraction after slightly modified to accommodate a specific nature of the sample. First, colloidal separation yielded fraction C1-8A, which was presumably enriched in presolar diamond. The rest of the sample was separated according to their densities with sodium polytungstate [$Na_6(H_2W_{12}O_{40})$], yielding 9 fractions with different densities. After washing, a known portion of the fractions was taken for noble gas analysis and their abundances in C1-8 were calculated. All five noble gases were analyzed with the VG 5400 at Osaka University.

RESULTS AND DISCUSSIONS

From the abundances and ^{132}Xe concentrations of all the fractions, we obtained that the sum of ^{132}Xe of the fractions is 1.33×10^{-7}ccSTP/g. It is about the same as the ^{132}Xe concentration of C1-7 (1.4×10^{-7}ccSTP/g) [11], another aliquot from the floating fraction extracted from 3.846g of Allende. This indicates that no significant portion of Q has been lost during the separation.

All the fractions as well as floating fractions A1, A1A, and C1-7 [9, 11], which were previously measured, have $^{134}Xe/^{132}Xe$ and $^{136}Xe/^{132}Xe$ ratios very close to those of 3C1, implying that all the separated fractions have the same proportion of Q and diamond. Especially, the fact that C1-8A has the isotopic ratios indistinguishable to those of other fractions indicates that the colloidal separation apparently failed to isolate presolar diamond.

Another possibility is that Q and diamond are closely related and that it is not feasible to separate them. In fact, Anders and Zinner [12] have proposed that Q is not a discrete phase but is the surfaces of carbonaceous matter, possibly graphitized coatings on presolar diamonds.

Interestingly, 48 percent of the ^{132}Xe of starting fraction C1-8 is concentrated in C1-8D with density of 1.65±0.04g/cm^3 (Fig. 1). Amari and Matsuda [13] analyzed carbonaceous grains in A1 by the ion probe and have found that there are two kinds of grains. One type has high CN^-/C^- ratios ranging from 0.3 to 1.3 (N is measured as CN^-) and the other type has lower ratio (<0.3). Grains of the first type have high F peaks (equal or higher than C peak) upon SEM (secondary electron microscope) examination at 10kV. It remains to be seen whether either type of grains is enriched in C1-8D. We plan to examine C1-8D as well as other fractions with the SEM and the NanoSIMS (secondary ion mass spectrometry), which was recently delivered at Washington University.

REFERENCES

[1] Lewis R. S., Srinivasan B. and Anders E. (1975) *Science* 190, 1251-1262. [2] Lewis R. S. et al. (1987) *Nature* 326, 160-162. [3] Bernatowicz T. J. and Zinner E. (1997) *Astrophysical Implications of the Laboratory Study of Presolar Materials* (New York: AIP). [4] Zinner E. (1998) *Ann. Rev. Earth Planet. Sci.* 26, 147-188. [5] Zadnik M. G., Wacker J. F. and Lewis R. S. (1985) *Geochim. Cosmochim. Acta* 49, 1049-1059. [6] Wacker J. F. (1989) *Geochim. Cosmochim. Acta* 53, 1421-1433. [7] Busemann H., Baur H. and Wieler R. (2000) *Meteori. Planet. Sci.* 35, 949-973. [8] Verchovsky A. B. et al. (2001) *Lunar Planet. Sci.* XXXII, Abstract #1706. [9] Matsuda J., Amari S. and Nagao K. (1999) *Meteorit. Planet. Sci.* 34, 129-136. [10] Amari S., Lewis R. S. and Anders E. (1994) *Geochim. Cosmochim. Acta* 58, 459-470. [11] Zaizen S. et al. (2000) *Antarct. Meteorite Res.* 13, 100-111. [12] Anders E. and Zinner E. (1993) *Meteoritics* 28, 490-514. [13] Amari S. and Matusda M. (1998) *Lunar Planet Sci.* XXIX, Abstract #1844.

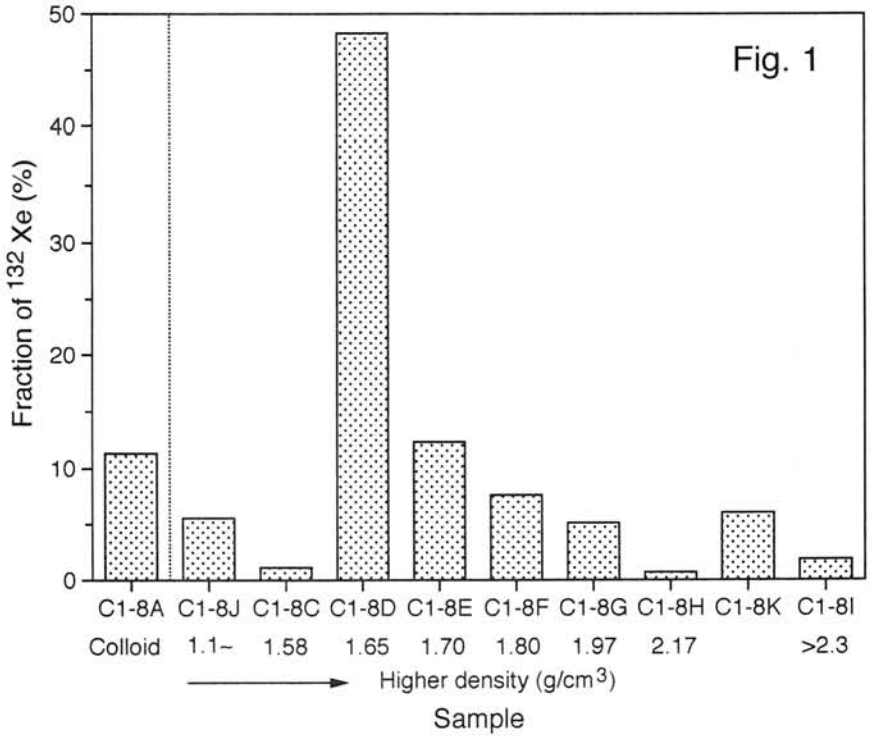

Mineralogical Study of Lunar Mare Meteorite EET 96008

Tomoko ARAI

Centrifuge Project Team, Office of Space Utilization Systems, National Space Development Agency of Japan (NASDA), Tsukuba Space Center, 2-1-1 Sengen, Tsukuba, Ibaraki 305-8505 Japan, arai.tomoko@nasda.go.jp

Introduction: Lunar meteorites are valuable sources of information about crustal evolution of the Moon. Since Apollo/Luna collected samples cover only limited regions of central nearside [1], discovery of lunar meteorites does contribute to our further understanding of the Moon. Elephant Moraine (EET) 96008, which was discovered in Antarctica, is the 6th lunar meteorite of mare origin [2]. Among the five pre-found mare meteorites, Yamato (Y) 793169 and Asuka (A) 881757 are unbrecciated, Ti-poor (bulk-rock TiO_2 = 1.5 ~ 2.0 wt %) mare basalts [e.g., 3, 4, 5], while Y 793274, EET 87521 and Queen Alenxandra Range (QUE) 94281 are brecciated mare basalts with some highland components and their source mare basalts are very Ti- poor (bulk-rock $TiO_2 \leq 1.0$ wt%) [6]. QUE 94281 and Y 793274 are derived from a common source crater [6]. In this study, mineralogy of EET96008 is investigated to identify its source mare-basalt suite and to assess its genetic relationship with other lunar-meteorite mare breccias.

Sample and Methods: The polished thin section (PTS) EET96008, 41 is provided by NASA Johnson Space Center. Analyses of mineral compositions were done by a JEOL 733 electron probe microanalyzer (EPMA) at the Ocean Research Institute, University of Tokyo.

Results:

EET96008 is a fragmental breccia (Fig. 1a), abundant in mineral fragments of pyroxene, less amount of plagioclase and olivine of apparent mare-basalt deriviation with accessory minerals, such as ilmenite, titanian chromite silica minerals and whitlockite. Pyroxene fragments of 0.5 – 1.0 mm in size are dominant across the PTS. Two mare basalt clasts (1 mm across) consisting of pyroxene, plagioclase and olivine, are found (Clast MB1 and MB2) (Fig. 1b). For non-mare components, the PTS includes a "poikilitic impact melt clast" (1.2 mm across) of highland origin (IM1) (Fig. 1c), and an "equigranular clast" (EQ1) (1 mm across) (Fig. 1d). The IM1 clast mostly consists of fine-grained anorthite. The EQ 1 clast is compositionally "evolved" and includes fine-grained (up to tens of micron in diameter), equant-shaped hedenbergite, fayalite, silica minerals and a trace of FeTi-oxide, with no plagioclase found. These mineral fragments and lithic clasts are typically set in fine-grained dark-brown glassy matrix (Fig. 1a). Pristine volcanic glass spherule is not found. At one corner of the PTS, a light brown fusion crust (0.5 mm across) is found with several vesicles in it.

Major compositional variation of pyroxene fragments (> 100 μm) and pyroxenes in MB1 and MB2, are plotted in pyroxene quadrilateral (Fig. 2). One fragment shows a Fe, Ca-rich hedenbergite composition circled in a dotted line. Most of mare pyroxene fragments show exsolution of around 1 μm in width. The hedenbergite in EQ1 clast shows homogeneous composition ($Fs_{46}En_{14}Wo_{40}$), which is notably analogous of that of the hedenbergite fragment in the Fig. 2.

Minor compositional variation of the pyroxenes are shown in a plot of Fe# (= molar Fe/(Fe+Mg)) vs. Ti# (=molar Ti/(Ti+Cr)) (Fig. 3), because both Ti# and Fe# are good indicators to record a primary compositional trend produced during fractional crystallization from a source magma [6]. The EET96008 pyroxenes constitute a series of trend, which is typical of zoned pyroxenes in the Ti-poor mare basalt, and the trend is similar to that of Apollo17 VLT basalt and EET87521 [7].

Based on an empirical correlation between Ti# in pyroxene and bulk-rock TiO_2 abundance [6], a source basalt of EET96008 mare pyroxenes is estimated to have a bulk-rock $TiO_2 \approx 1.0$ wt % (Fig. 4), with a mean Ti# = 0.46 at Fe# =0.5 in Fig.3.

Plagioclase compositions are An=69-73 and An=85-95 for mineral fragments, while An=80-90 for MB1/MB2 clasts, and An=90-96 for IM1 clast.

Olivine shows bimodal compositional variation; Fo=50-52 in mineral fragments and Fo=89-91 in MB1 clast, Fo=90 in EQ1 clast).

The fusion crust shows slight compositional variations: SiO_2 = 44.5 - 46.7, TiO_2 = 0.9 - 1.6, Al_2O_3 = 12.2 - 13.7, FeO = 18.4 - 20.4, MnO = 0.2 - 0.3, MgO = 5.8 - 6.6, CaO = 11.5 - 12.4, Na_2O = 0.3 - 0.4, K_2O = 0.1, Cr_2O_3= 0.1 - 0.3 (all in wt%).

Discussions:

The texture, the size of abundant pyroxene/plagioclase fragments and the dark gassy matrix are very similar to those found in YQ meteorites [6], while EET87521 is more abundant in larger basaltic clasts with coaser-grained (1-2 mm across) pyroxene and plagioclase [e.g., 7, 8]. The coase exsolution of pyroxene (≈1 μm in width) by mare standard is also reported [9, 10]. The coarse exsolution is also commonly found in EET87521 and YQ meteorites [6]. This indicates that mare-basalt remnants (mainly pyroxene) in four lunar mare breccias preserve a common cooling process, implying that their source basalt experienced relatively slow cooling, such as relatively slow-cooling in a thick lave flow or lava pond.

Pyroxene quadrilateral (Fig. 2) shows that EET96008 pyroxenes have very similar compositional variation to that of EET87521, except Fe, Ca-enriched hedenbergite, while YQ meteorites show more diverse variation. The Ti# vs. Fe# plot (Fig. 3) also confirms that EET96008 and EET87521 contain pyroxenes which record almost identical crystallization trend, and neither includes "exotic" pyroxenes with different crystallization history and source magma composition, that are observed in plots of YQ meteorites. Note that the composition of the hedenbergite from EQ1 clast is plotted within this trend. The estimated source-basalt TiO_2 content (≈ 1.0 wt %) is almost identical to that of EET87521 and YQ meteorites [6], which indicates the source basalts for the four lunar breccias is commonly Very Low Ti (Fig. 4).

A highland impact-melt clast (IM1) is also found in other thin section of EET96008 [9]. Such clast is commonly found in YQ meteorites [e.g., 6, 8]. The "evolved" clast (EQ1) is also reported in other thin sections [9, 10, 11]. This "evolved" clast is not common in EET87521 and YQ meteorites, although there are some reports of similar clasts [8, 12]. Its mineral assemblage of hedenbergite-fayalite-silica minerals suggests that this clast would be a derived from a break-down of pyroxferroite which is a product of a late-stage fractionation.

Compared with bulk-rock major compositions of EET87521 and YQ meteorites [e.g., 6], EET96008 composition estimated from its fusion crust composition is the closest to that of EET87521 with a slightly enrichment of FeO (by 1.2 wt%) and TiO_2 (by 0.3 wt%). It is noted that the estimated TiO_2 content of the source basalt (≈ 1.0 wt %) (Fig. 4) closely matches the bulk-rock TiO_2 based on the fusion-crust composition.

Lack of pristine glasses in EET96008 and EET87521 distinguish these two from YQ meteorites with pristine glasses [6] as to maturity of breccia and deriviation (=source-crater) on the Moon surface.

Conclusions: Texture, mineral compositions and exsolution of pyroxene, mixing of minor highland components and lack of pristine glass all supports EET96008 and EET87521 have provenance from a common source crater. This is consistent with their paired entry supported by the "Find" location in Antarctica [1] and the exposure ages [13]. EET96008/87521 and YQ meteorites commonly include Very-Low-Ti suite mare basalt with relatively slow cooling by mare standard.

References:

[1] Feldman W. C. et al. (1998) *LPS* **29**, abstract #1936. [2] McBride K. & Mason B. (1998) *AMN* **21**, 12. [3] Yanai K. & Kojima H. (1991) *Proc. NIPR Ant. Met.* **4**, 70-90. [4] Warren P. H. & Kallemeyn G. W. (1993) *Proc. NIPR Ant. Met.* **6**, 35-57. [5] Takeda H. et al. (1993) *Proc. NIPR Ant. Met.* **6**, 3-13. [6] Arai T. & Warren P. H. (1999) *MPS*, **34**, 209-234. [7] Arai T. et al. (1996) *MPS*, **31**, 877-892. [8] Takeda H. et al. (1992) *Proc. LPSC*, **22**, 355-364. [9] Warren P. H. & Ulff-Møller F. (1999) *LPS* **30**, abstract #1450. [10] Mikouchi T. (1999) *LPS* **30**, abstract #1558. [11] Snyder G. A. et al. (1999) *LPS* **30**, abstract #1499. [12] Joliff B. L. et al. (1996) *LPS* **26**, 615-616. [13] Nishiizumi K. et al. (1999) *LPS* **30**, abstract #1980.

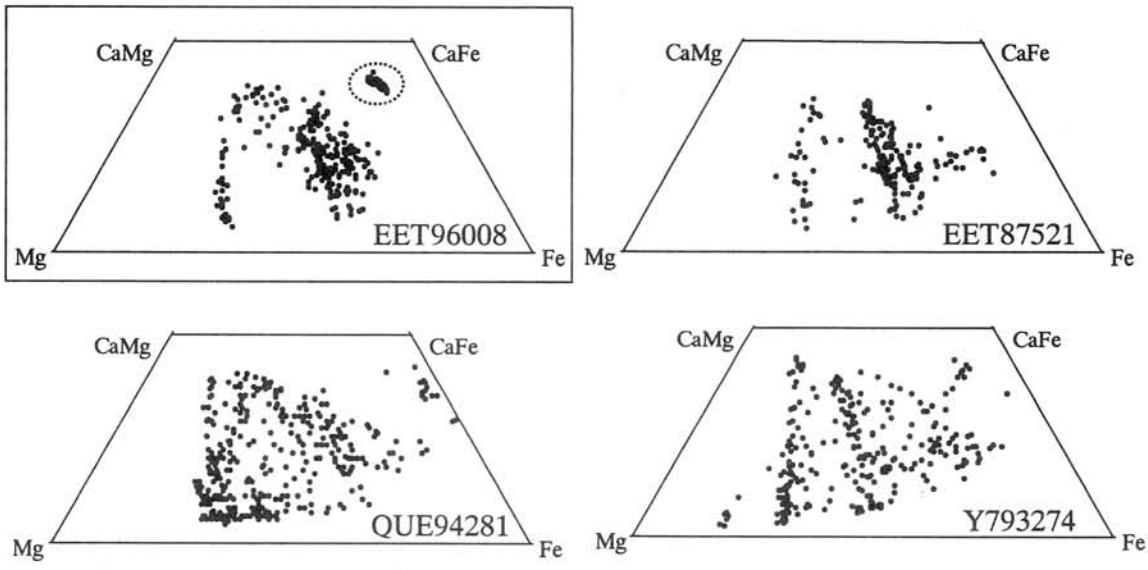

Fig. 2 Pyroxene quadrilaterals for EET 96008 and other mare breccias

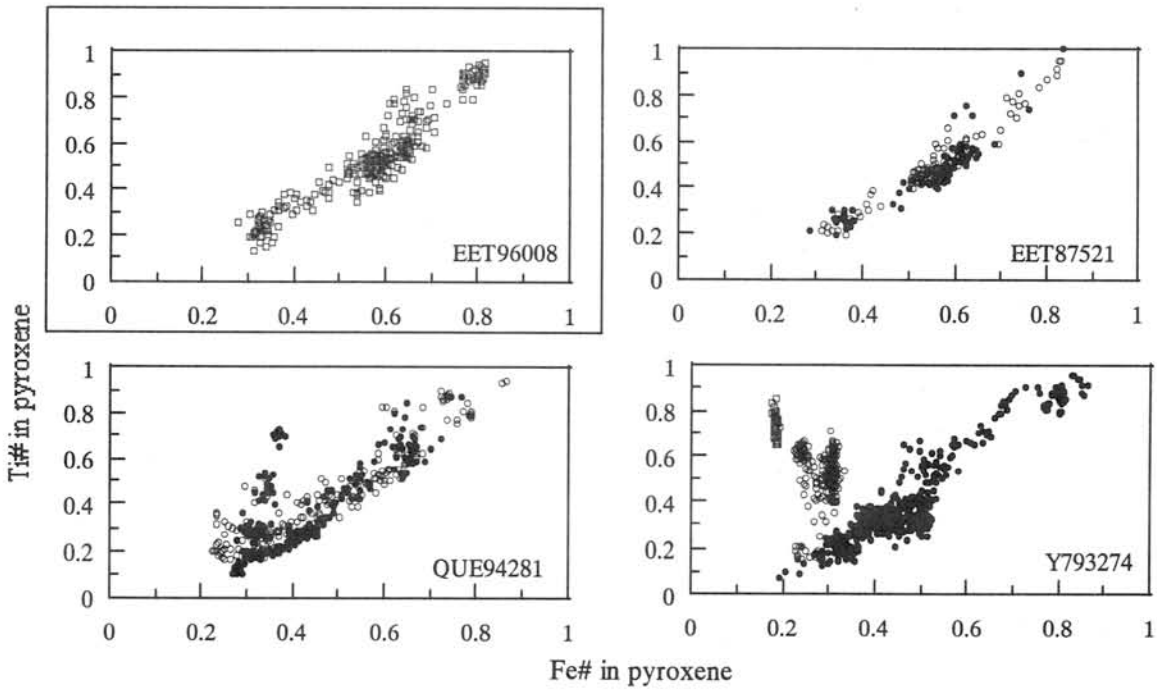

Fig. 3 Plots of Fe# vs. Ti# for pyroxenes of EET 96008 and other mare breccias

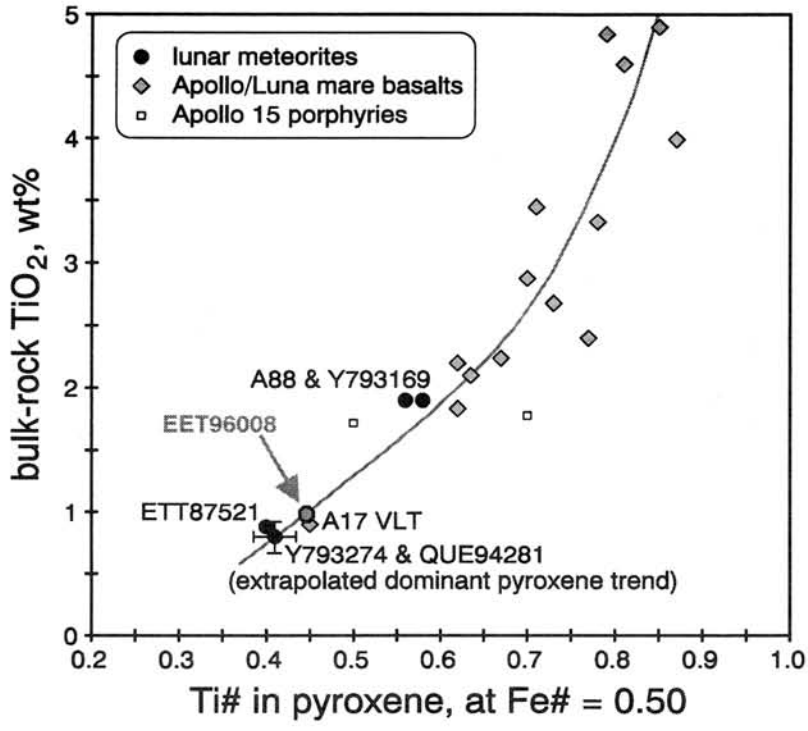

Fig. 4 Fe#-nomalized Ti# vs. bulk-rock TiO_2 (wt%) for Ti-poor mare basalts.

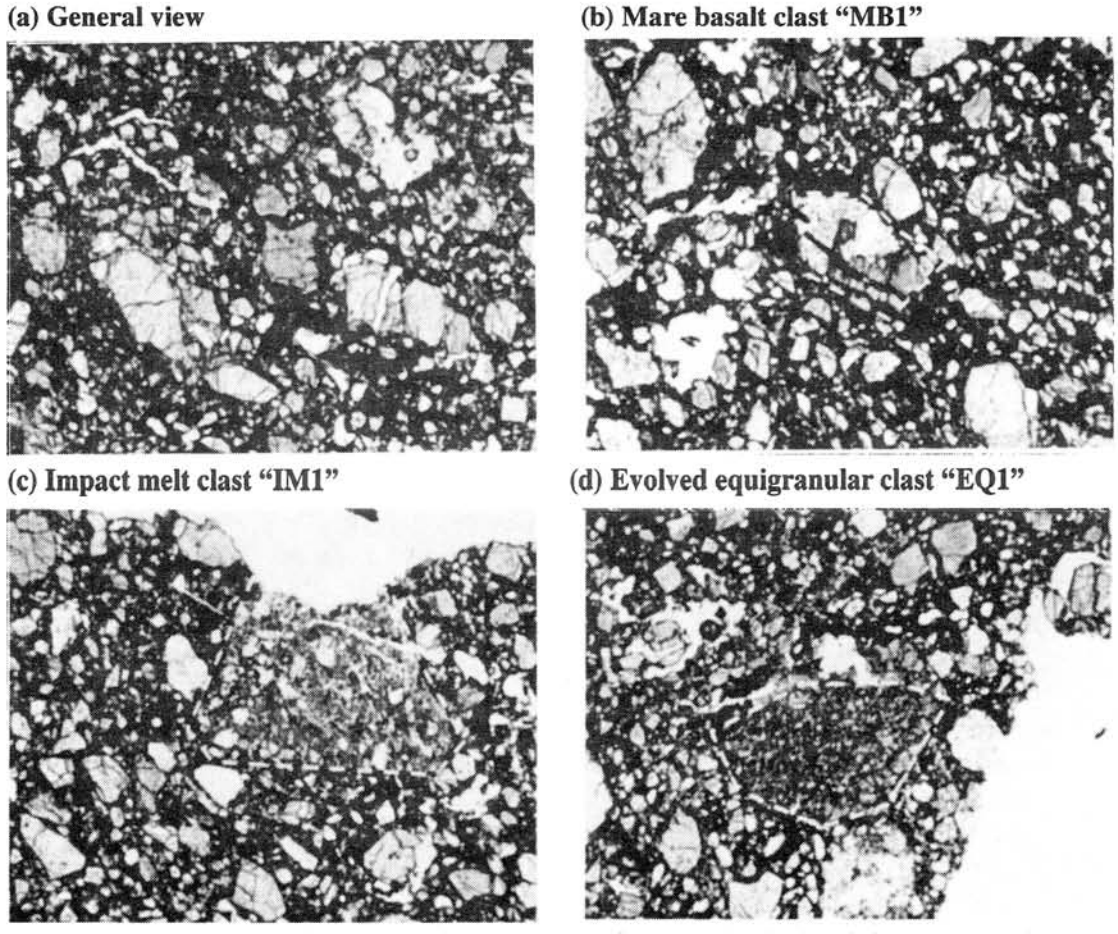

Fig. 1 Transmitted light photomicrographs of EET96008, 41 (3.3mm across).

TENTATIVE TTT-DIAGRAM FROM TEXTURES OF BASALTS AND BASALTIC CLASTS OF THE NASA LUNAR EDUCATIONAL SET: COMPARISONS TO TERRESTRIAL BASALTS

Bérczi Sz.[1,2], Józsa S.[2], Szakmány Gy.[2], Dimén A.[1], Deák F.[3], Borbéi F.[3], Florea N.[3], Peter A.[3], Fabriczy A.[4], Földi T.[1], Gál A.[3], Kubovics I.[2], Puskás Z.[2], Unger Z.[5],

[1]Eötvös University, Dept. G. Physics, Cosmic Materials Space Res. Group, H-1117 Budapest, Pázmány Péter s. 1/a. Hungary, (bercziszani@ludens.elte.hu)
[2]Eötvös University, Dept. Petrology and Geochemistry, H-1088 Budapest, Múzeum krt 4/a. Hungary,
[3]Babes-Bolyai University, Dept. and Museum of Mineralogy, RO-3400 Cluj, Kogalniceanu 1. Romania,
[4]Eötvös University, Teachers Training College H-1126 Budapest, Kiss J. altb. 42. Hungary,
[5]Hungarian Geological Survey, H-1146 Budapest, Stefánia út 14. Hungary.

ABSTRACT

We studied NASA Lunar Educational Thin Section Set's basalts and basaltic clast from breccias and soil samples. 1) We arranged them according to their silicate paragenetic sequences, textural characteristics, and estimated cooling rates, 2) we reconstructed a tentative TTT-diagram for a lunar basaltic lava flow, 3) we compared these textures to those of a terrestrial flow (tholeiitic composition), 4) we compared our results to cooling rates and industrial TTT diagrams used in hardening in the steel industrial textures.

INTRODUCTION

Basaltic textural types, their grain size, crystal morphology are in systematic relation with the cooling rates in the magma body [1]. In an undisturbed magma body from the edges toward the deeper layers gradually slower cooling rates result in gradually coarser textural types. From crystal morphology, paragenetic sequences [2] we arranged NASA lunar set textures of a 8-10 meters thick lunar basaltic flow [1-5]. according to cooling rates and textural types. This study was an international cooperation between teachers and students from Eötvös University, Hungary, and Babes-Bolyai University, Cluj, Romania. First in this work, 5 of us (Deák, Borbély, Florea, Peter, Unger) translated the Lunar Petrographic Thin Section Set book of C. Meyer (1987) [6] to Romanian language. We focused on basaltic samples of the lunar set, because Carpathian Basin petrology is rich in different basalts and gabbros for comparisons. From Carpathian Basin basalts we selected an ophiolitic textural series of the Darnó Hill, Heves C., Hungary [7]. Forming a continuous sequence of textures we used parallel both terrestrial and lunar samples [3]. (The following thin sections were used from NASA set: 74220, orange soil; 68501, clasts in soil s.; 14305, clasts in breccia; 72275, clasts in breccia; 12002 porphyritic s.; 70017, poikilitic s.; 12005 poikilitic s.) The reconstructed tentative TTT diagram represents a lunar "average" flow, which solidifies between 1250 and 950 C, contains the textural fabrics of the Fig. 1. sequence, with the cooling rates from glassy quenching 1000 C/min. rate till 0.5-0.05 C/hr. Our tentative TTT-diagram form a common background for detailed basaltic textural studies for students.

TEXTURAL SEQUENCE OF BASALTIC SAMPLES AND CLASTS IN NASA LUNAR EDUCATIONAL SET

On the basis of the sequence of terrestrial textures we estimated (interpolated) the place (probable original depth) of the lunar set textures in a lunar basaltic lava flow. We also used literature data for cooling rates. The samples in a sequence starting from the greatest cooling rate are:

74220 The "highest" position (the greatest cooling rate) had the orange soil spherules in the **74220,** because their ejection as a lava fountain ([6],[9],[11]) had glass quenching cca. 1000 C/min. cooling rate [12].

68501 Variolitic clast. (We remember from earlier loans, that in NASA Lunar set No. 6. 72275,509 breccia contained a larger vitrophyric-variolitic clast. 72275 is the thin section with the largest surface in the lunar set). Recent (No. 4.) set contains a clast with spherulitic-variolitic texture among the soil grains of **68501.** This clast had second highest cooling rate in our sequence (tentatively: some hundred degrees Celsius per day).

12002 This Apollo 12 porphyritic sample **12002** represents slower initial cooling rate for the large olivine

grains and higher cooling rate (wide range) for the surrounding (variolitic) laths of clinopyroxenes and plagioclase feldspars[12]). In a revised model cooling rates may vary from some degrees Celsius to 2000 C/hour [17].

14305 The breccia **14305** contains intergranular type clasts, such representing the third texture in the cooling rate sequence (tentatively: hundred degrees Celsius per week)

72275 The subophitic clast of **72275**,128 breccia represents an even slower cooling. Over breccias all three basaltic samples represent well crystallized beautiful specimens.

70017 This poikilitic sample of **70017** has paragenetic sequence similar to A-11 High Ti- basalts [2] [15], rich occurrence of sector zoned clinopyroxenes. The rich population of ilmenites make dark the thin section: this ilmenite rich specimen has a counterpart near to Darnó Hill (at Szarvaskő), in a gabbro with high ilmenite cont. bw. 8-10 % wt.)

12005 The Apollo 12 poikilitic **12005** sample had the slowest cooling, so this specimen closes our cooling rate series. It contains large, zoned pyroxene oikocrystals with embedded idiomorphic (euhedral) olivine grains of chadacrysts [12].

TERRESTRIAL COUNTERPART TEXTURES: AN OPHIOLITIC SEQUENCE OF DARNO HILL

In the Darnó Hill (basalts and microgabbros) textural sequence of an ophiolite can be found. From the outer edge high cooling rate textures to the bottom of the lava layer (or to the center of a pillow lava "sphere") the following textures represent this series: spherulitic, variolitic, intersertal, intergranular, subophitic, ophitic, poikilitic. [7]. Although important details are different in a terrestrial flow and in a lunar flow (chemical compositions, - e.g. 74220 and 12002 are picritic basalts [5], [10], [16]. - water content can change paragenetic sequence of crystallization for plagioclase feldspar and pyroxene), the main textural characteristics determined by cooling rates remains important basis for comparisons and TTT diagrams.

COOLING RATES FOR LUNAR AND TERRESTRIAL BASALTS AND TENTATIVE TTT DIAGRAM FOR THE LUNAR BASALTS

On the basis of experimental determination of the cooling rates and also from TEM measurements of clinopyroxenes both cooling rate sequences and TTT-diagrams were studied and determined [1], [3], [13-15]. The lunar basalt layer was 8-10 meter thick [13] [15]. This thickness is larger, but comparable to pillow lava units as terrestrial pairs. A pillow lava cools during 2 days, but 8-10 meters thick lunar layers cooled for months or years in their inner regions. In a pillow lava textural sequence only the intergranular texture could be reached because of the quick cooling and smaller lava body size. In the lunar basalt case all textural types in our sequence could be reached. The corresponding cooling rates were given by [3] as 3 C/min. for a vitrophyric, 30 C/hr for a coarser vitrophyric and 3 C/day for a porphyritic Apollo 15 sample. Data of a pillow lava are in table 1. as follows: [7]

textural type	cooling rate	depth in a pillow lava	length of cooling time
glassy	45000 - 1800 C / min.	1 centimeter	1 min.
spherolitic	22000 - 1000 C / min.	some centimeters	some minutes
variolitic	1000 - 200 C / min.	decimeter	10 minutes - 0,5 hour
intersertal	200 - 30 C / min.	some decimeters	0,5 - 2 hours
intergranular	0,5C / min.	central region of pill.l.	1 - 2 days

SUMMARY

We constructed: 1) from lunar basaltic textural characteristics a paragenetic and cooling rate sequence, 2) a tentative TTT-diagram of basaltic lava flow layers, which was 3) compared to a terrestrial basaltic flow textural layers and these were 4) applied to compare steel industrial TTT diagrams. 5) By translating the NASA Lunar Set Petrology Book of JSC to Romanian, in an international cooperation between teachers/students of Hungary and Romania.

ACKNOWLEDGMENT: Thanks to NASA JSC for loan of Lunar Educational Thin Section Set, 5th term.

REFERENCES: [1] Lofgren, G.E., Donaldson, C.H., Williams, R.J., Mullins, O. (1974): *5th LSC*, 458-460.; [2] Bence, A.E., Papike, J.J. (1972): *3th LSC*, 59-61.; [3] Grove, T.L. (1977): *8th LSC*, 380-382.; [4] Grove, T.L., Bence, A.E. (1977): *8th LSC*, 383-385.; [5] Grove, T.L. et al. (1973): *4th LSC*, 323-325.; [6] C. Meyer: (1987): *The Lunar Petrographic Thin Section Set.* NASA JSC Curatorial Branch Publ. No. 76. Houston, Texas, USA. [7] Józsa S. (2000): Thesis. Eötvös University, Dept. Petrology/Geochemistry, ELTE, Budapest; [8] Szakmány Gy. (1995): The main textural types of igneous rocks. (In Hungarian). Eötvös Univ. Lect. N. Ser. Dept. Petrology.; [9] Delano, J.W., & Livi, K. (1981): Lunar Volcanic Glasses. *GCA* **45**, 2137.; [10] Grove, T.L., et al. (1973): *4th LSC*, 323-325.; [11] D.S.McKay, D. S. & Wentworth, S. J. (1992): *Geology of Apollo 17 Landing site, WS.*, LPI Techn. Rep. No. 92-09, Part 1. p.31.; [12] Dungan, M. A., Brown, R. W. (1977): The Petrology of the Apollo 12 Basalt Suite. *Proc. Lunar Sci. Conf. 8th.* 1339.; [13] Grove T. L. (1982): *Am. Min. 67*, 251-268.; [14] McConell, J.D.C. (1975): An. Rev. Earth. Planet Sci. 3. 129.; [15] Nord, G.L., Heuer, A.H., Lally, J.S., Christie, J.M. (1975): *6th LSC*, 601-603.; [16] Walker, D., et al (1974): *5thLSC*, 814-816.; [17] Walker, D., Kirkpatrick, R.J., Longhi, J., Hays, J.F. (1975): *6th LSC*, 841-843.

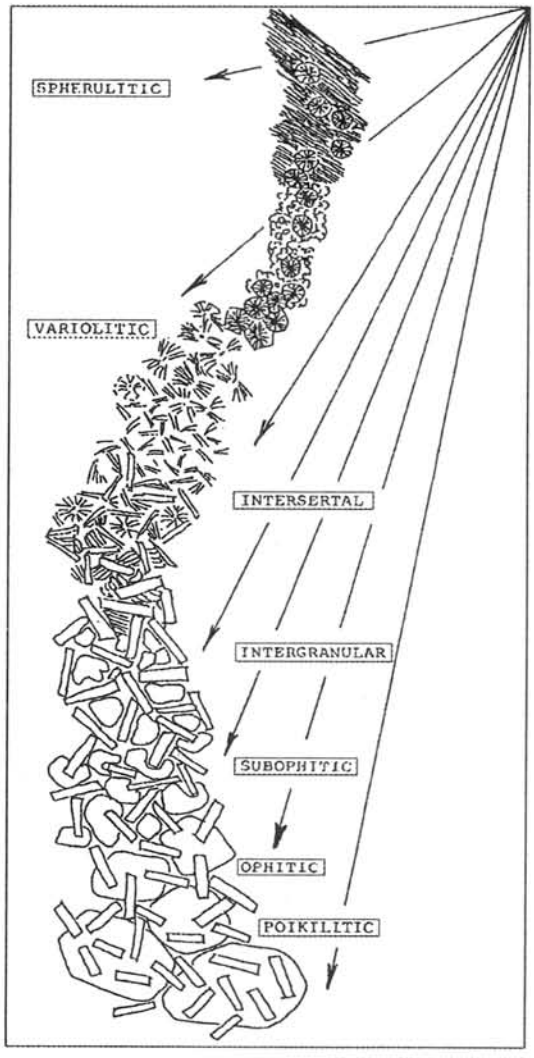

Fig. 1. Textural sequence and main cooling rate arrows for an average lunar basaltic flow. Horizontal axis is Temperature with a 950 C to 1250 C interval. Vertical axis is Time with seconds on the top till months at the bottom of the axis.

A comparative Raman spectroscopic study of maskelynite in SNC meteorites and diaplectic plagioclase glass from the Ries crater: Implications to their origin

M. Chen[1,2], A. El Goresy[2], B. Reynard[3], P. Gillet[3]

[1] Guangzhou Institute of Geochemistry, Chinese Academy of Sciences, Guangzhou 510640, China (mchen@gig.ac.cn)

[2] Max-Planck Institut für Chemie, D-55128 Mainz, Germany

[3] Laboratoire de Sciences de la Terre, Ecole Normale Supérieure, 46 Alléé d'Italie, F-69364 Lyon cedex 07, France

Introduction

The Raman spectrum of feldspar is usually characterized by three groups of bands in the 300-500 cm^{-1}, 550-580 cm^{-1} and 900-1200 cm^{-1} regions [1,2]. The bands in the 300-500 cm^{-1} and 900-1200 cm^{-1} ranges are attributed to the bending vibration and stretching vibrations of four-membered rings of tetrahedral (TO_4), respectively. The bands at 550-580 cm^{-1} ("defect " band) correspond to the bending vibration of three-membered rings of tetrahedra. The intensity variation of the defect bands is proportional to the increase of density of glass, which corresponds to a decrease of average ring size and the formation of three-membered rings at high pressure [1,2]. Recent investigation indicated that the maskelynite in shocked meteorites is a dense plagioclase glass quenched from a dense melt at high-pressures [3], whereas diaplectic glass is shock-induced amorphous phase formed from solid-state transformation [4]. Since the formation mechanism of maskelynite is distinct from diaplectic feldspar glass, there should be some differences in the Raman spectra of these two kinds of glasses. In this paper, we report the results of Raman spectroscopic investigation in the SNC meteorites and diaplectic plagioclase glass from the Ries crater.

Samples and analytical techniques

Several SNC meteorites including Zagami, Shergotty, Shergottite (SAU) and Dar al Gani 476, and granites and gneisses from the Ries crater, Germany, were made into polished thin sections for investigations by optical microscope, SEM and Raman spectroscopy. Raman spectra of maskelynite and diaplectic glass were recorded at Ecole Normale Suprerieure de Lyon, using a XY Dilor spectrometer equipped with a nitrogen-cooled CCD detecter.

Results and discussion

Maskelynite in the SNC meteorites usually contain no inherited fractures, cleavage, and shock-induced fractures. Most of these grains display smooth feature in the thin sections. Two types of maskelynites have been identified: (1) Densified maskelynite, such as those in Zagami and Shergotty. These maskelynites are usually surrounded by many radiating cracks emerging from their surface into surrounding minerals. Raman spectra of maskelynite display an intensive Raman band at ~580 cm^{-1} (Fig.1). This indicates that these maskelynites were quenched from a dense melt under high-pressure. (2) Maskelynite with lower density, such as those in the Shergottites (SAU) and Dar al gani 476. The radiating cracks surrounding these maskelynites are usually missing. The Raman spectra of these maskelynites display a weak shoulder at ~560 cm^{-1} (Fig.1), hence indicating that they were solidified from a plagioclase melt at lower pressure.

The feldspar glass in the Ries crater is typical diaplectic glass formed through solid-state phase transformation. Most of diaplectic plagioclase glass contains PDFs with both diaplectic plagioclase glass and crystalline lamellae. It indicates that these grains were never molten during the shock event. Diaplectic K-feldspar glass usually contains circular fractures. No radiating cracks were observed on both diaplectic plagioclase glass and feldspar glass. The Raman spectra of these diaplectic glasses display a weak shoulder in 560-570 cm^{-1} region (Fig.2). In comparison, this shoulder is much weaker than that from maskelynites in Dar al Gani 476 or Shergottite

(SAU). This indicates that the maskelynites contain much higher amount of three-membered rings of tetrahedra than the diaplectic glasses, and that the maskelynite is denser than the diaplectic glass.

The Raman band at 560-580 cm^{-1} is a diagnostic spectral tool to characterize the nature of glass. The intensity of this band, for a given composition, is correlated to the degree of densification. Densified glass has an intensive Raman band at 560-580 cm^{-1}, and normal glass has only a weak shoulder at this position. Our investigation revealed the presence of several types of feldspar glasses that we characterized by laser microRaman spectroscopy in meteorites and terrestrial craters. The maskelynites in the SNC meteorites are evidently different from the diaplectic feldspar glasses in the Ries crater both in petrologic and Raman spectroscopic features. Our investigation confirms that maskelynite quenches under pressures, and that diaplectic glass forms through solid-state transformation followed by relaxation after decompression.

References: [1] Mastson, D.W., Sharma, S.K., Philpotts, J.A. (1986) Amer Mineral 71: 694-704. [2] Reynard, B., Okuno, M., Shimada, Y., Syono, Y., Willaime, C. (1999) Phys Chem Minerals 26: 432-436. [3] Chen, M., El Goresy, A. (2000) Earth Planet Sci Lett 179: 489-502. [4] Engelhardt, W.v., Arndt, J., Stöffler, Müller, H., Jeziorkowski, R.A. (1967) Contrib Miner Petrol 15: 91-100.

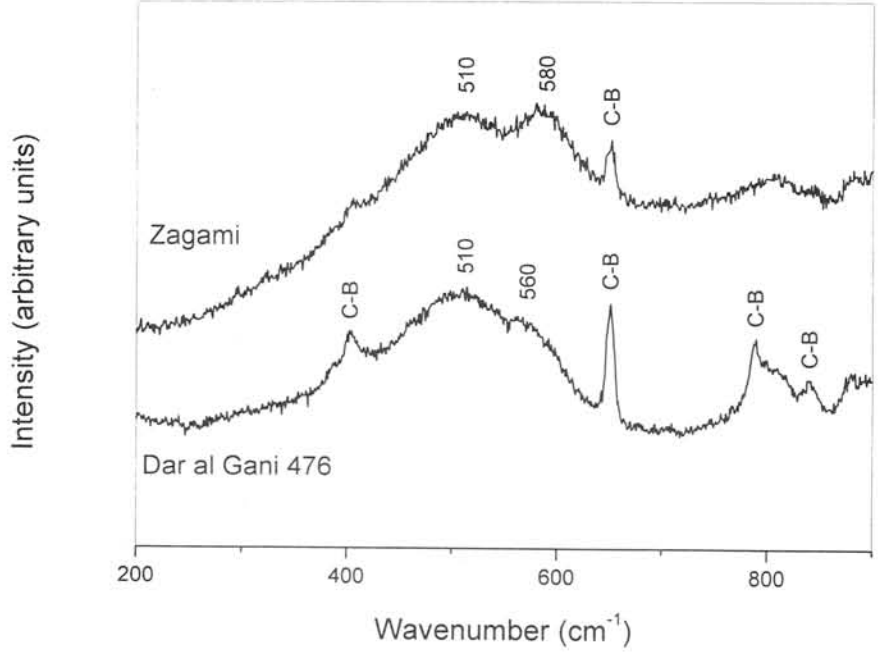

Fig.1 Raman spectra of maskelynite in the Zagami and Dar al Gani 476 meteorites. Raman band at ~580 cm^{-1} in the Zagami is much stronger than that at ~560 cm^{-1} in the Dar al Gani 476. The peaks of C-B are from the crystal bond epoxy.

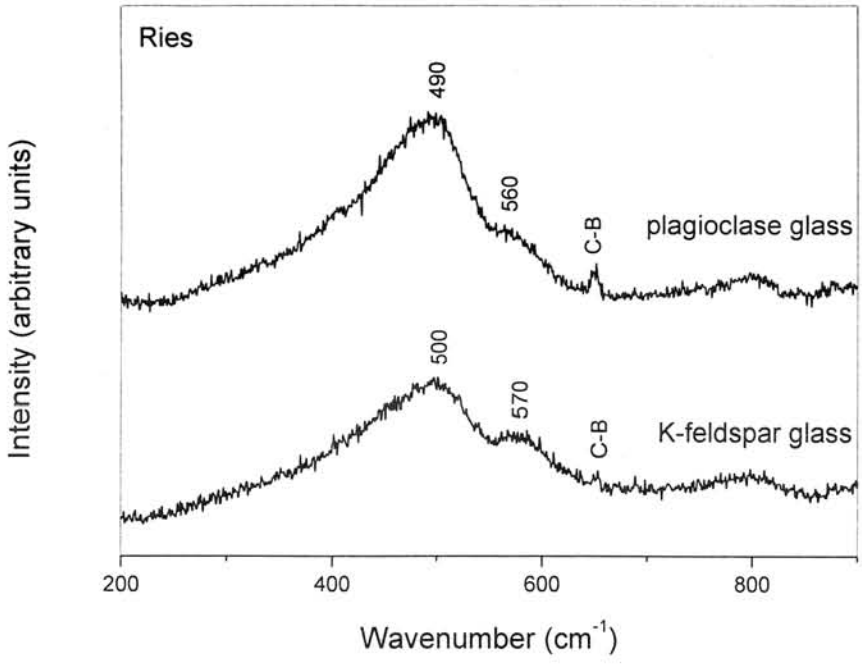

Fig.2 Raman spectra of diaplectic plagioclase and K-feldspar glasses in the Ries crater. The peaks of C-B are from the crystal bond epoxy

Possible giant buried meteorite crater identified in South-West Hungary

DETRE, CSABA H. (1), - KALAFUT, MIKLOS (2), - DETRE-LOMBAY, KAMILLA (1)
(1) Geological Institute of Hungary, Stefánia út 14., Budapest, H-1143 Hungary, E-mail: detre@mafi.hu, (2) MAGEO, Tó-utca 4., Diósd, H-2049, Hungary

On the basis of analysis of vertical intensity anomalies of the geomagnetic field presented on the Geomagnetic Map of Hungary (1989) became evident that at the South-Western final part of the Southern Magnetic Anomalies (SMA) a well identified circular formation is arranged.(see figure). This spectacular magnetic arrangement suggests the similar arrangment of the magnetic stone-masses. The phenomenon is interpreted as crust-structural feature which could be a print of an ancient astrobleme.On the territory of the Carpathian Basin many similar circular formations were identified by other methodes (e.g. geomorphology by space-photo interpretations.(DETRE, CS.H., 1995, KALAFUT, M. 1987), but on the basis of exact geophysical data, these results are the first presentation.

The main circle has regular elliptical form, with 80 km major axis and 40 km minor axis. In the inside of the ellipse an interior circle of 15 km diam. is distinguishable which is connected from Eastern direction with a line of anomalies of 20 km length, whose direction is identical with the SMA.

There are outer arcs which are connected with the main elliptical circle, therefore, the territory of the anomaly-arrangement is in the neightbourhood of 100 x 100 km. The Western part of the anomaly territory is buried by Pannonian (Upper Miocene) loess (see KOKAY, A. 1997), which has argumented the Pre-Pannonian age of the anomaly and the giant impact event. We can suppose that the impact event came from the intense bombardment period of the Earth, 4.0 - 2.0 billion years ago (see FRENCH, B.M., pp 104-105) This possible giant impact astrobleme effect could determine the later tectonic movements of the surrounding territory (GRACHEW, A.F. 1987, KALAFUT, M. 1987).
Further arguments for the impact event: On the North-Eastern edge of the main circle spherules of probably impact origin, shocked quartz and moissonite occurrences are known (ELEKES, Z. et al. 2001)

References cited:

DETRE, CS.H. 1995: Are there meteorite crtaers in Hungary? - Papers presented to the IGCP 384 Meeting: Spherules and Ecology, pp 10-12, Debrecen, Hungary.
ELEKES, Z., SZÖŐR, GY., KISS, Á.Z., RÓZSA, P., SIMON, Á., UZONYI, I., SIMILÁK, J. 2001: Carbon and Oygene Detremination in Magnetic Spherules by Deuteron Induced Gamma Ray Emission Method at a Nuclear Microprobe. - Nuclear Instruments and Methods in Physics, Research B. (In press)

FRENCH, B.M. 1998: Traces of Catastrophe. A Handbook of Schock Metamorphic Effects in Terrestrial Metamorphic Impact Structure. - Lunar and Planetary Institute, Houston.
GRACHEW, A.F. 1987: Rift-zones of the World. - Akad. Nauk, Moscow.
KALAFUT, M. 1987: Recognition of Crustal Platic Deformations. - Issled. Zemli iz Cosmosa, 4., 53-58, Moskva.
KOKAY, A. 1997: Geological Evaluation of the Üveghuta-1.Borehole. - Ann. Rep. Geol. Inst. Hungary, 1996/2, pp 59-69.
NATIONAL ATLAS OF HUNGARY, Geomagnetic Vertical Intensity Anomalies, 1989, p.48.

Acknowledgements
The investigations are supported by the National Scientific Foundations (OTKA) Project T025461 and by the Foundation for Interdisciplinary Research

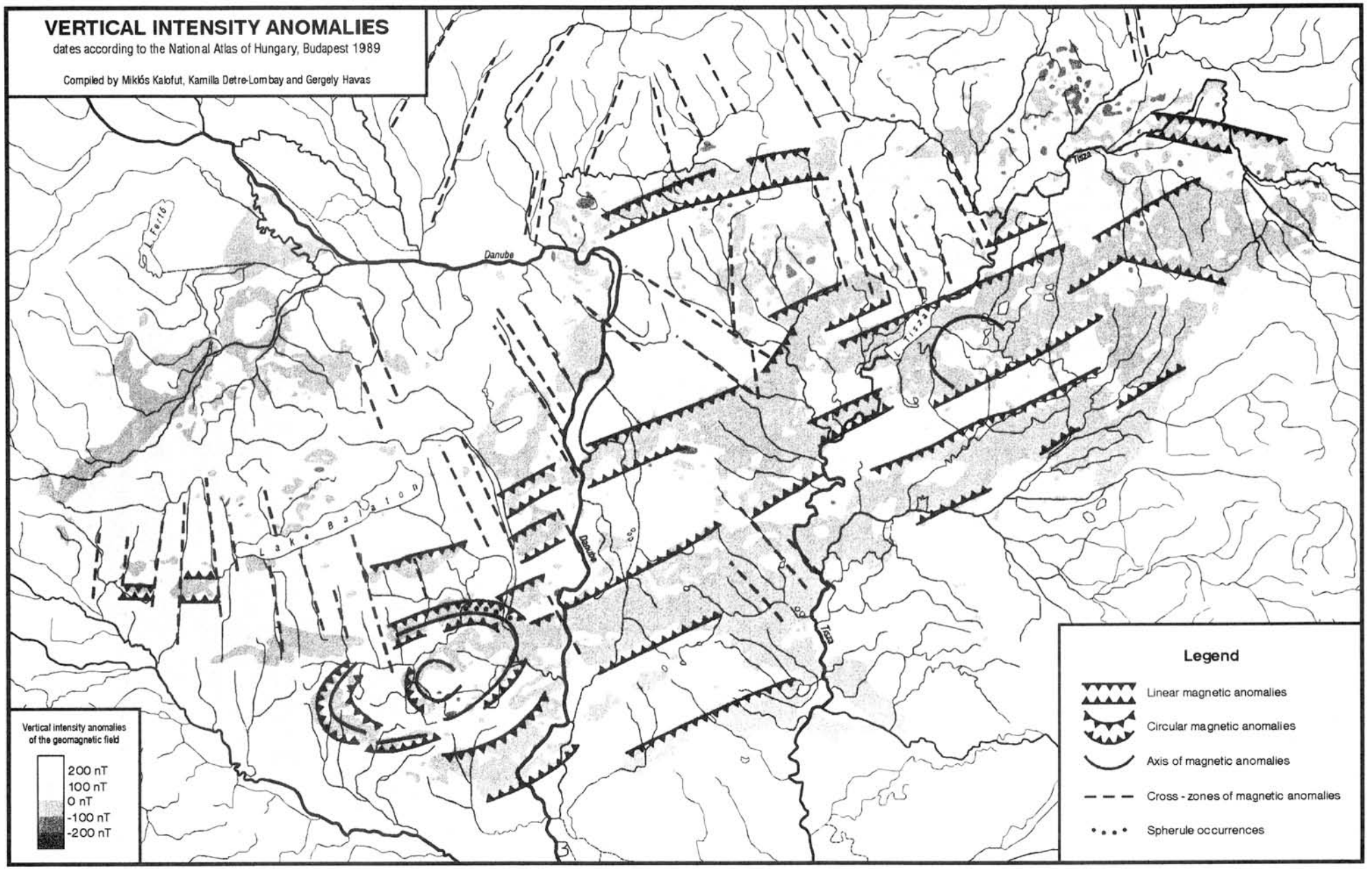
VERTICAL INTENSITY ANOMALIES
dates according to the National Atlas of Hungary, Budapest 1989
Compiled by Miklós Kalofut, Kamilla Detre-Lombay and Gergely Havas
Danube
Tisza
Lake Balaton
Vertical intensity anomalies of the geomagnetic field
200 nT
100 nT
0 nT
-100 nT
-200 nT
Legend
Linear magnetic anomalies
Circular magnetic anomalies
Axis of magnetic anomalies
Cross - zones of magnetic anomalies
Spherule occurrences

Laser microprobe analysis of noble gas composition in the Allende meteorite

N. Ebisawa[1], R. Okazaki[1], K. Nagao[1], and A. Yamaguchi[2]
1) Laboratory for Earthquake Chemistry, Graduate School of Science, University of Tokyo, Hongo, Bunkyo-ku, Tokyo 113-0033, Japan
2) Antarctic Meteorite Research Center, National Institute of Polar Research, Kaga, Itabashi-ku, Tokyo 173-8515, Japan

Introduction

Recently halite crystals have been discovered in two ordinary chondrites, Monahans (H5) and Zag (H3-6) [1, 2]. Whitby et al. [2] reported that the halite grains in Zag had excess of ^{129}Xe, the beta-decay daughter of extinct ^{129}I (half-life of 17 Myr) indicating that aqueous fluids existed on the H-chondrite parent body in the early solar system.

Micro-distribution of halogens provides us with the information of interaction between aqueous fluids and minerals in meteorites. A high sensitive mass spectrometer allows us to determine the small quantities of noble gases associated with halogens even in a few microgram of a meteorite. Measurement of noble gases produced from halogens by nuclear reactions on their parent body or in space does not need to consider terrestrial contamination of halogens on the Earth.

In this study, we investigated micro-distribution of noble gases in the Allende meteorite using two noble gas mass spectrometry systems equipped with laser microprobe for extraction, MS-II and MS-III at the Laboratory for Earthquake Chemistry, University of Tokyo. These mass spectrometers were modified to be available for various extraterrestrial materials such as meteorites [3, 4] and single micrometeorites [5].

Experimental procedures

Some chips of 10 mm x 10 mm x 800 μm were sliced up from the Allende meteorite with a diamond saw. One of the chips, which included a CAI with a diameter of about 2-mm, was fixed on a glass plate with crystal bond that can be easily dissolved with acetone. The sample was polished with carborundum and diamond paste to be 300 μm thick. To prevent water-soluble minerals from eluting, we used ethanol instead of water in preparation of the sample.

The sample coated with carbon film was analyzed for elemental compositions especially for chlorine with an electron microprobe in National Institute of Polar Research. Prior to noble gas analysis, we polished its surface again with diamond paste to remove the carbon film and washed it repeatedly in boiled acetone to remove diamond paste and crystal bond. In the sample chamber leading to a noble gas purification system, several penetrated holes with a diameter of about 50 μm were made in a small area, ca. 150 μm x 150 μm, in the sample with Nd-YAG laser. Noble gases extracted from those holes were introduced to the purification system together. We estimated the weight of fused material in a hole to be about 2 μg. Concentrations and isotopic ratios of the released noble gases from each area were determined with the mass spectrometer.

Results and discussion

More than 20 points traversing the disorderly part of CAI were measured for all noble gases (Fig. 1, along the white line). The other points of the CAI that had no detection of chlorine were measured as well to make a comparative study (Fig. 1, white circles).

Electron microprobe analysis revealed that a part of marginal area of the CAI was enriched in chlorine. The chlorine-rich part looked disorderly as compared with the other chlorine-poor area of the CAI. In matrix neighboring the disorderly chlorine-rich CAI part, chlorine was not detected (Fig. 2).

Shown in Fig. 3 is micro-distribution of ^{129}I-derived ^{129}Xe along the white line through the chlorine-rich portion and at the areas circled with white line. It is apparent that the chlorine-rich points of the CAI had significantly high concentrations of ^{129}Xe than the chlorine-poor points of CAI and matrix. High concentration of ^{129}Xe detected from one point that had no chlorine may be owing to a chlorine-rich phase under the surface. Excess of ^{80}Kr produced by neutron capture on ^{79}Br correlates with the ^{129}Xe distribution.

The results show that the halogen-rich area was formed in a period when ^{129}I was still alive. It is certain that the event was soon after the end of elemental synthesis. Although we cannot determine the absolute time of the event when the halogens were enriched in some parts of CAIs, it must occur in the early stage of solar system formation.

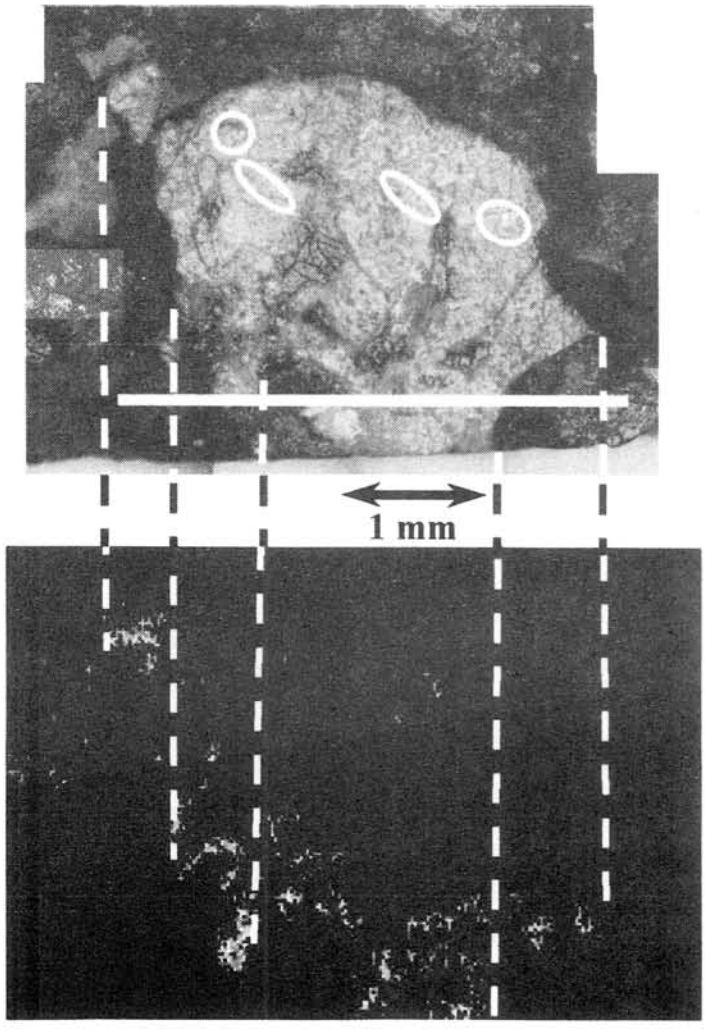

Fig. 1. Photomicrograph of the CAI in the Allende meteorite studied in this work. Reflected light was used. Noble gas analysis was performed along a white line and within four white circles. Chlorine is enriched in the area along the straight line.

Fig. 2. Micro-distribution of chlorine with an electron microprobe. White dots indicate chlorine. (The same scale as Fig. 1)

It is important that information concerning the location of the CAI during the formation of the halogen-rich area will be obtained from these data. Assuming that the CAI was already in its parent body, halogen must have been supplied from matrix materials contact with the halogen-rich portion or from inside the CAI. Neither the matrix nor the CAI have detectable concentrations of chlorine with our electron microprobe analysis. Therefore, it is probable that the halogens have penetrated into the CAI from outside in the early solar nebula. In all cases, it is an essential condition that the CAI has never experienced any great physical and/or heat impulse to lose the preserving ^{129}Xe.

Our noble gas data may give some constraints on the formation condition of halogen-rich portions in CAIs.

Reference

[1] Zolensky M. E. *et al.* (1999) *Science* **285**, 1377-1379.
[2] Whitby J. *et al.* (2000) *Science* **288**, 1819-1821
[3] Nakamura T. *et al.* (1999) *Geochim. Cosmochim. Acta* **63**, 241-255.
[4] Nakamura T. *et al.* (1999) *Geochim. Cosmochim. Acta* **63**, 257-273
[5] Osawa T. *et al.* (2000) *Antarctic Meteorite Res.* **13**, 322-341

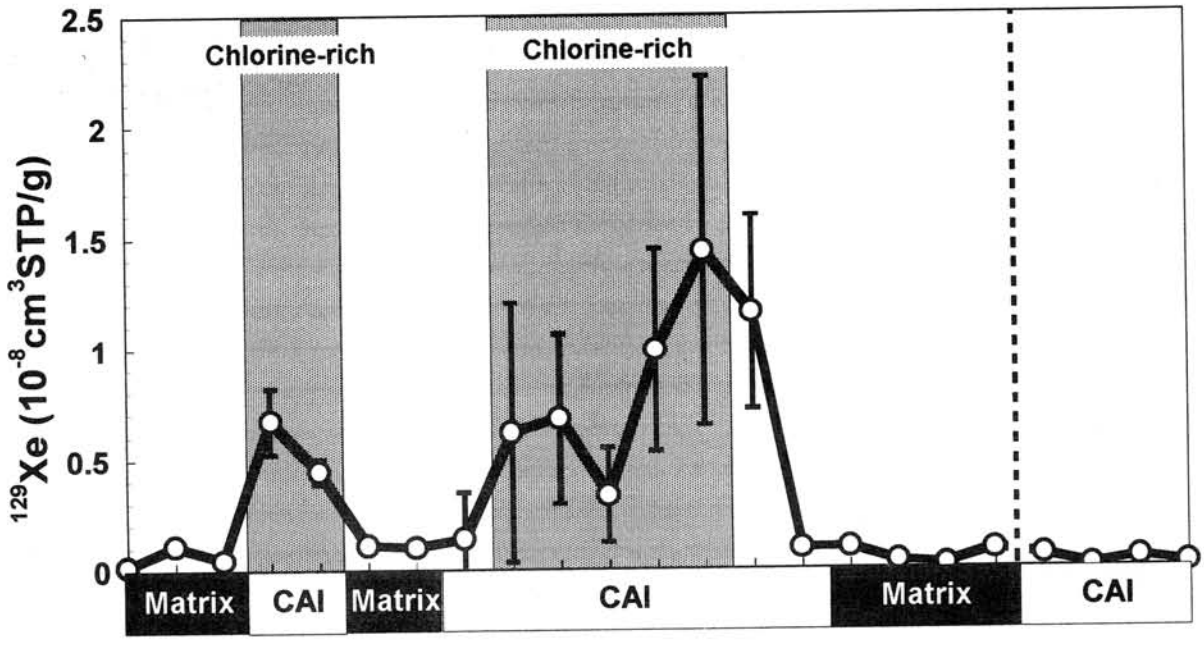

Fig. 3. Micro-distribution of ^{129}I-derived ^{129}Xe in the Allende meteorite. ^{129}Xe is enriched only in the chlorine-rich CAIs.

Magnetic field irradiated from An Odessa iron meteorite

M. Funaki[1], M. Koshita[2] and H. Nagai[2]
1: National Institute of Polar Research, Tokyo
2: Shinshu Univ. Faculty of Sciences, Matsumoto, Japan

1. Introduction

Octahedrite is a mass of iron-nickel of a dominant chemical composition, suggesting the multi-domain (MD) of its magnetic structure. Theoretically the isotropic MD material cannot take any magnetization in the nonmagnetic space. Nevertheless, the cubic sample prepared from octahedrite in laboratories carries the natural remanent magnetization (NRM) as investigated for a long time. The reasons are estimated due to the original magnetization (tetrataenite, present of single-domain and/or pseudosingle grains, magnetic anisotropy resulting from the Widmanstätten structure) associated from remagnetization on the earth such as the atmosphere heating and strains resulting from collisions with the earth and the effect of being cut etc. However, we do not know whether the natural state octahedrite has magnetization or not. In this sutdy, we measured the distribution of magnetic field irradiated from one block of Odessa octahedrite (3.7kg) and the results were compared with the samples cut from the block.

Several parts of the surface of Odessa were polished and etched by acid to identify the crystallization from Widmanstätten structure. Seven small cubic samples were cut from a tip of one hump to measure the magnetic properties. The block was set up to a binary axial rotation stage and was installed in the μ-metal magnetic shield case whose residual magnetic field was reduced to more than 53nT. The magnetic field toward the radius direction was measured by a uniaxial fluxgate magnetometer at every 5° or 10° apart from the surface of 1, 5, 10, and 40cm in distance. The cut samples were examined for NRM stability against AF demagnetization, magnetic anisotropy, hysteresis and thermomagnetic properties and microscopic structures.

2. Magnetic anomaly

In the measurement apart from 1cm, wide area of the sample irradiated the weak magnetic filed from -9 to 9 μT, but the strong field was irradiated from 2 areas (A and B) for positive anomaly and 3 ones (C, D and E) with the peak valres of-59.0 and 38.1 nT. The anomalies of A, C and E located at the corners or humps, but those of the B and D were located at flat or smooth surfaces. At the distance of 5cm, as shown in Fig. 1, the anomalies of A, B, C and D appeared with more broad spectrum with the peak intensity between -9.959 and 4.244 μT. The anomaly of E almost disappeared in this distance. At the distance of 10cm, the anomaly of the peak intensity (-2.128 to 1.088 μT) decreased to about 1/30 versus that of 1cm, and more broad anomaly pattern at A, B, C and D appeared. However, any meaningful magnetic anomalies were not measured at 40cm in distance due to the same level with the residual magnetic field in the magnetic shield case.

The irregular shape of this sample consists of single crystal defined by the Widmannstän structure, although many FeS inclusions were included by the microscopic observation. From the field measurement, it can be characterized that the larger magnetic anomalies appear at the hump and the corner, but weaker anomaly was also located at the relatively flat area (B). This tendency did not change throughout these measurements. However, there is poor correlation between the crystallization and the anomaly pattern, because the anomalies were not located systematically as controlled by octahedron. From these viewpoints, it is concluded that the anomaly is strongly controlled by shape anisotropy of the sample rather than crystallization.

3. Basic magnetic properties

The NRM ($0.24x10^{-2}$-$1.19x10^{-2}$Am2/kg) of 7 cut samples has the stable NRM components between 15 and 50mT, although the directions are classified into 2 groups; one group shifted to the other one during the AF demagnetization. The magnetic coercive force was small as $H_{C=}$2.4mT, but the magnetic remanent coercive force was large as H_{RC}=11.8mT suggesting small amount of higher coercive minerals in the sample. The thermomagnetic curve indicated the phase transition from kamacite to taenite ($\alpha \rightarrow \gamma$ phase) at 739°C in the heating curve and $\gamma \rightarrow \alpha$ phase at 565°C in the cooling curve, indicating 7% nickel content in the sample. Probably no tetrataenite is included inferred from the coercive force and thermomagnetic curve. The direction of magnetic anisotropy was almost parallel among the stable NRM components, isothermal remanent magnetization and the maximum axis of anisotropy magnetic susceptibility. These basic magnetic experiments suggest that the stable NRM of cut sample is strongly controlled by magnetic anisotropy resulting from fine grained magnetic grains in kamacite.

Fig. 1 The magnetic anomaly pattern apart 5cm from the surface.

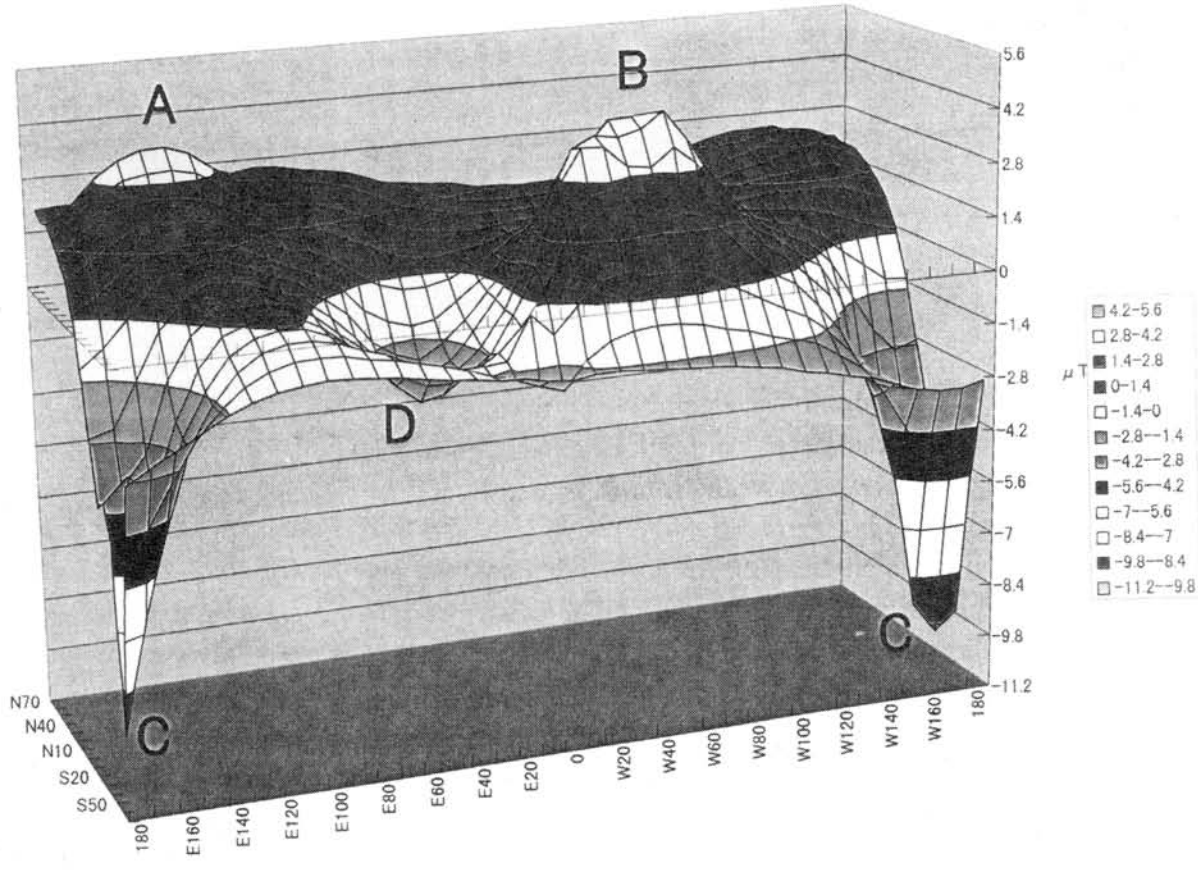

QUASIATMOSPHERIC ELECTROSTATIC PROCESSES ON DUSTY PLANETARY SURFACES: ELECTROSTATIC DUST AND WATER MOLECULE COAGULATION AND TRANSPORT TO THE POLES

T. Földi [1], Sz. Bérczi [2],

[1]FOELDIX, H-1117 Budapest, Irinyi J. u. 36/b. Hungary,
[2]Eötvös University, Dept. G. Physics, Cosmic Materials Space Research Group, H-1117 Budapest, Pázmány Péter sétány 1/a, Hungary, (berczi szani@ludens.elte.hu)

ABSTRACT

United acts by UV radiation and solar wind from the Sun and the micrometeorite bombardment produce a quasiatmosphere above the dusty (i.e. lunar) planetary surface. In this quaisiatmosphere the levitating charged dust particles can agglutinate by the alternating receiving and loosing charge and the electrostatically charged dust particles may produce larger and larger grains. These grains may also attract and include H_2O molecules on these dusty planetary surfaces. The composite agglutinated molecules are dragged by the solar radiation pressure toward the poles. In the vicinity of poles they are discharged, fall down and accumulate on the surface. We studied these electrostatic mechanisms of planetary quasiatmospheres and we suggest a model of accumulation of H_2O molecules in the polar regions of dusty planetary surfaces.

INTRODUCTION: FORMATION OF QUASIATMOSPHERE ABOVE THE LUNAR SURFACE

Micrometeorite bombardment is a continuous source of dust production on the Moon. The distribution of dust particles from impact may cover the size range from 200 micrometers to the molecular region. The ultraviolet radiation of the Sun, (depending on the escape energy for electrons) causes strong electron emission from the lunar surface. Most of the emitted electrons escape the lunar surface therefore the lunar surface becomes charged up positively (which retards the electron escape and which may produce a negative field charge similarly to that of virtual cathode in the electron tube).

Above the negative space charge field of the electron cloud a layer of positively charged dust cloud forms in the lunar vacuum. That dust cloud consists of ion-agglutinated, great mass, and low velocity particles, which are alternately charged up and discharged. These positively charged large particles levitate in the near vicinity of the surface (between 15-20 cm from surface) and we call it lunar quaisiatmosphere. With negatively charged water molecule-ions these agglutinated particles gradually grow larger and oscillate in the near vicinity of the surface. But where is the water molecule from?

It was found in electron-tube industry that water molecules may retain one negative electric charge (Tungsram Factory, Budapest, 1935, Bródy and Palócz, 1953). On the inner surface of the electron tube, in hypervacuum, a monomolecular water molecule layer was found. This molecular water layer was negatively charged while the glass surface wall was positively charged. Later, Israel (1957) found that the negatively charged water molecules have very longer lifetime and they do not recombine. (This lifetime is an order of magnitudes longer, then that of the small positive ions. Such charged water molecules can survive the cosmic travel time from the Earth upper atmosphere to the surface of the Moon.)

EXPERIMENTAl

We studied production of cosmic dust in an electrostatic experiment (Földi et al, 1999). In this work we studied the possibility of the experimental production of extrafine dust fraction. We used a chamber with 2000 X 1000 X 250 millimeters volume. There were atmospheric pressure and laboratory temperatures. Two systems of electrodes were arranged in this space. One operated on + 15 kV and the other on - 15 kV potential. The electrodes were 800 mms long, their diameter was 10 mms. In a distance of 45 mm from each electrodes a 0.1 mm diameter special nickel wire was placed. The large electrodes with opposite potential were arranged in a comb like pattern (Földi et al, 1999).

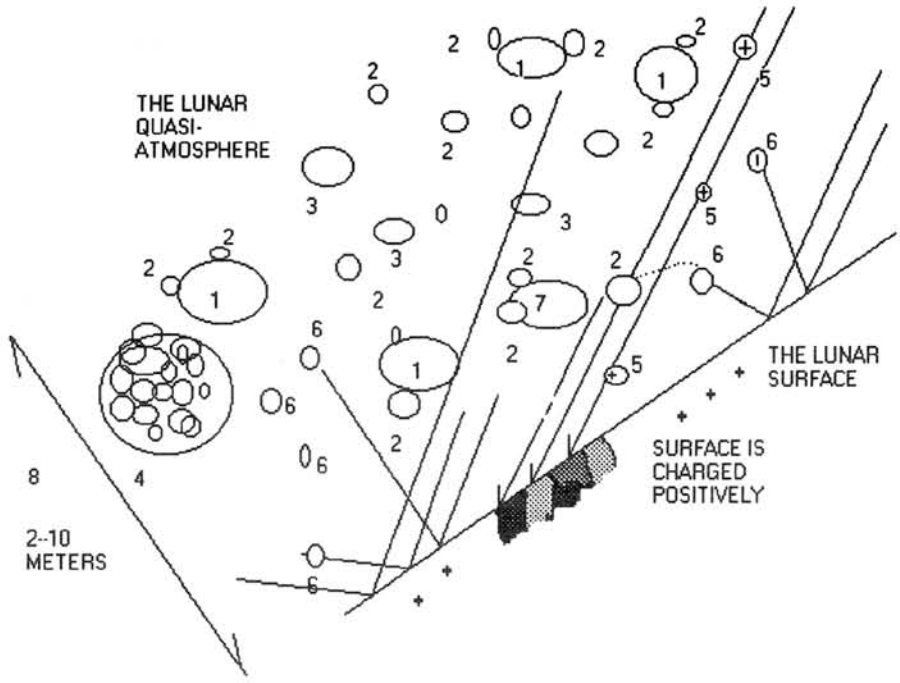

1 -- OXYGEN, 2 -- HYDROGEN, 3 -- DUST PARTICLE, 4 -- COAGULATED PARTICLE (THIS PARTICLE INCLUDES WATER MOLECULES), 5 -- SOLAR WIND PROTON, 6 -- ELECTRON EMITTED BY SOLAR UV RADIATION, 7 -- WATER MOLECULE, 8 -- THE HEIGHT OF THE LUNAR QUASIATMOSPHERE, WHERE COLLISIONS ARE FREQUENTLY OCCURRING, THERMAL PARAMETERS (ESTIMATED VALUES): 1: 600 K, 2: 5000 K, 3: 400 K, 4: 300 K, 5: 6000 K, 6: 12000 K.

We used a power supply which can be varied between 8 kV to 15 kV potemtial. If the system is opened to the free air, the air molecules begin to move through the instrument, by getting constant velocity of 1 meter/secundum along the alternating electrodes.

In the experiments the instrument was in a columnal arrangement, open up and down: on the bottom of the tube liquid stirol was placed. The wapor of stirol - together with the air - streamed into the space of the instrument. The stirol molecules polimerized to resin particles, as a result of their going through the alternating potential of electrodes. The coagulated particles have a spherulitic form. Getting through 20 electrodes, the final mass of the coagulated particles was 540.000. times that of the initial molecular mass.

THE SOURCE OF LUNAR ATER MOLECULES

During full Moon the tail of the Earth (magnetic and radiation belts of the Earth) sweep over the Moon. Terrestrial magnetosphere tubes retain the escape of charged particles from this tube, because for the ionized particles the "wall" of terrestrial magnetosphere tail behaves as a reflecting wall. Together with ionized particles the water molecules, which have one negative electric charge (adhered to the water molecule) are also reflected on this tube wall. The reflecting force from the wall is: v X B (where v is velocity, B is magnetic induction) the electrostatic accelerating force is e X E (where e is the electron charge unit, E is electric field strength in V/m) the acceleration by E is F_E Electric Force per molecular mass.

Reaching the lunar surface the negatively charged water particle meets the positively charged (from UV radiation) dust particles. With charged dust particles water molecule forms a complex coagulated particle. At the same time, in the near vicinity of the lunar surface there exist a space charge of electron cloud, which recharge and so neutralize the coagulated particle. But this coagulated particle will not remain neutral for a long time, but it becomes charged again by the space charge of electron cloud. This periodic charging up and discharge 1) enlarges the coagulated particle, and 2) levitates the particle which will be the object of a transporting mechanism which moves it toward the lunar pole. The step by step drag by the solar radiation pressure toward the poles, where agglutinated particles become discharged, results in their fall-down, and accumulate on the surface.

DRAG OF PARTICLES TOWARD THE POLES

Let us follow the way of a coagulated particle. Start the observation at the 45 degrees latitude. Three main forces act on this particle: gravity, solar wind pressure and electrostatic force. The gravity force, determined by particle mass and G specific gravity, remains constant (a good approximation). The solar wind pressure force is determined by the effective cross section (surface given by the diameter of coagulated particle): solar wind force is also constant in absolute value, but its components projected to the gravitational force, changes according to the cosine function with latitude. The electrostatic force is determined by the field strength coming from the surface charge of the planetary body multiplied by the charge of the coagulated particle. This force is oscillating depending on the absorption of negative or positive ions. As a result of the combined action of the three forces the coagulated particle periodically sinks or rises to the surface. But because the components of the solar wind force gradually changes with latitude, **the tangential component of the solar wind pressure force** (changing with sinus function of the latitude) **will drift the particle toward the poles between two** (rising and sinking) **oscillations**. (Fig. 1.) When the particle approaches the polar region the local vertical component of this force becomes zero ($\cos 90° = 0$) while the tangential component becomes almost one ($\sin 90° = 1$). Therefore, if the coagulated particle reached the pole, it will remain in the vicinity of the pole (there is no force to move it out from this region).

CONSEQUENCES

On the surface of the dusty planetary body the size distribution of the dust particles in the vicinity of the equator will not exhibit a gaussian because the fine fraction of the dust slowly moves toward the poles.

In the vicinity of a new great impact crater the dust produced by sublimation from the plasma originally have a gaussian size distribution. After some time elapsed the size distribution will loose the fine fraction because of the drift toward the poles. We suggest that the age of the crater can be estimated on the extent of lacking fine fraction drifted.

The coagulated particles - together with the accompanying water component, - will accumulate in the vicinity of those craters (in the planetary polar regions) which are always in shadow.

SUMMARY

On the basis of Surveyor and Apollo observations and theoretical considerations we defined a lunar (and dusty planetary) quasiatmosphere. This quasiatmosphere mainly consists of charged dust particles. On the basis of our experimental experiences on coagulation in an electrostatic tube, we proposed a mechanism acting in the lunar quasiatmosphere. There the agglutination of electrostatically charged dust particles may produce larger and larger grains. These grains attract H_2O molecules on dusty planetary surfaces and continue in growing during time. The coagulated particles will be dragged by the solar radiation pressure toward the poles where they are discharged, fall down and accumulate on the surface. This electrostatic mechanism accumulates H_2O molecules on polar regions of dusty planetary surfaces in craters which are always in shadow.

REFERENCES

Allen, Morris, Lindstrom,et al. (1998): Martian Regolith Simulant JSC MARS-1. LPSC XXIX, #1690

Bérczi Sz., T. Földi, I. Kubovics, A. Simonits, A. Szabó (1998): LPSC XXIX. Houston, LPI, CD-ROM, #1082

Bródy I., Palócz K. (1953): Lecture on Techn. Univ. Budapest (personal communication),

Földi T., Ezer R. Bérczi Sz., Tóth Sz. (1999): Creating Quasi-Spherules from Molecular Material Using Electric Fields (Inverse EGD Effect). LPSC XXX. LPI, CD-ROM, #1266

Horányi M., Walch, B., Robertson, S. (1998): Electrostatic charging of lunar dust. LPSC XXIX. LPI, CD-ROM, #1527

Israel, H. (1957): *Atmospherische Elektricitet*. Leipzig.

Manfred von Ardenne (1958): *Tabellen für Angewanten Physik*, Leipzig

McKay, Carter, Boles, Allen,(1995): JSC-1. A New Lunar Regolith Simulant. LPSC XXIV, 963.

Reid, G. C. (1997): On the influence of electrostatic charging on coagulation of dust and ice particles in the upper mesosphere. *Geophysical Res. Letters*, **24,** No. 9. 1095.

Vanzani, V., Marzari, F., Dotto, E., (1997): LPSC XXVIII, 1481. Houston, LPI, CD-ROM, #1025

Exposure History of the Kobe (CK4) Meteorite: Constraints from Nuclear Track and Cosmogenic Nuclide Data. J. N. Goswami[1], N. Sinha[1], N. Nakamura[2] and K. Nishiizumi[3]; [1]Physical Research Laboratory, Ahmedabad 380 009, India; [2]Kobe University, Nada, Kobe 657-8501, Japan; [3]Space Science Laboratory, University of California, Berkeley, Ca-94720, USA.

Cosmogenic noble gases and radionuclide data suggested a two-stage exposure history of the Kobe (CK4) meteorite, involving a short duration recent exposure in space as a small object and a long duration prior exposure under relatively high shielding within a large object [1,2]. Studies of nuclear tracks produced by galactic cosmic ray Fe-group nuclei now allow us to further constrain the exposure history of this meteorite and construct plausible scenarios for its delivery from the parent asteroid to earth within the framework of dynamical evolution of meteorites in the main belt [3,4].

We have studied two samples of Kobe meteorite for nuclear track records. Both the samples (C-4b and C-3-2) came from a 13.6g piece of this meteorite (Kobe C). Aliquots of the sample C-3-2 were studied earlier for cosmogenic nuclide records [1]. We have separated olivine grains from these two samples and etched them to reveal nuclear tracks using standard procedure [5]. Because of the small size of the olivine grains and the very low track densities in them, we have exposed some of the olivine grains to fission fragments from a ^{252}Cf source and etched them to infer appropriate track etching parameters. Combined data for both the samples, that are located very close to each other within the fragment Kobe-C, yielded a track density of $(1.4\pm0.3)\times10^4$ cm^{-2}. The analyzed samples are at least a few mm away from the visible fusion crust in the Kobe C fragment and the observed tracks are also well developed and partial annealing of tracks leading to this low track density may be ruled out.

If we consider an exposure age of 38 Ma for the Kobe meteorite [1] and a simple single stage exposure history, the track data suggest a shielding depth of ~28-23 cm within meteoroids of radius ≥30 cm. However, cosmogenic nuclide data, particularly the low ^{60}Co and ^{26}Al activities and the high ^{10}Be-^{21}Ne model age rule out this possibility. We, therefore try to construct a plausible two-stage exposure history of this meteorite that is consistent with both the track and cosmogenic isotope data.

A constraint on the preatmospheric size of the Kobe meteoroid and the shielding depth of the analyzed sample during its recent exposure in space can be placed from the track data if we know this exposure duration. Based on the cosmogenic nuclide data, particularly the measured activity of ~18 dpm/kg for the relatively longer-lived isotope ^{10}Be (half-life=1.5Ma), we infer a range of recent space exposure durations of 3 to 5 Ma corresponding to pre-atmospheric radii of 20 to 10 cm. For this range of exposure ages, the track data suggest minimum shielding of 15 cm and a preatmospheric radius ≥15 cm. Thus, a preatmospheric radius of ~15-20 cm, a shielding depth of ~15 cm and an exposure of ~3 Ma appear to be a plausible configuration for the recent space exposure of the Kobe meteorite. While these parameters can explain the ^{10}Be and ^{36}Cl data and is marginally consistent with the low ^{60}Co activity, the expected ^{26}Al activity is at least 20-

30% higher than the measured value of ~38 dpm/kg. The ^{26}Al data as well as ^{36}Cl and the track data will be consistent if we assume a lower value of 1.5 Ma for the recent exposure age. Although the expected ^{10}Be activity will be much lower than the measured value of ~18 dpm/kg, this shortfall may be explained by considering the residual ^{10}Be activity from the first stage of cosmic ray exposure of Kobe as a part of a much larger object.

Since the recent space exposure of the Kobe meteoroid is sufficient to account for the observed low track density, its shielding depth during its earlier cosmic ray exposure duration of ~35 Ma was at least ~30 cm within an object of ~50 cm to a few meter in size. The expected track density from such an exposure will be less than the uncertainty in the measured track densities. The cosmogenic data for the Kobe samples do not provide definitive evidence for cosmic ray exposure on a much larger parent (asteroidal) body.

The nuclear track and cosmogenic nuclide data for the Kobe meteorite can be used to constrain its dynamic evolution history. The Kobe meteoroid was initially ejected as a meter-sized object from a deep-seated layer from its parent asteroid ~40 Ma back and acquired cosmogenic records while shielded by ≥30 cm for most of this duration. A collisional event ~1.5 Ma ago led to fragmentation of the original meteoroid and Kobe underwent a second stage of exposure to cosmic rays as a small object (radius ~15-20 cm) prior to its fall on the earth. Recent studies of dynamical evolution of meteorites in the main belt [3,4] demonstrated the importance of injection of asteroidal fragments into the main resonances in the asteroidal belt for delivering these objects into earth crossing orbits. Drift of these objects under the influence of chaotic diffusion as well as diffusion induced by thermal forces has been proposed for placing these objects in the resonances. The cosmogenic data for Kobe would suggest that such drift could persists for several tens of Ma for meter sized objects before they are placed in the resonance. These data, however, cannot ascertain whether collisional fragmentation of such objects, as in the case of Kobe, terminated the drift and injected one or more of the fragments into the resonance or the fragmentation event took place later during the orbital evolution of the objects that placed them in earth crossing orbits.

References: [1] Caffee, M. W. et al., *MAPS 35*, A37-38, 2000. [2] Takaoka, N. et al., *MAPS 35*, A154-155. [3] Morbidelli, A. and Gladman, B. *MAPS 33*, 999-1016, 1998. [4] Bottke, W. F. Jr, Rubincam, D. P. and Burns, J. A. *Icarus 145*, 301-331, 2000. [5] Krishnaswami S. et al., *Science 174*, 287-291, 1973.

Single grain N-Ar analyses of lunar regoliths: Estimation of micrometeoritic flux at the Moon surface.

Ko HASHIZUME[1,2], Bernard MARTY[2,3] and Rainer WIELER[4]

1: Department of Earth & Space Sciences, Osaka University, Toyonaka, Osaka 560-0043, Japan
2: CRPG-CNRS, BP 20, 54501 Vandoeuvre-lès-Nancy Cedex, France
3: Ecole Nationale Supérieure de Géologie, 54501 Vandoeuvre-lès-Nancy Cedex, France
4: Institut for Isotope Geochemistry, ETH Zürich, Sonneggstrasse 5, CH-8092 Zürich, Switzerland
Corresponding email address: kohash@ess.sci.osaka-u.ac.jp

Surface of the Moon is irradiated or bombarded by various kinds of ions and objects, such as solar wind (SW), cosmic rays, and planetary materials like micrometeorites, comets or meteors. Absence of igneous activity at the recent Moon provides us a precious opportunity to obtain present and past information on, *e.g.*, chemical/isotopic composition of the Sun, production rate of cosmogenic nuclides, or flux and nature of planetary materials arriving onto the Moon, which are all necessary to understand the present situation and the history of formation of the solar system. Supply of these ions and objects onto the surface of the Moon is evidenced markedly by the highly volatile elements such as the rare gases, N, C, and H, those which are strongly depleted in igneous lunar rocks.

Among these elements, we are particularly interested in nitrogen, whose isotopic ratio $^{15}N/^{14}N$ is observed to be largely variable among lunar regolith samples, and the cause of such variation had not been understood over the past three decades. Analyses of the nitrogen isotopic composition in lunar soils reveal at least two isotopically distinct trapped components (besides the in-situ component produced by cosmic rays) with $\delta^{15}N$ (= $\{[(^{15}N/^{14}N)_{sample}/(^{15}N/^{14}N)_{terrestrial\ air}] - 1\} \times 1000$) values varying widely between –200 and +100 ‰. Though the proportion of these components differs largely among different samples, it is commonly observed that these components coexist in the same soils, extracted at slightly different temperature by stepwise heating. The cause of the variation is a matter of debate. Some argue that the N isotopic composition of the solar wind changed during the last 3×10^9 years (*e.g.*, Kerridge et al., 1993), while others claim that a significant fraction of the nitrogen in the lunar regolith is of non-solar origin (e.g., Wieler et al., 1999). The latter view is also based on the fact that N in lunar soils is ~10 times more abundant than one may expect from the concentrations of solar wind rare gases.

To decipher the complex lunar nitrogen archive, we have performed a series of microscopic N isotopic analyses at CRPG-Nancy aiming to precisely characterise the possible end-members contained in the lunar regoliths. Hashizume et al. (2000), using an ion microprobe, identified the N isotopic composition of the SW from the surface 100 nanometer layers of lunar regolith grains. The SW-N, associated with D-free H, a strong proof for its solar origin, showed a $\delta^{15}N$ value as low as –240 ‰, whereas non-solar N correlated with D-rich H possessed positive $\delta^{15}N$ values, as high as +50 ‰. Here in this study, we performed single mineral grain N-Ar isotope analyses to further tackle this problem. We analysed single grains, mostly of ~200 μm sized ilmenite, from Apollo 17 samples 71501, 79035 and 79135.

Experimental: In Nancy, a mass spectrometry system to analyse the isotopic composition of extremely small quantities of nitrogen has been developed, whose full detail is published elsewhere (Hashizume and Marty, 2001; Wieler et al., 1999). We analyse the N and Ar (^{38}Ar & ^{36}Ar) isotopic composition of the gas extracted from a single 200 μm sized ilmenite grain. The gas is extracted from single grains with a CO_2 laser in CW mode to minimize the blank gas. Stepwise analyses are performed by controlling the power of the laser. Though the temperature control is not accurate (presumably around 100 °C), we can constantly control the release of gas components: >90 % of the trapped gas is released at low temperature (600-1000 °C), while >90 % of the cosmogenic gas is released during the final fusion step.

1. Cosmogenic Nitrogen

In our analyses, the $\delta^{15}N$ values varied in a range of –200 ‰ to +2700 ‰. The highest values are observed mostly in fusion steps, and are due to contributions of cosmogenic nitrogen ($^{15}N/^{14}N \sim 1$). A good linear correlation between the amounts of cosmogenic ^{15}N and ^{38}Ar was obtained (Fig. 1) from which we were able to calculate the production rate ratio of these two nuclides. We obtained a value of $^{15}N_c/^{38}Ar_c = 14.4 \pm 1.0$ atoms/atoms for ilmenite grains. We are therefore, able to derive a $^{15}N_c$ production rate in bulk lunar rock of 10.4 ± 0.7 pg-^{15}N/g-rock/Ma, when the following values are known: (i) $^{38}Ar_c$ production rate in lunar ilmenites calibrated by the ^{81}Kr-Kr age (Eberhardt et al., 1974), although for lunar rocks different from our sample; (ii) concentration of oxygen, the target element for $15N_c$ production, in bulk lunar rocks and ilmenites.

The obtained production rate is significantly higher than literature values of 3.6 (Becker et al., 1976), or 5.8 (Mathew and Marti, 2001). Such a discrepancy might be caused by differences in mean burial depths between the samples studied here and the rocks previously studied, combined with the significant difference in dependence of production rates of $^{15}N_c$ and $^{38}Ar_c$ on the burial depth.

2. Trapped Nitrogen – *the trapping mechanism*

In the low temperature steps (600 - 1000°C), where the contribution of cosmogenic N is much smaller than in the fusion step, N with $\delta^{15}N$ ranging from -200 to +100 ‰ and large amounts of trapped solar Ar were released. In Fig. 2, the $\delta^{15}N$ values of the trapped components are plotted against the $^{36}Ar/N$ ratios normalized to the solar abundance ratio. The general picture is consistent with previous works. All grains show $^{36}Ar/N$ ratios much lower (0.01 - 0.45x) than the solar ratio. The mean $N/^{36}Ar$ and $\delta^{15}N$ values ($N/^{36}Ar$ = 391, $\delta^{15}N$ = 0 ‰ for 71501; $N/^{36}Ar$ = 473, $\delta^{15}N$ = -60 ‰ for 79035) for the ~200 μm sized grains obtained by this study is not largely different from literature values for corresponding samples ($N/^{36}Ar$ = 299, $\delta^{15}N$ = +18 ‰ for 71501 ilmenites [Frick et al., 1988]; $N/^{36}Ar$ = 705, $\delta^{15}N$ = -78 ‰ for 79035 ilmenites [Becker and Pepin, 1989]).

Single grains, which all experienced widely different exposure history, exhibit wide spread in the $^{36}Ar/N$ ratios and the $\delta^{15}N$ values, which must reflect mixture of multiple N-Ar components in various proportions. Those enriched in the solar component should show higher $^{36}Ar/N$ ratio and lower $\delta^{15}N$ value, as low as –240 ‰ (Hashizume et al., 2000), while those enriched in planetary components should generally be depleted in ^{36}Ar relative to N (*e.g.*, $(^{36}Ar/N)_{chondrite} < 10^{-5} \times (^{36}Ar/N)_{solar}$) and the $\delta^{15}N$ higher than solar (*e.g.*, $-100 < \delta^{15}N_{chondrite} < +1000$ ‰). Among the three regolith samples involved in this study, the 79035 ilmenite grains show the simplest and clearest trend in this diagram: A negative correlation (r = 0.93) between the $\delta^{15}N$ values and the $^{36}Ar/N$ ratio can be explained by a binary mixing of two end-members, one of which with a $\delta^{15}N$ value as low as –240 ‰, the upper limit for the solar value. An important point to be noted here is that the $^{36}Ar/N$ ratio of the solar component trapped in the lunar sample seems to be significantly lower (~0.2 x) than the solar abundance ratio. Since SW is considered to possess almost the same $^{36}Ar/N$ ratio (0.7 - 0.8 x) with the solar abundance ratio (Geiss et al., 1994), the only possible cause for the solar N enrichment in lunar samples is the preferential loss of solar rare gases from the lunar samples. However, Wieler et al. (1996) conclude, based on the single grain rare gas analysis of lunar samples where they found the relative abundances of Ar, Kr and Xe to be constant irrespective to their absolute concentration, that such loss is unlikely to have occurred by diffusion-like processes. We propose a three-stage SW trapping mechanism as follows to satisfactorily explain the observed N-rare gas abundance patterns in lunar grains.

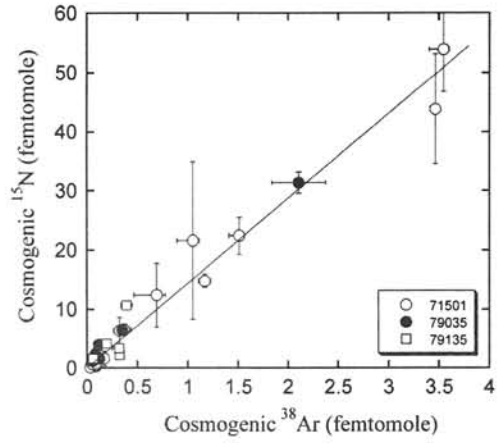

Fig. 1 Amounts of cosmogenic ^{15}N plotted against those of cosmogenic ^{38}Ar in Apollo 17 ilmenite grains. Each data represents fusion or 1000°C step of single grains. All fractions that show $\delta^{15}N$ values higher than +100 ‰ are selected for this plot. The $\delta^{15}N$ values for the trapped components are assumed to be –20 ± 75 ‰ for 71501 and –175 ± 75 ‰ for 79035/79135, which are the ones assumed by Becker and Pepin (1989). The assumed trapped $^{38}Ar/^{36}Ar$ ratios are $0.188\ ^{+0.010}/_{-0.004}$ for 71501 and $0.190\ ^{+0.016}/_{-0.007}$ for 79035/79135. The mean values are calculated from the results of stepwise etching analyses by Benkert et al. (1993). Error bars represent 1σ errors. Uncertainties assumed for the isotopic ratios of the trapped components are included in the error bars. Correlation factor for the best fit line is 0.97.

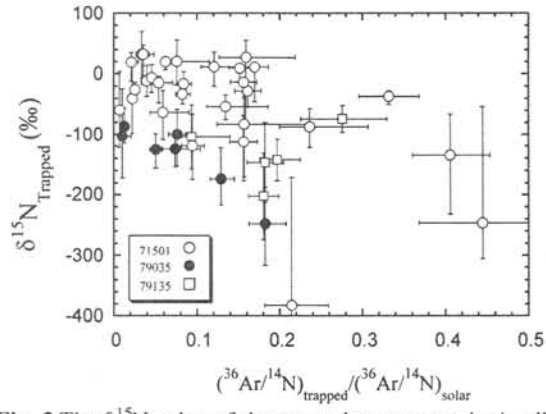

Fig. 2 The $\delta^{15}N$ value of the trapped component in Apollo 17 single ilmenite grains plotted against the $^{36}Ar/N$ ratio normalized by the solar abundance ratio (0.0272). Each data represent averaged values taken from the ≤1000°C temperature steps of respective grains. Contribution of the cosmogenic ^{15}N is subtracted from the measured $\delta^{15}N$ values using the measured $^{38}Ar/^{36}Ar$ ratios and the production rate ratio of $^{15}N_c/^{38}Ar_c$ obtained in this study.

I. The SW with substantially high energy (1KeV/nucleon) is implanted onto the surface of the lunar

regoliths. The trapping probability of ions with an energy of several KeV or higher is considered to be unity (*e.g.*, Manka and Michel, 1971). Therefore, no fractionation of solar rare gases to nitrogen will occur at this stage. **II.** As the surface of the mineral becomes saturated with the implanted SW, the implanted solar gases will be sputtered out from the mineral by high energy ions (SW, SEP or cosmic rays) continuously hitting the mineral surface. Such a process is known to be an all-or-nothing process, therefore, implanted ions are sputtered out from the sample without fractionation. **III.** The sputtered out solar gases, forming a dilute atmosphere at the lunar surface, are ionized by the high energy ions and re-implanted into the lunar regolith grains by a process so called Manka-Michel process (Manka and Michel, 1971). At this stage, the energy of the ions to be re-implanted should be substantially low compared to the original SW, where the implantation probability must be lower than unity. At such low energy range, implantation probability must be largely affected by the chemical nature of the elements to be implanted. Nitrogen behaves as a chemically active element at a reducing condition like the proton-rich surface layer of the lunar regolith.

3. Solar and Meteoritic N Association on the Moon – *Estimation of the micrometeoritic flux.*

We consider that the nature of the non-solar N trapped in the lunar regolith is the N contained in meteoritic solid material falling onto the Moon, most likely the micrometeoritic material like those on Earth which dominates the contemporary flux of extraterrestrial material on Earth. (See review by Engrand and Maurette, 1998.) The microimpactors at the Moon surface are melted or vaporized at the time of their impact, when the contained N is released into the lunar atmosphere. The meteoritic N will then be re-implanted, together with the sputtered-out SW component, by the process III we described above.

The trapping mechanism of the non-solar (micrometeoritic) N we propose here explains the general characteristics of the non-solar N trapped in the lunar regoliths, summarized by Kerridge (1993): (i) the non-solar N is extracted by stepwise heating at similar temperature with the solar N, suggesting that the non-solar and solar N are trapped at similar site and/or form in the minerals; (ii) abundance of bulk N in lunar regolith is roughly proportional to those of the solar heavy rare gases, even when the N is dominated by the non-solar component (*i.e.*, when the bulk $\delta^{15}N$ value is much higher than the solar value), because the implantation of the meteoritic component into the lunar mineral is driven by the SW.

Although the full detail of the N isotopes in micrometeorites on the Earth is yet unknown, study of those in interplanetary dust particles (IDPs) sampled in the stratosphere suggest that they contain N as abundant as the CI chondrites (~1000 ppm) (Keller et al., 1996), and are enriched in ^{15}N relative to solar ($-90 < \delta^{15}N_{IDP} < +480$ ‰; Messenger, 2000). The bulk $\delta^{15}N$ values for the trapped lunar N, by our hypothesis, represent the mixing proportion of the solar and the micrometeoritic N flux accreting onto the Moon. The bulk $\delta^{15}N$ value for various lunar samples covers roughly the entire range between the solar and IDP range ($-200 < \delta^{15}N_{lunar} < +100$ ‰; reviewed by Kerridge, 1993), suggesting that the solar and micrometeoritic N supply rates on the Moon are comparable. The estimated SW ^4He flux (7.2×10^6 atoms/cm^2/sec; Manka and Michel, 1971) and the solar abundance ratios gives a SW N flux of 1.6×10^4 atoms/cm^2/sec, and a comparable rate for the micrometeoritic N flux. If IDP-like materials with 1000 ppm N have accreted on the Earth with the same rate, the accretion rate is calculated to be 67000 tons-material/year. Our estimated rate shows remarkable agreement with the estimated flux of 40000 ± 20000 tons/year by direct measurements of IDPs in near-Earth interplanetary space (Love and Brownlee, 1993).

Becker R. H., Clayton R. N. & Mayeda T. K. (1976) *Proc 7th Lunar Sci. Conf.*, 441-458.
Becker R. H. & Pepin R. O. (1989) *Geochim. Cosmochim. Acta* **53**, 1135-1146.
Benkert J-P., Baur H., Signer P. & Wieler R. (1993) *J. Geophys. Res.* **98**, 13147-13162.
Engrand C. & Maurette M. (1998) *Meteorit. Planet. Sci.* **33**, 565-580.
Frick U., Becker R. H. & Pepin R. O. (1988) *Proc. 18th Lunar Planet. Sci. Conf.*, 87-120.
Geiss J., Gloeckler G. & von Steiger R. (1994) *Phil. Trans. R. Soc. Lond. A* **349**, 213-226.
Hashizume K., Chaussidon M., Marty B. & Robert F. (2000) *Science* **290**, 1142-1145.
Hashizume K. & Marty B. (2001) In *Handbook of stable isotope analytical techniques, Elsevier, In Press.*
Keller L. P., Messenger S., Miller M. & Thomas K. L. (1996) *Lunar Planet. Sci. Conf.* XXVIII, 1811-1812 (Abstract).
Love S. G. & Brownlee D. E. (1993) *Science* **262**, 550-553.
Kerridge J.F. (1993) *Rev. Geophys.* **31**, 423-437.
Manka R. H. & Michel F. C. (1971) Proc. 2nd Lunar Sci. Conf. **2**, 1717-1728.
Mathew K. J. & Marti K. (2001) *Earth Planet. Sci. Lett.* **184**, 659-669.
Messenger S. (2000) *Nature* **404**, 968-971.
Wieler R., Humbert F. & Marty B. (1999) *Earth Planet. Sci. Lett.* **167**, 47-60.
Wieler R., Kehm K., Meshik A. P. & Hohenberg C. M. (1996) *Nature* **384**, 46-49.

The Tagish Lake Meteorite: First Sample from the D Asteroids

Takahiro Hiroi[1*], Michael E. Zolensky[2], Carle M. Pieters[1]

[1] *Deptartment of Geological Sciences, Brown University, Providence, RI 02912, USA*
[2] *Earth Science and Solar System Exploration Division, NASA Johnson Space Center, Houston, TX 77058, USA.*

Virtually all meteorites are believed to come from asteroids, excluding known lunar and martian meteorites, and the parent asteroid of each meteorite class can be determined through reflectance spectroscopy. However, there are several spectral types of asteroids [1] whose meteorite counterparts have not been found. Among them are the P and D asteroids which are by some believed to be made of "supercarbonaceous" chondrites [2]. Here we report the identification of the first meteorite that most likely came from a D-type asteroid: the Tagish Lake meteorite, a new ungrouped C2 chondrite [3].

Tagish Lake is a very carbon rich (4-5 wt.%), aqueously altered carbonaceous chondrite, containing an exceptionally high concentration of presolar grains and Ca-Fe-Mg carbonates, but an unusually low amount of high-temperature nebular materials such as chondrules and calcium-aluminum rich inclusions (CAI) [3]. These characteristics match with expectations to the P and D asteroids or comets [2]. A chip sample of Tagish Lake carbonaceous chondrite was ground and dry-sieved into powder of <125 μm in grain size. UV-Visible-NIR and FT-IR spectra of the sample were measured, and they did not show any significant evidence of terrestrial weathering such as abosorption bands due to iron hydroxides.

The spectrum of Tagish Lake meteorite is compared with average reflectance spectra of the G, B, C, F, T, P, and D asteroids taken from the eight-color and the 52-color asteroid surveys [4] scaled by their albedo measurements [5] in Fig. 1. Because the reflectivity of Tagish Lake is very low (2-4 %), comparison of its reflectance spectrum was made only with dark asteroid spectra. The spectrum of Tagish Lake has a characteristic red slope which is typical of carbon-containing powdered materials. The fact that the C, G, B, and F asteroids have brighter and flatter reflectance spectra than Tagish Lake suggests that Tagish Lake has a greater carbon content, which is consistent with results of its mineralogical studies [2]. In terms of the overall spectral slope seen in Fig. 1, the T, P, or D asteroids are the best spectral match with Tagish Lake. In fact, comparison of the reflectance spectra of Tagish Lake with all the available reflectance spectra of the C, G, B, and F asteroids did not reveal any acceptable match. Many of the C, G, B, and F asteroids are believed to be thermally metamorphosed CI/CM/CR chondrites [6], which is completely inconsistent with the mineralogy of Tagish Lake. To save time and space in this paper, only the comparison with the T, P, and D asteroids are shown.

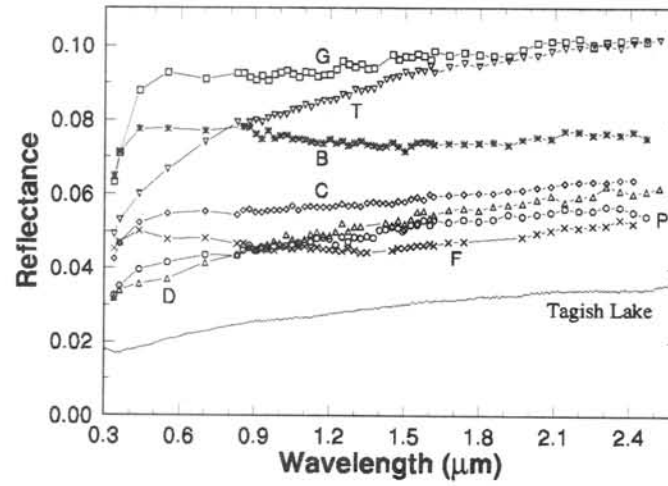

Fig. 1. Comparison of reflectance spectrum of a Tagish Lake meteorite sample and averages telescopic spectra of low-albedo asteroid classes.

In Fig. 2, the scaled reflectance spectrum of Tagish Lake is compared with each one of asteroid spectra used for calculating the average T, P, and D asteroid spectra in Fig. 1 in search of the best asteroid candidate. As seen in Fig. 2A, while the T asteroids have good spectral matches with Tagish Lake up to 1.5 μm, they show systematically flatter spectra than Tagish Lake in the longer wavelengths. In addition, the T asteroids also show a much higher albedo than the visible reflectivity of the Tagish Lake sample. The T asteroids are believed to be made of materials similar to troilite-rich iron meteorites [7], which is incompatible with the observed mineralogy of Tagish Lake. Next, as seen in Fig. 2B, while most of the P asteroids show good spectral matches with Tagish Lake in the wavelength range longward of 0.9 μm, they are significantly different in the shorter wavelength range. On the other hand, all the D asteroids in Fig. 2C have good spectral matches with Tagish Lake throughout the entire measured range. Among these D asteroids, the asteroid 368 Haidea is the best spectral match with Tagish Lake.

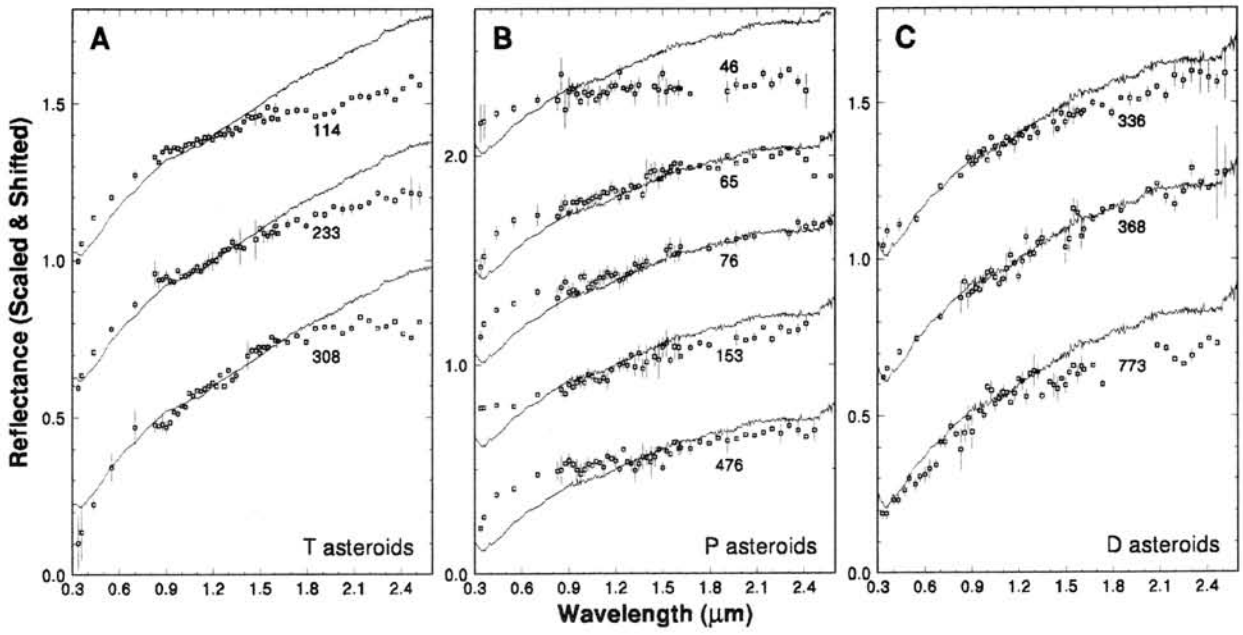

Fig. 2. Comparison of reflectance spectra (0.3-2.6 μm) of Tagish Lake with reflectance spectra of the T, P, and D asteroids [4,5] used for calculating the average spectra in Fig. 1. Reflectance spectra of the asteroids (open squares) are scaled to 1.0 at 1.2 μm and offset from one another for clarity, and Tagish Lake spectrum (solid line) is plot in the same way for comparison.

As seen in Fig. 1, the average albedo of the D asteroids is also the closest to the visible reflectance of the Tagish Lake powder sample prepared in this study.

We should also pay attention to the 3-μm water band features of Tagish Lake and the D asteroids. Shown in Fig. 3 are available telescopic 3-μm spectra [8] of four D asteroids. Because the asteroid spectra in Fig. 3 (a) are too noisy to compare individually with Tagish Lake, they are averaged together with band wavelengths binned at the same time in Fig. 3 (b). Even though this comparison is a very rough one in that all four asteroids are averaged from their very noisy spectral measurements, there seems to be a trend that the asteroid spectra show little water abosorption band while Tagish Lake meteorite shows a shallow but sharp band. Considering the excellent match between Tagish Lake and the D asteroids in the wavelength range of 0.3-2.6 μm which makes Tagish Lake meteorite only one candidate for the D asteroids, we are inclined to suggest a possible space weathering effect that could dehydrate the surfaces of the D asteroids, causing shallower 3-μm water absorption band.

Assuming Tagish Lake came from a D asteroid, which one is likely to be its parent body? Although 368 Haidea has the most similar reflectance spectrum to Tagish Lake, the asteroid

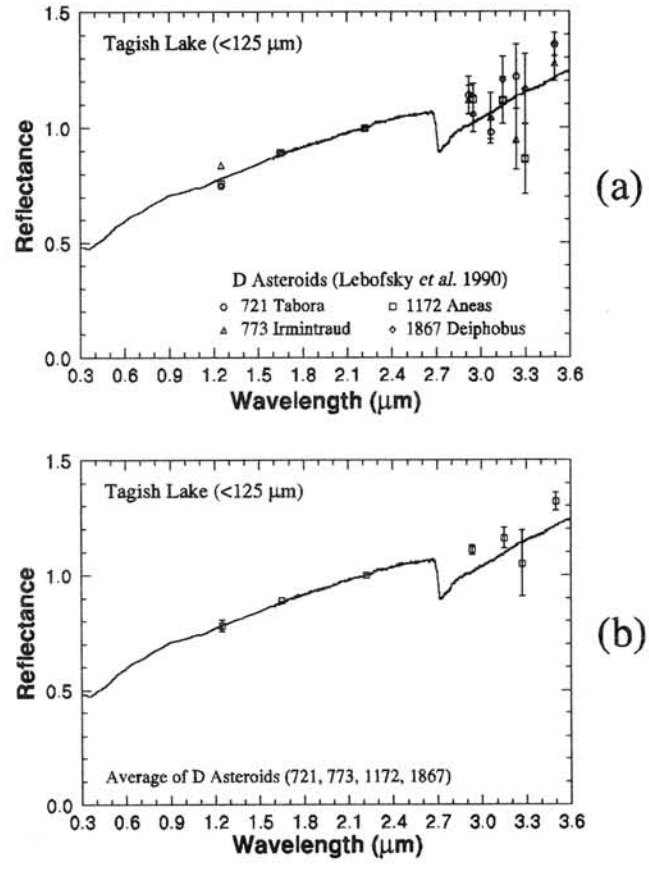

Fig. 3. Comparison of 3-μm reflectance spectra of the D asteroids [8] with reflectance spectrum of Tagish Lake meteorite. (a) Individual observations. (b) Wavelength binned and all spectra averaged.

is located at as much as 0.114 AU outside the 7:3 gap and as much as 0.206 AU inside the 2:1 gap as listed in Table 1. On the other hand, 732 Tjilaki, 415 Palatia, 773 Irmintraud, 1702 Kalahari, and 3501 Olegiya are located only 0.034~0.043 AU away from a resonance gap. Considering the highly accepted idea that the HED meteorites came from Vesta which is about 0.2 AU inside the 3:1 resonance, these D asteroids could supply their fragments to the Earth as meteorites. The mechanism can be the same as that of HEDs delivered from Vesta such as impact ejection followed by transport by the Yarkovsky effect [9] which works the more strongly, the smaller the asteroid is.

However, the huge crater on Vesta [10] and the existence of Vestoids [11], which strengthened the connection between Vesta and HED meteorites are not known for any of the D asteroids. Also, the low density (1.7 g/cc) [12] and mechanical weakness of the Tagish Lake meteorite parent body may cause any kinetic energy of its impactors to have been absorbed more efficiently than in Vesta's case, resulting in a smaller kinetic energy of ejecta. Therefore, delivering a meteorite from 368 Haidea may be more difficult than from 4 Vesta. More spectral measuremnts of the D asteroids including the 3-μm wavelength range would be necessary to specify the parent body of Tagish Lake meteorite.

Table 1. Albedos, diameters, and orbtal elements of the D (or DP) asteroids near the gaps due to mean motion resonances with Jupiter.

Albedo	D/km	a	e	sin(i)	No.	Class	Name
0.042	72.0	2.252	0.091	0.110	336	D	Lacadiera
0.058	39.0	2.457	0.068	0.192	732	D	Tjilaki
		2.500					**Gap 3:1**
0.050	33.1	2.716	0.096	0.253	1471	D	Tornio
0.049	80.1	2.788	0.277	0.144	415	DP	Palatia
		2.824					**Gap 5:2**
0.033	99.1	2.858	0.047	0.301	773	D	Irmintraud
0.050	36.8	2.858	0.102	0.157	1702	D	Kalahari
	32.0	2.922			3501	D	Olegiya
		2.956					**Gap 7:3**
0.032	74.5	3.070	0.170	0.163	368	D	Haidea
		3.181	0.218	0.252	2375	D	1975 AA
		3.276					**Gap 2:1**
0.029	53.6	3.384	0.184	0.233	2266	D	Tchaikovsky
0.039	69.0	3.413	0.073	0.114	1167	D	Dubiago
0.036	45.2	3.499	0.040	0.072	2208	D	Pushkin
0.050	82.6	3.551	0.083	0.135	721	D	Tabora
0.029	61.0	3.636	0.023	0.097	2311	D	El Leoncito
0.039	78.0	3.904	0.024	0.090	1256	D	Normannia

Acknowledgment: We thank Jim Brook, Peter Brown, and Alan Hildebrand for recovering Tagish Lake meteorite. Reflectance spectra of the meteorite samples were measured at RELAB, a multiuser facility supported by NASA grant NAGW5-3871.

References: [1] D. J. Tholen (1984) Ph.D. thesis, Univ. Arizona. [2] F. Vilas and B. A. Smith (1985) *Icarus* **64**, 503; J. F. Bell *et al.* (1989) in *Asteroids II*, R. P. Binzel *et al.*, Eds. (Univ. Arizona Press), pp. 921. [3] P. G. Brown *et al.* (2000) *Science* **290**, 320. [4] B. Zellner *et al.* (1985) *Icarus* **61**, 335; J. F. Bell *et al.* (1989) *Lunar Planet. Sci.* **19**, 57. [5] E. F. Tedesco (1989) in *Asteroids II*, R. P. Binzel *et al.*, Eds. (Univ. Arizona Press), pp. 1090. [6] T. Hiroi *et al.* (1993) *Science* **261**, 1016; T. Hiroi *et al.* (1996) Meteoritics & *Planet. Sci.* **31**, 321. [7] M. J. Gaffey *et al.* (1993) *Meteoritics* **28**, 161. [8] Lebofsky *et al.* (1990) *Icarus* **83**, 16-26. [9] E. J. Öpik (1951) *Proc. R. Irish Acad.* **54**, 165. [10] P. C. Thomas *et al.* (1997), *Science* **277**, 1492. [11] R. P. Binzel and S. Xu (1993) *Science* **260**, 186. [12] M. Gounelle *et al.* (2001) *Lunar Planet. Sci.* **32** [CD-ROM].

AN ION MICROPROBE STUDY OF OXYGEN ISOTOPES IN ANTARCTIC MICROMETEORITES.

[1)]Hajime Hiyagon, [1)]Sadahiro Mizutani, [2)]Takaaki Noguchi, [3)]Tomoki Nakamura and [3)]Toru Yada.

1) Department of Earth and Planetary Science, University of Tokyo, Bunkyo-ku, Tokyo 113-0033, Japan.

2) Department of Materials and Biological Science, Ibaraki University, Bunkyo 2-1-1, Mito 310-8512, Japan.

3) Department of Earth and Planetary Sciences, Kyushu University, Hakozaki Fukuoka 812-8581, Japan.

1. Introduction

Micrometeorites may represent a population of the extraterrestrial material which may be different from those represented by conventional meteorite collections [1]. Some of them are only partially melted upon entry to the Earth's atmosphere, and hence, may retain their original extra-terrestrial signatures. Oxygen isotopes are different among different meteorite groups and are widely used to classify meteorites [2,3]. Hence, in order to understand the origin of micrometeorites, it is important to analyze their oxygen isotopic compositions and to compare them with those of known meteorite groups. In the last NIPR Symposium we reported our preliminary ion microprobe data on Antarctic Micrometeorites (AMMs) collected at the Dome Fuji station [4]. In the present study, we further performed ion microprobe analyses of oxygen isotopes on AMMs using better experimental configurations.

2. Samples and experimental procedures

The AMMs used in the present study were recovered from the Minami-Yamato Ice Field in Antarctica in 1998 by the 39th Japan Antarctic Research Expedition (JARE) [5]. Each AMM was examined with SEM-EDS and only the grains showing chondritic compositions (i.e., showing strong Mg, Fe and Si peaks) were selected for the ion microprobe study. Each AMM was fixed using resin on the top of a cylindrical sample holder (6mm in dia. x 8mm in length), polished, carbon coated and re-examined with SEM-EDS. Maximum of six sample holders were put together in a conventional sample holder for the CAMECA ims-6f ion microprobe. The surfaces of the samples were carefully adjusted to the same level. This made us possible to analyze both samples and standard (San Carlos olivine) in the same geometrical conditions, which would minimize the instrumental mass fractionation. The analytical procedure of the ion microprobe at the University of Tokyo was essentially the same as described in [5]. Typical error was $\pm$ 3.2-3.4‰ (2σ) both for $\delta^{17}O$ and $\delta^{18}O$.

Oxygen isotopes were analyzed for 9 AMMs (TN5, TN14, TN21, TN23, IB14,

IB31, IB35, IB38N and IB39). For comparison, one deep sea spherule (DDS) recovered from deep sea sediment near Hawaii by one of the authors (SM) was also analyzed.

IB31 (~80x90 μm) is a coarse-grained crystalline AMM consisting only of olivine ($Fa_{28.5}$). TN23 (~50x100 μm) is also a coarse-grained crystalline AMM consisting mostly of olivine grains (Fa_{17}) with small sulfide grains. Three analyses were performed for olivine in these AMMs. IB39 (~70x90 μm) consists of matrix-like material with a large olivine grain (~20x40 μm; $Fa_{21.6}$) and some pyroxene grains (cpx; Fs_4Wo_{39}), and all three phases were analyzed. IB35 (~50x50 μm) shows chondrule-like texture on one side and matrix-like texture on the other. Analyses were performed for both of the two portions. TN5 (~40x50 μm), TN14 (~50x50 μm), TN21(~50x50 μm), IB14 (~40x80 μm) and IB38 (~50x90 μm) consist mostly of matrix-like material with small crystal (e.g., olivine) and sulfide grains. Among them TN5 and TN21 are highly porous. Analyses were performed for matrix-like portions of these 5 AMMs.

3. Results

The results for the crystals (olivine and pyroxene) and matrix-like phases are summarized in Figs. 1 and 2, respectively, including our previous results [4]. All the crystal data are plotted in the region between the TF (terrestrial fractionation) line and CCAM (carbonaceous chondrite anhydrous minerals) line and none of the data are plotted above the TF line. This suggests that AMMs are more closely related to the carbonaceous chondrite groups (i.e., all but CI are plotted below the TF line [6]) rather than ordinary chondrite groups. The present results as a whole are very consistent with the recent results by Engrand et al. [7], but tend to show more variations; some points are closer to the TF line and some points show lower $\delta^{18}O$ values.

Matrix-like phases are plotted more or less along the TF line with relatively large variations (Fig.2). The reason for this is not clear at present. However, the surfaces of these phases are rather rough, so that there may be larger instrumental mass fractionation effect. Furthermore, it was not possible to avoid the effect of resin contained in the pore spaces, which must have oxygen isotopic composition somewhere on the TF line. Hence, the present results for matrix-like phases must be considered rather preliminary.

The DDS datum is consistent with the DDS type S data reported by [8], indicating reliability of the present analyses.

References: [1] Engrand C. and Maurette M. (1998) *Meteoritics Planet. Sci.* **33**, 565-580. [2] Clayton R. N., Onuma N. and Mayeda T. K. (1976) *Earth Planet. Sci. Lett.* **30**, 10-18. [3] Clayton R. N. (1993) *Ann. Rev. Earth Planet. Sci.* **21**, 115-149. [4] Hiyagon H., Mizutani S., Noguchi T, Nakamura T. and Yada T. (2000) *Antarctic Meteorites* **XXV** (abstr.), 22-24. [5] Yada T. and Kojima H. (2000) *Antarctic Meteorite Res.* **13**, 9-18. [5] Hiyagon H. and Hashimoto A., *Science* **283**, 828-831, 1999. [6] Clayton R. N., and Mayeda T. K., *Geochim. Cosmochim. Acta* **63**, 2089-2104, 1999. [7] Engrand C., McKeegan K. D. and Leshin L. A., *Geochim. Cosmochim. Acta* **63**, 2623-2636, 1999. [8] Clayton R. N., Mayeda T. K. and Brownlee D. E. (1986) *Earth Planet. Sci. Lett.* **79**, 235-240.

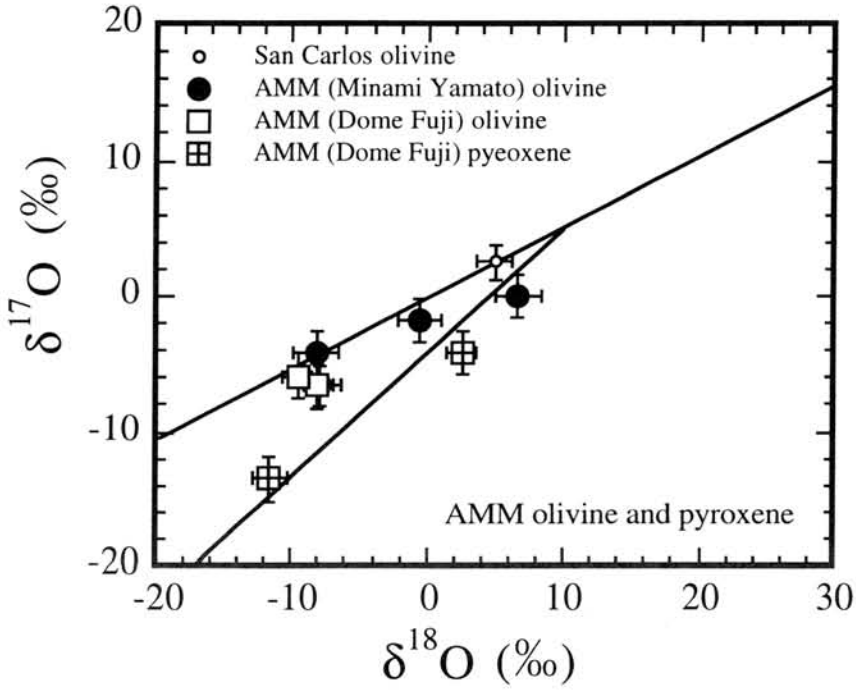

Fig. 1 Oxygen isotopic compositions of olivine and pyroxene grains in AMMs.

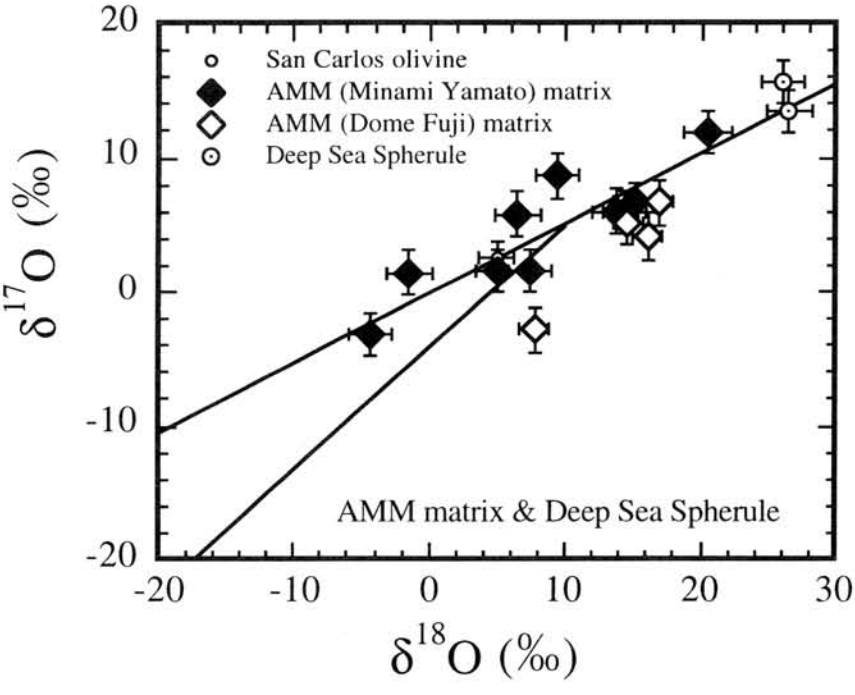

Fig. 2 Oxygen isotopic compositions of matrix-like portions of AMMs and a Deep Sea Spherule.

AN ION MICROPROBE STUDY OF OXYGEN ISOTOPES IN THE KOBE CK4 METEORITE.

1)Hajime Hiyagon, 2)Tomoki Nakamura and 3)Noboru Nakamura

1) Department of Earth and Planetary Science, University of Tokyo, Bunkyo-ku, Tokyo 113-0033, Japan;

2) Department of Earth and Planetary Sciences, Kyushu University, Hakozaki Fukuoka 812-8581, Japan;

3) Faculty of Science & Graduate School, Kobe University, Nada, Kobe 657-8501, Japan.

1. Introduction

The Kobe meteorite, fell on September 26, 1999 in northern part of Kobe City, Japan, was classified as CK4 based on its petrology, major and minor element chemistry and oxygen isotopic composition [1-5]. Since oxygen isotope study on CK chondrites is rather limited, we conducted ion microprobe analyses of oxygen isotopes for magnetite and some silicate phases of the Kobe meteorite. This work was done as a part of the consortium study of the Kobe meteorite [2].

2. Samples and analytical conditions

Two polished thin sections, P5-1 and P5-2, were prepared from the sliced specimen (~10mm x 7.8mm x 1mm), labeled P5, and one of the thin sections, P5-1, was used for the present ion microprobe study.

Chondrules (0.2-2.5mm) are well- to moderately-defined. Eight analyses were performed for olivine in 7 porphyritic olivine chondrules. Numerous opaque mineral grains exist within olivine grains and grain boundaries. They consist mostly of magnetite and pentlandite with minor amount of apatite or chlorapatite. Ilmenite and spinel exolusion lamellae are found in large magnetite grains [1,4]. Seven analyses were performed for 6 magnetite grains. Low Ca-pyroxene grains are often found within but near the margin of the opaque mineral assembly. One analysis was performed for one of the low-Ca pyroxene grains. A plagioclase-rich grain (~400μm in size) and other two plagioclase-rich portions in the thin section were also analyzed.

In situ analyses of oxygen isotopes were performed using a CAMECA ims-6f ion microprobe in the University of Tokyo. A Cs^+ primary beam with an impact energy of 19.5kV was used for the analyses. The beam size was ~20μm in diameter with an intensity of 0.7-1.0nA. An electron flood gun was used for charge compensation. Other analytical conditions were essentially the same as those described in [6]. Mexico magnetite ($\delta^{17}O$ = -1.40‰ and $\delta^{18}O$= -2.59‰ [7]) and San Carlos olivine ($\delta^{17}O$ = +2.54‰ and $\delta^{18}O$ = +4.92‰ [7]) were used as oxygen isotope standards for magnetite and silicate phases, respectively, and were analyzed repeatedly before and after the sample runs. The reproducibility of the analyses was ±0.8-1.0‰ (1σ) for $\delta^{17}O$ and ±0.9-1.2‰ (1σ) for $\delta^{18}O$, respectively.

3. Results and discussion

The results are summarized in Fig. 1. Also shown is the bulk composition of the

Kobe meteorite reported by Nakamura et al. [2,3]. Error bars are 1σ.

All the present data for magnetite, olivine in chondrules, low-Ca pyroxene and plagioclase-rich phases are plotted on the lower left (^{16}O-rich) side of the bulk composition and lying almost parallel to and slightly above the CCAM (carbonaceous chondrite anhydrous minerals) line [8]. Olivine data show relatively large variation toward an ^{16}O-rich composition (δ^{18}O from -5‰ down to -12‰). The present results for olivine are consistent with the olivine data reported for Karoonda CK4 meteorite [9]. The magnetite data (δ^{18}O from -7‰ to -3‰) are plotted slightly ^{16}O-poor side of the olivine data, but are still rather ^{16}O-rich. They are ^{16}O-rich even compared with the magnetite data for Karoonda, which show δ^{18}O from -5‰ to +2‰ [9].

An interesting observation of the present results is that *all* the data show compositions more ^{16}O-rich than the bulk composition. Hence, the bulk composition cannot be explained by combinations of the phases we analyzed in the present study. The present analyses were performed mostly on large magnetite and silicate grains but not on fine-grained matrix. Therefore, one possibility is that matrix is more ^{16}O-poor than the bulk composition. This interpretation, however, must be examined in future studies.

Another interesting observation is that magnetite grains show rather ^{16}O-rich compositions, not very different from those for olivine and other silicate phases. If magnetite was formed by aqueous alteration and its oxygen was introduced by fluid, one may expect much more ^{16}O-poor compositions for magnetite when it was formed. Exolution lamellae of ilmenite and spinel observed in large magnetite grains suggest that they have experienced relatively high temperatures during, most likely, a metamorphic event. During such event, it would happen that oxygen isotopes of magnetite became equilibrated with the surrounding silicate phases. Note that equilibrium partitioning of oxygen isotopes at high temperatures would result in a very small fractionation among different phases. Hence such a process may explain the similarities in the oxygen isotopic compositions in magnetite and silicates. More studies are required, however, to understand the origin of magnetite and its oxygen isotopic signature in the Kobe and other CK chondrites.

Acknowledgments

We express special thanks to Mr. Ryoichi Hirata for providing the Kobe meteorite specimen for the consortium studies.

References: [1] Nakamura N., Ebihara M., Hirota Y., Oura Y., Yoneda K., Kojima H., Tomeoka K., Kojima T., Komura K., Clayton R. N., Mayeda T. K. and Wang D. (2000) *Lunar Planet. Sci.* **XXXI**, #1234. [2] Nakamura N., Tomeoka K., Kojima H., Clayton R. N., and Mayeda T. K. (2000) *Meteoritics & Planet. Sci.* **35**, A116. [3] Nakamura N., Kojima H., Haramura H., Tomeoka K., Clayton R. N., and Mayeda T. K. (2000) *Antarctic Meteorites* **XXV**, 99-101. [4] Tomeoka K., Kojima T., Kojima H. and Nakamura N. (2000) *Antarctic Meteorites* **XXV**, 160-162. [5] Oura Y., Ebihara M., Yoneda S. and Nakamura N. (2000) *Antarctic Meteorites* **XXV**, 128-130. [6] Hiyagon H. and Hashimoto A. (1999) *Science* **283**, 828-831. [7] Jabeen I. (1999) *Dr. Thesis, Okayama Univ.* [8] Clayton R. N., Onuma N., Grosmann L. and Mayeda T. K. (1977) *Earth Planet. Sci. Lett.* **34**, 209-224. [9] Greenwood J. P., Wasson J. T. and McKeegan K. D. (2000) *Lunar Planet. Sci.* **XXXI**, #2042.

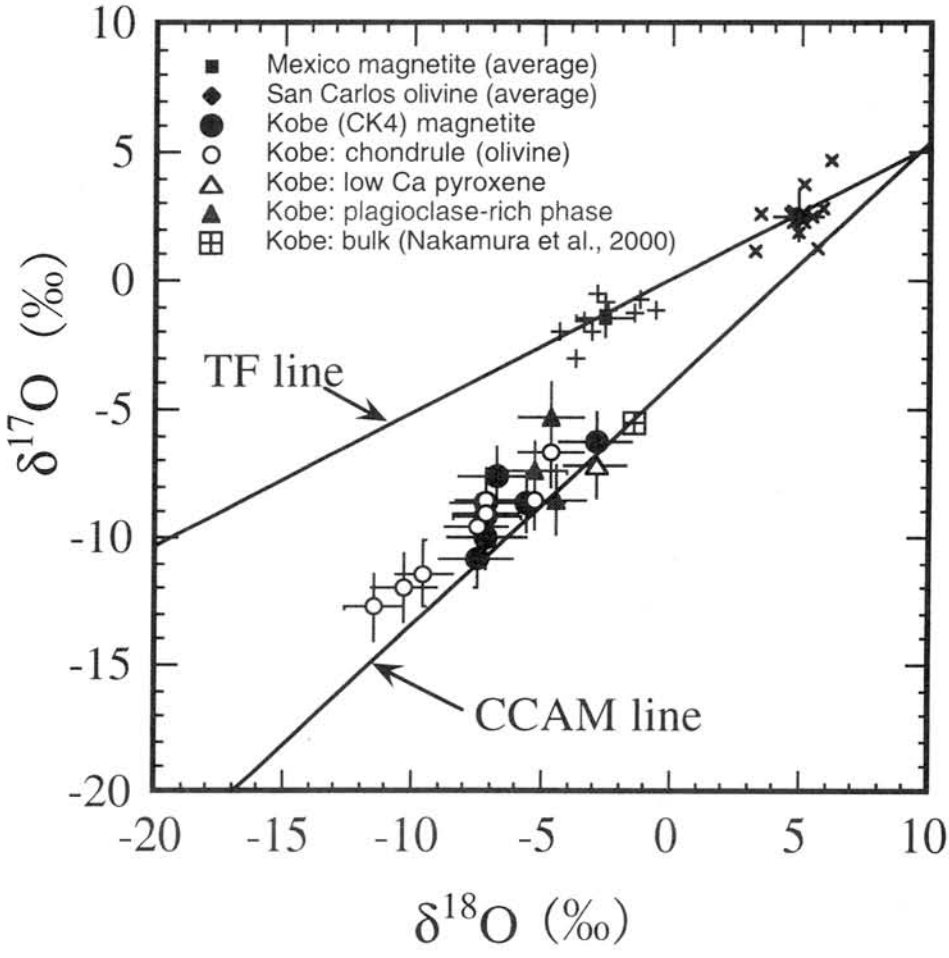

Fig. 1 Oxygen isotopic compositions of magnetite and silicate phases in the Kobe (CK4) meteorite measured with an ion microprobe. Also shown for comparison is the bulk composition of the Kobe meteorite reported by Nakamura et al. [2]. TF line = terrestrial fractionation line; CCAM line = carbonaceous chondrite anhydrous minerals line [8]. Repeated analyses of Mexico magnetite and San Carlos olivine standards were performed and their average values were used for normalization of the data of magnetite and silicate phases, respectively, of the Kobe meteorite. Individual data for these standards are also shown in the figure, which indicate the reproducibility of the present analyses. Errors are 1σ.

Preatmospheric Size of Large Irons by Cosmogenic Nuclides.

Masatake Honda

1). The contents of higher energy cosmogenic nuclides in near surface samples of large size irons are commonly high relative to those of other fragments. The examples are those of ^{26}Al and ^{10}Be. The levels reduce with depth, $d_{1/2}$ of about 100 g/cm^2.

2). Preatmospheric size of the meteoroid can be estimated from observed data of the lowest values which is attributed to the center.

3). The measurements with the fragments near center, however, are usually difficult because of the lowest contents. Even under a few meter below the surface, the production decreases rapidly. Estimation for the production in deep interior samples is also not reliable.

4). On the other hand, at some shallower depths the determination and estimations are much easier. In this work, we assume that the meteoroid was a simple spherical body and irradiation history was also the simplest.Problem may be in a reasonable sampling of the fragments in the spherical body. When we can collect the data sets from samples of known volume fractions, it is easy to estimate the original size of the meteoroid.

When the samples were from the depth deeper than 20% of the radius, they may contain relatively lower amounts of the products, whereas the other samples from shallower fragments contain higher contents. Because the volumes of shallower than d = 0.2R must be equal to the volume of deeper than that depth, the numbers of samples must be equal for both groups, if sampling has been performed uniformly or randomly throughout the object. The specific "d" described above may be expressed as a "representative" depth of the object. A similar test can be made employing data between the depths of radius.

5). To perform this operation, number of sampling must be extensive enough to cover evenly whole volume of the object. In fact plotting of the contents as a function of numbering of the samples is approximately expressed in a simple exponential function covering near surface down through the representative depth and decrease

rapidly toward center region. Even if the available measured points were not many enough from a view of statistics, corrections for the sequence of the data points can be made reasonably.

6). Some artificial model runs ($R=1000g/cm^2$) have been performed using several artificial sets of random numbers. Some series of 20 to 100 points have been tested and the representative member obtained has been compared. With 100 data points the test results quite reproducible. With 20 data, however, more than ±10% errors are found as unavoidable (Fig.1). The experimental determinations with up to 20 data points may be practical for each meteorite sample. On the whole, the estimation of the size has not been studied well, but this method might become useful.

7). Possible substantial loss of the nuclides may be expected due to ablation loss of the surface layer. The estimation for the common surface data can be suggested from many examples of large meteorites. For example, 2.5 dpm/kg with about 20% error for ^{10}Beand the somewhat smaller value can be estimated for ^{26}Al, such as 2 dpm/kg. They are classified to the highest energy products and the contents must be the highest at the surface respectively. For the stable nuclides, effects of multi-stage exposures must be considered.

On the other hand, the data of the deeper region must be included for the balance. The lowest data, however, may not necessary be those of very close to the center. The chance to encounter a sample from $d \geq 0.9R$ must be $\leq 1/1000$ of the total, which can be ignored from practical current statistical approach.

8). Actual Examples:

Campo del Cielo[4], recovered more than 30 tons. The lowest contents of cosmogenic nuclides among meteorites have been pointed out. The list of available data is poor, and the minimum size can only be estimated.

Gibeon[1], recovered 21 tons: Total 33 useful data could be collected. The representative depth is determined at 600 g/cm^2 which is 1/60 of the surface data, 0.03 dpm ^{10}Be/kg. The size is therefore estimated at $R = 3000g/cm^2$ or 2000 tons. In the deepest available sample it was E-4 dpm ^{10}Be/kg which corresponds to production at 1300 g/cm^2. A difference ± 1 to the sample number causes a 25% uncertainty in the depth which results an error of factor of 2 to the final estimate for the total weight.

Brenham[2]. recovered more than 4 tons: The sample of AMNH880 seems to be the representative among about 12 fragments examined;

The depth is estimated 400 g/cm^2. R = 2000 g/cm2 and density = 6, It corresponds to 900 tons. On the other hand, the minimum size was estimated at 600 tons.

Canyon Diablo, recovered 30 tons: Based on Heymann et al (1966)[5], more than 50 samples were determined for the ^{3}He contents ranged 0.03 – 300 x E-8 cc/g. The depth, 1000g/cm^2 , at the level of 1/300 relative to the surface seems to be the representative having about 1E-8 cc^{3}He/g, and 6000 tons are estimated. Shoemaker obtained 63,000 tons, however, based on a mega ton scale nuclear explosion and assuming 15 km/sec as the original velocity against the earth[3].The main part of the body seems to be disappeared by evaporation, and could never be recovered by us. This might be illustrating a limit of current method to the extreme example like Canyon Diablo. The current method is tacitly assuming 100% remaining of the fragments.

Ref.: 1). Nagai et al. abstract 24th,this symposium, 116(1999); 2). Honda et al. Meteoritics, submitted (2001); 3). Buchwald, "Iron Meteorites"(1975) 2, 381; 4). Nagai et al.Geochim.57,3705 (1993); 5). Heymann et al.(1966) JGR.71,619-641.

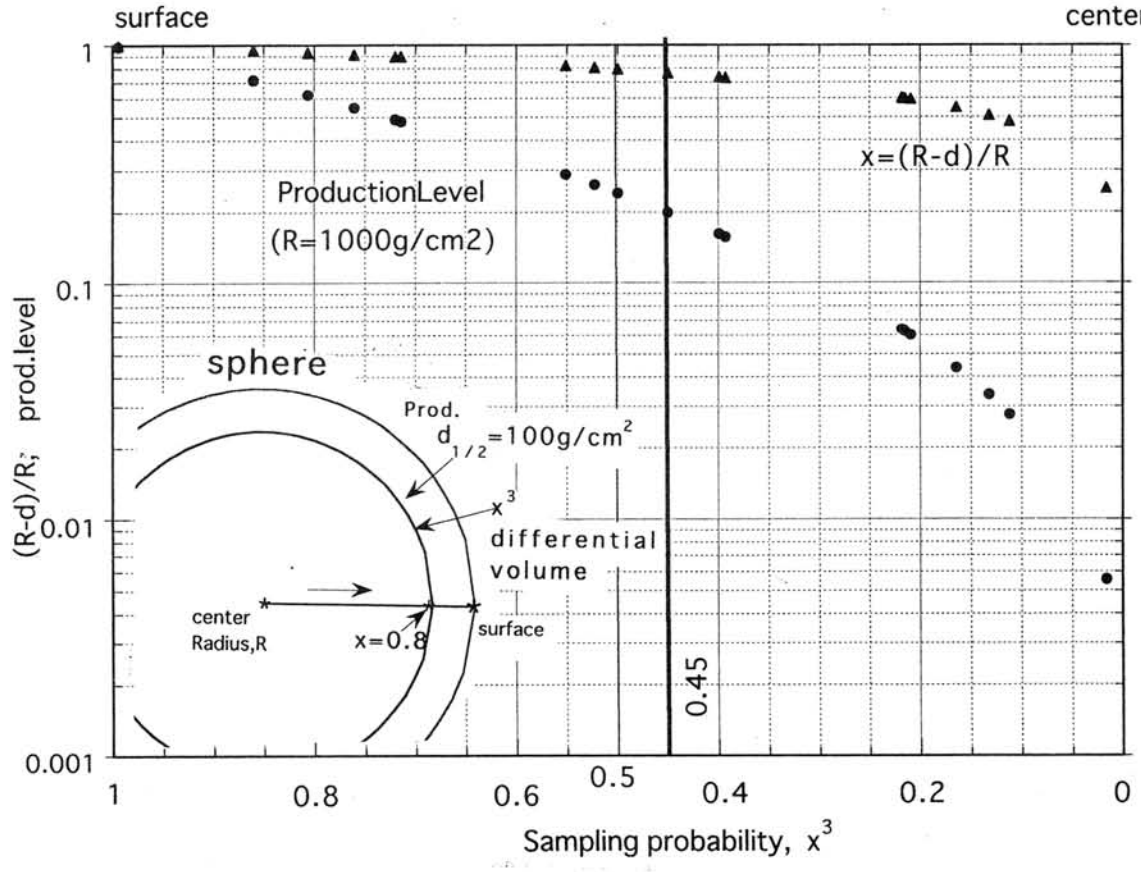

Fig.1. Random sampling model, 20 data points.

A preliminary report on the Mn-Cr chronology of IIIAB Iron meteorites

H.Hoshino and N.Sugiura

Dept. of Earth Planet. Sci., Univ. of Tokyo

sugiura@esp.s.u-tokyo.ac.jp

With a half-life of 3.7 m.y. Mn-Cr system is best suited for measuring time spans of events in small solid bodies in the early solar system. The presence of live ^{53}Mn in IIIAB irons was shown by pioneer studies by Hutcheon (1991,1992). The initial ^{53}Mn/^{55}Mn ratios in several IIIAB iron were of the order of $2x10^{-6}$. But the ratios showed some variation among the IIIAB irons and therefore it seemed that the IIIAB irons were not derived from a core of a single parent body, which is rather unexpected because IIIAB is a well defined group based on many properties. We reanalyzed the same IIIAB irons to find out the cause of the variation of the initial ^{53}Mn/^{55}Mn ratios and to clarify the thermal history of the IIIAB parent body.

The measurements of Cr isotopes were made with a CAMECA-6F ion microprobe with an O- primary beam. In order to make corrections for instrumental mass fractionation effects, the amount of ^{50}Cr was estimated by subtracting the contribution of Ti and V to mass 50. Also, in order to make corrections for cosmogenic ^{53}Cr, Cr+/Fe+ ratios were measured.

Grant, El Sampal, Bella Roca, Sandtown and Chupaderos were studied. A few other irons were examined mainly to obtain additional information on the cosmogenic ^{53}Cr production rate and relative sensitivity factors. Phosphates are the main Mn carriers in iron meteorites. Many phosphate species are present in the IIIABs which show different Mn/Cr ratios.

The production rate of ^{53}Cr in iron meteorites is known (Lugmair and Shukolyukov,1998). Therefore, it is possible to calculate the amount of cosmogenic ^{53}Cr for meteorites with known exposure ages. For meteorites with unknown exposure ages, we may assume that they have an exposure age of 650 m.y. which is a typical exposure age of IIIAB irons. It is also possible to estimate the exposure ages from the measurements of ^{53}Cr excesses in minerals (Fe-Ni metal and phosphide) with small Cr/Fe ratios. The relative sensitivity factor (Cr+/Fe+/Cr/Fe) is needed for this estimate. From these calculations, we found that the contribution of cosmogenic ^{53}Mn is not negligible but is smaller than that of radiogenic ^{53}Cr in many Mn-rich minerals. After the correction of cosmogenic ^{53}Cr, the excess ^{53}Cr is fairly well correlated with Mn/Cr ratios in the main phosphate minerals (Fig.1). The initial ^{53}Mn/^{55}Mn ratios estimated from the isochron is $2.6x10^{-6}$ which is in good agreement with that reported by Hutcheon et al.(1991,1992) . Data points for some minor phosphate minerals are located below the isochron, which suggests that they remained as an open system for a longer time during the slow cooling than the main phosphates. Minor deviations of the data points around the isochron may also be due to slight redistribution of Cr(and/or Mn) during the slow cooling. The present data suggest that all the IIIAB irons experienced the same cooling history and hence they were derived from a core of their parent body.

References
Hutcheon and Olsen (1991) LPS XXII, 605-606.
Hutcheon et al. (1992) LPS XXIII, 565-566.
Lugmair and Shukolyukov (1998) GCA, 62, 2863-2886.

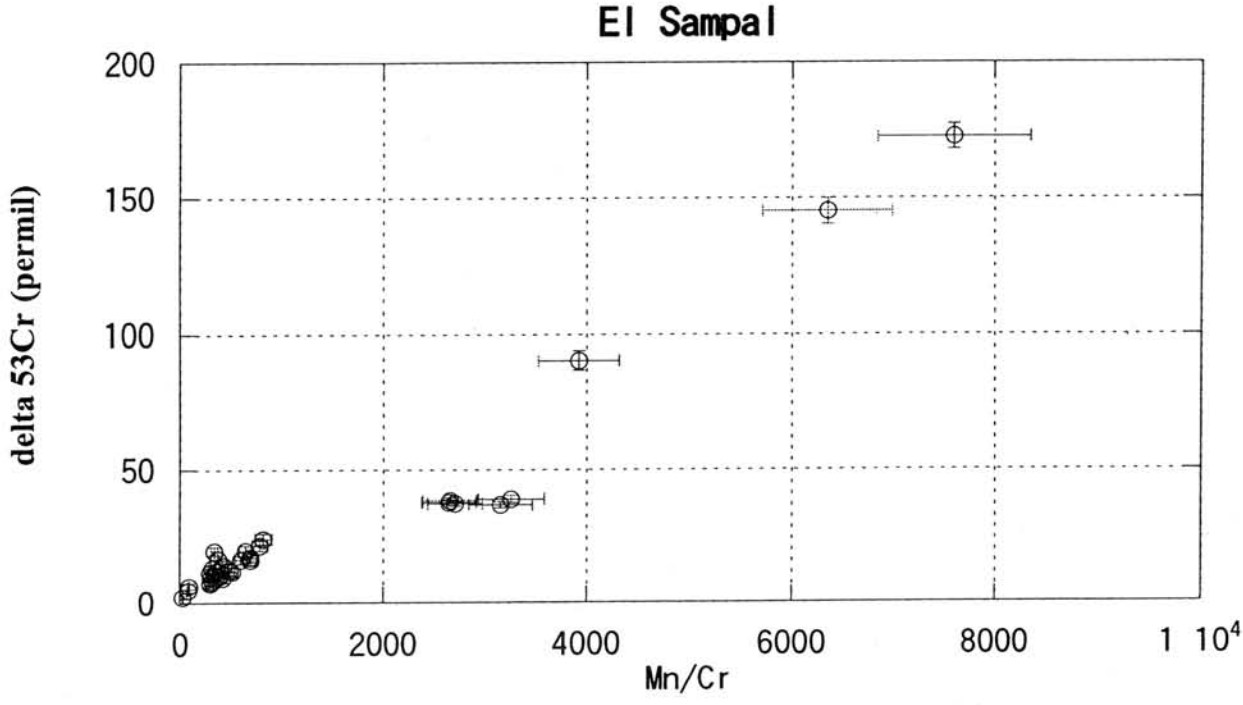

Magmatic Inclusions in the DaG 735 Shergottite

Y. Ikeda
Dept. Material & Biol. Sci., Ibaraki University, Mito 310, Japan
(ikeda@mito.ipc.ibaraki.ac.jp)

The Dar al Gani (DaG) 735 meteorite is a shergottite, which was recently recovered from Libyan Sahara and seems to be paired with other Libyan shergottites, DaG 476/489/670 [1, 2, 3, 4].

[Host Lithology] DaG 735 is a porphyritic basalt with millimeter-sized phenocrystic crystals set in fine-grained groundmass, and the phenocrystic crystals are mainly olivines and rarely low-Ca pyroxenes. The olivines show chemical zoning from magnesian cores ($Fo_{\sim 75}$) to ferroan rims ($Fo_{\sim 60}$), and the low-Ca pyroxenes zone from magnesian orthopyroxene ($En_{82\text{-}74}Wo_{1.5\text{-}4}$) to ferroan pigeonite ($En_{70\text{-}55}Wo_{7\text{-}14}$). The groundmass consists mainly of maskelynite ($An_{50\text{-}70}$), pigeonite, augite, olivine, chromite, ilmenite, and whitlockite. Minor pyrrhotite occurs in the groundmass. DaG 735 contains terrestrial calcite veins which are similar to those in the other Libyan shergottites, indicating that it was subjected to terrestrial weathering.

[Magmatic Inclusions] The phenocrystic olivines in DaG 735 contain magmatic inclusions, as well as mineral inclusions. The magmatic inclusions always occur in ferroan olivines with $Fo_{60\text{-}65}$, and the sizes are a few tens to several tens of microns across. They consist mainly of glassy materials with variable amounts of fassaite and/or a silica mineral. The magmatic inclusions are classified into two types, I and II, by existence of a fassaite mantle which lines the inclusion wall. The type I has no fassaite mantle and is glassy with variable amounts of quenched fassaite crystals. The type II has a fassaite mantle and contains variable amounts of a silica mineral and fassaite grains in devitrified glass.

[Crystallization of Magmatic Inclusions] The type I inclusions may have been produced from a trapped melt (L_0) by crystallization of wall-olivine followed by fassaite precipitation. The residual melts may have resulted in glass. The type II inclusions may have formed from L_0 by crystallization of wall-olivine and wall-fassaite around the inclusions. Then a silica mineral and fassaite crystallized in the inclusions, and the residual melts may have resulted in devitrified glass. Both types I and II occur in close association to each other in phenocrystic olivines, and the difference in crystallization may have been caused by unknown kinetic processes.

[References] [1] Grossman J.N. (2000 Meteorit. Planet. Sci. 35 (Suppl.), A199-A225; [2] Folco L. and Franchi I.A. (2000) Meteorit. Planet. Sci. 35 (Suppl.), A54-A55; [3] Wadhwa M. Lentz R.C.F. McSween H.Y. and Crozaz G. (2001) Meteorit. Planet. Sci. 36, 195-208; [4] Mikouchi T., Miyamoto M., and McKay G.A. (2001) Meteorit. Planet. Sci. 36, 531-548.

Search for Antarctic meteorites in the bare ice field around the Yamato Mountains by JARE-41

[1]Naoya Imae, [2]Naoyoshi Iwata and [3]Yasuyoshi Shimoda

[1]Antarctic Meteorite Research Center, National Institute of Polar Research, 9-10, Kaga 1-chome, Itabashi-ku, Tokyo 173-8515, Japan

[2]Faculty of Sciences, Yamagata University, 1-4-12 Kojirakawa, Yamagata-city, Yamagata, 990-8560, Japan

[3]Mizuho Junior High School, 1135-1, Saigo-shin, Mizuho-town, Minamitakaki-gun, 859-1206, Nagasaki, Japan

Introduction

Antarctic meteorites have been abundantly collected from bare ice regions accompanied with mountains or nunataks (Cassidy et al., 1992). About 10000 meteorites (total ~700kg) have been found from the bare ice area (~4000 km^2) around the Yamato Mountains (Kojima et al., 2000). The area potentially has still new meteorites mainly because the unsearched and insufficiently searched area has been left. The Wintering Party of the 41st Japanese Antarctic Research Expedition (JARE-41; 1999.11.14~2001.3.28) conducted the meteorite search in the bare ice field around the Yamato Mountains.

Meteorite Search and Results

The period of the meteorite search was 89 days. The departure from Syowa Station was on 2000 October 27, the entrance into the bare ice field around the Yamato Mountains on 2000 November 17, leaving the bare ice field on 2001 January 10, and the arrival at Syowa Station on 2001 January 23. Three large snow vehicles (SM100s) were used for the transportation between Syowa Station and the Yamato Mountains. Each vehicle pulled 7 sledges. And each sledge was capable of taking 2 tonnes on mostly for fuels. Figure 1 shows the route of meteorite search and searched area in detail. For the meteorite search in the bare ice field, one snow vehicle and 4~5 snowmobiles were used. The six men party among JARE-41 collected more than 3500 meteorites by the search. The total weight of recovered meteorites was about 196 kg. Then average weight was about 56 g. Most frequent weight was in the range of 3~10 g. There were 6 meteorites more than 10 kg and were 14 meteorites more than 1 kg. The heaviest meteorite among meteorites collected by the present expedition was the iron meteorite of 50.5 kg without Widmanstätten structure on the surface, which was found from the north-west region of JARE IV Nunataks (area II) (Fig. 1). This was also the heaviest meteorite among Yamato bare ice region since the first finding in 1969 (JARE-10). In area II, relatively large meteorites were found compared with other areas (number = ~1320; average weight =

~80g). Remarkably abundant meteorites have been collected from the bare ice region around Minami-Yamato Nunataks (area VIII) (Yanai, 1981; Kojima et al., 2000). Also in the present search, the abundant number of meteorites (~1800) were found. However, the average weight of meteorites in this area was small (~28g) compared with that of other areas. This will be because the southern part of the area VIII had been searched well. Meteorites found in area VII, the western side of Massif C of the Yamato Mountains (Fig. 1), had a unique distribution that 322 fragments mainly composed of two broken species of each more than 10 kg were found within a diameter of about 100 m. It has been known that area VII is a meteorite less concentrated area approximately more than one order smaller than area VIII and II.

Field Descriptions

The frequency of rough classification of collected meteorites in this search, that is, chondrites, achondrites, iron, or stony-iron in the field was 94.7, 4.9, 0.3, and 0.03%, respectively. The frequencies of chondrites and achondrites are nearly consistent with those of previous Antarctic finds, however, those of irons and stony-irons are both less than those of previous Antarctic finds (Harvey and Cassidy, 1989). In the field description, we defined the shape of a meteorite as "complete", "half", and "fragment". "Complete" means that a meteorite is completely covered with fusion crust, "half" shows that a meteorite is judged to be nearly half of the parent meteorite from the appearance, and "fragment" shows that a meteorite is tiny chip and often fusion crust absent. The relative number of each shape was 15.4, 13.0, and 71.6%, respectively. This will be related to the fragmentation at the time of fall of a meteorite and the fragmentation due to the weathering on the bare ice. We will need to consider it to estimate the meteorite flux in Antarctica.

Acknowledgements

We are grateful to Messrs. Mitsuaki Sakai (Surgery), Taku Kondo (Radio engineer), and Shintaro Nomoto (engineer of vehicles) who are members of the expedition for meteorites for the collaboration very much, and are also the leader of JARE-41 wintering team, Dr. Kentaro Watanabe for the management for the expedition. We are also grateful to members of JARE-41 of our colleague for the support of the expedition.

References:

Harvey, R. P. and Cassidy, W. A. (1989): A statistical comparison of Antarctic finds and modern falls: mass frequency distributions and relative abundance of type. Meteoritics, 24, 9-14.

Cassidy, W., Harvey, R., Schutt, J., Delisle, G., and Yanai, K. (1992): The meteorite collection sites of Antarctica. Meteoritics, 27, 490-525.

Kojima, H., Kaiden, H. and Yada, T. (2000): Meteorite search by JARE-39 in 1998-1999 season. Antarct. Meteorite Res., 13, 1-8.

Yanai, K. (1981): Collection of Yamato Meteorites in the 1979-1980 Field Seasons. Mem. of NIPR Spec. Issue, 20, 1-8.

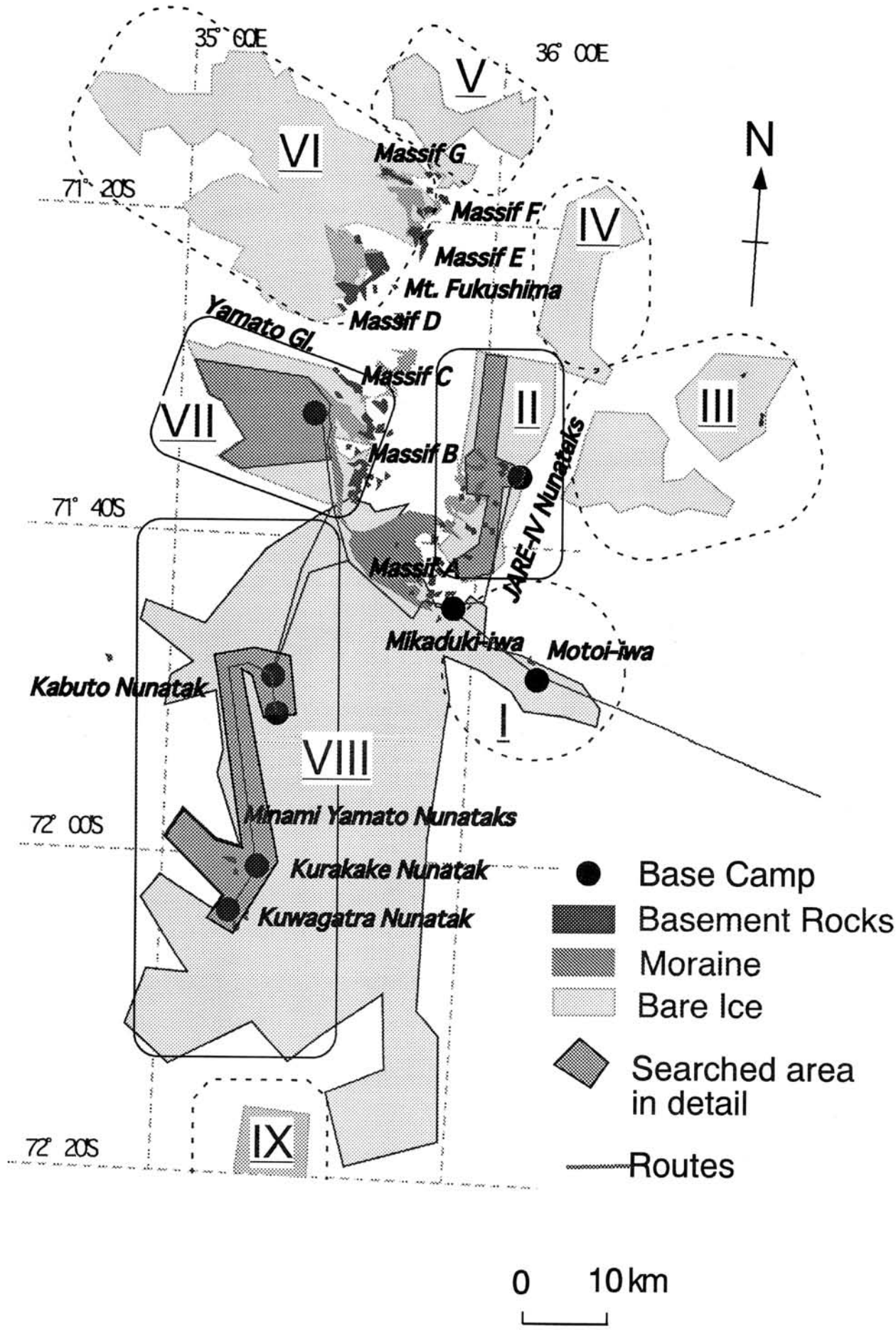

Fig. 1. Yamato bare ice field and meteorite searched area in detail. Bare ice area was divided into 9 (I~IX).

Phyllosilicate-bearing chondrules and clasts in the ALHA 77307 CO3 chondrite: Evidence for parent-body processes

Daisuke Itoh and Kazushige Tomeoka

Department of Earth and Planetary Sciences, Faculty of Science, Kobe University, Nada, Kobe 657-8501, Japan

Introduction

Type3 carbonaceous chondrites are regarded as being the least affected by aqueous alteration and thermal metamorphism among the various chondrite types. However, previous studies [1-4] suggested that some CO3 chondrites have experienced various minor secondary processes, including equilibration of olivine grains, Fe-alkali metasomatism of Ca-Al-rich inclusions (CAIs), formation of phyllosilicates, that may have occurred on the CO parent body. Especially, our recent study of dark inclusions in CO3 chondrites provided evidence suggesting that the CO parent body has experienced, at least partly, extensive aqueous alteration and subsequent thermal dehydration [5]. Whether these secondary processes also affected other components in the CO3 chondrites or not is a subject of great interest.

ALHA 77307 CO3 chondrite is classified into petrologic type 3.0 and considered to be the least processed among the known CO3 chondrites. Nonetheless, there have been some signs of secondary processes. Ikeda [6] found phyllosilicates in chondrules and matrix of ALHA 77307 and suggested that aqueous alteration occurred prior to final accretion of the meteorite. Keck and Sears [7] also suggested that ALHA 77307 may have been aqueously altered from its thermoluminescence property. Brearley [8] reported a minor occurrence of disordered mixed layer phyllosilicates in matrix of ALHA 77307. However, the studies of phyllosilicates in ALHA 77307 are still very limited and a more detailed study is needed to clarify the nature of phyllosilicates and to determine whether the alteration occurred before or after accretion. We here present the results of detailed petrographic and scanning electron microscopic observations of phyllosilicates in ALHA 77307.

Results

General Features

We surveyed a total of 124 chondrules, larger than 50 μm in diameter, in 14.5 mm^2 area, of which 97 (78 %) are, at least partly, enclosed by well-defined, fine-grained rims that range in thickness from 10 to 110 μm. We found that phyllosilicate is most abundant in chondrules and their rims; 55 of 124 (44 %) chondrules contain phyllosilicate grains (>3 μm in diameter) that can be observed by back-scattered electron imaging. We also found a total of 20 clasts that contain significant amounts of phyllosilicate; they are angular to irregular in shape and range in diameter from 50 to 700 μm. The phyllosilicates in those different objects are generally similar in composition; they are rich in Mg (5-13 wt% MgO) and Fe (20-31 wt% FeO) and contain 5-11 wt% Al_2O_3, and are compositionally close to Fe-bearing saponite (Fig.1). The compositions resemble those of phyllosilicates reported by Ikeda [6].

Phyllosilicate in chondrules and rims

Phyllosilicate occurs most commonly in mesostases of chondrules as a replacement product. Opaque nodules are also partially replaced by phyllosilicate. In type I chondrules, where phenocrysts of forsterite and enstatite coexist, enstatite is preferentially replaced by phyllosilicate, forming intimate intergrowths of enstatite and phyllosilicate,

whereas forsterite remains almost unaltered.

Chondrule rims consist of fine-grained olivine, magnetite, enstatite and Fe-sulfide. Some chondrule rims also contain rounded grains (3-10 μm in diameter) of phyllosilicate. The interface between chondrules and rims is commonly very irregular, and opaque nodules of chondrules are partly or completely exposed to rims due to preferential replacement of enstatite. The opaque nodules are also partially replaced by phyllosilicate. Where enstatite phenocrysts are exposed to rims, they show fine-scale irregular contacts and break down to fine grains of enstatite and phyllosilicate. The textural and mineralogical characteristics closely resemble those of phyllosilicate-rich rims on chondrules in the Vigarano CV3 chondrite [9].

A remarkable characteristic is that some chondrules contain narrow veins filled with Fe-hydroxide that range in width from 1 to 8 μm and in length from 30 to 100 μm. The veins extend from grains of Fe-Ni metal and magnetite in chondrules and penetrate into surrounding rims, but they always terminate at the boundaries between rims and matrix of the host meteorite.

Phyllosilicate-bearing clasts

Relatively large (>300 μm in diameter) clasts contain two to three chondrules and/or chondrule fragments, whereas small (<200 μm) clasts contain mineral fragments (5-40 μm in size), mostly of olivine and pyroxene. Chondrules in those clasts have no rims. Mesostases and opaque nodules of the chondrules are partially replaced by phyllosilicate, which is similar to the phyllosilicate-bearing chondrules in the host meteorite described above. The matrices of the clasts consist of fine-grained olivine, magnetite, enstatite and Fe sulfide; their mineralogy and compositions are closely similar to those of the chondrule rims. In addition, the matrices contain phyllosilicate as irregularly shaped patches (10-30 μm in diameter). The abundance of phyllosilicate in matrix differs considerably between clasts. As observed in the chondrule/rim assemblages, veins (1-3 μm in width and 80 μm in length) filled with Fe-hydroxide occur in some clasts; they terminate at the boundaries between clasts and matrix of the host meteorite

Discussion

Our study reveals that chondrules in ALHA 77307 contain abundant saponite, which was formed mainly by replacing mesostases, enstatite phenocrysts and opaque nodules in chondrules. Similar occurrences of saponite have been also reported from some CV3 chondrites [9-13]. Most of these workers concluded that saponite was formed by replacing chondrules during aqueous alteration. Our study also reveals that some clasts in ALHA 77307 contain abundant saponite. Both saponite-bearing chondrules and clasts show veins filled with Fe-hydroxide. These observations and evidence suggest that the saponite in ALHA 77307 was formed by aqueous alteration that occurred on the meteorite parent body.

The abundant occurrence of clasts in ALHA 77307 indicates that the meteorite has undergone brecciation processes on its parent body. The Fe-hydroxide veins in the clasts always terminate at the boundaries between clasts and matrix, indicating that the veins are extraterrestrial and formed prior to incorporation of the clasts to the present location. The texture also suggests that the clast formation occurred after aqueous alteration. Chondrules and clasts in ALHA 77307 show various degrees of aqueous alteration; some chondrules contain feldspathic mesostases, while other chondrules contain abundant phyllosilicate. These suggest that the meteorite parent body was heterogeneous in degree of aqueous alteration and the host ALH77307 meteorite is an assemblage of clasts from many different locations in the parent body.

References
[1] McSween H. Y. Jr. (1977) Geochim. Cosmochim. Acta 41, 477-491.
[2] Keller L. P. and Buseck P. R. (1990) Geochim. Cosmochim. Acta 54, 1155-1163.
[3] Scott E. R. D. and Jones R. H. (1990) Geochim. Cosmochim. Acta 54, 2485-2502.
[4] Kojima T., Yada S. and Tomeoka K. (1995) Proc. NIPR Symp. Antarct. Meteorites 8, 79-96
[5] Itoh D. and Tomeoka K. (2000) Meteoritics Planet. Sci. 35, A81 (Abstr.)
[6] Ikeda Y. (1983) Proc. NIPR Symp. Ant. Meteor Memoirs NIPR (Spec Issue.) 30, 93-108.
[7] Keck B. D. and Sears D. W. G. (1987) Geochim. Cosmochim. Acta 51, 3013-3021.
[8] Brearley A. J. (1993) Geochim. Cosmochim. Acta 57, 1521-1550.
[9] Tomeoka K. and Tanimura I. (2000). Geochim. Cosmochim. Acta 64, 1971-1988.
[10] Tomeoka K. and Buseck P. R. (1982) Nature 299, 327-329.
[11] Tomeoka K. and Buseck P. R. (1990) Geochim. Cosmochim. Acta 54, 1745-1754.
[12] Keller L. P., Thomas K. L., Clayton R. N., Mayeda T. K., DeHart J. M. and McKay D. S. (1994) Geochim. Cosmochim. Acta 58, 5589-5598.
[13] Kimura M. and Ikeda Y. (1998) Meteoritics Planet. Sci. 33, 1139-1146.

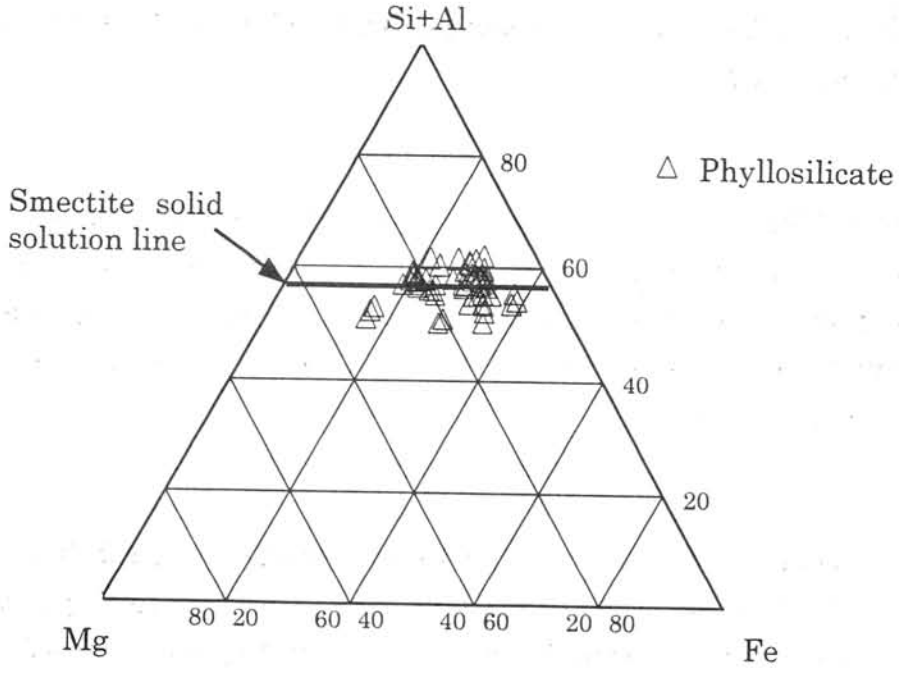

Fig. 1. Focused-beam EDS analyses of phyllosilicate in chondrules in ALHA 77307 in terms of atomic percents of Si+Al, Mg and Fe.

The collection of Antarctic micrometeorites at a bare ice region near the Tottuki Point of the Soya Coast in 2000

Iwata N. [1] and Imae, N. [2]

[1]Department of Earth and Environmental Science, Yamagata University, Yamagata, 990-8560, Japan
[2]Antarctic Meteorite Research Center, National Institute of Polar Research, Tokyo 173-8515, Japan

Introduction

Collections of Antarctic micrometeorites (AMMs) have been performed in the last decade. Maurette, et al. (1991) succeeded in the collection of AMMs on the bare ice near the Dumont d'Urville Station, near Cap-Prudhomme. Taylor, et al. (1998) collected AMMs from the bottom of the water well of the Amundsen-Scott Station at the South Pole. Collections of AMMs by the Japanese Antarctic Research Expedition (JARE) were carried out at the Dome Fuji Station (e.g. Nakamura, et al., 1999) and at the bare ice field in the Yamato Mountains Area (e.g. Yada and Kojima, 2000). Here, we report the latest collection of AMMs, which was carried out by JARE-41 in 2000.

Sampling Sites

We performed the collections at a bare ice region near the Tottuki Point of the Soya Coast. This point is 17 kilometers northeast of the Syowa Station. We located the sampling sites ~1.5 km inside from the coastline (elevations of ~140m), in order to avoid contamination of terrestrial materials from the basement rocks. Positions of the experiments were 68°55.2~55.3'S and 39°51.0~51.3'E.

Method

Sampling procedure was divided into two parts, melting of ice and filtering of the melted water. Non-freezing liquid (60% ethylene glycol solution) was heated by three boilers. A radiator that was warmed by circulation of the warm non-freezing liquid, melted ice on the surface of the bare ice field. The melted water was pumped up from a melted-water-filling pond and was sieved by four filters (openings were 10, 40, 100, 238 μm) to eliminate particles from the water.

The facility which was used in this experiments had been developed originally by JARE-39 (Yada and Kojima, 2000). We gave two improvements to the facility in this work. In the previous system, melted water was pulled up by only a vacuum pump. Since that system could not continue the pumping during the filtered-water draining, rates of filtering were limited

about only 200 liters per hour. In this work, we connected a water pump in parallel with the previous pump. As a result, a rate of filtering in the new system became 4~5 times larger than that of the previous system. Further, in order to estimate the volume of filtered water accurately, we added a water meter to a drain of the water pump.

Result

We carried out five trips to the bare ice field during austral fall and spring seasons in 2000. During twenty-one days, we made sixteen holes on the sampling site. Unfortunately, water sometimes leaked from the melted-water-filling pond in the experiments. Thus, we could not sieve a part of the melted water.

Volume of the filtered water was measured directly by the water meter in the earlier period of experiments. Unfortunately, the water meter was broken by an accident during the experiments at the 4th trip. Since then, amounts of filtered waters in the later experiments were estimated based on a relationship between the duration of pumping and water flux, which was established in the earlier period. We estimated that the total amounts of filtered waters were ~38 tons.

Obtained samples that were on the filters were dried off, and were sealed in Polyethylene bags at the Syowa Station. They were kept in room temperature while the transportation from the Syowa Station to Japan. These samples have been reserved in the Antarctic Meteorite Research Center of National Institute of Polar Research and are under preparation for investigation.

Acknowledgements

We acknowledged to members of the 41st Japanese Antarctic Research Expedition Wintering Party (Leader: Dr. Kentaro Watanabe) for the convenience of trips of the Antarctic micrometeorites collections. Especially, we thank to Messrs. Y. Shimoda and K. Abe who helped us in the field and in the improvement of facilities. We are also grateful to Dr. Yada in Kyushu University for the assistance of the use and improvements of the AMM collection apparatus.

References

Maurette, et al. (1991), Nature, 351, 44-47.

Nakamura, et al. (1999), Antarctic Meteorite Research, 12, 183-198.

Taylor, et al. (1998), Nature, 392, 899-903.

Yada and Kojima (2000), Antarctic Meteorite Research, 13, 9-18.

Refractory inclusions in enstatite and ordinary chondrites: A systematic study.

Kimura M.[1], Hiyagon H.[2], Lin Y.[3] and Nakajima H.[1]

[1]Ibaraki University, Mito 310-8512, Japan, [2]Dept. Earth and Planet. Science, University of Tokyo, Tokyo 113-0033, Japan, [3]Guangzhou Institute of Geochemistry, Chinese Academy of Sciences, Guangzhou 510640, China.

1. Introduction

Refractory inclusion is the important component of chondrites, because of mineralogy, chemistry and age, reflecting the early condensate in the solar nebula. The occurrence of the inclusions is typical in carbonaceous chondrites (hereafter CCs). However, rare inclusions have been studied in some ordinary (OCs) and enstatite chondrites (ECs) [1-4]. We also found 66 inclusions from an EH3 chondrite (Sahara 97159) [5] and 43 from probably paired 3 anomalous H3 chondrites (H3-an) [6].

Following our previous studies, we systematically studied refractory inclusions in OCs and ECs. The purposes of the study are as follows: 1) quantitative estimation of the abundance of inclusions in ECs and OCs, 2) comparison of their characteristic features with those in CCs, 3) exploration of the formation and alteration conditions of them in OCs and ECs. In addition to H3-an and Sahara 97159 (EH3), we studied 4 H (H3.7-4), 3 L (L3.2-3.6), 15 LL (LL3.0-6), 6 EH (EH3-5) and 2 EL-chondrites (EL3).

2. Results

Our systematic study showed that inclusions are usually very poor in abundance in OCs and ECs. Except H3-an and Sahara 97159, only 6 inclusions were observed in 6 OCs of type 3.0-3.9. The abundance of the inclusions in OCs ranges from 0.00 to 3.91 inclusions/cm^2 (ave. 0.87). On the other hand, the abundances in H3-an and Sahara97159 are extraordinarily high, 22.32 and 20.78, respectively. The inclusions are small in size, ranging from 17 to 306 μm (80 μm in average) in all OCs and 8-85μm (35 μm in average) in EC (Sahara

97159). Many inclusions, especially in OCs, are surrounded by rims usually consisting of high-Ca pyroxene.

Most of the inclusions consist predominantly of spinel. Some inclusions in OCs abundantly contain olivine. The inclusions in OCs and EC also contain high-Ca pyroxene, nepheline, sodalite and hibonite, with rare perovskite and rutile. An inclusion in A9046 (LL3.2) consists of melilite ($Åk_{11-16}$), perovskite and high-Ca pyroxene. Hedenbergite and ilmenite occur in OCs, whereas albite, corundum and Ti-rich sulfides are encountered only in EC. Many inclusions in both chondrites are similar to spinel-rich inclusions in CO chondrites.

Spinel contains 0-46.4 and 0-17.4% Cr_2O_3, 8.2-28.7 and 0-5.2 FeO, and 0-3.1 and 0-0.1 ZnO in OCs and EC, respectively. It is noted that Cr-rich spinels are encountered in the inclusions in both chondrites. A characteristic feature of spinels in OCs is high concentrations of FeO and ZnO, which are in general correlated with each other. High-Ca pyroxenes contain 0-12.0% TiO_2 and 0.6-26.1 Al_2O_3.

We measured the bulk compositions of the inclusions in OCs and EC. They are usually enriched in Al_2O_3 (ave. 36.3%) and Na_2O (3.5%), and depleted in CaO (3.7%), which agrees with mineralogy that spinels and feldspathoids are abundant, and Ca-phases are poor in them. The bulk compositions overlap with those of CCs.

The oxygen isotopic compositions of some inclusions in OCs and EC were measured [5-6]. They are plotted along the CCAM line, consistent with the other studies [2, 7-8].

Measurements of trace elements, including REE, of the inclusions are in progress, which will shed light on origins of them.

3. Discussion

Although the abundance varies widely, the inclusions both in OCs and ECs have close characteristic features to those in CCs: 1) primary mineral assemblage of spinel, hibonite, perovskite, melilite and high-Ca pyroxene (abundantly fassaitic), 2) the bulk compositions, 3) the oxygen isotopic

compositions, 4) the initial $^{26}Al/^{27}Al$ ratios [3, 9]. All these features strongly indicate that all inclusions were originated in the same condition.

Abundant feldspathoids and bulk compositions suggest high degrees of the secondary alteration of the inclusions in OCs and ECs. However, ilmenite and hedenbergite are not encountered in ECs, whereas Ti-rich sulfides and albite are observed only in ECs. Therefore, the alteration reaction in ECs took place under reducing [4], and SiO_2-rich conditions. This is supported by compositions of spinels, which hardly contain FeO and ZnO in ECs, contrasting with OC spinels.

Although the abundance of the inclusions in OCs and ECs is usually very low, some of these chondrites abundantly contain the inclusions. The distribution of refractory inclusions is highly heterogeneous in chondrites than reported before.

In summary, similar primary features of the inclusions in OCs, ECs and CCs, strongly support the idea that all the inclusions had formed in a common reservoir, and distributed into the different regions where the various chondrites formed [2-4, 7-8]. Through such process, the inclusions may have heterogeneously mixed with chondrules and matrices. Later, the inclusions were subjected to the alteration reaction under various redox conditions in the different regions.

References: [1] Bischoff A. and Keil K. (1984) GCA, 48, 693. [2] McKeegan K.D. et al. (1998) Science, 280, 414. [3] Guan Y. et al. (2000) Science, 25, 1330. [4] Fagan T. J. et al. (2000) MAPS, 35, 771. [5] Kimura M. et al. (2000) MAPS, 35, A87. [6] Kimura M. et al. (2000) Antarctic Meteorite XXV, 38. [7] Guan Y. et al. (2000) EPSL, 181, 271. [8] Fagan T.J. et al. (2001) MAPS, 36, 223. [9] Russell S. et al. (1996) Science, 273, 757.

Shock metamorphism of the Allende CV3 chondrite at 600 to 800 °C: An experimental study

Koji Kiriyama, Kazushige Tomeoka, and Toshimori Sekine*
Department of Earth and Planetary Sciences, Faculty of Science, Kobe University, Nada, Kobe 657-8501, Japan.
*National Institute for Materials Science, 1-1 Namiki, Tsukuba 305-0044, Japan.

INTRODUCTION

Previous shock experimental studies on the Allende CV chondrite [1, 2] and the Murchison CM chondrite [3] revealed a variety of shock effects at peak shock pressures from 5 to 50 GPa. Those shock effects, many of which have never been observed in natural CV and CM chondrites, provided us with plentiful insights into the shock history of the carbonaceous chondrites. Especially recent shock experimental studies on preheated chondrite samples [4, 5] revealed that shock effects at high temperature (300-650 °C) are different in many respects from those at room temperature. Thus it has become evident that the shock evaluation of Stöffler et al. [6] cannot be directly applied to meteorites that were shocked at high temperature. In this study, shock-recovery experiments were carried out on Allende at high temperature (600-800 °C), higher than that in the previous experiments [4]. We intended to gain our knowledge of shock effects of the carbonaceous chondrites at high temperature and to establish quantitative estimates of the shock intensities in the carbonaceous chondrites at high temperature.

MATERIALS AND METHODS

The shock-recovery experiments were performed by using a single stage 30-mm bore propellant gun at National Institute for Materials Science. The targets were disks of Allende, 12 mm in diameter and 2.5 to 3.0 mm in thickness. The Allende samples were preheated to 600-800 °C by kanthal wire heaters that surround sample containers. The samples were shocked in seven experiments at the following conditions: (1) 14 GPa/600 °C, (2) 18 GPa/625 °C, (3) 24 GPa/650 °C, (4) 30 GPa/650 °C, (5) 14 GPa/800 °C, (6) 21 GPa/800 °C, and (7) 24 GPa/800 °C. The pressure value designated for each experiment is the resultant peak shock pressure calculated from the measured velocity of the projectile. The velocity of the projectile can be controlled by the propellant mass but often deviates from what is initially intended. Polished thin and thick sections were made from each recovered sample by cutting along the shock compression axis. They were studied in detail by using an optical microscope, a scanning electron microscope (JEOL JSM-5800) equipped with an energy dispersive X-ray spectrometer (EDS), and an electron microprobe analyzer (JEOL JXA-8900) equipped with wavelength dispersive X-ray spectrometers (WDS). Chondrules larger than 100 μm in diameter are used for measuring aspect ratios and estimating preferred orientations. Details of the shock-recovery experimental procedures are described in [3, 7]

RESULTS

Impact at 14-30 GPa and 600-650 °C (14 GPa/600 °C, 18 GPa/625 °C, 24 GPa/650 °C, 30 GPa/650 °C)

Chondrules are flattened and show preferred orientations in directions roughly perpendicular to the shock compression axis at 14 GPa/600 °C, 18 GPa/625 °C, and 24 GPa/650 °C. At 30 GPa/650 °C, all chondrules are disrupted, so aspect ratios could not be measured. The mean aspect ratios of chondrules are 1.94 (14 GPa/600 °C), 2.48 (18 GPa/625 °C) and 1.94 (24 GPa/650 °C); these values are generally larger than those for the samples shocked at similar pressures but low temperature (20 °C) [1, 2]. At 14 GPa/600 °C and 18 GPa/625 °C, almost all olivine grains in chondrules are densely fractured with subgrains of 5-10 μm in size, but at 24 GPa/650 °C and 30 GPa/650°C, the subgrain size becomes larger and the fracture density becomes lower. The matrix is highly compacted, and the degree of compaction increases with increasing shock pressure. Wide (5-10 μm) and long (200-300 μm) fractures are produced in the matrix, and their density increases with increasing shock pressure. Local melting occurs as melt veins (10-20 μm in width and 0.5-1 mm in length) and melt pockets (50-300 μm in size) in the matrix at 18 GPa/625 °C and 24 GPa/650 °C. The melts are rich Si, Mg and Fe and contain numerous tiny vesicles and spherical grains of Fe-Ni sulfide, both 5-10 μm in diameter. The melts are similar in composition to the matrix, but they are slightly more enriched in Ca and S. In addition to the Si-Mg-Fe-rich melts, Fe-Ni sulfide in chondrules and matrix are melted and fill fractures of silicates and matrix, forming an intimate network of opaque veins, which is similar to that reported in the Allende sample shocked at 21 GPa/600 °C [4]. At 24 GPa/650 °C, the matrix is almost totally melted.

Impact at 14-24 GPa and 800 °C (14 GPa/800 °C, 21 GPa/800 °C, 24 GPa/800 °C)

Chondrules are flattened with a mean aspect ratio of 2.02 and show preferred orientations at 14 GPa, but at 21 and 24 GPa, chondrules are mostly disrupted, so aspect ratios could not be measured. Olivine grains in chondrules are densely fractured with subgrains of 5-10 μm in size at 14 GPa, but at 21 GPa and 24 GPa, the subgrain size becomes larger and the fracture density becomes lower. The matrix is more compacted than at 600-650 °C at any given pressure. Wide (5-10 μm) and long (200-300 μm) fractures are produced in the matrix. Local melting occurs as melt veins (10-20 μm in width and 0.5-1 mm in length) and melt pockets (100-300 μm in size) in the matrix. The melts are similar in composition and texture to the Si-Mg-Fe-rich melts described above. The amount of melts at any given pressure is distinctly larger than that at 600-650 °C. At all pressures/800 °C, Fe-Ni sulfide in chondrules and matrix is extensively melted, and opaque melt veins are distributed throughout chondrule silicates and matrix. At 24 GPa, major amounts of Si-Mg-Fe-rich melts occur pervasively throughout matrix. The melts penetrate into interstices between small olivine grains in the matrix, forming a complex network of veinlets that are typically 5 μm in width. Although the matrix is not totally melted at 24 GPa, from the texture, the shock pressure leading to total melting of matrix at 800 °C is estimated to be not much higher than 24 GPa, probably lower than 30 GPa.

DISCUSSION

Our experimental study reveals that most of the mechanical shock effects observed at low temperature (20 °C) (e.g., fracturing in silicate crystals and matrix and chondrule flattening) also occur at high temperature (600-800 °C). However, the degree of chondrule flattening at high temperature is apparently higher than that at low temperature at any given shock pressure. The fracture density of olivine generally increases with increasing shock pressure at low temperature [2]. However, the fracture densities of olivine at 24 GPa/650 °C and 30 GPa/650 °C are lower than those at 14 GPa/600 °C and 18 GPa/625 °C, and the fracture densities at 21 and 24 GPa/800 °C are lower than those at 14 GPa/800 °C. These are probably because fractures were recovered by thermal annealing. It is also evident that the shock at high temperature leads to the onset of melting at a distinctly lower shock pressure and produces a much larger volume of melts at any given pressure than the shock at low temperature [1, 2]. These results indicate that the onset of melting and the amount of melts are strongly dependent on preheated temperature of the samples.

Our previous experiments on unpreheated Allende [2] revealed that the matrix of Allende is extensively comminuted at 41 GPa, below the pressure (49 GPa) leading to total melting of matrix [2]. Such extensive comminution of matrix was also found to occur at 30 GPa and low temperature (20 °C) in Murchison [3]. However, in the present experiments on Allende preheated to 600-800 °C, such stage of matrix comminution appears to be absent. Instead, a network of fracture-filling veinlets of melts are produced pervasively throughout matrix, which is most clearly visible at 24 GPa/800 °C. We believe it is important to note that the texture closely resembles that of vesicular olivine-rich regions in the matrix of Kobe CK4 chondrite, where the silicate darkening is most pronounced [8]. This suggests that the vesicular olivine in Kobe resulted from partial melting of matrix material, mainly olivine, and supports the suggestion that the silicate darkening in Kobe was caused by shock metamorphism at high temperature (>600 °C).

REFERENCES

[1] Nakamura, T., Tomeoka, K., Sekine, T., and Takeda, H., Meteoritics, 30, 344 (1995).

[2] Kiriyama, K., Tomeoka, K., and Sekine, T., Meteorit. Planet. Sci. (abstr.), 35, A88 (2000).

[3] Tomeoka, K., Yamahan, Y., Sekine, T., Geochim. Cosmochim. Acta, 63, 3683 (1999)

[4] Nakamura, T., Tomeoka, K., Takaoka, N., Sekine, T., and Takeda, H., Icarus, 146, 289 (2000).

[5] Schmitt, R. T., Meteorit. Planet. Sci., 35, 545 (2000).

[6] Stöffler D., Keil K. and Scott E.R.D. (1991) Geochim. Cosmochim. Acta 55, 3845-3967.

[7] Sekine, T., J. Mat. Sci. Lett., 8, 872 (1989).

[8] Tomeoka, K., Ohnishi, I., Kiriyama, K. and Nakamura, N., *Papers presented to 26th NIPR Symp. Antarct. M*eteorites (this abstract volume).

Three-dimensional structures of metal-sulfides in a CO chondrite using X-ray CT

Masashi Kitamura[(1)*], Akira Tsuchiyama[(1)], Kentaro Uesugi[(2)], and Tsukasa Nakano[(3)]

(1) Department of Earth and Space Science, Graduate School of Science, Osaka University, 1-1 Machikaneyama-cho, 560-0043, Japan, *<kitamura@ess.sci.osaka-u.ac.jp>, (2) Japan Synchrotron Radiation Research Institute (JASRI), Mikaduki, 679-5198, Japan, (3) National Institute of Advanced Industrial Science and Technology, Tsukuba, 305-8567, Japan

Introduction

Chondrules are spherical objects characteristically included in chondrites. They were formed by heating and rapid cooling of solid precursor materials that mainly consists of silicates. Metal-sulfide aggregates are also major constituent of chondrites. They are not considered as metal-sulfide droplets because of their irregular shapes. However, their behavior during chondrule formation is not known well. Metallic chondrules are also present but they are rare [1].

We assume here that metal-sulfides have experienced heating and cooling processes as well as chondrules. Most of spherical metal-sulfides have been deformed by rigid chondrules and become irregular in their shapes after accumulation as chondrites. In order to verify this assumption we made three-dimensional observation of metal-sulfide aggregates in ALH77003 (CO3.5) using X-ray CT (computed tomograpy).

Experiments

X-ray CT is a non-destructive method to get spatial distribution of X-ray LAC (linear attention coefficient) of samples. We can obtain three-dimensional structures by piling up successive cross-sectional CT images.

In this study, we used ALH77003 chondrite (CO3.5) as a sample. CO chondrites have metal-sulfide aggregates and sufficient amount of matrix, which may preserve spherical metal-sulfides as well as deformed aggregates. The effect of thermal metamorphism is expected to be small in this sample.

A tip of the sample (about 4.7mm×7.0mm×7.8mm) was mounted into a resin with silicon powder to make a cylinder (7mm in diameter) to reduce artifacts such as beam-hardening [2]. An olivine crystal (Fo_{92}) was also mounted together with the meteorite as a standard to estimate LACs of the sample from CT values, which is quantitative expression of contrasts in CT images [2]. The sample was imaged by an industrial X-ray CT scanner (ELE SCAN, NX-LCP-C80-I(4)-0) at Osaka University. The acceleration voltage was 65kV and the tube current was 40 μA. Cross-sectional CT images were reconstructed from 360 projections. The pixel of each CT image is 15 μm×15 μm and the width is 12 μm. We obtained 651 cross sections for constructing the three-dimensional structure.

Results

Chondrules, matrix, (Fe, Ni)-metals and Fe-sulfides were distinguished in the CT images by using estimated LAC. Because most chondrules are poorer in FeO than matrix, they are darker than matrix in the CT images (Fig. 1). (Fe, Ni)-metals have larger LAC than Fe-sulfides. We selected some portions, which include representative metal-sulfide aggregates and chondrules. Three-dimensional structures of these metal-sulfides were examined.

Metal-sulfides and chondrules were extracted in the three-dimensional images. As shown in Fig. 2, a chondrule is located on a concavity of an irregular metal-sulfide aggregate. This suggests that the metal-sulfide aggregate is deformed by the chondrule. On the other hand, another metal-sulfide exists as an independent sphere.

The internal structures of metal-sulfide aggregates were also observed. They are not homogeneous. In many cases metal cores are surrounded by Fe-sulfide, especially in spherical metal-sulfide aggregates (Fig. 3).

Discussion

The present results suggest that metal-sulfide aggregates might have been present once as metal-sulfide (or metallic) chondrules. This is consistent with the chemical compositions of metal grains indicating that they were once melted [3]. Many of the aggregates became irregular in their shapes due to deformation by silicate chondrules at intermediate temperatures, where metal-sulfides are plastic while silicate chondrules were rigid after accumulation as a chondrite. If metal-sulfide chondrules were surrounded by matrix, their spherical shapes remained. (Fe, Ni)-metals surrounded by Fe-sulfides may be the evidence of recondensation of evaporated sulfur onto metal-sulfide aggregates [4].

The present spatial resolution of the CT images was not sufficient to analyze detailed three-dimensional structures of the sample. We have removed the selected portions of the sample, which include metal-sulfide aggregates of interest, and they have imaged by X-ray microtomography system using synchrotron radiation at SPring-8, where higher spatial resolution is attained [5]. The results have not been analyzed yet. We are planning to compare the CT images with SEM observation after cutting samples.

Acknowledgment : We are grateful to National Institute of Polar Research for providing the chondrite sample used in this study.

References : [1] Gooding J. L. and Keil, K. (1981) Meteoritics, **16**, 17-43. [2] Tsuchiyama A. et al. (2000) Jour. Geography, **109,** 845-858. [3] Kong, P and Ebihara M. (1996) Earth Planet. Sci. Lett., **137**, 83-93. [4] Imae N. (1994) Proc. Japan Acad., **70**, Ser. B [5] Uesugi et al. (1999) Proc. SPIE, **3772**, 214-221.

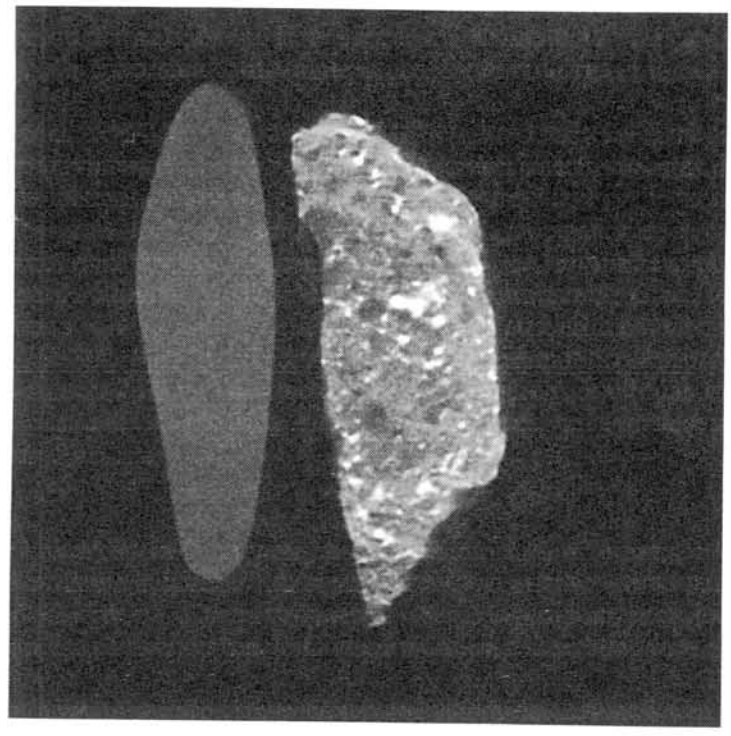

Fig. 1 : An example of a CT image of ALH77003 (CO3.5). Chondrules are recognized as rounded objects with slightly dark contrasts. Metal and sulfide (white) cannot be distinguished in this contrast of the image. A sub-rounded object on the left is an olivine crystal used as a standard for estimating LAC values of the sample. The width of the image is 7.6mm.

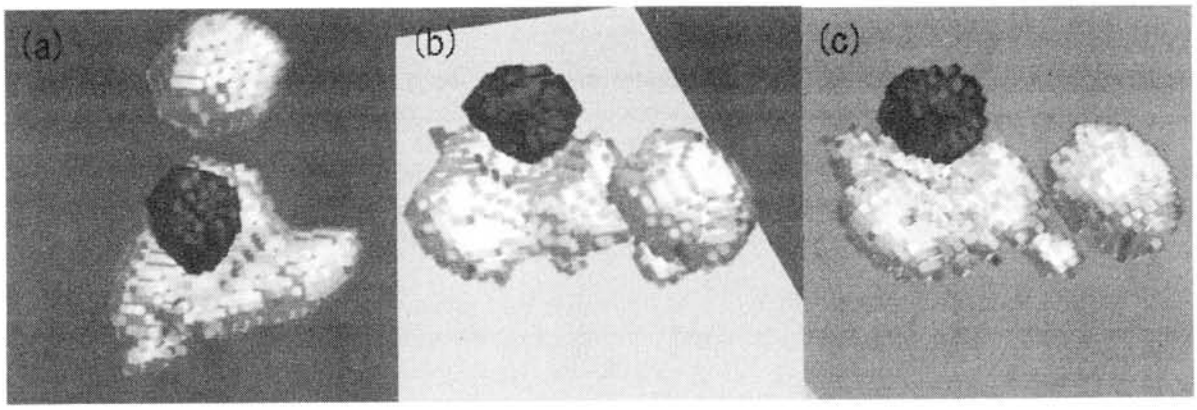

Fig. 2 : Thee dimensional images of a chondrule (dark) and metal-sulfide aggregates (bright) extracted from CT images. The same objects are viewed from different angles. The chondrule is about 0.17mm in diameter. A spherical metal-sulfide of about 0.23mm in diameter is recognized on the top of (a). An irregular metal-sulfide aggregate seems to be deformed by a chondrule in (b) and (c).

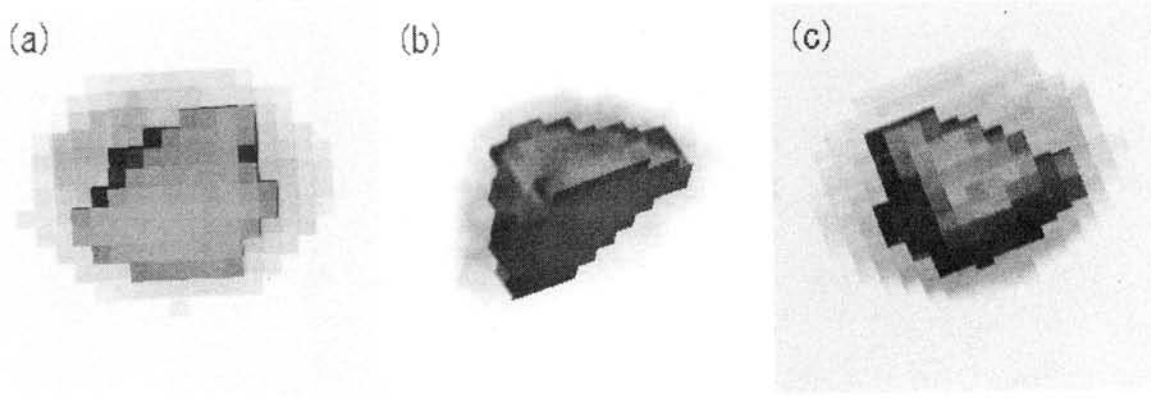

Fig. 3 : Three-dimensional images of a spherical metal-sulfide aggregate, which is cut in half by a computer. The width of each image is about 0.44mm. Fe-sulfide is shown as semi-transparent, whereas (Fe, Ni)-metal is opaque. The same object is viewed from different angles.

Distribution of Yamato 98 meteorites

Hideyasu Kojima [1], Hiroshi Kaiden[1] and Toru Yada[2]

1 National Institute of Polar Research, 1-9-10, Kaga, Itabashi-ku, Tokyo 173-8515, Japan

2 Department of Earth and Planetary Sciences, Graduate School of Sciences, Kyushu University 33, Hakozaki, Fukuoka 812-8581, Japan

Meteorite search party of the 39th Japanese Antarctic Research Expedition (JARE) searched meteorites in bare ice fields around the Yamato Mountains and the Belgica Mountains for approximately three months from November 1998 to January 1999. The party collected 4148 meteorites in bare ice fields around the Yamato Mountains and also collected 32 meteorites in northwest bare ice field of the Belgica Mountains. Positions of all 4180 meteorites were recorded by Global Positioning System (GPS). A figure plots the positions of all Yamato 98 meteorites. Three meteorite concentrated fields are distinguished; around the JARE IV Nunataks, around the Minami Yamato Nunataks, and northern field of the Minami Yamato Nunataks. 1800 meteorites were collected around the Minami Yamato Nunataks. 1000 meteorites were collected in northern field of the Minami Yamato Nunataks. 1000 meteorites were collected around the JARE IV Nunataks.

43 of coarse-grained cumulate eucrites were found in bare ice field of 50km^2, southwest of Minami Yamato Nunataks. Many of them are individual complete stones. The field occurrence and the feature of stones indicate that these eucrites are derived from the same single fall.

9 of brownish green diogenites are found near the Yamato A Massif. These are classified into type A diogenites (Yanai and Kojima, 1995). These type A diogenites are derived from a single fall. 8 of type B diogenites (Yanai and Kojima, 1995) are found in narrow bare ice field between the Yamato A Massif and the JARE VI Nunataks. These diogenites are also derived from the same fall.

16 of ureilites are distinguished at the field. Many of them are found in bare ice field around the Minami Yamato Nunataks and northern field of Minami Yamato Nunataks. PTS's of three of these ureilites show different texture. It indicates at least that all 16 ureilites are not the same type of ureilites.

Distribution of all Yamato 98 meteorites

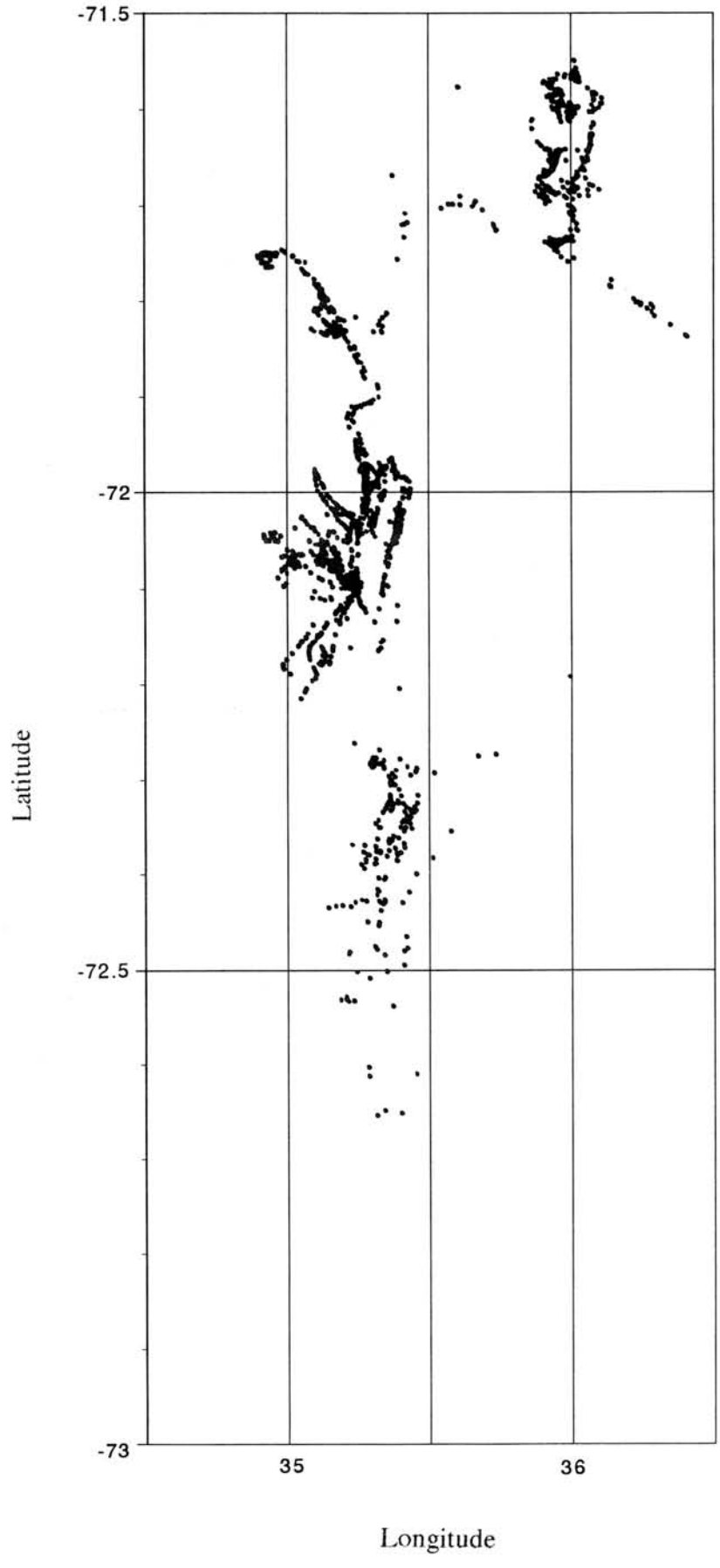

Diffuse Reflectance Spectra in the UV-VIS-NIR Wavelength Region of YAMATO 75258 (LL6) Heated at Different Oxygen Fugacities: Relationship between Spectral and Mineralogical Changes.

Mutsumi Komatsu, Masamichi Miyamoto, and Takashi Mikouchi
Dept. of Earth and Planetary Science, Graduate School of Science, University of Tokyo
(mutsumi@space.eps.s.u-tokyo.ac.jp).

Introduction

Reflectance spectral studies of experimentally heated meteorites have been done in order to examine possible thermal metamorphism of asteroids [e.g., 1]. Recently, we have investigated the spectral changes of the Y75258 LL6 chondrite heated at different oxygen fugacities and demonstrated that the spectra of the sample heated under two log units above the IW buffer (IW+2) show the changes characterized by low spectral contrast and low reflectance in comparison with the unheated samples [2]. In this abstract we report our initial examination of textural and compositional changes observed for the heated LL6 chondrite under different oxygen fugacities in order to identify the responsible phases(s) that affected the spectra.

Experimental Procedures

We studied Y75258 (LL6) chondrite supplied by NIPR. A small rock chip was ground in a pestle to pass through a 100 ì m sieve. A pellet of about 80 mg was placed in Pt-foil and heated to temperatures of 700 and 800 °C, and held for 48 hours in a vertical 1-atm H_2/CO_2 gas-mixing furnace at constant oxygen fugacities of $\log fO_2$ = IW-1 and IW+2. The reflectance spectra were acquired using the JASCO UV-Visible-Near IR spectrophotometer. The samples were measured relative to halon, at an incidence angle of 30° and a reflection angle of 30°. We also analyzed the powdered samples (both unheated and heated) by Hitachi S-4500 FEG-SEM. Chemical analyses of the samples were acquired using the JEOL JX-733 and JX-840A electron microprobes.

Results

Major constituent minerals in Y75258 are olivine, low-Ca pyroxene, (Fe, Ni) metal (mostly taenite and rare kamacite), and troilite. Plagioclase and high-Ca pyroxenes are not abundant. As is expected from its high petrologic type, both olivine and low-Ca pyroxene are homogeneous in their major element compositions (olivine: Fa_{32-33}, pyroxene: $Fs_{24-25}Wo_{1.9-2.3}$). Na-rich plagioclases occur as small grains.

There is little difference in composition of olivine and low-Ca pyroxene between heated samples and unheated samples. Average Fa content of olivine in both unheated and heated samples is $Fa_{32.5}$, while average Fs content of low-Ca pyroxene is $Fs_{24.5}$.

<Heated samples at $\log fO_2$=IW+2>

Fig.1 shows the diffuse reflectance spectra of the samples heated at 700°C and 800°C under the oxygen fugacity of $\log fO_2$=IW+2. The spectrum of the unheated sample is also shown for comparison and all spectra are scaled to 1.0 at 560nm. The spectra of the heated samples show lower spectral contrast and lower reflectance at 560 nm compared with the unheated sample (Fig.2).

SEM and microprobe analyses reveal that olivine and pyroxene in the samples heated at 700 °C and 800 °C show no obvious difference from the unheated sample in both microscopic appearance and compositions. Only the opaque minerals such as (Fe, Ni) metal and troilite appear to have changed during heating. In the sample heated at 700 °C, magnetite and hematite are observed as well as (Fe, Ni) metal. No troilite is found. Some olivine and low-Ca pyroxene grains are enclosed within magnetite and hematite. In

the sample heated at 800 °C, (Fe, Ni) metal, magnetite, hematite and small amount of an Fe-Ni-S phase are observed. No troilite is observed in this sample, as it is absent in the 700 °C sample. Magnetite and hematite enclose olivine and low-Ca pyroxene, and commonly include large vesicles (Fig. 3). The Fe-Ni-S phase is rimmed by magnetite (Fig. 4). It is unclear whether it is crystalline or not, but its variable Fe/Ni ratio suggests that it is amorphous.

<Heated sample at logfO_2=IW-1>

The reflectance spectrum of the heated sample at 800 °C shows slightly higher reflectance compared to that of the unheated sample (Fig.2).

Olivine and pyroxene in the samples heated at 700 °C and 800 °C show no obvious difference from the unheated sample like the samples heated at logfO_2=IW+2. Both Ni-free iron and (Fe, Ni) metal are found in the heated sample at 800 °C. We do not find troilite in this sample. (Fe, Ni) metal shows little change in texture and composition from an unheated sample. Ni-free iron grains show a unique spongy structure, which is absent in the IW+2 samples.

Discussion

Because troilite is the only phase absent in the heated samples at both IW+2 and IW-1, it may be a key phase to understand the observed textural change. Evaporation study of troilite by Tuchiyama et al. showed that troilite began evaporation as low as 600°C to form sulfide-free iron under H_2-rich conditions. In our experiment, one of the most remarkable observations in the heated samples at IW+2 is that a mixture of magnetite and hematite shows a unique texture that appears to penetrate into grain boundaries of the adjacent silicate fragments (Figs. 3 & 4). In contrast, such a texture is absent in the sample heated at IW-1. Instead, Ni-free iron with a spongy structure that is similar to the iron texture shown in [3] is present.

The presence of these different phases at different oxygen fugacities may be explained by evapolation of S from troilite as low as 700 °C at logfO_2 of IW+2. Magnetite and hematite may be formed from molten FeS under the oxidizing condition of IW+2.

The spectra of Y75258 sample heated at the IW+2 condition show low spectral contrast and low reflectance at 560 nm in comparison with the unheated sample, nevertheless little change is shown in the spectra of IW-1 samples. Miyamoto et al. [4] showed that addition of a few percent of magnetite to the Y75258 sample lowers the reflectance and significantly reduces the spectral contrast. The formation of magnetite and hematite The results of our heating experiments imply that the low spectral contrast of samples heated at the IW+2 condition can be attributed to the replacement of troilite by magnetite and hematite. It is not clear whether the process observed in this study had really occurred on the LL chondrite parent body. However, our results suggest that iron which is produced by troilite decomposition affect its spectral characteristics when it is heated at the temperature range700-900°C.

References: [1] Hiroi T. et al. (1996) *Meteorit. and Planet. Sci.*, 31, p321. [2] Miyamoto M. et al. (2000) *Proc. 33rd ISAS Lunar Planet. Symp.*, CD-ROM #1261 [3] Tsuchiyama et al. (1993) *Antarct. Meteorites*, 18, p121. [5] Miyamoto M. et al. (1982) *Mem. of NIPR 25, Antarct. Meteorites, 3*, 55.

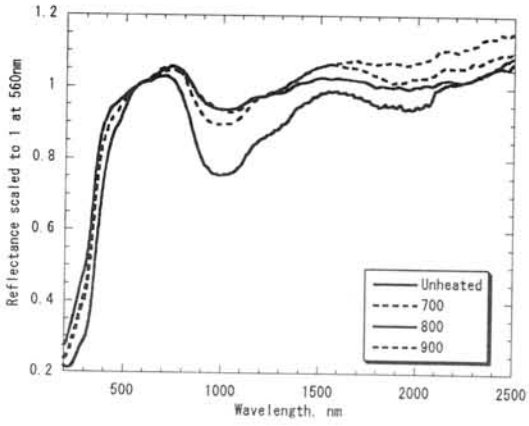

Fig.1. Diffuse reflectance spectra of the Y75258 LL6 chondrite. The spectra are scaled to 1.0 at 560nm and offset for clarity. The Reflectances at 560 are: unheated; 0.30; 700°C, 0.29 ; 800 °C, 0.24.

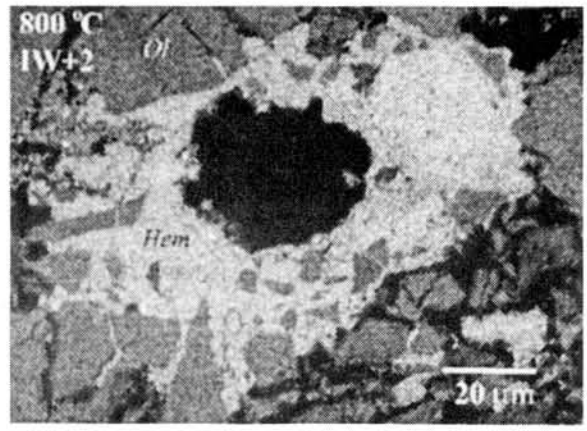

Fig.3. BSE image of the hematite(Hem) grain(s?) in the sample heated at 800°C (IW+2). Fragmental olivine grains are scattered within hematite. A large vesicle is present in the center of hematite. Ol;olivine.

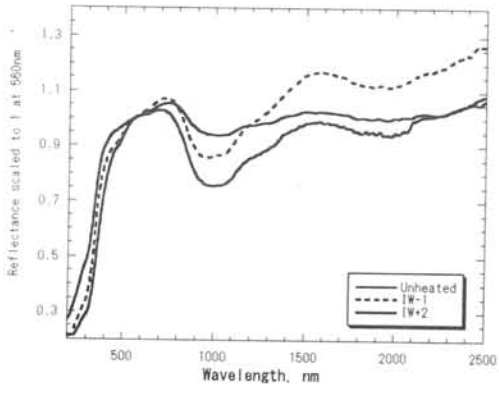

Fig.2. Diffuse reflectance spectra of the Y75258 LL6 chondrite heated at 800°C under the condition of IW+2 and IW-1. The reflectances at 560nm are unheated; 0.30; IW+2; 0.26, IW-1; 0.3.

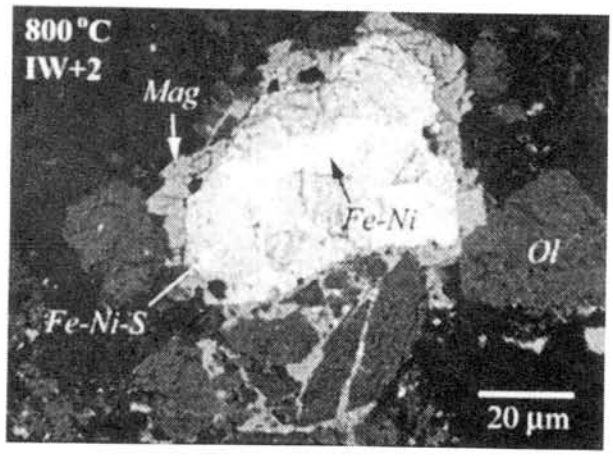

Fig.4. BSE image of Fe-Ni-S phases in the sample heated at 800oC (IW+2). The mixture of Fe-Ni metal and Fe-Ni-S phase (Fe-Ni-S) is rimmed by magnetite. Ol; olivine.

Three-dimensional structure of a radial pyroxene chondrule using X-ray microtomography.

KUSAKA Hiroto[(1)*], TSUCHIYAMA Akira[(1)], NOGUCHI Takaaki[(2)], UESUGI Kentaro[(3)], NAKANO Tsukasa[(4)]

(1) Department of Earth and Space Science, Osaka University, 1-1 Machikaneyama-cho, Toyonaka 560-0043, JAPAN, *kusaka@ess.sci.osaka-u.ac.jp (2) Materials and Biological Sciences, Ibaragi University, Bunkyo 2-1-1, Mito 310-8512, JAPAN, (3) Japan Synchrotron Radiation Research Institute, Mikaduki, 679-5198, JAPAN, (4) National Institute of Advanced Industrial Science and Technology, Tsukuba, 305-8567, JAPAN.

Introduction

Chondrule is defined to be a spherical object formed from either fully or partially molten droplet of silicate by rapid cooling process. Chondrules, the most abundant constituent of chondrite, size from 0.1mm to 1mm, contain a record of many important features of the solar nebula. The major internal textures of chondrules are prophyritic (P), barred olivine (BO) and radial pyroxene (RP). P chondrules were partially molten, while BO and RP chondrules were fully molten. X-ray computed tomography (CT) using synchrotron radiation (SR) can provide three-dimensional structures in high resolution without breaking samples. Kawabata et al. [1] revealed that parallel sets of olivine plates in BO chondrules are nearly perpendicular to the minor axes of their oblate shapes. They proposed that these features were the result of spinning of the chondrules as well as concentration of voids along the minor axes of some P chondrules. However, three-dimensional structure of RP chondrule has not been known. In this study, the structure was examined by X-ray CT method to obtain new information during their formation.

Sample and experimental procedure

The proportion of RP chondrules is relatively high in ordinary chondrites. We used the Bjurböle meteorite (L4) because chondrules are easily removed from the meteorite.

Thirty-two chondrules were imaged by a micro focus X-ray CT scanner (ELESCAN, NX-LCP-c80-I(4)-0) at Osaka University as a first step to select suitable candidates for detailed study by an X-ray CT system using SR, which has better spatial and contrast resolution [2]. They were mounted into cylinders of epoxy (about 3mm in diameter) to reduce artifacts of CT images and to reserve the slice directions.

These samples were imaged at SPring-8 of SR facility in Japan. Monochromatic beam of 25keV was used. Cross-sectional images were reconstructed from 360-720 projections with a convolution back projection method. Each CT image has a contrast, which corresponds to the X-ray linear attenuation coefficients of materials. Three-dimensional structures were reconstructed from successive CT images with the voxel size of $5.83 \times 5.83 \times 5.83\ \mu$m, which gives spatial resolution of about $13\ \mu$m [2].

At least one chondrule was recognized as a RP chondrule (the diameter is about 1.6 mm). This was thin-sectioned as parallel as possible to the sliced direction of the CT images. The thin sections were observed under a polarized optical microscope and a scanning electron microscope (SEM). The chemical compositions were analyzed with an electron probe micro analyzer (EPMA). A three-dimensional plaster figure of the RP chondrule was also formed by rapid prototyping method.

Results

Examples of the CT images of the RP chondrule are shown in Figure 1, where bright and dark bands are pyroxene and mesostasis, respectively. Observation of the thin sections under an optical microscope showed that each elongated pyroxene is a single crystal of orthopyroxene and the crystal direction changes successively. The chemical analysis showed that the pyroxene crystals are uniform with the composition of $En_{78}Wo_1$. The mesostasis were composed of microcrystalline silicates, Fe-Ni alloys and Fe sulfides. Three-dimensional structure of the RP

chondrule was obtained from 323 slices (Fig. 2). In some CT images four straight lines were drawn along the elongational directions of the mesostasis parallel to the pyroxene crystals (Fig. 3). A three-dimensional image, which includes these lines (Fig. 4), showed that the RP chondrule consists of a radial set of planar pyroxene crystals three-dimensionally. These pyroxene plates are also recognized on the surface of the chondrule. The surface of the plaster figure (Fig. 5) showed that this chondrule consists of at least eight sets of the radial plates with different directions.

Discussion

So far, RP crystals were believed to be radial sets of needles (e.g., [3]). The present result is different from the previous RP texture model. One possibility is that all of RP crystals are planar. However, some chondrules in thin sections shows a set of dotted pyroxene crystals, which may be cut nearly perpendicular to the needle crystals. The pyroxene crystals in the present RP chondrule are generally coarser than those in other RP chondrules. Accordingly, there is another possibility that fine crystals are needle and coarse ones are plates. This should be examined for further study by imaging more RP chondrules.

The lines along the pyroxene plates have a focus point in each CT image (Fig. 3). Three-dimensionally, each focus point is aligned on a line forming a focus line. As shown in Figure 4, the focus line is located clearly in the outside of the chondrule. It is reasonable that the radial set of pyroxene plates was formed by nucleation on the focus line. If this is the case, the chondrule has been abraded after crystallization. Another possibility is that the nucleation for the RP has not occurred on the focus line although mechanism of RP plates formation is not clear at present.

Acknowledgment: We are grateful to Smithsonian Natural Museum for providing chondrule samples used in the present study.

References: [1] Kawabata et al. (1999) Antarctic Meteor. **XXIV**, 64-66. [2] Uesugi et al. (1999) Proc. SPIE, **3772**, 214-221. [3] Kitamura et al. (1983) Earth Planet. Sci. Lett., **63**, 189-201.

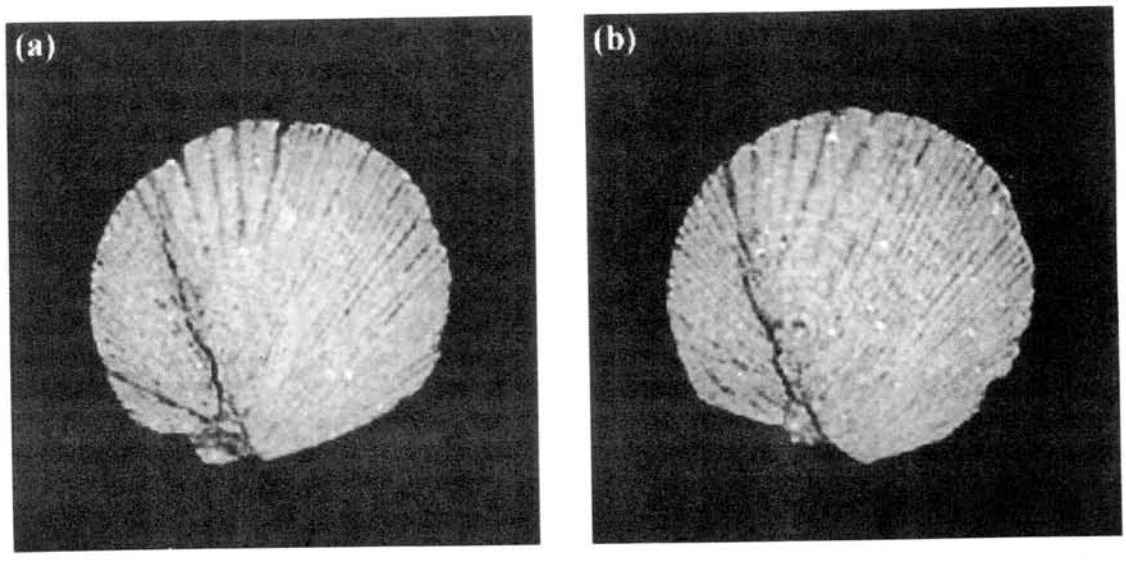

Figure 1: Examples of X-ray CT slice images of a RP chondrule removed from the Bjurböle chondrite (L4). Pyroxene (bright gray), mesostasis (dark gray), Fe-Ni alloy or Fe sulfide (white) and crack (black) are seen. The width of each figure is 2.3mm. (a) Slice number-140. (b) Slice number-160.

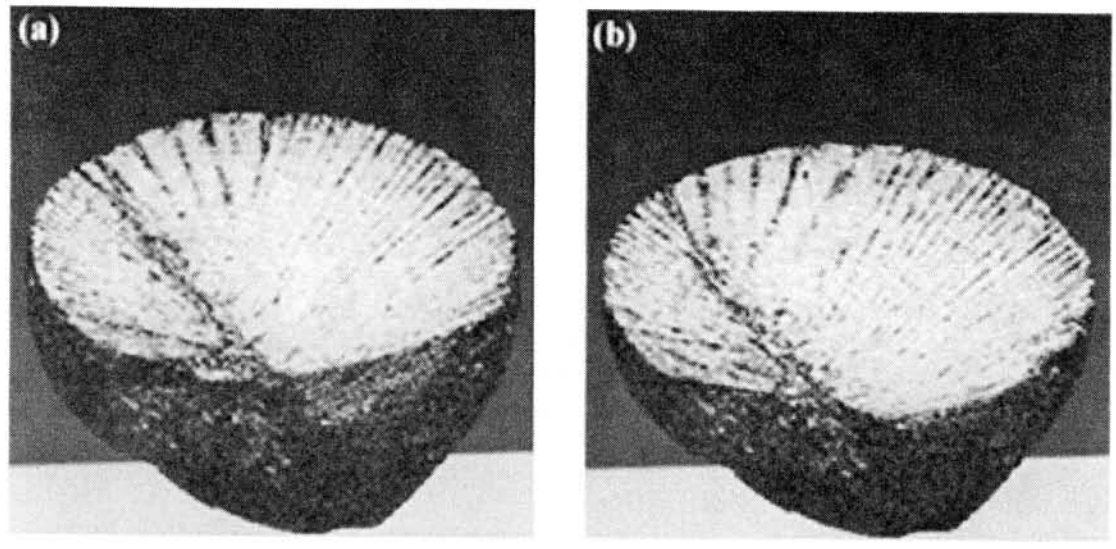

Figure 2: Three-dimensional structure of the RP chondrule. Each cut surface corresponds to the CT slice image in Figure 1.

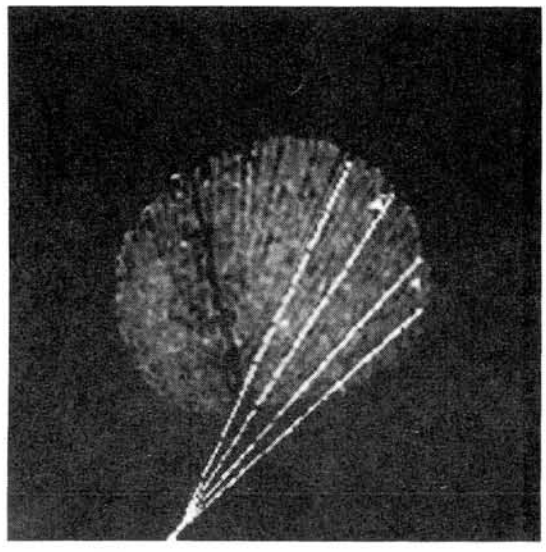

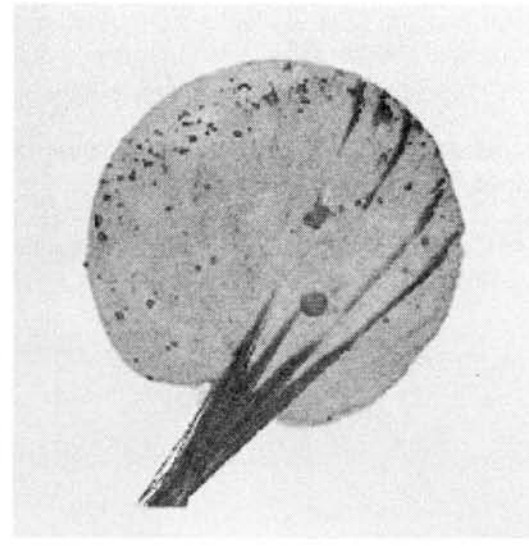

Figure 3 (left): Four lines along elongated directions of mesostasis, which is parallel to the pyroxene crystals. Extensions of these lines have a focus point.
Figure 4 (right): Three-dimensional structure including lines parallel to pyroxene crystals in Fig.3. The focus line is located outside the chondrule.

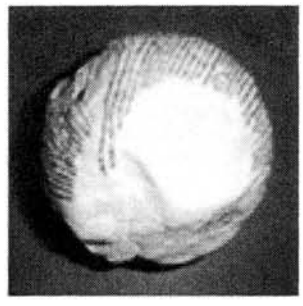

Figure 5: A three-dimensional plaster figure of the RP chondrule viewed from the same angle as Fig. 4. Lines on the surface are pyroxene plates.

PRESOLAR GRAINS IN THE QINGZHEN (EH3) METEORITE

Yangting Lin[1], Sachiko Amari[2] and Olga Pravdivtseva[2]

[1]Guangzhou Institute of Geochemistry, Chinese Academy of Sciences, Guangzhou 510640, China.
[2]Laboratory for Space Sciences and Physics Dept., Washington University, St. Louis, MO 63130-4899, USA.

1. INTRODUCTION

Presolar grains in enstatite chondrites may play a key role of clarifying their distribution in the primitive solar nebula. However, up to date, only limited studies have been conducted on presolar grains in enstatite chondrites. The most intensively studied meteorite is Indarch (EH4) which experienced significant asteroidal metamorphism. The majority of SiC grains in enstatite chondrites have isotopic compositions of C, N and Si within ranges of the mainstream type in the Murchison (CM2) meteorite, and only five grains of rare Type X SiC were confirmed so far [1,2]. Most Si_3N_4 in enstatite chondrites have normal isotopic compositions [1,3-5], different from those in carbonaceous and ordinary chondrites [6]. Recently, Besmehn et al [2] reported three presolar Si_3N_4 grains from Indarch. In addition, most SiC grains in Indarch are submicron-sized, smaller than in Murchison [1,7,8].

Qingzhen (EH3) is one of the most primitive enstatite chondrites [9,10], hence best suited to study preserved presolar material from the most reduced location of the nebula. Here we report preliminary results of presolar grains isolated from Qingzhen.

2. RESULTS

From 28 grams of the sample, 2 mg of nano-diamond were isolated, indicative of a bulk content of 72 ppm. Bulk abundance of the final etched residue is 17.9 ppm, consisting predominantly of spinel, SiC and Si_3N_4, with minor Al_2O_3. Submicron-sized baddeleyite, and a few grains of TiC (several μm in size) were also identified using SEM equipped with an ultra-thin Be window. SEM observation of the etched residue showed size-dependent fractions of spinel, SiC and Si_3N_4. For grains >1 μm, ratio of spinel: Si_3N_4: SiC: Al_2O_3 is 21:13:5:1. The smaller grain size, the more abundant SiC. For grains < 0.3 μm, SiC is predominant.

Ion mapping of the etched residue was conducted on only two size fractions, namely QZR5 (0.8-2 μm) and QZR 4 (0.4-0.8 μm), using $^{12}C^-$, $^{13}C^-$, $^{16}O^-$, $^{18}O^-$, $^{28}Si^-$, and $^{30}Si^-$. Four out of 23177 O-rich grains of QZR4, 2 out of 31233 of QZR5 were ^{18}O-deficit. The ^{18}O-deficit candidates have very low intensities of $^{16}O^-$, suggestive of rather small grain sizes in comparison with the predominant normal grains. Twenty-four out of 20425 Si-rich grains of QZR4, 32 out of 17492 of QZR5 showed significant ^{30}Si-deficits. High mass-resolution analyses of C, N and Si isotopes were carried out for the ^{30}Si-deficit candidates. All 32 candidates from QZR5 fraction were confirmed to have C, N and Si isotopic compositions similar to type X of SiC from Murchison. Of them, 26 grains are SiC, and the other 6 grains are Si_3N_4. This is the first report of presolar Si_3N_4 in an enstatite chondrite. Only 16 out of 23 candidates from QZR4 were analyzed for C, N and Si isotopes, confirming 10 grains of type X SiC, 3 grains of type X Si_3N_4 and 3 grains of mainstream SiC. In addition, 32 random selected SiC grains were also analyzed; their isotopic compositions of C, N and Si overlap with the mainstream SiC of Murchison. Only one grain has low $^{12}C/^{13}C$ (4.7±0.1) similar to Type A. Another five randomly selected Si_3N_4 grains of QZR5 showed normal isotopic compositions of C, N and Si.

The X-SiC grains tend to cluster into two subtypes in $\delta^{29}Si/^{28}Si$-$\delta^{30}Si/^{28}Si$ diagram. The majority (27 out of 36 grains) overlaps with those from Murchison and other chondrites, plotting on a line with a slope of 0.77. The other 9 grains (25% of the total) plot on a mixing line between the solar material and predicted Si/O zone of a supernova II with 25 Sun mass.

We describe the majority of X-SiC as subtype X1 and the other ^{29}Si-deficit grains as subtype X2. All 9 grains of subtype X2 are ^{13}C-deficient, while 4 out of 27 grains of subtype X1 are ^{13}C-enriched relative to solar. Most presolar Si_3N_4 grains (6 out of 9) have the same Si and N isotopic compositions of subtype X1 SiC, except one on the mixing line between the pure ^{28}Si and the solar components and another grain with significant ^{29}Si-enrichment. However, all 5 analyses of C isotopes of the presolar Si_3N_4 are normal or slightly anomalous (^{12}C/^{13}C: 44±5~98±19).

3. DISCUSSION AND CONCLUSIONS

This is the first report of X-SiC in Qingzhen, and it increases the total of X-SiC in enstatite chondrites to 41 grains up from the previous five reported in Indarch [1,2]. The abundance of X-SiC is ~1/400 relative to SiC, after correction for Si_3N_4. This is about a factor of four lower in comparison with Murchison SiC (~1%). The low abundance of X-SiC was confirmed by results in Indarch, which suggested a ratio of 1/1000 based on discovery of two grains of X-SiC [2]. Furthermore, 25% of X-SiC grains in Qingzhen showed evident ^{29}Si-deficit relative to ^{30}Si, and they are referred to as subtype X2. In contrast, only 11 out of 169 X-SiC grains in Murchison (based on data of WU and [11]) plotted within the range of subtype X2, much less abundant than in Qingzhen. The distinct isotopic compositions of Si and C between subtypes X1 and X2 probably suggest different interstellar sources. Regardless of low abundance of presolar Si_3N_4 in Qingzhen, its Si_3N_4/SiC ratio of Type X (9/36) is higher than that of Murchison (1/30) [6] and Acfer 094 (5/60) [12]. Besmehn et al. [2] reported 3 grains of presolar Si_3N_4 with 2 grains of X-SiC from Indarch, suggestive of an even higher ratio.

High mass-resolution analyses of O isotopes have not yet been conducted on the ^{18}O-deficient candidates. However, its ratio to O-rich refractory grains (spinel, Al_2O_3), referred to as maximum ratio of presolar oxides, is about 1/10000, at least a order of magnitude lower in comparison with Murchison. Only one ^{18}O-deficit spinel was found by ion mapping ~1000 O-rich grains [1]. However, the candidate was not analyzed under high mass-resolution condition. Such a low abundance of presolar oxides in enstatite chondrites is somewhat surprising, because these reduced meteorites contain much less Ca-Al-rich inclusions in comparison with Murchison, which would dilute presolar oxides.

An explanation for differences of presolar grains between enstatite chondrites and Murchison is a size sorting process in the nebula, because majority of SiC grains in enstatite chondrites are submicron-sized, distinctly smaller than those in Murchison. However, this may not be true if we compare the above observations of the 0.4-2 μm size fractions of Qingzhen SiC with those of Murchison grains with size of 0.5-1.5 μm [11]. Asteroidal metamorphism probably destroyed small presolar grains, but not selectively the rare types that did not show size-dependent abundances. Another possibility is heterogeneous distribution of presolar grains in the primitive nebula, since enstatite chondrites and Murchison formed under very different nebular conditions.

References: [1]X. Gao, et al. *Meteoritics.* 1995, **30**, 508. [2]A. Besmehn & P. Hoppe. *LPSC.* 2001, **32**, #1188. [3]M. R. Lee, et al. *Meteoritics.* 1992, **27**, 248-249 (abstr.). [4]C. M. O. D. Alexander, et al. *Meteoritics.* 1994, **29**, 79-84. [5]S. S. Russell, et al. *MPS.* 1995, **30**, 399-405. [6]L. R. Nittler, et al. *Astrophysical Journal Letters.* 1995, **453**, L25-L28. [7]S. S. Russell, et al. *Meteoritics.* 1993, **28**, 425. [8]S. S. Russell, et al. *Meteoritics.* 1997, **32**, 719-732. [9]Y. Lin (1991) Qingzhen enstatite chondrite (EH3): Petrology, mineral chemistry and evolution. Chinese Academy of Sciences, Guiyang. [10]A. El Goresy, et al. *Proc. NIPR Symp. Antarct. Meteorit.* 1988, **1**, 65-101. [11]P. Hoppe, et al. *MAPS.* 2000, **35**, 1157-1176. [12]X. Gao, et al. *MAPS.* 1996, **31**, A48 (abstr.).

GENETIC RELATIONS BETWEEN CHONDRITES AND IRON METEORITES: EXPERIMENTAL RESEARCH

A.A.Marakushev*, Yu.B.Shapovalov*, O.V.Chaplygin**

**Institute of Experimental Mineralogy, Russian Academy of Sciences, Chernogolovka, Moscow District, 142432 Russia; **Chair of Petrology, Geological Department, Moscow State University, Vorob'evy Gory, 119899 Moscow, Russia*

The problem of genetic interrelations between chondrites and iron meteorites appeared after studying of octahedrite Netschaevo. Inclusion of Fe-rich chondrite and chondrules were found in this sample for the first time: "Chondrules: first occurrence in an iron meteorite" (Olsen, Jarosevich, 1971). Extremely rich in Fe HH-chondrites are of particular interest as their composition is similar to the calculated composition of the planet Earth. This fact serves as the basis to "chondrite model" of Earth formation. Such extremely rich in Fe chondrite (Fe = 24.77, FeO = 8.82, FeS = 3.70 wt.%) was described in Netschaevo meteorite as a silicate inclusion. The silicate chondrules consist of bronsite ($Mg_{0,85}Fe_{0,15}SiO_3$), olivine ($Mg_{1,79}Fe_{0,29}SiO_4$), plagioclase ($Na_{0,78}Ca_{0,16}K_{0,06}Al_{0,16}Si_{2,84}O_8$) and diopside ($Ca_{0,91}Mg_{0,98}Fe_{0,11}Si_2O_6$) and contain chromite ($Fe_{0,79}Mg_{0,21}Al_{0,5}Cr_{1,5}O_4$), vitlockite ($Ca_{2,7}Mg_{0,3}P_2O_8$) and graphite.

The suggested model of formation of this chondrite and the iron meteorite Netschaevo which contains the chondrite is showed on a diagram (fig. 1). The development of liquid immiscibility in initial chondrite melt (*1* in fig. 1) accounted for their formation. As a result of immiscibility silicate chondrules (*4*) separated from metal nickel-iron phase (*3*) which formed a matrix in the chondrite part of the meteorite, along with separating of some Fe in the iron meteorite.

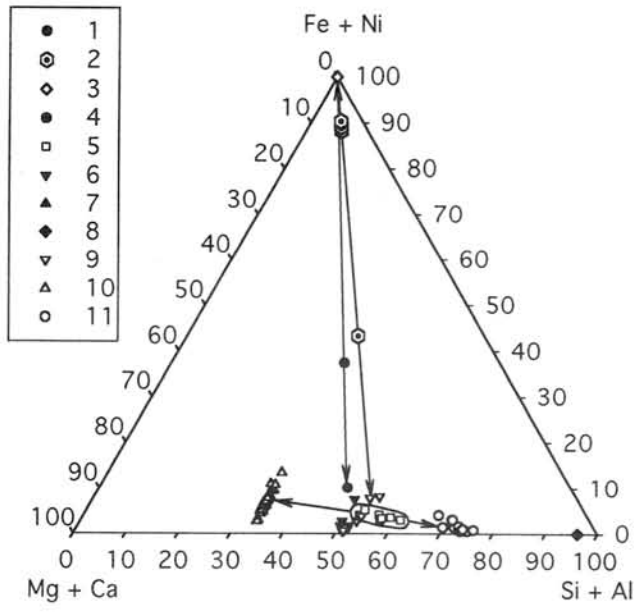

Fig.1. The suggested model of formation of chondrite Netschaevo marked by divergent arrows (3←1→4) and its experimental basis (3←2→5). *1,2* – bulk compositions of the meteorite (*1*) and experimental mixtures (*2*); *3–5* – products of their splitting: nickel-iron phase (*3*), silicate phases of the meteorite (*4*) and experimental silicate phases (*5*); *6–11* – products of their consolidation: *6–8* – pyroxene (*6*), olivine (*7*) and plagioclase (*8*) of the meteorite, *9–11* – experimental pyroxene (*9*), olivine (*10*) and glass (*11*).

To confirm this model we have carried out special experimenal research. We used iron-silicate mixtures composed of picrite glass and chemical reagents – Fe, Ni and S. The compositions of the mixtures compared with Netschaevo chondrite (HH) and the average compositions of H, L and LL chondrites are given in table. Experimental mixtures placed in graphite tubes were hold at 1200°C during one hour and then quenched on the air. Presence of graphite tubes proved the reducing regime and necessary addition of some carbon to the melt which is characteristic to the chondrite magmas.

Table. Compositions of ordinary chondrites and the mixtures used in experiments, wt.%

oxide	chondrites				experimental mixtures						
	LL	L	H	HH	1	2	3	4	5	6	7
Fe	3.41	7.72	17.27	24.97	36.00	80.00	65.00	60.00	68.00	78.00	84.00
Ni	0.96	1.12	1.58	2.52	2.00	0.00	13.00	10.00	8.00	6.00	2.00
Co	0.05	0.06	0.08	0.10	-	-	-	-	-	-	-
FeS	5.91	6.19	5.36	3.73	-	-	-	-	-	-	-
S	-	-	-	-	2.00	10.00	12.00	20.00	14.00	6.00	4.00
SiO_2	39.62	39.99	36.61	32.63	28.26	4.71	4.71	4.71	4.71	4.71	4.71
TiO_2	0.19	0.15	0.13	0.21	0.48	0.08	0.08	0.08	0.08	0.08	0.08
Al_2O_3	2.22	2.32	2.44	1.83	5.49	0.92	0.92	0.92	0.92	0.92	0.92
Cr_2O_3	0.30	0.44	0.36	0.59	0.00	0.00	0.00	0.00	0.00	0.00	0.00
FeO	17.81	13.16	8.89	8.89	6.09	1.01	1.01	1.01	1.01	1.01	1.01
MnO	0.32	0.27	0.25	0.35	0.01	0.00	0.00	0.00	0.00	0.00	0.00
MgO	25.56	24.96	23.54	19.81	14.50	2.42	2.42	2.42	2.42	2.42	2.42
CaO	1.97	1.91	1.82	1.65	3.79	0.63	0.63	0.63	0.63	0.63	0.63
Na_2O	0.88	0.88	0.85	0.77	0.98	0.16	0.16	0.16	0.16	0.16	0.16
K_2O	0.21	0.14	0.14	0.19	0.34	0.06	0.06	0.06	0.06	0.06	0.06
P_2O_5	0.22	0.26	0.23	0.54	0.06	0.01	0.01	0.01	0.01	0.01	0.01
H_2O	0.37	0.34	0.33	0.98	-	-	-	-	-	-	-
C	-	0.09	0.10	0.21	-	-	-	-	-	-	-

Note: LL, L, H – average compositions, HH-chondrite – silicate inclusion in the iron meteorite Netschaevo.

All experiments clearly showed liquid immiscibility in melts peculiar to the chondrite magmatism, although structural relations of metal and silicate phases differ depending on the compositions of the initial mixtures. When composition is close to the chondrite Netschaevo (#1 in table and symbol in the middle of the diagram, fig. 1) liquid immiscibility appear as metal drops in silicate matrix. However in chondrites we observe the opposite relations – emulsion of silicate drops (chondrules) in a matrix enriched with Fe and Ni. In conducted experiments such chondritic structure was obtained only in melts with iron–silicate ratio much greater than in chondrites. Bulk compositions of the chondrules (fig. 2), allocated in the Ni-Fe matrix are similar to the silicate phase of Netschaevo meteorite in their position on the diagram and by composition of crystallizing minerals (pyroxene and olivine). The only difference is the degree of crystallization. There is monoclinic Ca-pyroxene and plagioclase in Netschaevo chondrules instead of the residual glass of the same composition in experiments. Minerals obtained in experiments are zoned as a rule. The cores of olivine grains have composition close to $Mg_{1.71}Fe_{0.29}SiO_4$ and the rims are richer in Mg – $Mg_{1.85}Fe_{0.15}SiO_4$. Pyroxene grains are smaller and more homogeneous ($Mg_{1.30}Fe_{0.05}Ca_{0.65}Si_{1.98}Ti_{0.02}O_6$). The resemblance is not only in mineral composition but also in structural peculiarities of the chondrules and in compositions of the silicate phases.

The fact that the chondritic structure formed only in melts highly rich in Fe could be the evidence that formation of chondrites (of HH-type at least) is connected to the formation of iron meteorites and pallasites. Experimentally proved iron – silicate (chondrule – matrix) splitting of melts corresponded to splitting into the iron and iron-silicate (HH-chondrite) phases in the natural samples. The combination of iron meteorite (octahedrite) and Fe-rich HH-chondrite is described in Netschaevo meteorite. Probably, this could be the evidence of presence of iron and pallasite cores even in the planets of the most primitive (chondritic) level of evolution. This planets underwent explosive disintegration in the asteroid belt – the only source of chondrites. In any case iron meteorites and pallasites enter all chondrite families in the system of genetic groups based on oxygen isotopes (Marakushev et al., 2000). In these

families iron meteorites placed in areas of chondrites enriched with light oxygen isotope (fig. 3). Besides meteorite Netschaevo ($\delta^{17}O$ = 2.21, $\delta^{18}O$ = 3.53‰) meteorites Steinbach ($\delta^{17}O$ = 3.50, $\delta^{18}O$ = 4.49‰), Sao Joao Nepomuceno ($\delta^{17}O$ = 3.39, $\delta^{18}O$ = 4.09‰) and Elga ($\delta^{17}O$ = 3.10, $\delta^{18}O$ = 4.65‰) also related to the family of ordinary chondrites (H–L). Meteorite Deep Springs ($\delta^{17}O$ = –2.96, $\delta^{18}O$ = 0.27‰) – to the family of enstatite and forsterite chondrites (F–E) and pallasites Eagle Station ($\delta^{17}O$ = –5.96, $\delta^{18}O$ = –2.78‰) and Itzawisis ($\delta^{17}O$ = –6.33, $\delta^{18}O$ = –2.82‰) belong to the family of carbonaceuous chondrites and ureilites. All these primitive iron meteorites and pallasites result from iron – silicate splitting of melts closely connected with formation of chondrites. However most of the iron meteorites and pallasites form their own family (I–Pal) clearly isolated from all chondrite families and connected to the family of achondrites (Dio–Euc). This reflects their relation to the later stages of stratification of planets and their sattelites.

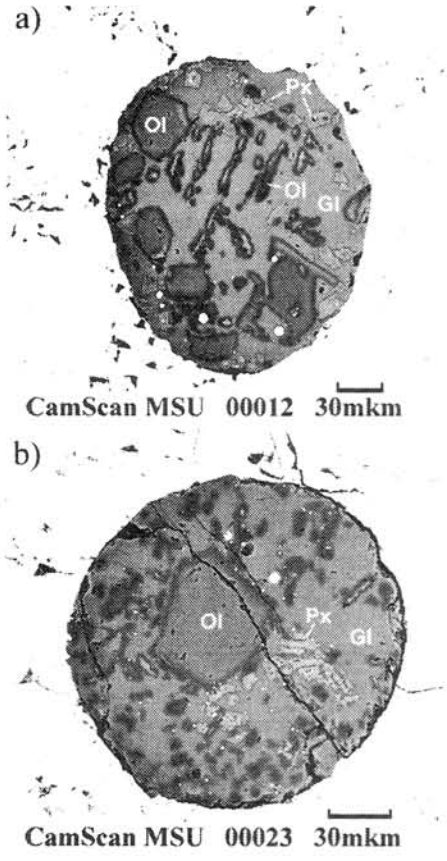

Fig. 2. Experimental chondrules enclosed in sulphide-nickel-iron matrix. Chondrules consist of olivine (Ol), pyroxene (Px) and glass (Gl) and characterized by barred olivine stucture (a) along with porphiric structure (b). Small sulphide-iron drops can be seen in the glass.

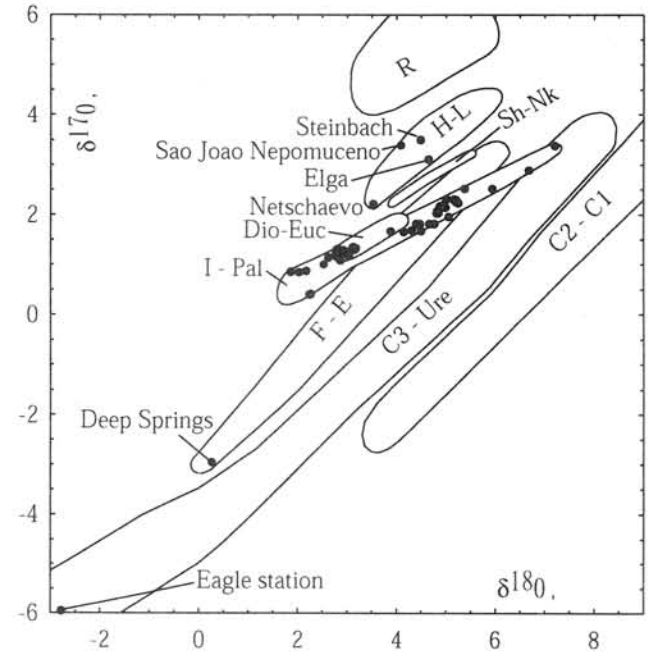

Fig. 3. Iron meteorites and pallasites (black circles) in the system of genetic groups of meteorites on a three oxygen isotope plot. The families of Rumuruti-chondrites (R), ordinary chondrites (H-L), forsterite and enstatite chondrites (F-E), shergottites, nakhlites and chassignites (Sh-Nk), diogenites, eucrites and howardites (Dio-Euc), carbonaceous chondrites C3 and ureilites (C3-Ure) and carbonaceous chondrites C2 and C1 (C2-C1) are shown by contours. Iron meteorites and pallasites which belong to the families of chondrites are named. Irons shown without names form their own group (I-Pal).

References:

Olsen E., Jarosevich E. Chondrules: the first occurence in an iron meteorite. – Science. 1971. V. 174. P. 583-585.

Marakushev A.A., Chaplygin O.V. and Bobrov A.V. Petrology of the meteorites based on oxygen isotope data. – Vestnik MSU, Series 4 Geology, 2000, N 5, P. 14-30.

Noble gases in the Kobe meteorite: II. Measurements by stepwise heating

Yoshiki Matsumoto[1], Takuya Matsumoto[1], Jun-ichi Matsuda[1] and Noboru Nakamura[2]

[1]*Department of Earth and Space Science, Graduate School of Science, Osaka University, 1-1 Machikaneyama, Toyonaka, Osaka 560-0043*
[2]*Department of Earth and Planetary Sciences, Faculty of Science, Kobe University, Nada-ku, Kobe 657-8501*

INTRODUCTION

About a decade ago, the CK group was defined by Kallemeyn *et al.* [1], but only one meteorite, Karoonda, had been known as a fall CK-normal chondrite until recently. In that situation, the Kobe meteorite fell in 1999 with a rare episode that it penetrated a roof of a house. The preliminary petrological investigation revealed that the Kobe meteorite belongs to the CK-normal group. Provided with two fragments of the meteorite from the finder, the Kobe Meteorite Consortium was organized by leading laboratories in Japan and the U.S.A. in order to elucidate the history and nature of CK chondrites [2]. As members of the consortium, we investigate noble gases in the Kobe meteorite.

In our preliminary study [3], we investigated elemental and isotopic compositions of noble gases in a chip of the Kobe meteorite (C-3-1, 28 mg) by single-step heating. The results showed that it has low concentrations of primordial heavy noble gases and a high $^{129}Xe/^{132}Xe$ ratio, which are consistent with characteristics of CK chondrites reported previously by Scherer and Schultz [4]. We also obtained the calculated cosmic-ray exposure age based on cosmogenic ^{21}Ne (41 Ma) and the K-Ar age (2.1 Ga). These ages are longer than the exposure age based on cosmogenic ^{3}He (12 Ma) and U,Th-^{4}He age (1.0 Ga), respectively, which indicates that Kobe has partially lost both radiogenic and cosmogenic He by solar heating during the time of cosmic-ray exposure. Also, there is an inconsistency in exposure ages derived from ^{21}Ne and ^{38}Ar, which may be strongly influenced by textural inhomogeneity due to the small sample size. On the other hand, there are some anomalies such as high $^{136}Xe/^{132}Xe$ ratio ($^{136}Xe/^{132}Xe$ = 0.377), but we were not able to discuss them in detail from only a single step measurement.

In this study, we investigated a larger mixed sample by step-wise heating in order to eliminate textural inhomogeneity and to obtain more detailed noble gas elemental and isotopic compositions, and discuss cosmic-ray exposure ages, gas retention ages, and isotopic anomalies in Xe.

EXPERIMENTAL PROCEDURE

In this study, we used Kobe C-3mix-1 of 296 mg without chemical treatment. This sample is one of the fractions of C-3 mixture (~1 g). The gases in the sample were extracted by a resistively-heated Ta furnace at the temperatures of 600, 800, 900, 1000, 1100, 1200, 1400, and 1600°C. For the gas fraction of each temperature step, elemental and isotopic compositions of He, Ne, Ar, Kr, and Xe were analyzed by a VG5400 mass spectrometer. An additional gas extraction at 1700°C was carried out, but the amount of each noble gas was less than 1% of the total amount,

indicating complete extraction of noble gases at 1600°C.

The calibration of sensitivity and mass discrimination for the noble gases was made by analyses of aliquots of atmospheric gas of known volume and isotopic compositions and an artificial helium gas mixture ($^3He/^4He = (2.862 \pm 0.049)\times10^{-5}$). The corrections of hot blanks and interference were also made. The detailed procedure is shown in Matsumoto *et al.* [5].

RESULTS

The observed Ne was released from 900 to 1600°C as a pure cosmogenic components ($^{20}Ne/^{22}Ne = 0.83$ and $^{21}Ne/^{22}Ne = 0.93$). Helium was also released from 900 to 1600°C with $^3He/^4He$ ratios constant ($^3He/^4He = 0.038$). Because Ne did not contain trapped gas, the $^3He/^4He$ ratio can be explained by a mixture of cosmogenic ^3He and ^4He and radiogenic ^4He ($(^3He/^4He)_c = 0.2$). On the other hand, the peak of released Ar shifts to higher temperature (Fig. 1a). At the temperatures of 600 and 800°C, extracted Ar can be considered to be trapped air because the ratios of $^{38}Ar/^{36}Ar$ and $^{40}Ar/^{36}Ar$ are close to those of air (Figs. 1a, b). At higher temperatures, extracted Ar can be explained by a mixture of cosmogenic ^{36}Ar and ^{38}Ar, primordial ^{36}Ar and ^{38}Ar, and radiogenic ^{40}Ar ($(^{38}Ar/^{36}Ar)_c = 1.5$, $(^{38}Ar/^{36}Ar)_p = 0.188$).

Most of Kr and Xe were released from 1400 to 1600°C. Isotopic character of Kr shows that the extracted Kr is a mixture of primordial and cosmogenic (including neutron-produced) components [5]. A $^{130}Xe/^{132}Xe$ *vs.* $^{136}Xe/^{132}Xe$ diagram is shown in Fig. 2. From 600 to 900°C, the fractions are influenced by air. From 1000 to 1600°C, the fractions seem to be not a simple mixing of Q and spallogenic components but include fissiogenic component and considerable Xe-HL.

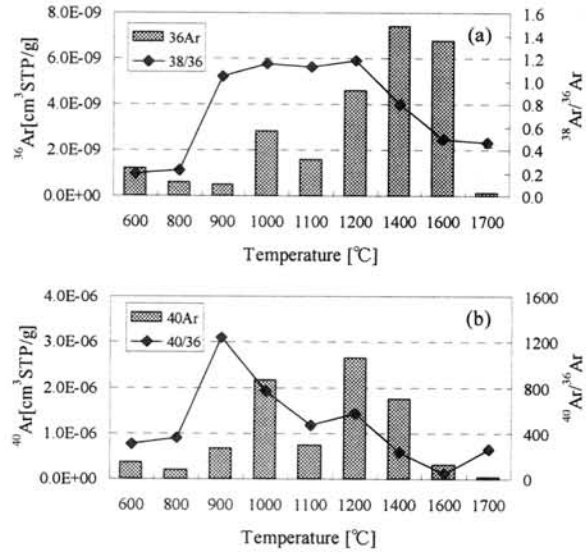

Fig. 1. (a) Release pattern of ^{36}Ar and $^{38}Ar/^{36}Ar$ ratios.
(b) Release pattern of ^{40}Ar and $^{40}Ar/^{36}Ar$ ratios.

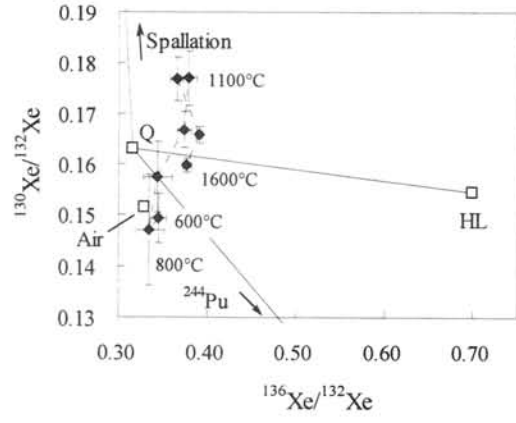

Fig. 2. A diagram of $^{130}Xe/^{132}Xe$ *vs.* $^{136}Xe/^{132}Xe$.

DISCUSSION

Cosmic-ray exposure ages and gas retention ages

We calculated cosmic-ray exposure ages (T_3, T_{21}, and T_{38} from cosmogenic ^3He, ^{21}Ne, and ^{38}Ar, respectively) and U,Th-^4He and K-Ar gas retention ages (T_4 and T_{40}, respectively). Production rates of cosmogenic ^3He, ^{21}Ne, and ^{38}Ar were evaluated by using formulae given in Eugster [6] with the elemental composition of Kobe C [7], Kobe E [8], or mean CK [9].

The obtained exposure ages of T_3, T_{21}, and T_{38} are 14, 38, and 39 Ma, respectively. The previously observed inconsistency between T_{21} and T_{38} ages are not observed, which supports the explanation that the shorter T_{38} age in the previous study is affected by chemical inhomogeneity due to a small sample size. The calculated gas retention ages of T_4 and T_{40} are 1.2 and 3.1 Ga, respectively. The present T_{40} age remains shorter than those of most carbonaceous chondrites (4.6 Ga), indicating that Kobe experienced thermal events such as impact or collision around or less than three billion years age. Also, the present T_3 and T_4 ages remain shorter than T_{21} and T_{40} ages, respectively (T_3/T_{21} = 0.37, T_4/T_{40} =0.41), which can be explained by He loss caused by solar heating during the time of cosmic-ray exposure because both of T_3/T_{21} and T_4/T_{40} are less than one and T_3/T_{21} is nearly equal to T_4/T_{40} [3, 5, 10].

High HL/Q ratio

From Fig. 2, Xe in the fractions from 1000 to 1600°C seems to be a mixture of Q, HL, spallogenic, and fissiogenic components. Therefore, we decomposed the fractions into these four components using the ratios of $^{124}Xe/^{132}Xe$, $^{130}Xe/^{132}Xe$, and $^{136}Xe/^{132}Xe$. There remains no significant excess after the subtraction of the above components from the measured values except for ^{128}Xe at 1600°C and ^{129}Xe at all temperature steps. The excess in ^{128}Xe at 1600°C is possibly derived from neutron capture of ^{127}I. The large excess in ^{129}Xe can be assumed to be a radiogenic component produced from ^{129}I.

The obtained HL/Q ratio of 0.17 (^{132}Xe basis) is much greater than that of AVCC (HL/Q = 0.012). Such a high relative abundance of a HL component has never been reported in total bulk measurements of carbonaceous chondrites. In IAB iron, the graphite nodule in El Taco with a high HL/Q ratio of ~0.2 was reported [11]. It is reported that a shock event can elevate a HL/Q ratio as this preferentially releases Q-gas over HL-gas [12]. However, the estimated shock pressure on Kobe (5-10 GPa; [13]) does not reach the required pressure (>70 GPa) to achieve such a high HL/Q ratio. Therefore, another process in parent body or solar nebula is required to explain the observed HL/Q ratio.

Acknowledgement: We thank Mr. Hirata for providing us with a sample of the Kobe meteorite.

REFERENCES

[1] Kallemeyn *et al.* (1991) Geochim. Cosmochim. Acta, **55**, 881-892.
[2] Nakamura *et al.* (2000) Antarct. Meteorites, **25**, 99-101.
[3] Matsumoto *et al.* (2001) Antarct. Meteorite Res., **14**, 61-70.
[4] Scherer and Schultz (2000) Meteorit. Planet. Sci., **35**, 145-153.
[5] Matsumoto *et al.* Geochem. J., submitted.
[6] Eugster (1988) Geochim. Cosmochim. Acta, **52**, 1649-1662.
[7] Hirota *et al.* (2000) Antarct. Meteorites, **25**, 16-18.
[8] Oura *et al.* (2000) Antarct. Meteorites, **25**, 128-130.
[9] Lodders and Fegley (1998) The Planetary Scientist's Companion.
[10] Eugster *et al.* (1993) Geochim. Cosmochim. Acta, **57**, 1115-1142.
[11] Maruoka (1999) Geochem. J., **33**, 343-350.
[12] Nakamura *et al.* (1997) Lunar Planet. Sci., **28**, no. 1416.
[13] Tomeoka *et al.* (2000) Antarct. Meteorites, **25**, 160-162.

Experimental crystallization of the QUE94201 basaltic shergottite: Support for the Martian Magma hypothesis

G. McKay[2], E. Koizumi[1], T. Mikouchi[1,2], L. Le[3], and C. Schwandt[3]

[1]Mail Code SN2, NASA Johnson Space Center, Houston, TX 77058, USA, [2]Department of Earth and Planetary Science, Graduate School of Science, University of Tokyo, 7-3-1 Hongo, Tokyo 113-0033, Japan, [3]Lockheed Martin, 2400 Nasa Road 1, Houston, TX 77058, USA

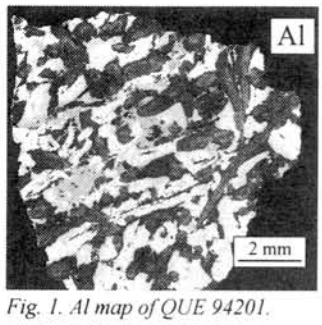

Fig. 1. Al map of QUE 94201. Light areas are plagioclase; medium gray areas are impact melt pockets; and dark gray areas are pyroxene.

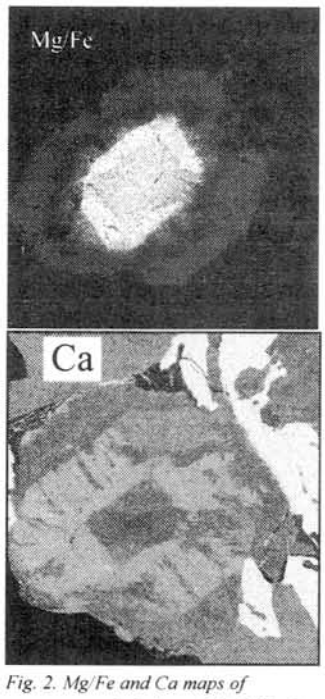

Fig. 2. Mg/Fe and Ca maps of pyroxene grain in lower left of Fig. 1. Light areas in Al map are plagioclase, and those in Ca map are whitlockite.

Introduction: There are now 8 recognized basaltic shergottites (Shergotty, Zagami, EETA79001, QUE94201 (QUE), Dar al Gani 476/489/735/670, Los Angeles, Sayh al Uhaymir 005/008/051, and Dhofar 019), making this the largest group of Martian meteorites. Most basaltic shergottites have high pyroxene/plagioclase ratios, suggesting they are "cumulate" rocks with excess pyroxene. However, because of its different mineralogy and chemistry from the other basaltic shergottites, QUE is believed to be the first Martian meteorite that represents its original magmatic composition [1-3]. In particular, it is rather plagioclase-rich (Fig 1) compared with other basaltic shergottites, and it also has a higher Fe/Mg. Moreover, QUE pyroxenes display extreme and complex compositional zoning (Fig. 2) that no doubt records information about the crystallization history of this sample. In this abstract, we present initial results of our ongoing crystallization experiments on a synthetic QUE analog in order to advance our understanding of the crystallization history and petrogenesis of this interesting meteorite.

Our goals in these experiments are to (1) determine the equilibrium phase assemblage and phase compositions as a function of temperature and oxygen fugacity, (2) determine the effects of cooling rate on phase assemblage, texture, and compositional zoning patterns, and (3) compare the phase compositions with those from the QUE meteorite to determine if the combination of experimental starting composition and crystallization conditions produces a good match with the natural sample. Information from these experiments will help constrain the crystallization conditions of QUE (e.g., fO_2, size of magma body), and will provide evidence bearing on the question of whether QUE actually represents a magma.

Experiments: A synthetic glass having the bulk composition of QUE94201 [4] was used as starting material (Table 1). 125 mg pellets were placed on Pt wire holders and suspended in a vertical gas mixing furnaces at the Johnson Space Center (CO/CO_2) and the University of Tokyo (H_2/CO_2). Samples were held for 48 hours at 1300°C and IW+1 [1], and quenched to room temperature. Then, they were put back into

the furnace at lower temperature and either held at constant temperature to grow crystals, then quenched after another 48 hr, or cooled to around 900°C, then quenched. Polished mounts were prepared from quenched charges and analyzed by electron microprobe.

Results and Discussion: Phase assemblages produced in the isothermal experiments at fO_2 = QFM are given in Table 2. These runs all contain olivine, despite the fact that there is no indication of any olivine in QUE. Moreover, the MELTS program [5] indicates augite as the liquidus phase at 1155°C, with no olivine appearing anywhere in the crystallization sequence. Possibly the melt composition at QFM is slightly Fe-enriched because it lost less Fe to the Pt wire. Additional experiments will be required to resolve this issue.

Table 1. Bulk compositions of QUE94201 and synthetic glass starting material

	Bulk composition of QUE94201	*Synthetic glass composition*
SiO_2	*47.66*	*46.39*
TiO_2	*1.92*	*1.86*
Al_2O_3	*10.14*	*10.30*
FeO	*19.60*	*22.09*
MnO	*0.49*	*0.47*
MgO	*6.33*	*6.24*
CaO	*11.18*	*10.70*
Na_2O	*1.46*	*1.02*
K_2O	*0.05*	*0.05*
Cr_2O_3	*0.15*	*0.10*
P_2O_5	*1.01*	*0.88*

Table 2. Phase assemblages produced in the experiments at QFM

Temperature (°C)	*Phases present*
1160	*Glass, Olivine*
1150	*Glass, Olivine, Pyroxene*
1140	*Glass, Olivine, Pyroxene*
1130	*Glass, Olivine, Pyroxene*
1117	*Glass, Olivine, Pyroxene, Plag*

Table 3. Phase assemblages produced in the experiments at IW+1

Temperature (°C)	*Phases present*
1180	*Glass*
1175	*Glass*
1170	*Glass, Pig, Aug (?)*
1170	*Glass*
1150	*Glass, Pig*
1125	*Glass, Aug, Plagioclase (?)*
1125	*Glass, Pig, Aug, Plagioclase*
1100	*Glass, Pig, Aug, Plagioclase*
1050	*Glass, Pyx (Pig, Aug), Plagioclase, Ilmenite*

Isothermal phase assemblages at IW+1 are given in Table 3. Two experiments, one at 1170° and the other at 1125° appear to give results that are inconsistent with those of experiments at bracketing temperatures, and are indicated by ? in Table 3. Running additional experiments at these two temperatures gave results consistent with those of bracketing experiments. The inconsistent experiments suggest that either we are having minor experimental difficulties (e.g., imprecise temperature control or minor Fe loss), or the energy difference between pigeonite and augite crystallization is so small that random nucleation effects can cause metastable augite crystallization. We will ignore the inconsistent experiments in the following discussion.

At IW+1, the onset of pigeonite crystallization occurs between 1170° and 1165°, while the onset of both augite and plagioclase crystallization occurs between 1137° and 1125°. The crystallization sequence at IW+1 is consistent with that predicted by MELTS (Fig. 3).

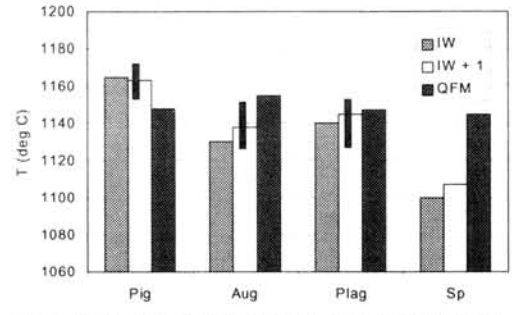

Fig. 3. Predicted phase crystallization temperatures for QUE bulk composition for three different oxygen fugacities [5]. Observed onset of crystallization occurs in the temperature interval indicated by the vertical bars.

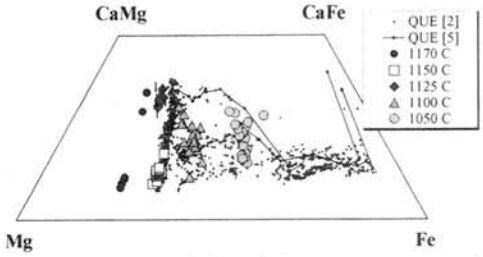

Fig. 3. Pyroxene quadrilateral showing comparison of pyroxenes from isothermal with natural QUE94201 pyroxenes [2,6,7].

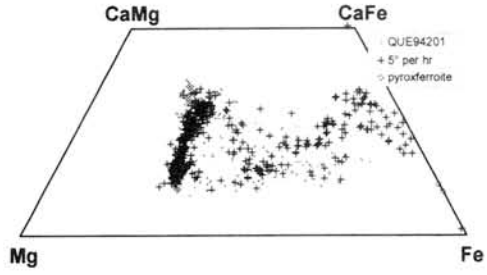

Fig. 4. Pyroxene quadrilateral showing comparison of pyroxenes from 5°/hr run with natural QUE94201 pyroxenes [2,6,].

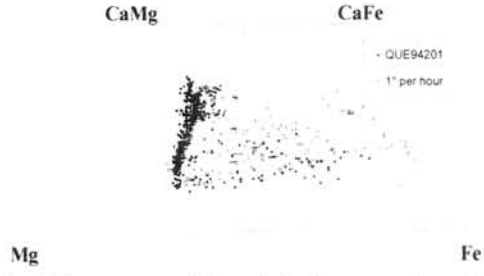

Fig. 5. Pyroxene quadrilateral showing comparison of pyroxenes from 1°/hr run with natural QUE94201 pyroxenes [2,6].

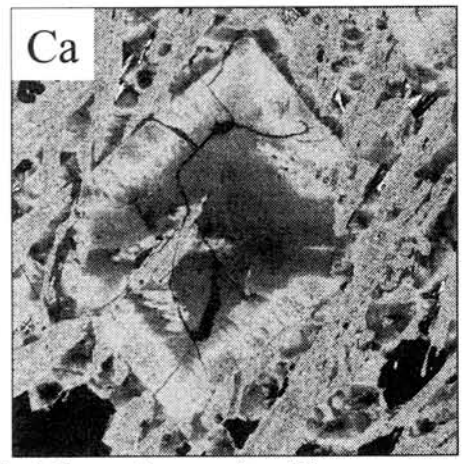

Fig. 6. Ca map of pyroxene from 1°/hr run.

Pyroxene compositions from isothermal IW+1 experiments are compared with QUE pyroxenes in Fig. 3. For each run temperature, there is a group of pyroxenes roughly aligned along lines of constant Fe/Mg. At each Mg/Fe, the synthetic pyroxenes show a spread in Ca content that is comparable to that seen in the natural pyroxenes.

Pyroxene compositions from runs that were cooled at 5°C/hr and 1°C/hr are shown in Figs. 4 and 5. These pyroxenes (esp. 1°/hr) closely resemble the zoning patterns of QUE. In particular, the synthetic pyroxene cores match the natural cores very well, except for a slight shift in the orientation of the pigeonite-augite tie lines. This shift may be the result of slight differences in oxygen fugacity between the meteorite and the experiments, an idea that we plan to test with further experiments.

Discussion: The good agreement between natural and synthetic core pyroxene compositions and zoning trends supports the idea that the QUE composition represents a Martian magma. Our starting composition is nearly multiply saturated with pigeonite, augite, and plagioclase, but has a slight excess of pigeonite. If our starting composition accurately represents the QUE bulk composition, (1) QUE may have undergone a small interval of pigeonite crystallization before augite and plagioclase joined the crystallization sequence, and thus was last in equilibrium with a pigeonite residuum prior to eruption, or (2) the intrinsic conditions of QUE crystallization (e.g., P, fO_2) may have been slightly different than our experimental conditions.

References: [1]McSween H. Y. Jr. et al. (1996) *GCA. 60.* 4563-4570. [2]Mikouchi T. et al. (1998) *Meteoritics & Planet. Sci., 33.* 181-189. [3]Wadhwa M. et al. (1998) *Meteoritics & Planet. Sci., 33.* 321-328. [4]Mittlefehldt, pers. com. [5] Ghiorso and Sachs (1995) *Contr. Min. Pet. 119.* 197-212. [6] McKay G. et al. (1996) *LPS XXVII.* 851-852. [7] Mikouchi T. et al. (2001) *LPS XXXII*, #2100.

Magnesian olivine xenocrysts in angrites Lewis Cliff 87051, Asuka-881371 and D'Orbigny: Their relationship and origin

T. Mikouchi[1], M. Miyamoto[1], and G. McKay[2]

[1]*Deptartment of Earth & Planetary Science, University of Tokyo, Hongo, Tokyo 113-0033, JAPAN*
[2]*Mail Code SN2, NASA Johnson Space Center, Houston, TX77058, USA*

Introduction

Angrites form an intriguing group of basaltic achondrites represented by unique mineralogy and very old crystallization ages (4.56 b.y.) [*e.g.*, 1-4]. Because angrites are depleted in volatile elements whereas enriched in refractory elements, their major constituent minerals are Ca-, Fe-rich olivine, fassaitic clinopyroxene, and anorthitic plagioclase. In spite of these interesting characteristics never seen in other meteorite groups, only four angrites (Angra dos Reis, Lewis Cliff 86010, Lewis Cliff 87051, Asuka-881371) were known until recently and they were all small (especially, Antarctic angrites). Sahara 99555 was recovered from the Sahara in 1999 and D'Orbigny was then discovered in Argentina in 2000 [5-9]. Sahara 99555 and D'Orbigny weigh 2.71 kg and 16.55 kg, respectively, by far larger than the previously known angrites. Therefore, the discovery of these new angrites is expected to provide useful information to better understand their enigmatic origins. Especially, D'Orbigny contains xenocrystic olivine megacrysts similar to those in Lewis Cliff 87051 (LEW87051) and Asuka-881371, which suggest their relationship [6]. In this abstract we present petrological and mineralogical study of these exotic olivines in LEW87051, Asuka-881371, and D'Orbigny. Then, we calculate their cooling rates by the method similar to [10] and discuss their relationship and origin.

Olivine Mineral Chemistry

LEW87051: LEW87051 consists of porphyritic olivine crystals set in a fine-grained groundmass that clearly represents a crystallized melt. Olivine grains are euhedral to subhedral and usually ~500 μm across. We previously described that some of the largest olivine grains have magnesian cores up to Fa_9, although regular phenocrystic cores are Fa_{20} [4,11,12]. These cores are enriched in Cr (0.2 wt% Cr_2O_3) and poor in Ca (0.2 wt% CaO) in contrast to the Cr-poor (<0.05 wt% Cr_2O_3) and Ca-rich (0.5 wt% CaO) regular phenocryst cores. Our interpretation is that these cores are xenocrysts that crystallized from a different melt than the groundmass, and the outer part of the crystals constituting the majority of olivine in LEW87051 are overgrown phenocrysts [4,11,12].

Asuka-881371: Asuka-881371 shows a medium-grained ophitic texture. Rare olivine megacrysts (up to 2 mm across) are scattered in the samples studied. They are remarkably homogeneous in most parts of the grains except for the extensively zoned outermost rims of several tens of μm from the edge. The rims show a reaction relationship between the megacrysts and the surrounding groundmass melt. Despite being internally homogeneous, these olivines show variations in composition (*e.g.*, Fa, Ca, Cr) from one crystal to another, suggesting that they have not been in equilibrium with one another [12]. Furthermore, these megacryst cores are clearly more Mg-, Cr-rich and Ca-poor compared to the groundmass olivines. The xenocrystic cores are Fa_{11-20}, 0.15-0.7 wt% Cr_2O_3, and 0-0.7 wt% CaO, whereas the groundmass cores are Fa_{30}, 0.05 wt% Cr_2O_3, and 0.8 wt% CaO. Therefore, it is obvious that these megacrysts are xenocrysts that are not in equilibrium with the Fe-rich groundmass melt [4,11,12].

D'Orbigny: D'Orbigny contains rare olivine megacrysts reaching 5 mm and texturally similar to Asuka-881371. Another new angrite, Sahara 99555 also shows a generally similar ophitic texture, although it does not contain any olivine megacrysts [5]. Kurat et al. [7] reported great heterogeneity of D'Orbigny (e.g., distribution of olivine megacrysts, vesicles, and glass), but we found only one grain of olivine megacryst in our samples studied. The megacryst shows a granoblastic texture composed of tiny (~10 μm) olivine grains. The inner portion of the megacryst is homogeneous like those in Asuka-881371, and is extensively zoned at the rim (~50 μm from the edge) presumably due to reaction with the surrounding Fe-rich melt. The megacryst core is Fa_{11}, and contains 0.25 wt% Cr_2O_3 and 0.4 wt% CaO. In contrast, the groundmass

olivine cores are Fa_{37}, <0.05 wt% Cr_2O_3, and 0.8 wt% CaO. Thus, we believe that the D'Orbigny olivine megacryst is also a xenocryst as those in LEW87051 and Asuka-881371 [6].

Cooling Rates of Olivines

We calculated cooling rates of olivine xenocrysts in LEW87051, Asuka-881371, and D'Orbigny by fitting the calculated Fa and Ca zoning profiles to the observed ones. We presumed that the original compositions were homogeneous due to internally homogeneous nature of the megacrysts. We then calculated the zoning profiles produced by interaction with the surrounding melts at various cooling rates from 1300 °C down to 1000 °C. We used the diffusion coefficient of Fe-Mg in olivine from Misener [13] and the Ca diffusion rate from Jurewicz and Watson [14]. We calculated the diffusion rates at logfO_2 of IW+1, which is the estimated fO_2 during angrite crystallization. The best fitting cooling rates for all three meteorites are 7 to 13 °C/hour, only ranging within factor of two (Fig. 1). These cooling rates are very fast, and the burial depths are shallower than 0.5 m from the surface if we consider that they were covered by rock-like material [10].

Discussion and Conclusion

As others and we have already pointed out [6-9], LEW87051, Asuka-881371, and D'Orbigny plus Sahara 99555 are very similar rocks if we look at the groundmass portions of these rocks. This study also demonstrates that LEW87051, Asuka-881371, and D'Orbigny contain olivine xenocrysts of similar compositions (Mg-, Cr-rich, and Ca-poor). Furthermore, they have nearly identical cooling rates (7-13 °C/hour) consistent with the quenched textures of the groundmass. Sahara 99555 would have cooled at a similar cooling rate as 50 °C/hour cooling experiments well reproduced its mineralogical and petrological properties [5]. The clear differences among these angrites are the abundance and size of olivine xenocrysts. In LEW87051 and Asuka-881371, their abundance is about 10 vol.% whereas they are less than 1 vol.% in D'Orbigny. No xenocrysts are found in Sahara 99555. The size of olivine xenocrysts in LEW87051 (~500 μm) is much smaller than those of Asuka-881371 and D'Orbigny (2-5 mm). Nevertheless, their characteristic composition indicates that such exotic olivine grains share the common origin and these three angrites are closely related. If this is the case and the original xenocrysts are millimeter-sized, we might be able to explain that the most mafic nature of LEW87051 groundmass are due to incorporation of a large amount of the magnesian xenocryst content into the magma. Thus, we suggest that they might have crystallized from the same magma with locally different abundances of entrained olivine xenocrysts. Minor difference in the groundmass compositions are attributed to locally different (only minor) melt compositions in the same magma body due to different degrees of dissolved olivine xenocryst component.

The calculated cooling rates suggest crystallization of the groundmass near the surface of the parent body. Impact melting is one of the most plausible heat sources to explain such shallow setting of the magma. Although angrites show little evidence for shock metamorphism, the presence of granoblastic olivines in D'Orbigny [6] and Asuka-881371 [15] suggests a shock event prior to the crystallization of the groundmass. However, we can not rule out the possibility that the magma was produced by endogeneous melting.

The origin of the olivine megacryst itself is unclear. Especially, the presence of variable compositional xenocrysts (though each is homogeneous) in Asuka-881371 makes the interpretation of their origin more puzzling. Among olivines in differentiated meteorites, ureilite olivines have similar compositions to olivine megacrysts in angrites in their forsteritic composition with high Cr and Ca abundance. In fact, a granoblastic olivine is found in some ureilites (*e.g.*, ALH81011) [16]. However, Warren and Davis [17] reported that one olivine xenocryst in Asuka-881371 has the O isotopic composition fallen within the angrite group. Therefore, this scenario is implausible, and the xenocrysts are probably related to the angrite parent body. In any case, these angrites appear to have experienced complex histories prior to incorporation of xenocrysts into the groundmass melt and subsequent rapid crystallization.

Acknowledgement: We thank Prof. T. Tagai (The University Museum, Univ. of Tokyo) and Dr. S. Yoneda (Natl. Science Museum, Tokyo) for supplying the D'Orbigny samples. This work was partly supported by the Japanese Ministry of Education, Science and Culture (No.12740297).

References: [1] Prinz M. *et al.* (1977) *EPSL* **35,** 317-330. [2] Mittlefehldt D. W. and Lindstrom M. M. (1990) *GCA* **54,** 3209-3218. [3] Nyquist L. E. *et al.* (1994) *Meteoritics* **29,** 872-885. [4] Mikouchi T. *et al.* (1996) *Antarct. Meteorite Res.* **9,** 174-188. [5] Mikouchi T. *et al.* (2000) *LPSC* **XXXI,** #1970. [6] Mikouchi T. and McKay G. (2001) *LPSC* **XXXII,** #1876. [7] Kurat G. *et al.* (2001) *LPSC* **XXXII,** #1737. [8] Mittlefehldt D. W. *et al.* (2001) *LPSC* **XXXII,** #2057. [9] Floss C. *et al.* (2001) *LPSC* **XXXII,** #1201. [10] Mikouchi T. *et al.* (2001) *MAPS* **36,** 531-548. [11] Mikouchi T. *et al.* (1995) *LPSC* **XXVI,** 973-974. [12] McKay G. (1995) *Antarct. Meteorites* **XX,** 155-158. [13] Misener D. J. (1974) In *Geochemical Transport and Kinetics,* ed. Hoffmann A. W. *et al.* pp. 117-129, Carnegie Inst. of Washington. [15] Jurewicz A. J. G. and Watson E. B. (1988) *Contribut. Mineral. Petrol.* **99,** 186-201. [16] Yanai K. (1994) *Proc. NIPR Symp. on Antarct. Meteorites* **7,** 30-41. [17] Takeda H. (2001) pers. comm. [18] Warren P. H. and Davis A. M. (1995) *Antarct. Meteorites* **XX,** 257-260.

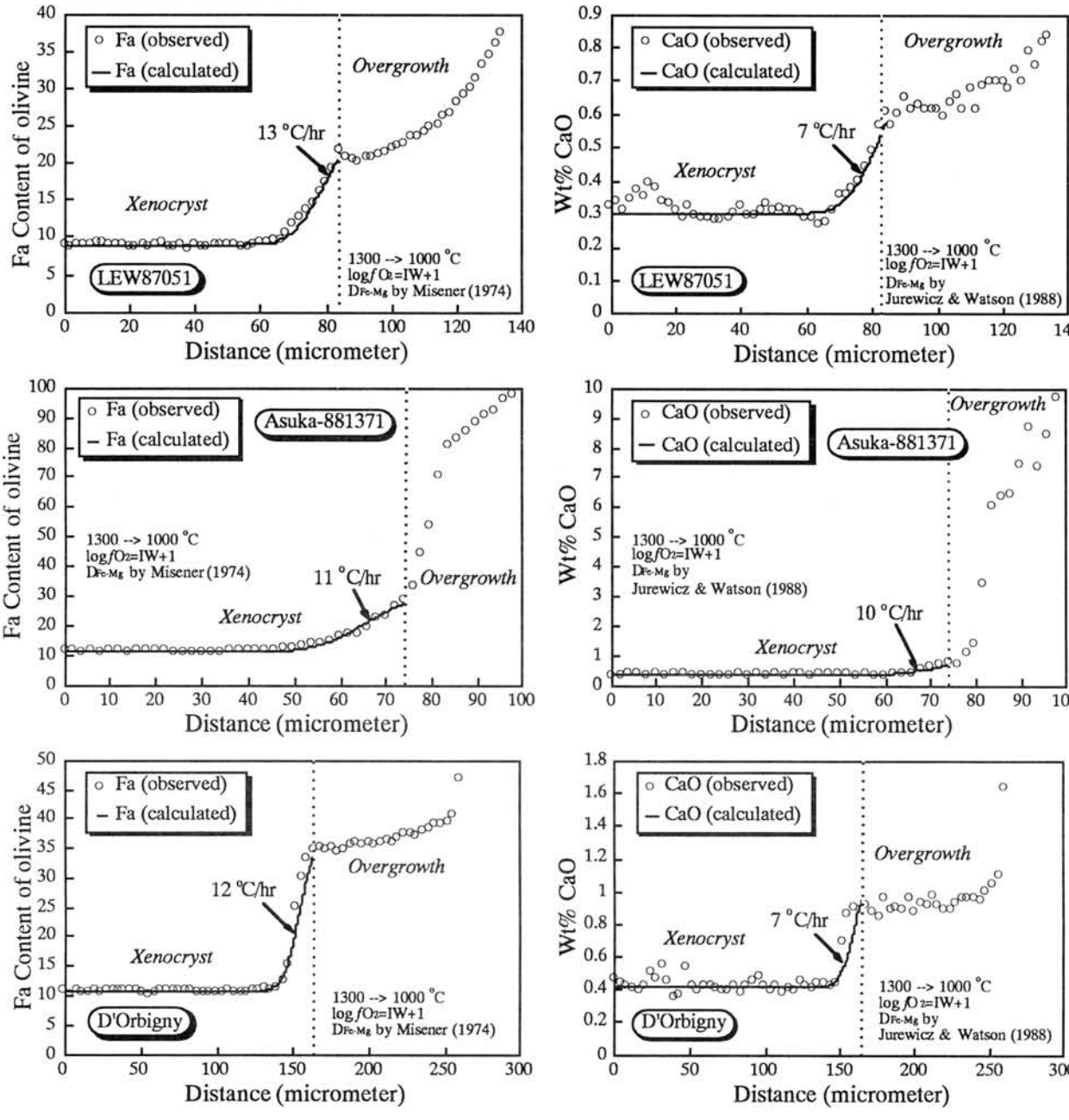

Fig. 1. Observed (circles) and calculated (solid lines) Fa and Ca zoning profiles of olivine xenocrysts in LEW87051, Asuka-881371, and D'Orbigny. The best fit cooling rates from 1300 °C to 1000 °C are 7-13 °C/hour) for all three meteorites, suggesting similar rapid cooling histories of these meteorites.

U-Pb ISOTOPIC SYSTEMATICS OF ZIRCONS FROM BASALTIC EUCRITES

Keiji Misawa and Akira Yamaguchi
Antarctic Meteorite Research Center, National Institute of Polar Research
1-9-10 Kaga, Itabashi, 173-8515 Tokyo (misawa@nipr.ac.jp)

Introduction: On the basis of isotopic studies using long- and short-lived chronometers, there is mountain evidence for early differentiation on the HED parent body [*e.g.*, 1]. Most eucrites tend to have experienced complex thermal histories after initial crystallization. Thus, there still remain open questions about timing and duration of early basaltic volcanism as well as metamorphism on the HED parent body. The ^{207}Pb-^{206}Pb mineral isochron ages of ~4510 Ma were determined for brecciated eucrites Nuevo Laredo and Bouvante [2]. The U-Pb ages of zircon and baddeleyite in eucrites suggest that they recorded the initial formation of the rocks [3-7]. The purpose of this study is to date the U-Pb age of eucritic zircon to reveal whether internal Pb-Pb and Sm-Nd ages reflect formation ages, thermal resetting through shock metamorphism, or slow cooling. We have examined eucritic clasts in breccia and granulitic eucrites, and focused on the U-Pb isotopic systematics of well-documented eucritic zircon. Here, we report the U-Pb and ^{207}Pb-^{206}Pb ages of zircon in unmetamorphosed eucritic clast in Yamato 75011 [8-10] and in unbrecciated, highly metamorphosed eucrites Asuka 881388 and Asuka 881467 [11, 12].

Experimental: We have examined polished sections of 16 basaltic eucrites. Zircons were identified by X-ray mapping with an electron probe microanalyzer. Backscattered electron images (BEIs) of eucritic zircon are shown in Fig. 1. Detailed occurrence, mineralogy, and petrography of eucritic zircons are described in the companion paper [13]. The U-Th-Pb isotopic analysis was carried out using thin sections with the SHRIMP II ion microprobe at Antarctic Meteorite Research Center, NIPR. An oxygen primary beam was focused on a spot with a diameter of ~10μm. Common lead was monitored using ^{204}Pb and assumed to be surface related and of Cañon Diablo Troilite (CDT) lead isotopic compositions [14]. Standard zircons were used for U/Pb normalization (SL13 [15]) and for age reference (FC1, ^{207}Pb-^{206}Pb age = 1099.0 ± 0.6 Ma [16]). Mass resolving power of the mass analyzer was ~6500 (M/ΔM) at 1% peak height. Because of the low concentrations of uranium in eucritic zircon as well as their fine-grained sizes, we could not obtain enough counting of signals at the first attempt for A-881388 zircons. Thus, we calculated preliminary ^{207}Pb-^{206}Pb ages with relatively large errors for A-881388 zircons.

Results and Discussion: Zircon in the unmetamorphosed eucritic clast in Y-75011 is distinct group in chemically with high uranium contents (>100ppm) and high Th/U ratios (~0.5) compared with those in equilibrated eucrite zircons (~50ppm U, Th/U = ~0.2). Concentrations of uranium and thorium in zircon from highly metamorphosed eucrites A-881388 and A-881467 are almost similar range to those reported previously [3-7] (the exception is an extremely high uranium content in a Pasamonte zircon up to 300ppm [6]). Combined with bulk data for basaltic eucrites [17-19], the facts suggest that parent melt of unmetamorphosed eucrites was rich in incompatible elements.

Analytical results are plotted on a concordia diagram (Fig. 2). Several data points are reverse discordance, *i.e.*, plotted above the concordia, suggesting an excess radiogenic lead component. Since eucritic zircons we analyzed are fine-grained and sometimes cracked during preparation of polished sections (Fig. 1b), the excess component could be partly derived from the primary beam overlap onto the surrounding ilmenite and/or due to inadequate U/Pb normalization. Excess radiogenic lead components were also observed in previous study [7]. If we assume U-Pb systems of eucritic zircon analyzed in this study are closed, calculated ^{207}Pb-^{206}Pb ages of eucritic zircons are ~40 Myr older than the ^{207}Pb-^{206}Pb isochron ages of brecciated eucrites Nuevo Laredo and Bouvante [2]. The ^{207}Pb-^{206}Pb ages of zircon in unmetamorphosed clast in Y-75011 are nearly identical to those from the highly metamorphosed eucrite A-881467, suggesting that basaltic volcanism on the HED parent body could have occurred at a very early stage of solar system history, and that volcanism occurred within very short periods. Whether the unmetamorphosed eucrites formed later than the metamorphosed eucrites or not is still unclear in this study. The U-Pb systems in 10-20μm-sized zircon have a closure temperature grater than 800°C depending on cooling rate [20]. Thus almost U-Pb ages of eucritic zircon do not represent metamorphic ages but crystallization ages of extrusive lavas.

Whether highly metamorphosed eucritic zircon was originally depleted in incompatible elements or depletion occurred during thermal metamorphism still remains unsolved. Some evidence for redistribution of REE are suggested for partially melted eucrites Y-86763, Ibitira, and EET90020 [12]. On the other hand, pigeonites in granulitic eucrites A-881388 and A-881467 retained their original zirconium abundances [12]. Zircon closes to tetravalent cation exchange at significantly higher temperatures (>100°C) than the trivalent rare earths [21]. We suggest that uranium and thorium depletions in zircons from granulitic eucrites A-881388 and A-881467 are not metamorphic but indigenous.

REFERENCES: [1] Carlson R.W. & Lugmair G.W. (2000) in *Origin of the Earth and Moon*, Univ. Arizona Press, pp. 25-44. [2] Tera F. *et al.* (1997) *GCA* **61**, 1713-1731. [3] Bukovanská M. *et al.* (1991) *Meteoritics* **26**, 325. [4] Ireland T.R. *et al.* (1992) *LPSC* **XXIII**, 569-570. [5] Ireland T.R. & Bukovanská M. (1992) *Meteoritics* **27**, 237. [6] Bukovanská M. & Ireland T.R. (1993) *Meteoritics* **28**, 333. [7] Bukovanská M. *et al.* (1996) *Meteoritics* **31**, A24. [8] Takeda H. & Graham A.L. (1991) *Meteoritics* **26**, 129-134. [9] Nyquist L.E. *et al.* (1991) *JGR* **91**, 8137-8150. [10] Takeda H. *et al.* (1994) *EPSL* **122**, 183-194. [11] Yamaguchi A. *et al.* (1997)

AMR **10**, 415-436. [12] Floss C. *et al.* (2000) *AMR* **13**, 222-237. [13] Yamaguchi A. & Misawa K. (2001) *this volume*. [14] Tatsumoto M. *et al.* (1973) *Science* **180**, 1279-1283. [15] Compston W. (1999) *Mineral. Mag.* **63**, 297-311. [16] Paces J.B. & Miller J.M. (1993) *JGR* **98**, 13997-14013. [17] BVSP (1981) Basaltic Volcanism on the Terrestrial Planets, Pergamon Press, pp. 1286. [18] Shimizu H. & Masuda A. (1986) *GCA* **50**, 2453-2460. [19] Warren P.H. & Jerde E.A. (1987) *GCA* **51**, 713-725. [20] Lee J.K.W. *et al.* (1997) *Nature* **390**, 159-162. [21] Cherniak D.J. *et al.* (1997) *CMP* **127**, 383-390.

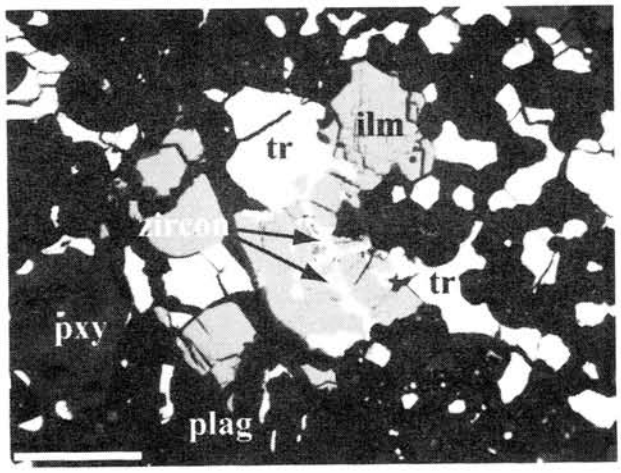

Fig. 1a. BEI of unmetamorphosed euctitic clast in Yamato 75011. Zircons occur as veins and contacts with ilmenite in silica-rich mesostasis, suggesting that they were formed at final stage of crystallization from the melt. Scale bar is 50μm.
tr: troilite, ilm: ilmenite, pyx: pyroxene, plag: plagioclase.

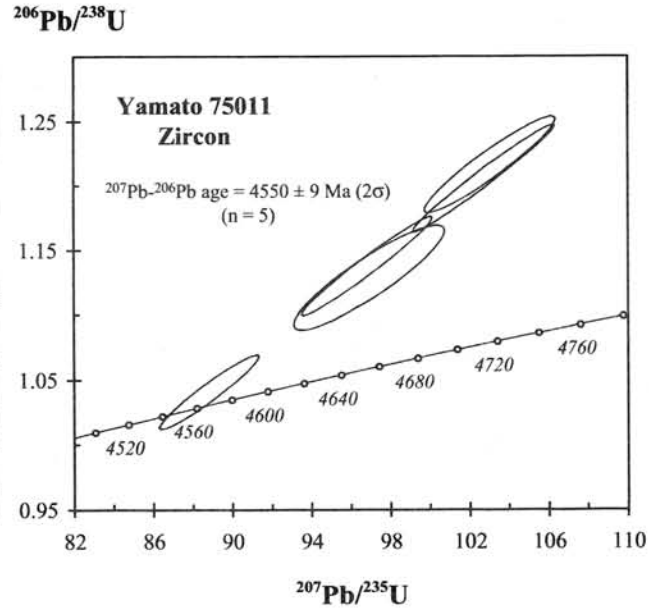

Fig. 2a. Concordia plot for Yamato 75011 zircons. Data points show a large degree of reverse discordance, suggesting an excess radiogenic lead component. Assuming initial isotopic compositions of CDT lead [14], we obtained an averaged ^{207}Pb-^{206}Pb age of 4550 ± 9 Ma (2σ).

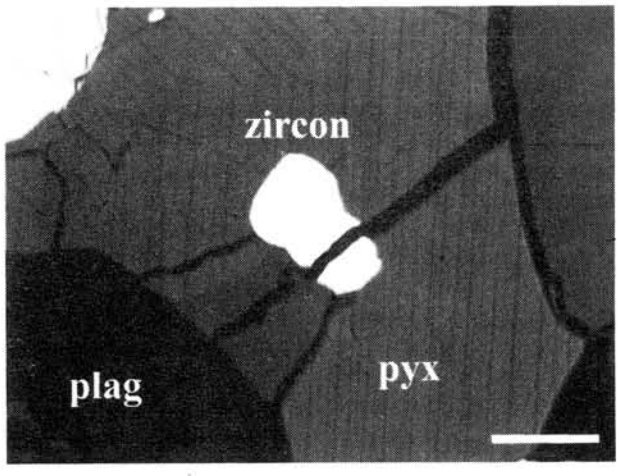

Fig. 1b. BEI of unbrecciated, highly metamorphosed eucrite Asuka 881467. Zircon in Asuka 881467 occurs as an equant grain in pyroxene. Scale bar is 30μm.
pyx: pyroxene, plag: plagioclase.

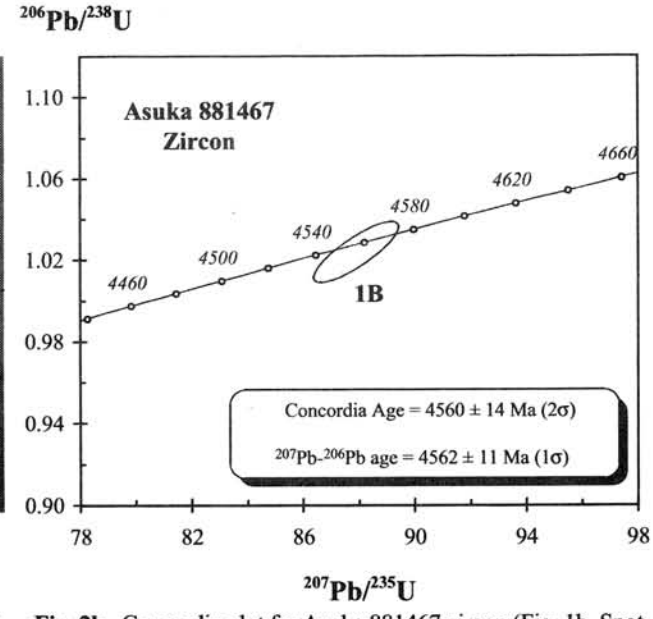

Fig. 2b. Concordia plot for Asuka 881467 zircon (Fig. 1b, Spot 1B). The U-Pb systems are concordant, yielding a ^{207}Pb-^{206}Pb age of 4562 ± 11 Ma (1σ) assuming initial isotopic compositions of CDT lead [14].

Noble gas studies on CO3 and L3 chondrites : An Ar-rich component related to isotopically light nitrogen

Yayoi N. Miura[1], Naoji Sugiura[2], Kaoru Kiyota[1] and Keisuke Nagao[3]

[1] Earthquake Research Institute, University of Tokyo, Yayoi, Bunkyo-ku, Tokyo 113-0032, Japan.
[2] Department of Earth and Planetary Science, University of Tokyo, Hongo, Bunkyo-ku, Tokyo 113-0033, Japan.
[3] Laboratory for Earthquake Chemistry, Graduate School of Science, University of Tokyo, Hongo, Bunkyo-ku, Tokyo 113-0033, Japan.

Introduction

Sugiura *et al.* (1998) [1] and Kiyota *et al.* (2000) [2] found that isotopically light nitrogen is released with a large amount of Ar in some unequiribrated ordinary chondrites (UOCs) and CO chondrites under combustion experiments. In order to characterize release profiles and elemental and isotopic compositions of Ar and other noble gases and in order to clarify relation between the light nitrogen and noble gases, we have carried out noble gas analyses for two UOCs studied in [1] and four CO chondrites in [2].

Samples and Ar-rich gas

Samples In the previous work [1], 8 out of the measured 24 UOCs were reported to have isotopically light nitrogen component (hereafter ALH-77214-type based on the name of the representative sample). Most ALH-77214-type that includes H, L, LL chondrites released more abundant Ar than other UOCs. The release profiles of ^{36}Ar correlated with those of isotopically light nitrogen in stepped combustion experiments and the HF/HCl treatment removed large amounts of ^{36}Ar and light nitrogen from the crushed bulk samples, hence origin and trapping site(s) may be the same for Ar and light nitrogen. The same chemical feature has also been indicated based on noble gas data for 8 UOCs [3], where HF/HCl treatment removed Ar-rich component and HF/HCl residue showed Q-gas composition. Last year, [2] reported that CO chondrites have release patterns of nitrogen and Ar similar to ALH-77214-type. They also found that 80 or 90 % of light nitrogen and Ar is removed by HCl etching. In this study, we selected two L3 chondrites classified into ALH-77214-type [1] (ALH-77167 and ALH-78119, the former is a paired meteorite with ALH77214) and four CO chondrites which were studied for nitrogen in [2] (Y-790992, Y-791717, Y-82094 and ALH-77003) for noble gas study. We measured noble gases for the six samples by stepwise heating and two samples so far by laser-microprobe experiments. A modified VG-5400 at Laboratory for Earthquake Chemistry, Univ. of Tokyo was used for the noble gas mass spectrometry.

Ar-rich gas The measured six samples contain Ar-rich gas with Ar/Xe ratios significantly higher than Q-gas. Q-gas and Ar-rich gas are major primordial noble gas components in chondrites. Q-gas, trapped in "phase Q", is found widely in different classes of chondrites. Ar-rich gas, characterized by higher Ar/Xe ratio than Q-gas, is also found in some classes of chondrites and ureilites. Some enstatite chondrites show Ar/Xe ratio greater than 1000 (*e.g.* 2700 for South Oman [4]), much higher than 50 –100 for Q-gas [5,6]. Recently Ar-rich gas in enstatite chondrites (named subsolar gas) has been identified to be contained in chondrules [7]. Although Ar/Xe ratio is lower than those of the subsolar gas, Ar-rich component with Ar/Xe ratio between Q-gas and subsolar gas has been found in some ordinary and carbonaceous chondrites [*e.g.*, 3]. The present study investigates the Ar-rich gas in UOCs and CO chondrites.

Experiments

Stepwise heating Several small pieces weighting about 10 – 20 mg were used for the stepwise heating. Noble gases have been extracted at 700, 900, 1000, 1100, 1200, 1300, 1500 and 1700℃, and elemental and isotopic compositions from He to Xe have been determined.

Laser-microprobe Laser-microbe experiments were carried out on sliced samples of Y-791717 and ALH-77167. After observation of their polished surfaces with a scanning electron microprobe, we tried to extract noble gases from metal, troilite and graphite grains, chondrules, matrices, and chondrule-matrix boundaries using a Nd-YAG laser with the beam size of ~50μm in diameter, though the present results may have not fully characterized noble gas compositions of individual phases. From one to twenty-three pits were made for a single analysis, and eleven and twelve analyses were performed so far for Y-791717 and ALH-77167, respectively.

Results and discussion

The release profiles of Ar, Kr and Xe are similar among measured chondrites except Y-82094. As seen in Fig. 1, the temperature of the largest amount Ar released is higher for Y-82094 than for the others. Since the total concentrations of Ar, Kr and Xe are more than two times higher and Ar/Xe ratio is lower than the others, Y-82094 might contain more abundant Q-gas. In the following, we summarize characteristic obtained for the measured five chondrites excepting Y-82094. The total concentrations of Ar, Kr and Xe are (4.8-12) x 10^{-7}, (3.7-8.3) x 10^{-9} and (3.2-6.2) x 10^{-9} cm^3STP/g, respectively. About 80 % and 40 – 60 % of the totals have been released from 1000 to 1200 ℃ with a peak at 1100 ℃ for Ar and Xe, respectively. The Ar/Xe ratios are significantly higher than Q-gas (Fig. 2), that is, Ar-rich component was released around these temperatures. The Ar-release profiles are similar to those observed in the stepped combustion experiments [1,2], where the largest amounts of ^{36}Ar as well as isotopically light nitrogen were also released at 1100 ℃. From both experiments, it is suggested that Ar-rich component and light nitrogen is trapped in the common phase(s).

The isotopic compositions of Ar, Kr and Xe for the Ar-rich gas around 1100 ℃ of the measured chondrites are not different from those of Q-gas [5,6]. The $^{38}Ar/^{36}Ar$ ratio obtained here is about 0.190, *e.g.*, a less cosmogenic sample of ALH-77167 shows 0.1894 +/- 0.0006 at 1100 ℃, which is close to the ratio reported for Q-gas. The Xe isotopic ratios are similar to those of Q-Xe within experimental errors except for terrestrial Xe at 700 ℃ and Xe-HL around 900 ℃.

The present laser experiments for Y-791717 do not reveal significant variation in noble gas abundances and compositions among different phases. This may be due to technical condition; that is, the laser spots applied did not satisfy to hit a single phase and thereby extracting gases from several phases, and amounts of released gases so small that blank correction was relatively large. On the other hand, we found diversity of noble gas abundances and elemental composition for ALH-77167. The elemental compositions of Ar, Kr and Xe similar to Q-gas have been observed in gases from a graphite grain (probably accompanying Fe and FeS phases) and chondrule-matrix boundaries. The two FeS grains release Ar-rich component with the Ar/Xe ratio of ~200, equal to the ratio of the bulk sample. The measured three chondrules and Fe grain release less abundant noble gases, whose elemental compositions are uncertain. At now, possible candidate for the carrier phase of Ar-rich gas in UOCs is FeS. However, more detail investigation is need to conclude if troilite and/or related phase is truly the carrier phase.

Acknowledgements: We thank NIPR for providing us with Antarctic meteorite samples.

References

[1] Sugiura, Kiyota and Hashizume (1998) *Meteoritics Planet. Sci.* 33, 463-482. [2] Kiyota, Sugiura and Zashu (2000) *Antarctic Meteorites* XXV, 48-49. [3] Schelhaas, Ott and Begemann (1990) *Geochim. Cosmochim. Acta* 54, 2869-2882. [4] Crab and Anders (1981) *Geochim. Cosmochim. Acta* 45, 2443-2464. [5] Busemann, Baur and Wieler (2000) *Meteoritics Planet. Sci.* 35, 949-973. [6] Huss, Lewis and Hemkin (1996) *Geochim. Cosmochim. Acta 60*, 3311-3340. [7] Okazaki, Takaoka, Nakamura and Nagao (2000) *Meteoritics Planet. Sci.* 35, A123.

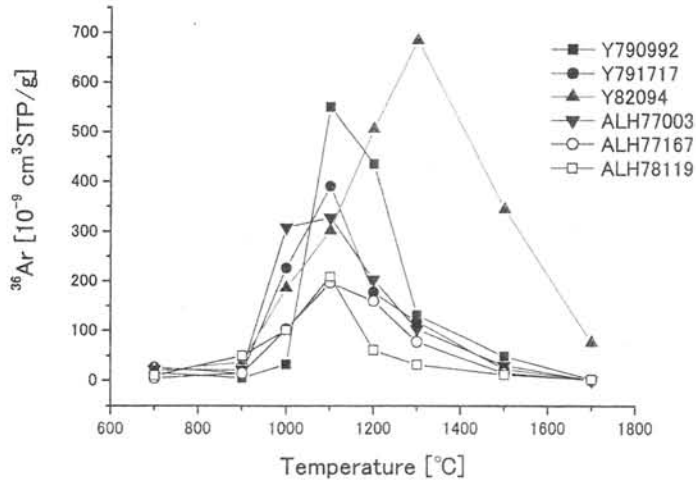

Fig. 1. Release profiles of ^{36}Ar against extraction temperatures. Abundant ^{36}Ar is released at 1100 ℃ except Y-82049. The closed symbols are for CO chondrites and open symbols for UOCs.

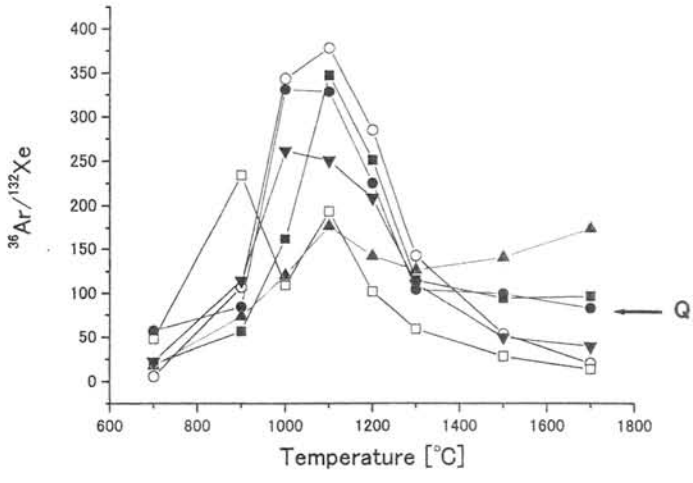

Fig. 2. ^{36}Ar/^{132}Xe ratios against extraction temperatures. The ^{36}Ar/^{132}Xe ratios are higher than that of Q-gas around 1100 ℃. See Fig. 1 for symbols.

Noble Gases in Muong Nong-type Tektites

Sayaka Mizote[1], Takuya Matsumoto[1], Jun-ichi Matsuda[1] and Christian Koeberl[2]

1. Department of Earth and Space Science, Graduate School of Science, Osaka University, 1-1 Machikaneyama, Toyonaka, Osaka, 560-0043, Japan

2. Institute of Geochemistry, University of Vienna, Althanstrasse 14, A-1090 Vienna, Austria

Introduction

Tektites are a group of natural glasses that have an appearance similar to other natural glasses, such as obsidians. They are found in four strewn fields (North American, Central European, Ivory Coast, and Australasian) on Earth. Tektites can be divided into three groups according to their form. Splash-form tektites and aerodynamically shaped tektites are the two of three groups and differ only in their appearances [1]. They are chemically homogeneous and often spherically symmetric objects that are several centimeters in size. The third variety is called Muong Nong-type tektites. These have irregular and blocky shapes, and are much larger in size than the other types, reaching up to a few kg in weight. In addition, they are not chemically homogeneous and have a layered structure. The origin of this unusual type of tektites and their relationship with other "normal" tektites are not understood well. Because noble gases in tektites can be good tracers for deciphering their origin, we have carried out noble gas analyses on a suite of well-documented Muong Nong-type tektites from Thailand.

Sample and Experiments

We prepared eight Muong Nong-type tektites for the present study. These are from Ubon Ratchatani in East Thailand, and are the same samples that had been studied for major and trace element composition (except for X-103;[1]). Noble gases were extracted from the coarse grained samples (1.5 mm) by vacuum crushing technique. After purification, the elemental and isotopic compositions of the noble gases were analyzed by a noble gas mass spectrometer VG5400 at Osaka University. Before the sample analyses, the crusher blank level was measured prior to the sample run, and appropriate corrections were made (the typical crusher blank contributed about 5% of the sample value for the heavy noble gases).

Results and Discussion

Neon enrichments in Muong Nong Teketites

Anomalous neon enrichment relative to atmospheric composition is a common characteristic of many tektites studied so far [2, 3, 4]. The present samples also showed distinct enrichments in neon, with F(20) values varying from 2.5 to 36 (Fig. 1), whereas the relative abundance of Ar, Kr, and Xe are consistent with the normal atmospheric composition. Because we extracted the gases by crushing the samples, we can safely regard the neon enrichment as the signature of the noble gases trapped in abundant vesicles. Matsubara and Matsuda [5] demonstrated that a significant amount of neon can diffuse into obsidian glasses (i.e., a type of natural glasses). The observed high F(20) in vesicles in Muong Nong-type tektites might also be accounted for by the diffusive input of neon from the atmosphere to vesicles. Note, however, that the obtained F(20) values are somewhat smaller than those reported previously for normal tektites. For example, Matsubara and Matsuda [4] reported that the F(20) of splash form tektites varies from 200 to 7130. As will be shown, this difference in F(20) might be explained by systematically more abundant heavier noble gases (Ar, Kr and Xe) in the Muong Nong-type tektites relative to normal tektites.

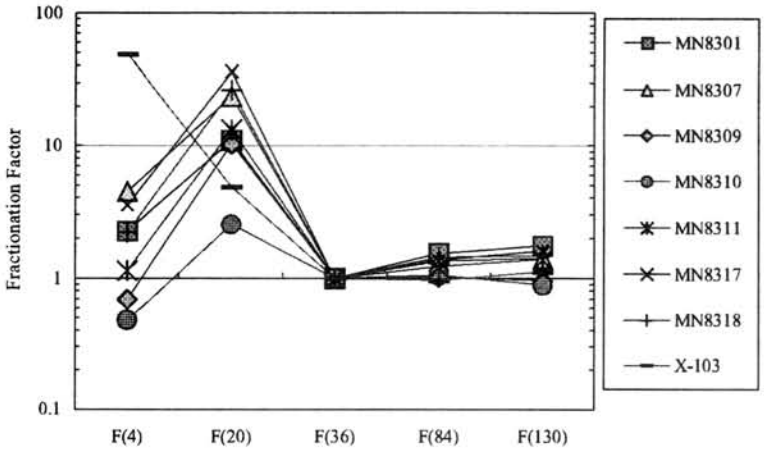

Fig. 1 Fractionation Factor F(m)

F(m) defined by
$F(m) = ({}^{m}X/{}^{36}Ar)_{sample} / ({}^{m}X/{}^{36}Ar)_{air}$
where ^{m}X represents a noble gas isotope of mass "m".

Heavy noble gas abundances in Muong Nong-type tektites

Matsuda *et al.* [3] reported that the concentrations of ^{36}Ar in impact glasses are systematically higher than those in tektites by about two orders of magnitude, while they have comparable amounts of ^{20}Ne (~10^{-7} cm^3STP/g) (see Fig.2). As shown in Fig. 2, the amounts of ^{36}Ar in Muong Nong-type tektites appear to be significantly higher than those in normal tektites. Note, however, that there is no systematic difference in ^{20}Ne concentrations. In this respect, the present results suggest that the noble gas compositions in the Muong Nong-type tektites have a close similarity to impact glasses and that the observed smaller F(20) values in the Muong Nong-type tektites are likely to result from the relatively large concentration of Ar. In fact, Koeberl [1] pointed out that the Muong Nong-type tektites are distinct from other normal tektites in their enrichments in volatile elements (e.g., Cl, Br, Zn, Cu, Pb). The present results demonstrate that this observation can be extended to include the highly volatile noble gases as well, because the observed Kr and Xe contents are also systematically higher than those in the normal tektites and are similar to those in impact glasses (Fig. 3).

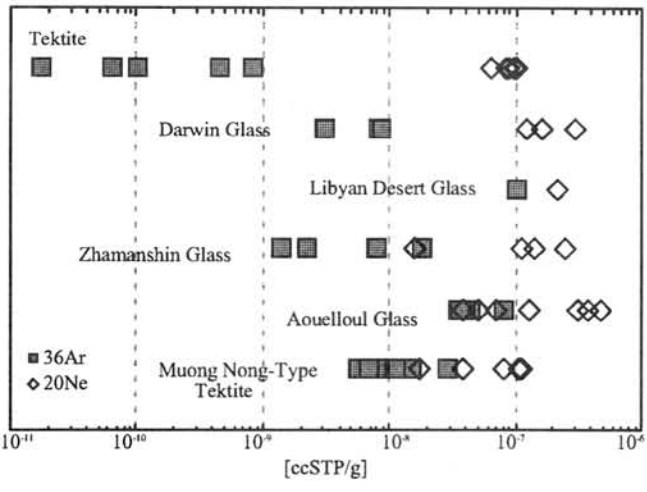

Fig. 2 Concentrations of ^{20}Ne and ^{36}Ar

Neon concentrations in all samples are confined to a narrow range. Argon concentrations in Muong Nong-type tektites and impact glass. Impact glasses are from Aouelloul (West Africa), Zhamanshin (Khazakhstan), Libyan Desert Glass (Egypt) and Darwin (Australia). Tektites are normal splash-form ones from near Thailand in the Australasian strewn field. Muong Nong-type tektites are from Thailand (this study).

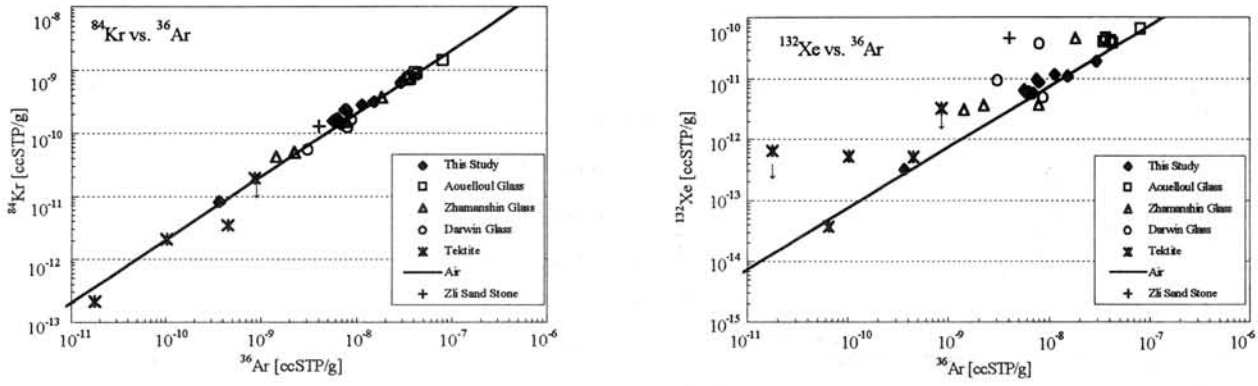

Fig. 3 Heavy noble gases vs. ^{36}Ar

^{84}Kr(left) and ^{132}Xe(right) contents are plotted against ^{36}Ar content in Muong Nong-type tektites, normal tektites and impact glasses. Impact glasses are from Aouelloul crater (West Africa), Zhamanshin crater (Khazakhstan), Libyan Desert Glass (Egypt) and Darwin crater (Australia). Normal tektites are splash-form ones from near Thailand in the Australasian strewn field. "Air" shows the line corresponding to the ratio of noble gases in terrestrial atmosphere.

Conclusion

We have analyzed the noble gas composition of Muong Nong tektites by a vacuum crushing technique, followed by mass spectrometry. Muong Nong-type tektites are characterized by having relatively large amounts of heavy noble gases compared to normal tektites. The observed ranges are similar to those reported for impact glasses. In contrast, there is no significant difference in the neon abundances between normal and Muong Nong-type tektites and impact glasses. Consequencely, a relatively low F(20) value is also characteristic for Muong Nong-type tektites.

Reference

[1] Koeberl C. (1992) Geochemistry and origin of Muong Nong-type tektites. *Geochim. Cosmochim. Acta* **56**, 1033-1064.

[2] Matsubara K., Matsuda J. and Koeberl C. (1991) Noble gases and K-Ar ages in Aouelloul, Zhamanshin, and Libyan Desert impact glasses. *Geochim. Cosmochim. Acta* **55**, 2951-2955.

[3] Matsuda J., Matsubara K. and Koeberl C. (1991) Origin of tektites: Constraints from heavy noble gas concentrations. *Meteoritics* **28**, 586-599.

[4] Matsubara K., Matsuda J. (1991) Anomalous Ne enrichments in tektites. *Meteoritics* **26**, 217-220

[5] Matsubara K. and Matsuda J. (1995) Laboratory experiments on the Ne enrichments in terrestrial natural glasses. *Geochemical Journal* **29**, 293-300

Suppression of isotopic mass fractionation during evaporation in the ambient gas and its application to chondrule formation

Hiroko Nagahara
Dept Earth Planet Sci, Univ Tokyo, Hongo, Tokyo 113-0033, Japan
(hiroko@eps.s.u-tokyo.ac.jp)

Chondrites as well as the Earth, Moon, and Mars show significant chemical fractionation, which is well shown in the degree of depletion of elements according to the volatility. These materials, however, do not show isotopic fractionation that is expected for high temperature evaporation processes responsible for the chemical fractionation. Several possibilities have been proposed: the volatile loss without isotopic fractionation to condensation in the solar nebula that preceded chondrule, chondrite and planet formation (Humayun and Clayton, 1995), the role of diffusion (Ozawa and Nagahara, 1999; Young, 2000), and back reaction (Nagahara and Ozawa, 2000; Alexander *et al.*, 2000; Nagahara, 2000). Theoretical consideration on the decoupling of chemical and isotopic fractionation during evaporation of a condensed phase indicates the importance of back reaction (Ozawa and Nagahara, 2001). In order to understand chemical and isotopic fractionations in the presence of ambient gas and to evaluate the role of back reaction quantitatively, we have carried out evaporation experiments for partially molten chondrite in the presence of ambient gas and studied. The results will be discussed in the light of the theoretical consideration.

The experiments and results on alkali evaporation were described in Nagahara and Ozawa (2000). Powdered chondrite from which metal and troilite were extracted was heated in a Knudsen cell (cell with an orifice). Cells with various sizes of orifice were put in a vacuum chamber simultaneously. The evaporation rate was calculated from the initial and final chemical composition of the glass, surface area of the sample, and experimental duration. The partial pressure of Na and K in the capsule or cell was obtained from the mass loss, which is corrected for the conductance of the capsule and the orifice. Potassium isotopic fractionation was measured with Cameca 6f SIMS at the Dept Earth Planet Sci, Univ Tokyo. The degree of mass fractionation was calculated against the experiment in a closed capsule that should show no mass fractionation from the starting material. The validity of this assumption is supported by the fact that there was no chemical fractionation in experiments with different durations, which indicates no mass loss in closed capsule experiments.

Potassium isotopic composition shows mass dependent fractionation, and the degree of fractionation decreases with decreasing the size of orifice for a series of experiments with a fixed temperature and duration. It reaches about 20 ‰ in capsules with orifice larger than a certain size, and decreases to zero with decreasing orifice size. The value of 20‰ is much smaller than that expected for Rayleigh fractionation. The results were analyzed with the model of Ozawa and Nagahara (2001), which describes the chemical and isotopic fractionation in the presence of ambient gas. The model is based on the Hertz-Knudsen equation, which comprises two terms; evaporation reaction and condensation reaction. The net rate of the reaction is shown as the balance of these two reactions. The vacuum evaporation rate includes equilibrium vapor pressure and the kinetic parameter (evaporation coefficient, α_e), and the condensation rate includes the pressure of the ambient gas kinetic parameter (condensation coefficient, α_c). Because the kinetic parameters are not known, the ratio α_c / α_e is used as a parameter and its effect on chemical and isotopic fractionation was examined. The results are well explained with the ratio smaller than 0.2 for 10 hours ad 1300°C experiments and less than 03 for 3 hours experiments. These values indicate the presence of very large kinetic barrier for condensation in the presence of ambient gas. If the evaporation coefficient is assumed to be constant, the actual number of α_c varies by an order. The variation of α_c depending on the ambient gas composition is also shown for Fe (Tachibana et al., 2001) and forsterite (Onaba et al., 2001).

The experimental results were applied for chondrule formation conditions. The plausible condition for the large elemental fractionation and the scarce isotopic fractionation is wide variation of dust enrichment factor ranging from 0.01 to 10.0 in order to generate at a constant cooling rate. The factor less than 1.0 is necessary to produce the marked K depletion. The cooling rate should be smaller than ~1°C/min at ~1400°C, and a cooling rate greater than this value does not cause the observed range of elemental fractionation by three orders of magnitudes. If the initial temperature was 1500°C this limit may be increased by a factor of 5. Small isotopic fractionation and the wide variation in concentration of K are realized in the temperature range between 1200 and 900°C.

References

Alexander, C. M. O'D. *et al.* (2000) *Meteorit. Planet. Sci.* **35** 859-868
Humayun, M. and Clayton, R. N. (1995) *Geochim Cosmochim Acta*, **59** 2131-2148
Inaba, H. et a;. (2001) *LPSC* **XXXII** (CDROM)
Nagahara, H. (2000) *Mteeorit. Planet. Sci.* **35** A116
Nagahara, H. and Ozawa, K. (2000) *LPSC* **XXXI** (CDROM)
Ozawa, K. and Nagahara, H. (1999) *LPSC* **XXX** (CDROM)
Ozawa, K. and Nagahara, H. *Geochim Cosmochim Acta* (in pressd)
Tachibana, S. et al. (2001) *LPSC* **XXXII** (CDROM)
Young, E. D. (2000) *EPSL* **183** 321-333

LABORATORY SIMULATION OF SPACE WEATHERING: MICROSTRUCTURES AND IRON NANOPARTICLES IN THE LASER IRRADIATED SAMPLES

Keiko Nakamura

Department of Earth and Planetary Sciences, Kobe University, Kobe 657-8501 Japan *(keiko@shidahara1.planet.sci.ac.jp)*

Sho Sasaki, Yoshimi Hamabe, Erika Kurahashi

Department of Earth and Planetary Science, University of Tokyo, Tokyo 113-0033, Japan

Takehiro Hiroi

Department of Geological Science, Brown University, Providence, RI 02912, U.S.A.

Introduction of Space Weathering : The S-type asteroids have been considered as parent bodies of ordinary chondrites since both of them are silicate-rich and the most abundant among asteroids and meteorites, respectively. However, the steep reddened reflectance spectra of S asteroids are different from those of ordinary chondrites. The term *Space Weathering* applied originally to explain the spectral differences between lunar soils and underlying rocks due to micrometeorite impacts and/or solar wind irradiation may define also the mismatch of reflectance spectra between ordinary chondrites and S-type asteroids. Formation of nanophase reduced iron on regolith is credited with one of the key processes of optical property changes [1-3]. Such submicroscopic metallic iron particles were found on the vapor-deposited rims of lunar soil grains (Fig.1a)[4-6]. We have succeeded in simulating space weathering of silicates, which produces reflectance spectrum very similar to S-type asteroids [7-11] and recently confirmed the suspected link between the occurrence of nanophase iron in the vapor-deposited rims and the spectroscopic optical effects of darkening and reddening [12]. Here we report an extended study of microtextures of the simulated samples examined by transmission electron microscope (TEM).

Samples of Pulse Laser Irradiation Simulation: In order to simulate the space weathering by high-velocity dust impact, we irradiate powder and pellet samples of olivine San Carlos (8.97 wt% FeO) and enstatite Bamble (9.88wt% FeO) by a pulse laser beam (1064 nm) with pulse duration 6-8 ns, which is comparable with a real dust impact [7,8]. The pellet samples with size of 2cm are made of grains smaller than 75 μm. Experiments are performed under a vacuum at $(1\text{-}2)\times10^{-5}$ torr. The total irradiation energy in unit area were 240 mJ mm^{-2} for 30 mJ pulse energy. After the laser irradiation, bidirectional reflectance spectra of samples were measured[7,8]. Laser-irradiated samples show significant reddening: reduction of spectra is much larger in a visible region than in a near-infrared region. The important finding was that reflectances of olivines are more easily changed than those of pyroxenes[8]. This is compatible with the compiled asteroid data: using areas of 1 μm and 2 μm absorption bands, olivine-rich asteroids have more reddened spectra than pyroxene-rich asteroids[9-11].

TEM Investigation: For TEM measurements, several grains from each olivine pellet sample after five times and twenty times irradiation were picked up and embedded in low viscosity epoxy and thin-sectioned with ~50-80nm thickness using an ultramicrotome. For systematical comparable study, irradiated pyroxene samples were also prepared in the same procedure as well as the initial olivine and enstatite. Imaging and electron diffraction were performed with a JEOL2010 (200keV) TEM equipped with an energy-dispersive X-ray (EDX) spectrometer. Electron diffraction was calibrated with a Au-coated carbon film.

Results *Olivine samples*: The rim regions of the irradiated olivine samples show a highly mottled contrast indicative of high density of defects. Amorphous rims in ~200nm thickness are developed along the grain rims(Fig.2). Average atomic percents of the amorphous materials of the rims from six different areas are O 59.05 (57.07), Si

18.10 (14.08), Mg 20.60 (25.05), Fe 2.25 (3.80), where values in brackets are composition data of host olivine. The amorphous material is more silica rich than underlying olivine crystal.

In high resolution TEM images, nanophase particles (several to 30nm in size) are recognized which are widely dispersed throughout the amorphous rims (Fig.1b). These particles appear to be single- to poly-crystallines embedded in amorphous material which have never been observed on initial unirradiated olivine samples.

Doubled- to multiple amorphous layers are frequently observed in 30mJ twenty repetitions irradiated samples (Fig.3). The outer rims are more widely developed than both the inner rims and those of five times irradiated samples. Nanophase particles in the outer rims are slightly larger and more poly-crystalline than those rims.

The EDX analysis on the regions where these nano-phase particles densely occur indicate that the beam-indent area is enriched in iron (The EDX focused probe size is 15~20nm.) Selected area electron diffraction (SAED) and nano-beam diffraction (NBD) patterns (~3nm beam spot size) both in 33-60 seconds exposure time were taken from both the single- and poly-crystalline particles. The diffraction patterns from poly-crystallines are well-matched with αFes' (body-centered cubic, the unit length a_0=0.2874nm.) The observed interlayer spacing: 0.204nm in average (Fig.3) is also consistent with the (110) spacing of αFe (d_{110} =0.203nm).

***Enstatite samples*:** Consistent with the spectral data, the optical color of the irradiated enstatite grains is much brighter than the olivines'. Even though the hardness of enstatite crystal (3.2) is lower than olivine's (6.5), distinct cleavage due to the fibrous habit of enstatite crystal has been seen both in the initial enstatite grains and the irradiated microtomed samples. No such amorphous rims nor nanophase particles as seen in the olivine has been identified so far.

Discussions and Conclusions: Electron diffraction patterns and interlayer spacing measurement of each crystalline particle reveal that these are nanophase αFe particles. Our observed αFe nanophase particles are clearly similar to those found in the rim of lunar soil grains in occurrence and size[4-6]. Doubled, possibly multiple, amorphous layers which are rather frequently seen in 20 times at 30 mJ olivine sample than 5 times'. The microscopic characteristics in the simulation samples – the formation of nanophae iron in the vapor deposited rims - are linked to optical property change especially reddening. The defects observed close to the irradiated grain rims may be caused by rapid heating. In space, heating by micrometeorite impacts on the regolith surface should produce the vapor, part of which subsequently deposit on nearby grains. Through this process, nanophase crystalline iron particles should be formed. Our results show that reduction by implanted hydrogen from solar wind is not necessary to form nanophase iron. Hereby both the spectral and these microscopic data, the magnitude of space weathering on air-less planetary surface is highly dependent on the chemical composition, such as olivine-to-pyroxene. Our experimental method for space weathering simulation can be applied for determination of exposure age of asteroidal and lunar regolith surface.

References: [1] Hapke B. *et al.* (1975). *Moon* **13**, 339-353 [2] Hapke B. (2000) *Lunar Planet. Sci.* **31**, #1087. [3] Pieters C. M. *et al.* (2000) *Meteoritics and Planet. Sci* **35**, 1101-1107 [4] Keller L. P. & McKay, D. S. *Science* **261**, 1305-1307 (1993) [5] Chiristoffersen R., Keller L. P. & McKay D. S. (1996) *Meteoritics and Planet. Sci* **31**, 835-848 [6] Keller L. P. & McKay D. S. (1997) *Geochim. Cosmochim. Acta.* **61**, 2331-2341 [7] Yamada M. *et al* (1998) *Antarctic Meteorites* XXIII, 173-176 (National Inst. Polar Res., Tokyo) [8] Yamada M. *et al.* (1999) *Earth Planets Space* **51**, 1255-1265 [9] Hiroi T. and Sasaki S. (1999) *LPSC* XXX, #1444. [10] Hiroi T. and Sasaki S. (2001) *Meteoritics and Planet. Sci.* (in review) [11] Sasaki S. et al.(2001) LPS XXXII. [11] Sasaki S. et al.(2001) *Nature* **410**, 555-557 .

Fig.1a left: rim of anorthosite grain of Apollo lunar soil sample. **Fig1b right:** a bright field image of an amorphous rim from 30mJx5 irradiated olivine sample.

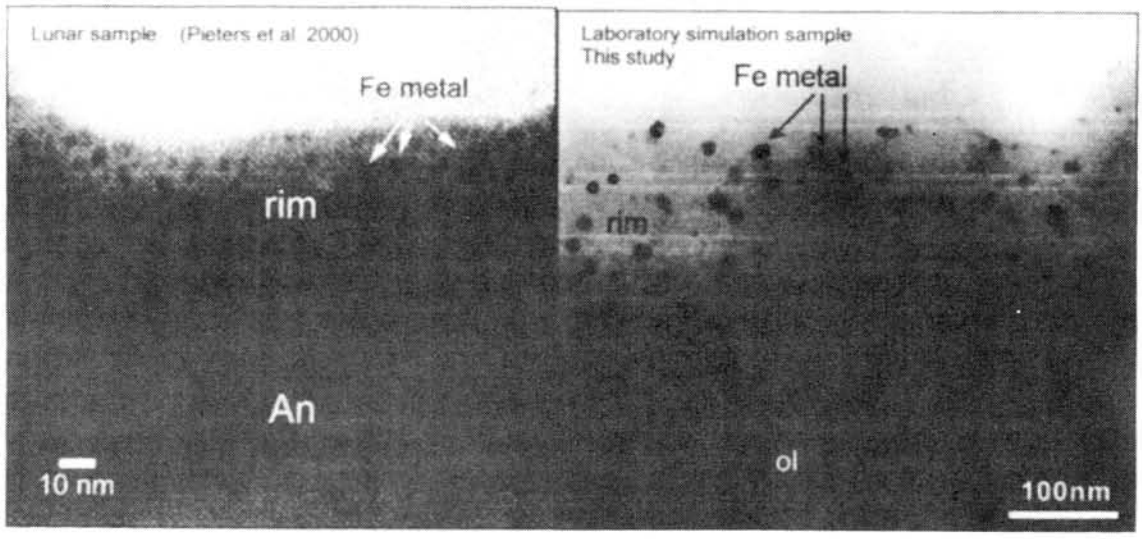

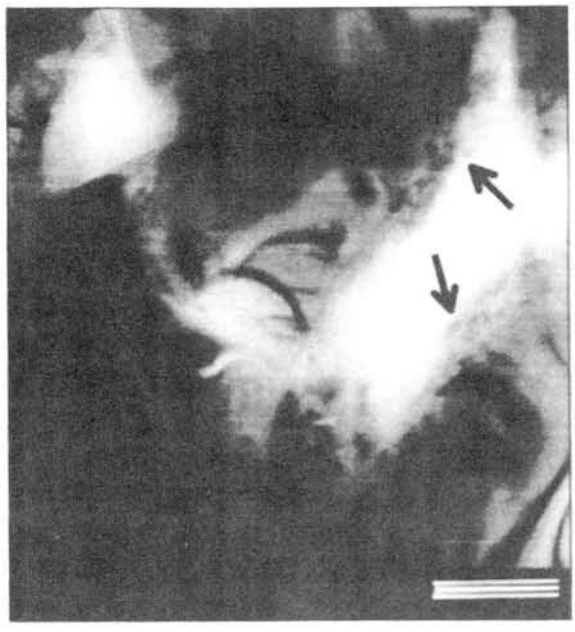

Fig 2 (left) : a bright field image of the grain rim region from olivine 30mJx5 irradiated sample. Arrows indicate amorphous rims (~100nm in thickness) developing along the grain rims. The scale bar equals 200nm.

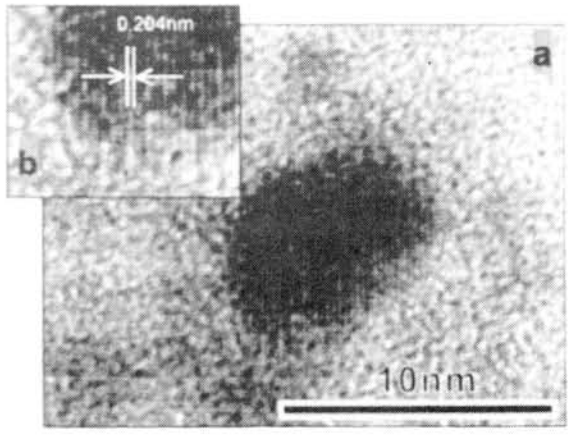

Fig 3 (a): A bright field high resolution TEM image of nanophase particle in the rim of 30 mJ x 20 irradiated olivine grain. The grain size is about 7.7nm. **Fig3(b):** An enlarged image of Fig.3(a). The measured interlayer spacing is 0.203-0.205nm,

SAYAMA METEORITE: A PCP-POOR HEAVILY ALTERED CM CHONDRITE

Nakamura T[1], Noguchi T[2], Tonui E[3], Gounelle M[4], Zolensky M. E[3], Yoneda S[5], and Takaoka N[1]

[1]Department of Earth and Planetary Sciences, Faculty of Sciences, Kyushu University, Hakozaki, Fukuoka 812-8581, Japan, [2]Department of Materials and Biological Science, Ibaraki University, Bunkyo 2-1-1, Mito 310-8512, Japan, [3]SN2, NASA/JSC, Houston Texas 77058, USA, [4]C. S. N. S. M., CNRS-IN2P3, F-91405 Orsay, France, [5]National Science Museum, 3-23-1 Hyakunincho, Shinjuku, Tokyo 169-0073, Japan.

Introduction: Sayama meteorite is a newly recognized meteorite fell in Saitama prefecture [1]. Preliminary examination by Yoneda *et al.* [1] showed that the meteorite contains chondrules, 1.99 wt% of carbon, and 12 wt% of H_2O, and has a bulk oxygen isotopic composition in the range of CM chondrites, thus they proposed that it is a CM chondrite. In this paper, we report the results of detailed mineralogical examination performed by the methods of optical microscopy, scanning electron microscopy (SEM and EPMA), X-ray diffraction analysis using synchrotron radiation, and transmission electron microscopy (TEM). Our results confirmed that Sayama is a CM chondrite, but it underwent extensive aqueous alteration on the meteorite parent body.

Results and discussion: Sayama contains chondrules with diameter from 200 to 600 μm. They have fine-grained dark rims with thickness from 50 to 100 μm. The abundance of chondrules is low and similar to that of other typical CM2 such as Murchison and Murray. Approximately half chondrules are completely replaced by greenish phyllosilicates, while others retain limited amounts of olivine phenocrysts. In many places in chondrules, preexisting anhydrous phases are pseudomorphically replaced. The degree of aqueous alteration of chondrules is apparently higher than that of Murchison and Murray. SEM observation showed that matrix consists of coarse serpentine-rich aggregates from 50 to 400 μm in size, FeS-rich PCP-like objects from 30 to 200 μm in size, dolomite crystals from 10 to 100 μm in size, sulfide, magnetite, and fine-grained phyllosilicates. Texture of matrix is similar to that of primary accretionary rock defined by [2]. Carbonates occur predominantly as dolomite, although a few calcite grains are present. Dolomite shows slightly high MnO contents (1-2.5 wt%). Sulfide occurs as irregular to sub-rounded small grains of pentlandite up to 50 μm in diameter. Pyrrhotite occurs but is rare. Magnetite rims commonly occur around the pentlandite grains. Other minor phases identified are apatitie and chromite. Some coarse phyllosilicate-rich aggregates contain remnant anhedral olivine cores, suggesting that they are replacement products of coarse anhydrous mineral fragments.

Synchrotron X-ray diffraction analysis using gandolfi camera was performed on 100 μm-sized lumps removed from portions of a meteorite slice that was characterized by SEM and EPMA. The results showed that Sayama chondrules consists predominantly of well-crystallized serpentine (d_{001} = 7.22 Å) and minor amounts of Fe-sulfides. TEM observation showed that chondrules also contain clinochlore (d_{001} = 14.2 Å) whose amounts are very small so that it cannot be detected by the X-ray diffraction. Matrix is mainly composed of serpentine, moderate amounts of magnetite and pentlandite. Minor amounts of pyrrhotite also detected. But tochilinite, the major phase of PCPs, is

not detected. Serpentine 001 reflection is sharp and appears at 7.20 Å, which is larger than that of other CM chondrites such as Murchison [3]. This suggests that a low Fe^{3+} / Si^{4+} ratio in the tetrahedral layers in serpentine in Sayama. (02*l*) prism reflection due to disordered stacking is clearly recognized.

TEM observation was performed on the matrix lumps that were analyzed by X-ray diffraction. The most distinct features are almost all of pentlandite and pyrrhotite grains with diameter 500 Å or larger have a thin FeO-rich rind approximately 500 Å in width. The FeO-rich rinds are poor crystalline, but selected area diffraction analysis showed that they may be magnetite. There are two types of phyllosilicate in the matrix. First type is serpentine and occurs as coarse grains, which often reach ~ 10 μm in width. Their morphology suggests that some are pseudomorphs of anhydrous minerals such as olivine. The second type of phyllosilicates is aggregates showing fine-grained fibrous to tabular textures. High resolution TEM imaging and EDS analysis suggest that they are also serpentine. The chemical compositions of both coarse and fine serpentine crystals were determined by analytical TEM. Coarse serpentine crystals have variable Mg/(Mg+Fe) ratios from 0.2 to 0.6. Their composition suggests that they are mainly Fe-rich serpentine. On the contrary, the fine-grained serpentines tend to be more magnesian (0.55~0.75) than those of the coarse-grained serpentines. (Si+Al)/(Mg+Fe+Si+Al) atomic ratio of the fine serpentines ranges from 0.45 to 0.48, which is higher than that of pure serpentine and suggests that the fine-grained serpentines have an excess of Si. This means that there are SiO_2-rich materials among the fine-grained serpentine crystals.

Our mineralogical study of chondrules and matrix of Sayama indicates that it is a CM2 chondrite with a high degree of alteration. Matrix mineralogy is distinct from typical CM2s, including the presence of abundant pentlandite with ultrathin Fe-oxide rinds and the absence of tochilinite. The absence of tochilinite was reported in heavily altered CM chondrites EET 83334 and ALH 88045, which are assigned to CM1, and was ascribed to high fO_2 and temperature during progressive alteration [4]. Lack of tochilinite and the presence of Fe-oxide rinds in Sayama suggest that it experienced aqueous alteration under conditions similar to CM1 chondrites, but Sayama is much less altered than the CM1s. The degree of the alteration of Sayama is similar to that of a highly altered CM2 chondrite ALH 83100, but Sayama is still less altered. Because in ALH 83100 fewer than 5% of chondrules contain remnant olivine [4], while about 50% chondrules in Sayama contain such olivine. In spite of the higher degree of alteration, ALH 83100 still contains tochilinite [4], but Sayama do not contain it. Therefore, Sayama seems to have experienced aqueous alteration under physicochemical conditions different from a highly altered CM2 ALH 83100 but similar to CM1s.

Acknowledgments: We thank Drs. Tanaka, Nozaki, and Mori for technical support during X-ray diffraction analysis at KEK.

References: [1] Yoneda S. *et al.* (2001) LPSC XXXII, 2034 (CD-ROM). [2] Metzler K. *et al.* (1992) *GCA* 56, 2873-2898; [3] Nakamura T. and Nakamuta Y. (1996) *Proc. of the NIPR Symp.* 9, 37-50; [4] Zolensky M. E. *et al.* (1997) *GCA* 61, 5099-5155.

Metamorphic temperature of Kobe meteorite estimated by the plagioclase thermometer

NAKAMUTA Yoshihiro[1]*, NAKAMURA Tomoki[2], and NAKAMURA Noboru[3]

[1] The Kyushu University Museum, Kyushu University, Fukuoka 812-8581, Japan; [2] Dept. Earth and Planetary Sciences, Faculty of Science, Kyushu University, Fukuoka 812-8581, Japan; [3] Dept. Earth and Planetary Sciences, Faculty of Science, Kobe University, Nada, Kobe 657-8501, Japan.

Correspondence author's e-mail address: nakamuta@museum.kyushu-u.ac.jp

Introduction

The Kobe meteorite fell on 26th (local time: about 20:21) September 1999 in Kita-ku, Kobe [1]. The meteorite is the metamorphosed carbonaceous chondrite, Karoonda-type (CK normal group). The meteorite contains compositionally very homogeneous Fe-rich olivine and low-Ca pyroxene, abundant plagioclase with large grain-to-grain compositional variations, and abundant magnetite containing ilmenite [2]. Chondrules in the Kobe meteorite are well to moderately defined and matrix olivines have typical grain sizes of 5 to 50 μm, then, the Kobe meteorite is tentatively assigned to metamorphic type 4 [2].

It is thought to be very important to know the metamorphic temperature of the Kobe meteorite in order to uncover the thermal history of the meteorite. The pyroxene thermometer is usually used to know the igneous temperature of achondrites. However, metamorphic temperature of chondrites is known to be too low to be measured by pyroxene thermometer [3]. The plagioclase thermometer was applied to petrologic types 5 and 6 chondrites and shown to be useful to know metamorphic temperatures of chondrites that were metamorphosed at relatively low temperature [3]. In this study, the plagioclase thermometer was used to estimate the metamorphic temperature of the Kobe meteorite.

Metamorphic temperature

The X-ray powder patterns of individual plagioclase grains of about 50 μm in size of which chemical compositions have been analyzed by EPMA were obtained by using a Gandolfi camera. An X-ray powder pattern of plagioclase of the Kobe meteorite is shown in Fig. 1. Plagioclase in the Kobe meteorite is usually associated with medium to trace amounts of magnetite and trace amounts of diopside and shows very sharp X-ray reflections suggesting very well crystallinity of it.

The distance between 1–31 and 131 reflections in the X-ray powder pattern that represents structural state of plagioclase was precisely determined by applying a profile-fitting technique. The measured distance was corrected for the influence of Or content by using the correction diagram [4]. The corrected distance is directly related to the structural state of plagioclase, i.e. the degree of Al/Si order in the four symmetrically non-equivalent tetrahedral sites in the framework structure, and is correlated with the equilibration temperature of plagioclase [5].

Plagioclases from the Kobe meteorite are plotted on the diagram [5] that shows the relation between the 131 structural indicator and temperature of synthesis of plagioclase (Fig. 2). Plagioclases in the Kobe meteorite are plotted on the Ca-rich region where the equilibration temperature of plagioclase is not well known. However, higher vales of Δ131 of plagioclases from the Kobe meteorite distribute around the estimated temperature line showing 700°C, and reveal that the metamorphic temperature of the Kobe meteorite have reached about 700°C.

Discussion

Table 1 shows the maximum metamorphic temperature of the Kobe meteorite together with those of ordinary chondrites [3, 6, 7]. Metamorphic temperature of the Kobe meteorite is lower than those of petrologic type 6 ordinary chondrites and near to those of petrologic type 5 ordinary chondrites. The recrystallization textures of the Kobe meteorite, i.e. typical grain sizes of 5 to 50 μm of olivine and well to moderately defined chondrules, are correspond to petrologic type 4 of ordinary chondrites [2]. The degree of recrystallization of minerals during metamorphic processes depends on metamorphic temperature and also on duration time. The less recrystallized minerals of the Kobe meteorite compared to type 5 ordinary chondrites may suggest that the duration of metamorphism in the CK parent body is shorter than those in the ordinary chondrite parent bodies.

Acknowledgement— We thank Mr. R. Hirata for providing the meteorite sample.

References

[1] Nakamura N. et al. (2000), Antarctic Meteorites **XXV**, 99-101.

[2] Tomeoka K. et al. (2000), Antarctic Meteorites **XXV**, 160-162.

[3] Nakamuta Y. and Motomura Y. (1999), Meteoritics & Planetary Sciences **34**, 763-771.

[4] Kroll H. and Ribbe P.H. (1980), Amer. Mineral. **65**, 449-457.

[5] Smith J.V. (1972), Jour. Geology **80**, 505-526.

[6] Nakamuta Y. and Motomura Y. (1997), Antarctic Meteorites **XXII**, 137-139.

[7] Nakamuta Y. and motomura Y. (1998), Meteoritics & Planetary Sciences **32**, A97.

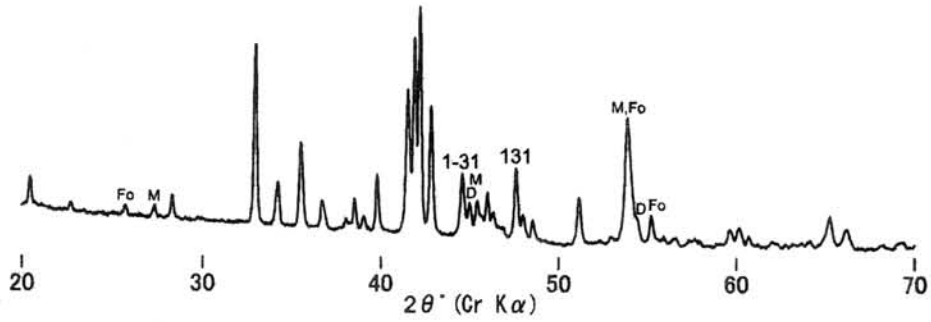

Fig. 1. X-ray powder pattern of plagioclase taken by a Gandolfi camera. Fo: forsterite, M: magnetite, D: diopside. 1-31 and 131: 1-31 and 131 reflections from plagioclase, respectiveely.

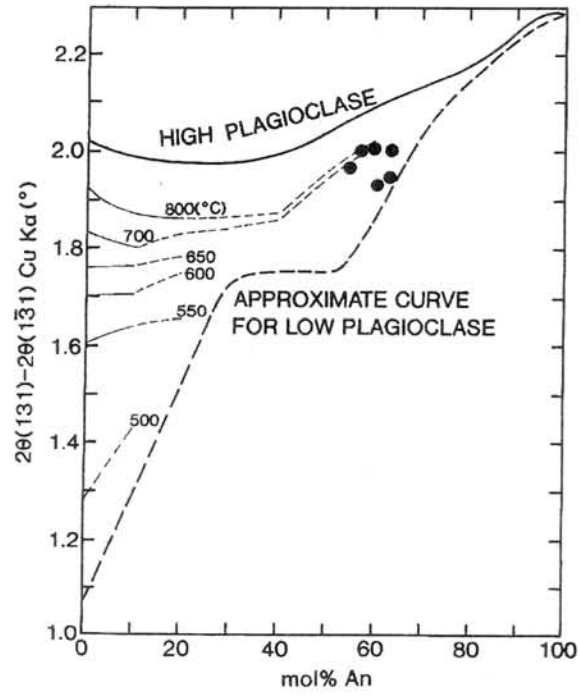

Fig. 2. Plots of individual plagioclase crystals on the relation diagram between the Δ131 parameter and the temperature of synthesis of plagioclase.

Table 1. Temperatures obtained by plagioclase thermometer.

Petrologic type	Temperature(°C)	References
H6	734(9)	3
L6	814(6)	3
LL6	800	3
LL5-6	710	6
LL5	758, 558	7
Kobe	≈ 700	this study

Cosmic Ray Exposure Age and Heliocentric Distance of the Parent Body of H Chondrites Yamato-75029 and Tsukuba

D. Nakashima[1)], T. Nakamura[2)], M. Sekiya[2)] and N. Takaoka[2)]

1) Department of Earth and Planetary Sciences, Graduate School of Science, Kyushu University 33, Hakozaki, Fukuoka, 812-8581

2) Department of Earth and Planetary Sciences, Faculty of Sciences, Kyushu University 33, Hakozaki, Fukuoka, 812-8581

Introduction

Anders [1] calculated the heliocentric distances of meteorite parent body on the basis of the noble gas data and the assumption that fluxes of solar wind (SW) and solar energetic particles (SEP) are in inverse relation to the square of heliocentric distance and flux of galactic cosmic ray (GCR) is constant in the solar system. Wieler et al. [2] calculated 20Ma for the parent body exposure age and 2～3AU for the heliocentric distance of H chondrite Fayetteville.

The purpose of this study is to determine the parent body exposure ages and the heliocentric distances for two H chondrites Yamato-75029 and Tsukuba. These meteorites contain solar gases as well as cosmogenic ones [3, 4]. From the concentrations of solar $^{20}Ne_S$ and $^{36}Ar_S$ and cosmogenic $^{21}Ne_C$, the parent body exposure ages, the heliocentric distances and the space exposure ages of these meteorites were calculated.

Experimental and calculation procedures

The parent body exposure age T_P is the duration for which the precursor materials of meteorite were exposed to solar cosmic ray (SCR) and GCR when they were on the parent body. The heliocentric distance r_P is the distance of the parent body of meteorites from the sun. The space exposure age T_S is the duration for which the meteoroids are exposed to GCR. T_P and r_P were calculated by,

$$T_P = \frac{(^{21}Ne_C)_P}{P_G + P_S / r_P^{\,2}} \qquad \cdots(1)$$

$$r_P = \sqrt{\frac{(^{36}Ar_S)_L}{T_L} \Big/ \frac{(^{36}Ar_S)_P}{T_P}}\,, \qquad \cdots(2)$$

where suffix P and L represent parent body and lunar, respectively, and P_G and P_S are the production rate of $^{21}Ne_C$ by GCR and SCR, respectively.

In equation (1), P_S is divided by r_P^2 because SCR flux is in inverse proportion to r_P^2. Since GCR production rates exceed the SCR contribution, Wieler et al. [2] calculated the parent body exposure age using only GCR production rate. But in fact, the surface of the meteorite parent body was exposed to both SCR and GCR. Therefore, we consider both contributions. The SCR contribution to T_P will be examined later. Each shielding depth for P_G and P_S is assumed to be 0～10g/cm^2 and SEP can penetrate this depth. These production rates are calculated from data given by [5].

As found in equation (2), the concentration of noble gas implanted on the meteorite parent body per unit time is in inverse proportion to r_P^2 because fluxes of SW and SEP are inversely proportioned to r_P^2. Since the distance from the sun to the moon is 1AU, r_P can be calculated by

comparing the concentration of solar gases implanted per unit time in lunar samples $(^{36}Ar_S)_L/T_L$ with those of meteorites investigated in this study $(^{36}Ar_S)_P/T_P$. Data for QUE93069 [5], ALHA81005 [5] and EET87521 [6] are used for $(^{36}Ar_S)_L$ and T_L. $(^{21}Ne_C)_P$ and $(^{36}Ar_S)_P$ are obtained by the noble gas analysis. Meteorite samples are agglomerates consisting of mineral grains, some of which contain much noble gas but others of which contain less noble gas. Thus samples are crushed into small grains to separate these grains as much as possible. Sample weights range from about 1mg to 30mg. We analyzed 23 and 20 grains for Yamato-75029 and Tsukuba, respectively. Each sample was heated at 1700℃ to extract noble gas.

Results and discussion

Good correlations were obtained between $^{20}Ne_S$ and $^{21}Ne_C$ for both meteorites. In Fig. 1, the ordinate intercept at which no implanted solar gases are found corresponds to the concentration of $^{21}Ne_C$ produced during the space exposure. And the excesses from the ordinate intercept are $^{21}Ne_C$ produced by GCR and SCR during the parent body exposure. This is because solar gases trapped on the meteoroid are lost when the meteoroid falls onto the earth, and thus noble gas added to meteoroid is only cosmogenic gases. From equations (1) and (2) with this assumption, we obtain $T_P=5.9\pm^{4.9}_{5.5}$ Ma and $r_P=2.2\pm^{0.7}_{1.6}$ AU for Yamato-75029, $T_P=9.3\pm^{4.9}_{7.4}$ Ma and $r_P=3.7\pm^{0.9}_{2.0}$ AU for Tsukuba. Space exposure ages are 3.7 ± 1.1Ma and 8.3 ± 1.1Ma for Yamato-75029 and Tsukuba, respectively, with the production rate of 3.1×10^{-9}cm^3/g·Ma from [8].

How does SCR contribution affect T_P ?. Without the SCR contribution, T_Ps are 7.5Ma and 10.1Ma for Yamato-75029 and Tsukuba, respectively. These are 27% and 8.6% larger than those calculated by considering SCR contribution. Thus SCR contribution affects T_P definitely in the case of shielding depth of $0\sim10$g/cm^2.

There is a possibility that the precursor materials were exposed to only GCR at depth that SCR could not reach on their parent body. In this case, we can not distinguish the irradiation on parent body from the space exposure. So T_P is a lower limit for the parent body exposure age and T_S an upper limit for the space exposure age.

The parent body of H chondrites is S-type asteroid [9]. The orbits of S-type asteroids are from 2 to 3.5AU [10]. The heliocentric distance for Yamato-75029 is in good agreement with this. The heliocentric distance for Tsukuba is also in the range given above, within experimental errors.

Reference

[1] Anders E. (1975) *Icarus*, **24**, 363-371.

[2] Wieler R. et al. (1989) *Geochim. Cosmochim. Acta* **53**, 1997-2017.

[3] Takaoka N. et al. (1981) Mem. Natl. Inst. *Polar Res*. Tokyo, Spec. Issue **20**, 264-275.

[4] Okazaki R. et al. (1998) *Symp. Ant. Met., NIPR* Tokyo **23**, 117-119.

[5] Hohenberg C. M. et al. (1978) *Proc. Lunar. Sci. Conf. 9th*, 2311-2344.

[6] Thalmann Ch. and Eugster O. (1995) *Meteoritics*, **30**, 585.

[7] Eugster O. et al. (1995) *Meteoritics & Plant. Sci*. **31**, 299-304.

[8] Eugster O. (1988) *Geochim. Cosmochim. Acta* **52**, 1649-1662.

[9] Pieters C. M. and McFadden L. A. (1994) *Ann. Rev. earth Planet. Sci*. **22**, 457-497.

[10] Gradie J. and Tedesco E. (1982) *Science*, **216**, 1405-1407.

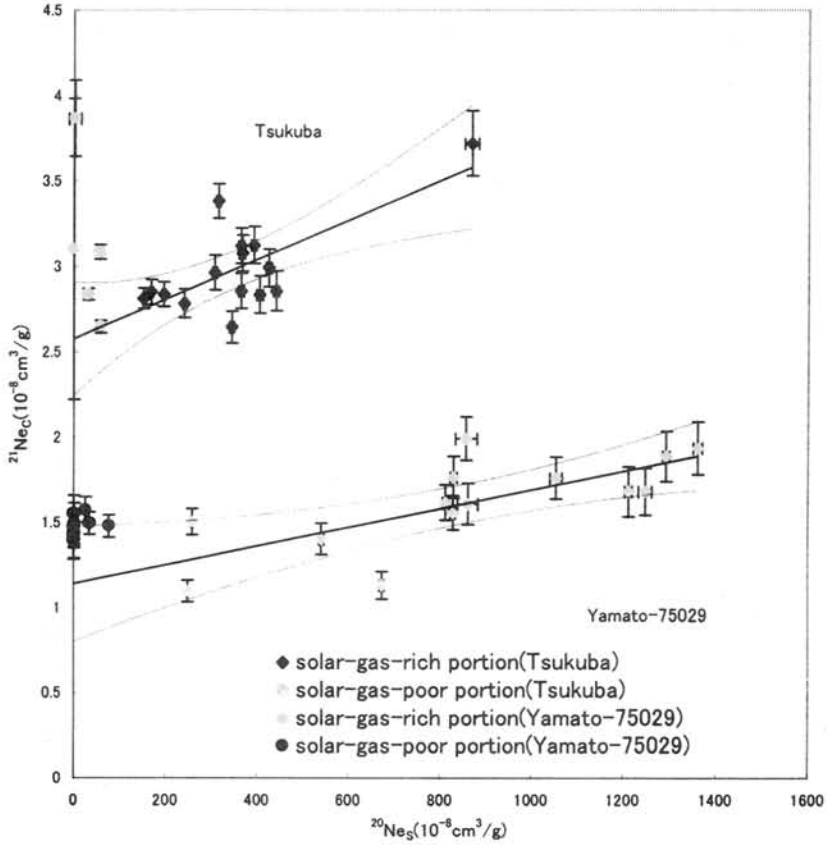

Fig. 1: Correlation between solar ^{20}Ne and cosmogenic ^{21}Ne in samples Yamato-75029 and Tsukuba. The areas between two curved lines are 95% confidence areas for correlation lines.

THE LONAR IMPACT CRATER (INDIA) IN A PLANETARY CONTEXT – AN APPRAISAL

V.K. NAYAK
Department of Applied Geology, University of Saugar, Saugar-3 (M.P.), India

ABSTRACT:

The Indian Impact Crater at Lonar is unique because it is the only known terrestrial crater in basalts and is the closest analog with the lunar craters. The target rocks, impact cratering process and various degrees of shock metamorphism are the important factors. The shocked and unshocked basalts, microbreccias, glass spherules and melt rocks of the Lonar crater are compared with the lunar materials. An appraisal of these aspects of the Lonar and lunar craters are presented in a planetary context.

INTRODUCTION:

As an outgrowth of scientific interest and awareness of planetary exploration programmes, there has been a rapid accleration in the study and understanding of terrestrial impact structures. Over the years, enormous information and ground truth data gathered from more than 150 terrestrial impact craters (Grieve, 1998) have been of critical significance in constraining various aspects of cratering processes. It is now established that impact cratering was a fundamental geological process which will certainly unravel the history of the solar system and planetary evolution.

One such meteorite impact crater is at Lonar (19°58'N : 76°31'E), in Buldana District, Maharashtra State, India. The young crater (30,000 to 50,000 yrs.) is nearly circular, 1830 m diameter, 150 m deep and the floor is occupied by a saline lake. Lonar is unique because it is the only terrestrial impact crater in basalts of the Cretaceous-Eocene age (Nayak, 1972; Fredriksson et al., 1973a). The main minerals in basalt are labradorite, augite, pigeonite, ulvospinel and palagonite. More than three decades of extensive researches of the Indian crater have proliferated with considerable information, data and new ideas (Fudali, 1999). Similarly, tremendous progress has been made with regard to the lunar craters and its rocks, soil and other materials, since the first manned flight to the Moon in 1969.

The purpose of this contribution is an attempt to present an appraisal of the shocked and unshocked basalts, microbreccias, glass and melt rocks of the Lonar crater and compare and correlate them with those of the lunar craters in a planetary context. Hopefully, such an approach will have multiple usefulness and benefits to resolve and comprehend extra-terrestrial geoscientific problems of the planets.

COMPARATIVE APPROACH:

Significant contributions on various aspects of the Lonar crater were made by Fredriksson et al. (1973a). The Lonar impact crater in basalt provides excellent opportunities for comparison with

lunar craters and lunar shocked basalt. The shock effects recognized at Lonar were quantified and the quantification extended to compare between Lonar basalts and shocked lunar basalts.

The mineralogy and chemistry of shock metamorphosed basalts, microbreccias and melt rocks of the Lonar crater are the closest terrestrial analogs to the impact generated rocks and soils of the Moon. A comparison between the two revealed a wide range of similar textures and forms. Besides, the isochemical nature of the Lonar glass and basalt demonstrates that lunar glasses may often be equated chemically with their parent rocks (Fredriksson et al., 1978).

The Lonar microbreccias show that plagioclase is completely transformed into maskelynite (Fredriksson et al., 1973a; Nayak, 1993) and is analogous to that found in lunar breccias, while the Lonar pyroxene exhibits closed-spaced twins, granulation and wavy extinction similar to their lunar counterparts. Fredriksson et al. (1973b) argued that impact-generated silicate spherules from the Lonar crater and from samples of all Apollo sites are analogous to meteoritic chondrules and also some micro-tektites. Further, they suggested that chondrites seem to be mainly impact breccias which are similar to Lonar and lunar microbreccias.

Schaal (1976) compared the results of shocked and unshocked basalts from the Lonar crater with microcraters on the surface of lunar rocks (anorthosite 62255; anorthosite norite 14314; basalt 10085; and polymict breccia 61175) and concluded that equivalent shock features with concentric zones underlying the lunar microcraters correspond to the scheme of five classes of progressive shock metamorphism devised by Kieffer et al. (1976) for basalts of the Lonar crater.

Schaal and *Hörz* (1977) investigated shock metamorphism of lunar and Lonar basalts under shock loaded controlled conditions upto 1000 kbar pressure and reported that the production of shock-induced basalt melt requires intense shock ≥800 kbar pressure.

Morgan (1978) studied the trace element volatilization and meteoritic contamination in the Lonar glasses and high-magnesium australites and reported that heavy volatile elements Re and Se are significantly depleted in the Lonar glasses and depletion and degree of shock can be correlated. Ir is present only in most heavily shocked Lonar glasses but is rather too low to characterize. Further, Morgan (1978) remarked that the Lonar glasses have not proved very rewarding for characterization of meteoritic component, but they do show abundant changes which are related with impact processes. On the other hand australite No. 46 is substantially and uniformly enriched in siderophile elements and the pattern for all nine elements resembles the 'carbonaceous' or 'cometary' component in lunar soil 61220 and somewhat favours the cometary impact origin for australites. As at Lonar, there is depletion of alkalies in the lunar glasses relative to parent basalt (Fredriksson et al., 1971).

Fudali et al. (1980) reconstructed the original morphology of the Lonar crater and presented an evidence for its mechanism of excavation. The depth/diameter ratio is normal but owing to less rock uplift, its rim height/diameter ratio is much smaller than fresh terrestrial and lunar impact craters. Lonar's low rim height/diameter ratio is not a consequence of post-cratering erosion but is due to the nature of the target rocks. This target configuration cannot be unique to the Earth but some lunar and

mercurian craters are expected to be low-rimmed because of Lonar-like target rocks. The continuous ejecta blanket and substrate surrounding Lonar is excellently preserved and this strongly supports that the dominant mechanism of debris transportation and deposition around Lonar was a ground-hugging, fluidized debris surge due to strong gravity field and atmosphere. Consideration of these aspects of Lonar, it should be a good analog for the 'fluidized craters' of Mars. Lonar crater is also compared with other impact craters on the Earth, Moon, Mercury and Mars with planetary considerations (Fudali et al., 1980).

CONCLUDING REMARKS:

Researches of the Lonar impact crater in basalt has certainly helped not only to understand the Indian crater but also to make comparison with the lunar craters, its rocks, soil and impact cratering process. Obviously, there are similarities and differences between the Lonar lunar craters. As such more work and researches on Lonar and lunar craters together with related aspects are imperative. It is believed that the present and future work will continue to provide opportunities in this exciting field to resolve the mysteries of nature in relation to planetary evolution.

Finally, the cosmic visitor which formed the magnificient Indian impact crater at Lonar should be considered as the world's best 'impact crater laboratory' in basalts. The Lonar crater appears like a giant eye staring-up into the sky, saying hallo to its brothers on the Moon and other planets.

REFERENCES:

Fudali, R.F., Milton, D.J., Fredriksson, K. and Dube, A. (1980). Moon and Planets, 23, 493-515.

Fudali, R.F. (1999). Geol. Soc. India, Mem. 43(1), 911-914.

Fredriksson, K., Nelen, J., Noonan, A., Anderson, C.A. and Hinthorne, J.R. (1971). Proc. 2nd Lun. Sci. Conf., 727-735.

Fredriksson, K., Dube, A., Milton, D.J. and Balasundaram, M.S. (1973a). Science, 180, 862-864.

Fredriksson, K. Noonan, A. and Nelen, J. (1973b). The Moon, 7, 475-482.

Fredriksson, K., Brenner, P., Dube, A., Milton, D., Mooring, C. and Nelen, J.A. (1978). Smithsonian Contribution-Earth Science, 22, 1-13.

Grieve, R.A.F. (1998). In Meteorites-Flux with Time and Impact Effects (Eds. Grady, Hutchison, McCall and Rothery), Geol. Soc., London Special Publication, 140, 105-131.

Kieffer, S.W., Schaal, R.B., Gibbons, R., Horz, F., Milton, D.J. and Dube, A. (1976). Proc. 7th Lun. Sci. Conf., 1391-1412.

Morgan, J.W. (1978). Proc. 9th Lun. Planet. Sci. Conf., 2713-2730.

Nayak, V.K. (1972). Earth & Planet. Sci. Letts., 14(1), 1-6.

Nayak, V.K. (1993). Jour. Geol. Soc. India, 41, 307-312.

Schaal, R.B. (1976). M.S. Thesis, University of California, U.S.A., 1-143.

Schaal, R.B. and Hörz, F. (1977). Proc. 8th Lun. Sci. Conf., 1697-1729.

Thermoluminescence Study of Japanese Antarctic Meteorites V

K. Ninagawa[1], M.Ohta[1], N. Imae [2], and Kojima[2]

[1] Department of Applied Physics, Okayama Univ. of Science, 1-1, Ridai-cho, Okayama 700, Japan
[2] National Institute of Polar Research, 9-10, Kaga 1-chome, Itabashi-ku, Tokyo 173, Japan

Natural TL (thermoluminescence), the luminescence of a sample that has received no irradiation in the laboratory, reflects the thermal history of the meteorite in space and on Earth. Natural TL data thus provide insights into such topics as the orbits of meteoroids, the effects of shock heating, and the terrestrial history of meteorites. Induced TL, the response of a luminescent phosphor to a laboratory dose of radiation, reflects the mineralogy and structure of the phosphor, and provides valuable information on the metamorphic and thermal history of meteorites. The sensitivity of the induced TL is used to determine petrologic type of type 3 ordinary chondrites.

As reliable pairing approach, TL properties within large chondrites were analyzed, taking advantage of the fact that serial samples from these meteorites is known to be paired [1]. Then a set of TL pairing criteria: 1) the natural TL peak height ratios, LT/HT, should be within 20%; 2) that ratios of raw natural TL signal to induced TL signal should be within 50%; 3) the TL peak temperatures should be within 20℃ and peak widths within 10℃ was proposed. This set of TL pairing criteria is less restrictive than previously used [1].

We have measured TL of ninety-seven Japanese Antarctic unequilibrated chondrites so far [1,2,3]. This time we measured TL of more twenty-eight Asuka meteorites. The TL data of them are listed in Table. The petrologic subtype was determined from their TL sensitivity. But no primitive chondrite under subtype 3.3 was found. Some of H chondrites, A-880713, 733 and 916, had low TL sensitivity. However, they had high TL peak temperature and wide width. Then microscopic observation of their sections is necessary to ascertain whether shock made them low TL sensitivity or not. Above pairing criteria were also applied to all of Asuka unequilibrated chondrites. A chain of paired chondrites was constituted in H chondrites, and A-880833 and 795 were paired in LL3 chondrites.

References: [1] Ninagawa *et al.* (1998): *Antarctic Meteorite Res.*, **11**, 1-17. [2] Ninagawa *et al.* (2000): *Antarctic Meteorite Res.*, **13**, 112-120. [3] Ohta *et al.* (2000): *Papers presented to the twenty-fifth Symposium on Antarctic Meteorites*, 120-121.

Table Thermoluminescence data of Okayama for twenty-eight unequilibrated Japanese ordinary chondrites

Meteorite	Class	Natural TL		Induced TL				LT /TL Sens. ($x10^3$)	Pairing
		LT/HT	LT (10^3 counts)	TL Sensitivity (Dhajala=1)	Peak Temp. (℃)	Width (℃)	TL Subtype		
A-880833	LL3	2.20 ± 0.01	156.3 ± 22.5	2.02 ± 0.16	143 ± 1	130 ± 4	3.8-3.9	77 ± 13	A-880795
A-880795	LL3	2.52 ± 0.02	141.0 ± 0.8	1.50 ± 0.02	154 ± 2	128 ± 1	3.8	94 ± 1	
A-880774	L3	0.08 ± 0.01	1.9 ± 0.1	0.85 ± 0.03	177 ± 5	145 ± 3	3.7	2.2 ± 0.1	
A-880820	L3	0.82 ± 0.01	18.3 ± 0.5	0.59 ± 0.06	176 ± 3	137 ± 2	3.7	31 ± 3	
A-880708	L3	1.00 ± 0.02	6.2 ± 0.6	0.08 ± 0.01	170 ± 2	151 ± 3	3.4	83 ± 11	
A-880908	L3	1.19 ± 0.06	10.7 ± 1.1	0.53 ± 0.05	162 ± 6	132 ± 1	3.7	20 ± 3	
A-880870	L3	1.33 ± 0.00	9.9 ± 0.1	0.22 ± 0.01	161 ± 9	142 ± 1	3.6	45 ± 2	
A-880709	H3	0.04 ± 0.01	0.2 ± 0.0	0.47 ± 0.02	161 ± 1	136 ± 3	3.6-3.7	0.36 ± 0.02	
A-880710	H3	0.06 ± 0.01	0.1 ± 0.0	0.20 ± 0.00	152 ± 2	138 ± 1	3.5-3.6	0.7 ± 0.1	
A-880901	H3	0.16 ± 0.01	0.7 ± 0.1	0.42 ± 0.02	179 ± 3	151 ± 1	3.6-3.7	1.7 ± 0.2	
A-880713	H3	0.28 ± 0.04	0.1 ± 0.1	0.07 ± 0.00	162 ± 2	151 ± 2	3.4	1.4 ± 0.4	
A-880733	H3	0.53 ± 0.01	0.3 ± 0.1	0.04 ± 0.00	142 ± 1	132 ± 1	3.3-3.4	6.4 ± 0.5	
A-880916	H3	0.62 ± 0.01	0.6 ± 0.1	0.03 ± 0.00	151 ± 2	133 ± 1	3.3	20 ± 1	A-880620
A-880676	H3	0.63 ± 0.03	4.3 ± 0.4	0.41 ± 0.00	152 ± 2	134 ± 1	3.6	10 ± 1	A-880620
A-880793	H3	0.64 ± 0.01	3.7 ± 0.2	0.36 ± 0.02	186 ± 1	155 ± 1	3.6	10 ± 1	
A-880620	H3	0.73 ± 0.01	7.8 ± 0.5	0.54 ± 0.01	161 ± 2	131 ± 1	3.7	14 ± 1	
A-880729	H3	0.87 ± 0.03	22.5 ± 1.5	1.15 ± 0.01	160 ± 5	133 ± 1	3.8	20 ± 1	A-880746
A-880746	H3	0.88 ± 0.01	18.9 ± 0.5	0.93 ± 0.05	158 ± 4	131 ± 1	3.7-3.8	20 ± 1	
A-880711	H3	1.14 ± 0.03	10.6 ± 0.3	0.51 ± 0.00	164 ± 4	131 ± 1	3.7	21 ± 1	A-880613
A-880613	H3	1.28 ± 0.04	60.4 ± 1.4	2.22 ± 0.26	163 ± 11	130 ± 4	3.8-3.9	27 ± 3	A-880624
A-880624	H3	1.51 ± 0.03	31.1 ± 1.9	0.96 ± 0.07	153 ± 6	134 ± 1	3.7-3.8	32 ± 3	A-880724, 684, 840
A-880724	H3	1.68 ± 0.01	47.4 ± 2.4	1.19 ± 0.02	150 ± 3	137 ± 1	3.8	40 ± 2	A-880684, 840, 641
A-880684	H3	1.68 ± 0.06	103.4 ± 5.7	2.23 ± 0.16	167 ± 5	129 ± 2	3.8-3.9	46 ± 4	A-880840, 788, 641
A-880840	H3	1.74 ± 0.06	23.0 ± 1.7	0.70 ± 0.01	154 ± 2	128 ± 1	3.7	33 ± 2	A-880788, 863
A-880788	H3	1.90 ± 0.01	51.7 ± 1.0	1.26 ± 0.15	154 ± 1	124 ± 4	3.8	41 ± 5	A-880641, 863
A-880641	H3	1.94 ± 0.01	40.7 ± 3.1	0.77 ± 0.09	159 ± 1	136 ± 1	3.7	53 ± 7	A-880863
A-880863	H3	2.05 ± 0.06	21.6 ± 0.5	0.47 ± 0.01	150 ± 4	129 ± 1	3.7	46 ± 1	
A-880869	H3	3.57 ± 0.01	77.4 ± 5.3	0.94 ± 0.09	155 ± 2	127 ± 1	3.7-3.8	82 ± 10	

Mineralogy of phyllosilicate-rich micrometeorites and their relationship with some CI and CM chondrites.

Takaaki NOGUCHI[1]*, Tomoki NAKAMURA[2], and Wataru NOZAKI[2]
[1] Department of Materials and Biological Sciences, Ibaraki University, Bunkyo 2-1-1, Mito 310-8512, Japan
[2] Department of Earth and Planetary Science, Kyushu University, Hakozaki, Fukuoka 812-8581, Japan

1. Introduction

Less heated MMs have been investigated chemically, petrologically, and mineralogically (e. g. Kurat *et al.*, 1994; Genge et al., 1997). Small population of the unmelted MMs contains abundant phyllosilicates. However, detailed mineralogical data of phyllosilicate-rich MMs are rare (Klöck and Stadermann, 1994; Noguchi and Nakamura, 2000). We investigated individual unmelted MMs by synchrotron radiation X-ray diffraction (SR-XRD) method, transmission electron microscopy (TEM). There are two types of phyllosilicate-rich MMs: saponite-rich ones and serpentine-rich ones. First TEM study of a phyllosilicate-rich MM revealed that the MM contains only saponite as phyllosiliate (Klöck and Stadermann, 1994). Noguchi and Nakamura (2000) reported a similar result for a saponite-rich MM. Recently Genge et al. (2001) found a large MM in which serpentine coexists with saponite like the case of CI chondrites such as Orgueil (Tomeoka and Buseck, 1988) although saponite in the MM had been already decomposed into amorphous material during atmospheric entry. Except for the exceptional MM found by Genge et al. (2001), the other saponite-rich MMs contains only saponite as phyllosilicates (Klöck and Stadermann, 1994; Noguchi and Nakamura, 2000 and 2001). Absence of serpentine in the saponite-rich MMs is different from the case of "normal" CI chondrites in which serpentine coexists with saponite. Noguchi and Nakamura (2000; 2001) and Nakamura et al. (2001b) discovered that some saponite-rich MMs contain fine-grained magnesiowüstite (MW)-Fe sulfide aggregates as well as fine-grained magnetite aggregates. Such MW-bearing aggregates have not been reported from known meteorites. In the previous studies on the saponite-rich MMs, the meteorite counterparts of the MMs have not been identified yet. In this study, we found a possible candidates for the meteorite counterparts of the MMs among the recently fallen meteorites. It is a carbonaceous chondrite Tagish Lake fell at British Columbia, Canada in January 18, 2000 (Brown et al., 2000). We investigated the meteorite and concluded that the saponite-rich MMs have similarity to the matrix of Tagish Lake. Noguchi and Nakamura (2001) also found another type of phyllosilicate-rich MM: a serpentine-rich MM that does not contain saponite like the case of CM chondrites. In this paper, we will show the mineralogy of the MMs and also compare the mineralogy of the saponite-rich MMs with Tagish Lake CI chondrite and those of the serpentine-rich MMs with a CM chondrite Sayama that experienced heavy aqueous alteration and discuss the origins of the phyllosilicate-rich MMs.

2. Samples and experimental procedures

Four phyllosilicate-rich MMs were investigated in this study. Three MMs are rich in saponite. Another one was rich in serpentine. The MMs that were investigated by SR-XRD technique at High Energy Accelerator Research Organization. We also investigated some fine-grained fragments of Tagish Lake CI chondrite and Sayama CM2 chondrite, to compare their mineralogy with the phyllosilicate-rich MMs investigated. Because the effects of heating during atmospheric entry is definite even though MMs contain abundant saponite, we performed heating experiments of fine-grained fragments of Tagish Lake matrix to compare bulk mineralogy and microstructure of the run products with some saponite-rich MMs. A vacuum furnace was used for the experiment. Each MM, each fragment of two carbonaceous chondrites, and a run product of the heating experiment were embedded in epoxy resin and microtomed by ultramicrotome for TEM observation. Microstructure, mineralogy, and chemical compositions of minerals of the samples were obtained by TEM equipped with EDS. Semiquantitative analysis was based on the modified

Cliff-Lorimer thin film approximation. Experimental k factors were determined from many mineral standards.

3. Results and discussion

Mineralogy of saponite-rich MMs We found three MMs that are rich in saponite. SR-XRD data revealed that the major constituent minerals are saponite, Fe sulfides, and magnetite although the relative abundance of pyrrhotite and magnetite widely varies among the MMs. In two saponite-rich MMs, magnesiowüstite (MW)-bearing aggregates were discovered. Based on TEM observation, the aggregates consist of < 50 nm across polygonal MW and a small amount of Fe sulfide grains that tend to be larger than MW. Serpentine and other hydrous phases except for saponite were not identified. Major minerals in the MW-bearing saponite-rich MMs are saponite, pyrrhotite, magnetite, and MW. Although MW is a rare mineral among meteorites, it is relatively common in moderately heated MMs in which MW coexists with low-Ca pyroxene (Nakamura et al., 2001b).

TEM observation of the saponite-rich MMs displays that the matrices contain abundant coarse irregularly shaped phyllosilicates. Among the phyllosilicates, there are aggregates of Fe oxide and sulfide as described above. High-resolution TEM imaging of the coarse phyllosilicates reveals that spacing of basal lattice fringes ranges from 0.95 to 1.05 nm except for one MM in which saponite has 1.35 nm lattice fringes. The spacing indicates that the coarse phyllosilicates are saponite.

Mineralogy of the matrix of Tagish Lake Two fine-grained (about 100 μm across) fragments of Tagish Lake CI chondrite were used for comparison with the saponite-rich MMs. We found that the matrix with Fe- and Mg-rich carbonate (magnesian siderite)-rich lithology contains abundant saponite and is very poor in serpentine (Nakamura et al., 2001). Major minerals in the matrix are saponite, pyrrhotite, magnesian siderite, and pentlandite. Magnetite is poor in the matrix. Serpentine was not found by the SR-XRD technique, although only a trace amount of serpentine layers that coexists with saponite having coherent boundaries was found by TEM observation.

TEM observation of the matrix of Tagish Lake shows that the matrix of Tagish Lake is composed mainly of abundant coarse irregularly shaped phyllosilicates and abundant fine-grained (mainly 100-300 nm across) pyrrhotite grains and coarse (> 500 nm across) magnesian siderite grains embedded in the phyllosilicates. Magnetite grains are rare in the matrix. The matrix texture is similar to those of the saponite-rich MMs although the matrix of Tagish Lake is more porous than those of the MMs and there is no magnesian siderite in the matrices of the saponite-rich MMs.

MW-bearing aggregates in the saponite-rich MMs MW-bearing aggregates often have fine-grained rims. The outlines of the aggregates suggest that they are pseudomorphs of precursor mineral grains. Shapes of each MW grain are polygonal and suggest that the MW grains were formed though decompositions and recrystallization of precursor minerals. Based on AEM data, MW grains in a saponite-rich MM contain about 3 wt % MnO. If the aggregates are not primary objects as the texture of the aggregates suggests, their precursor material often contains a small amount of Mn as well as abundant Mg and Fe. One possible precursor material of the aggregate is Mg- and Fe-rich carbonate. As described above, Tagish Lake matrix contains magnesian siderite, which often include a small amount of Mn. It is plausible that Mg- and Fe-rich carbonate is the precursor material of the aggregates. If the saponite-rich MMs contained Mg- and Fe-rich carbonate before entering the Earth's atmosphere, their major mineral assemblage is very similar to that of Tagish Lake matrix investigated in our study. The estimated assemblage is saponite, Fe sulfides, magnetite, and Mg- and Fe-rich carbonate.

Heating experiment of the matrix of Tagish Lake Can the Tagish Lake matrix transformed into material similar to the saponite-rich MMs by heating? We conducted heating experiments to answer this question. Small fragments (< several hundred μm across) of the matrix of Tagish Lake

were heated by an electric furnace under vacuum condition. Samples were set in a small open silica glass capsule. Temperature of the capsule was measured by a thermocouple. When the samples were heated at 600 °C for 120 sec under 10^{-2} Torr, SR-XRD and TEM data show that magnesian siderite was decomposed into the aggregates of MW. AEM data display that the Mg/(Mg+Fe) atomic ratios of the decomposed products were not greatly affected during the decomposition of their precursor material. On the other hand, XRD and TEM data revealed that saponite keeps its structure. The heating experiment clearly displays that Mg- and Fe-rich carbonate can be decomposed into oxide aggregates although saponite is not decomposed under the experimental condition. The experimental condition is reasonable for 100-500 μm-sized micrometeoroids that enter the Earth's atmosphere with about 12-15 km/sec (Yada et al., 1996). Therefore, it is plausible that MW-bearing saponite-rich MMs can be formed by decomposition of material similar to Tagish Lake matrix investigated in this study. This result strongly suggests that saponite-rich MMs (at least, MW-bearing saponite-rich MMs) were derived from parent bodies that are very similar to the parent body of Tagish Lake.

Bulk mineralogy and texture of a serpentine-rich MM We could find only one MM that bears abundant serpentine by SR-XRD technique. Reflections of serpentine are sharp indicative of well crystallinity. The serpentine has an average basal spacing (0.715 nm) shorter than that of normal serpentine (0.73 nm) due to exchange of parts of Si^{4+} by Fe^{3+} in the tetrahedral layers. (02*l*) prism diffraction due to disordered stacking was also found. This MM is composed mainly of serpentine and magnetite. Diffraction peaks due to tochilinite were not observed. Relict anhydrous silicates were not found in this MM. Fe oxides and sulfides are very rare.

Microstructure of a serpentine-rich MM and Sayama TEM observation of the MM revealed that its matrix is composed of coarse (0.1 to 1 μm across) serpentine crystals that were embedded in very-fine grained poorly crystalline serpentine. Minor mineral is fine-grained (< 100 nm across) magnetite. Fe sulfides are rare. 0.70~0.73 nm basal spacing and EDS analysis of the coarse serpentine indicates that it is cronstedtite. Mg/(Mg+Fe) atomic ratio of the cronstedtite ranges from 0.17 to 0.07. Although its composition is very similar to that in CM chondrites, cronstedtite does not coexist with tochilinite that usually coexists with cronstedtite in CM chondrites. EDS analysis of the very-fine grained serpentine indicate that it is much more heterogeneous in Mg/(Mg+Fe) ratios (0.46-0.05) and contains more Si than the coarse cronstedtite. Anhydrous silicates such as olivine were not observed in the MM.

SR-XRD data of matrix fragments of Sayama, which experienced severe aqueous alteration on its parent body display that the matrix contains abundant serpentine, pentlandite, and magnetite. TEM observation of the matrix shows that its texture is very similar to the case of the serpentine-rich MM. The matrix is composed of coarse serpentine grains that are embedded in fine-grained serpentine. Fine-grained (< 100 nm across) pyrrhotite, pentlandite, and magnetite are also set in the fine-grained serpentine. Different from the case of the serpentine-rich MM, the coarse serpentine in Sayama matrix is Fe-rich serpentine. Fine-grained serpentine in the matrix is more homogeneous and magnesian than those in the fine-grained serpentine in the MM. Zolensky (1993) reported that carbonaceous chondrites that experienced heavier aqueous alteration have more magnesian and homogeneous serpentine. Therefore, the matrix of Sayama experienced heavier aqueous alteration than the serpentine-rich MM.

Cronstedtite in the serpentine-rich MM does not coexist with tochilinite. Coexistence of these minerals is common among CM chondrites. One may think that the difference means that the serpentine-rich MM is different from CM chondrites. However, tochilinite decomposes at slightly lower temperature than the decomposition temperature of cronstedtite (Caillère and Hénin, 1957). It is plausible that tochilinite was preferentially decomposed into Fe-rich phase(s) by heating during atmospheric entry. Therefore, it cannot be denied that the serpentine-rich MM had similar mineral assemblage before entering the Earth's atmosphere to that of moderately altered CM chondrite matrix and that at least the serpentine-rich MM was derived from a parent body that is

very similar to those of moderately to heavily altered CM chondrites.

Acknowledgement

We thank H. Kojima, M. Maurrette, M. E. Zolensky, and S. Yoneda to give us specimens of MMs, Tagish Lake, and Sayama. We also thank M. Tanaka and T. Mori for technical support during X-ray diffraction analysis. We thank N. Takaoka for his encouragement to investigate MMs. H. Nagahara is appreciated for her permission to use an electric furnace for preliminary heating experiment of Tagish Lake. T. Yada, N. Matsumoto, J. Kamata, and Y. Uryu are also appreciated for their endeavor to search phyllosilicate-rich MMs with us. This study is partially supported by grant-in-aid for scientific research (main investigator: H. Kojima).

References

Brown, P. G. et al. (2000) Science, 290, 320-325.
Caillère S. and Hénin S. (1957) In: The differential thermal investigation of clays.
Genge, M. J. et al. (1997) GCA, 61, 5149-5162.
Genge M. J. et al. (2001) LPSC, XXXII, CD-ROM.
Klöck, W. and Staderman (1994) In: Analysis of Interplanetary dust, 51-87.
Kurat, G. (1994) GCA, 58, 3879-3904.
Noguchi, T. and Nakamura, T. (2000) Antarct. Meteorite Res., 13, 285-301
Nakamura, T. et al. (2001) LPSC XXXII, CD-ROM.
Nakamura, T. et al. (2001) GCA, in press.
Noguchi, T. and Nakamura, T. (2001) LPSC, XXXII, CD-ROM.
Tomeoka, K. and Buseck, P. *. (1988) GCA, 52, 1627-1640.
Yada, T. et al. (1996) Antarct Meteorite Res., 9, 218-236.
Zolensky, M. E. et al. (1993) GCA 57, 3123-3148.

DATING EUCRITE FORMATION AND METAMORPHISM. L. E. Nyquist[1] , Y. Reese[2], H. Wiesmann[2], C.-Y. Shih[2], H. Takeda[3], [1]Mail Code SN2, NASA Johnson Space Center, Houston, TX 77058, l.nyquist@jsc.nasa.gov, [2]Mail Code C23, Lockheed-Martin Space Mission Systems and Service Co., 2400 NASA Road 1, Houston, TX 77058. [3]Research Institute, Chiba Inst. of Tech., 2-17-1 Tsudanuma, Narashino City, Chiba 275-0016.

Introduction: The crystallization ages of eucritic basalts from the HED parent body (probably asteroid 4 Vesta [1,29]) were established to be ~4.56 Ga some time ago (e.g., [2]). However, ages determined by differing methods often are discordant, suggesting that in general eucrites have experienced a complex history since crystallization. Impact cratering on the HEDPB has had a major influence on the more easily reset chronometers. Thus, many ^{39}Ar-^{40}Ar ages and some Rb-Sr ages of eucrites have been reset to the interval ~3.4-4.1 Ga ago that characterizes a period of heavy bombardment in the inner solar system [3]. Several non-brecciated eucrites apparently were shielded from the heavy bombardment and give ^{39}Ar-^{40}Ar ages of ~4.49-4.50 Ga [4]. Pristine eucrite clast Y75011,84 has a Rb-Sr age of 4.56±0.05 Ga [5], but an ^{39}Ar-^{40}Ar age of only 3.95±0.05 Ga [6], showing that nearly complete Ar outgassing can occur without noticeable textural changes. Evidence of other thermal events affecting the eucrites is recorded in their texture and mineralogy, however. A metamorphic scale for the eucrites has been constructed based on observations of pyroxene homogenization and exsolution [7]. Other, more subtle textural evidence of thermal metamorphism also has been observed in eucrites [8,9]. This evidence, combined with isotopic studies, has been interpreted as indicating major thermal events affecting some eucrites in the time period of ~4.48-4.50 Ga ago [8,9].

We present a summary of recent chronological data obtained in consortia studies of several eucrites and eucritic clasts from howardites that combine textural, mineralogical, and Rb-Sr and Sm-Nd isotopic studies. Several eucrites have ages of ~4.50 Ga; it even can be argued that this is a preferred average age. In at least one case, that of the Ca-rich eucrite, A881394, the conventional Rb-Sr and Sm-Nd ages cannot be original crystallization ages. This conclusion arises from the presence of radiogenic ^{53}Cr* and ^{26}Mg*, decay products of ^{53}Mn ($t_{1/2}$ = 3.7 Ma) and ^{26}Al ($t_{1/2}$ = 0.72 Ma), in A881394. Thus, its crystallization age is close to the ~4566 Ma age of the solar system, in spite of younger conventional Rb-Sr and Sm-Nd ages.

Summary of ^{87}Rb-^{87}Sr Ages: An early study of bulk eucrites established a Basaltic Achondrite Best Initial (BABI) ^{87}Sr/^{86}Sr value that was among the lowest found for meteorites and lunar samples, suggesting that eucrites were among the oldest rocks in the solar system [10]. The corresponding whole rock isochron age was relatively imprecise, however.

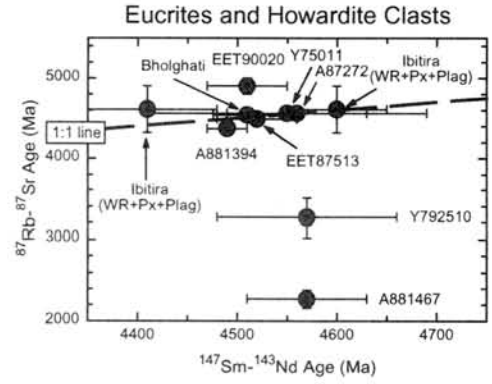

Figure 1. Comparison of ^{87}Rb-^{87}Sr and ^{147}Sm-^{143}Nd ages of eucrites and eucritic clasts in howardites.

Birck and Allegre [2] reported an "internal isochron" age of 4.53±0.13 Ga for combined samples from Juvinas and Ibitira, but the Rb-Sr systematics of several other eucrites they analysed were disturbed. (All Rb-Sr ages discussed here are recalculated for the decay constant λ_{87} = 0.01402 Ga^{-1} [11,12]). Nyquist et al. [5] found a Rb-Sr age of 4.56±0.05 Ga for the pristine eucrite clast Y75011,84 and 4.52±0.06 Ga for matrix material from the same eucrite. In Figure 1 we have plotted Rb-Sr ages from the JSC lab against Sm-Nd ages for the same samples. The Rb-Sr ages vary considerably more than the Sm-Nd ages. The youngest Rb-Sr ages, for A881467 and Y792510, have clearly been disturbed by "late" events, either impact on the surface of the HEDPB, or weathering in the Antarctic. The "too old" age of EET90020 is determined by data for tridymite, interpreted to have formed during a late event in which the mesostasis of the original basalt was melted and recrystallized [9]. The remaining data can be analysed in a number of ways, all of which suggest average ages that are apparently younger than the canonical ~4560 Ma age often assumed for eucrites. For example, data for Y75011,84 [5], the Bholghati clast [13], EET87513,18E [14], and A881394,53 [15], having individual precisions better than 2%, average to 4490±85 Ma (1σ) directly. A weighted average, weighted inversely as the square of individual uncertainties, is 4498±30 Ma (weighted 2σ). One of the better defined individual Rb-Sr ages is 4490±80 Ma (2σ) for EET87513, 18 Clast E [14], coincident with the average, and suggestive of a "young" age.

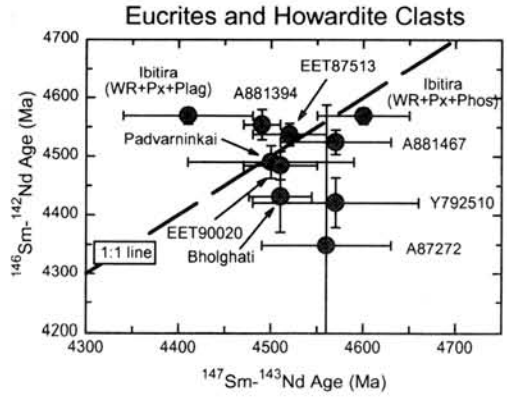

Figure 2. ^{146}Sm-^{142}Nd ages relative to $^{146}Sm/^{144}Sm$ = 0.0076 [21] and T = 4558 Ma for LEW86010 [22] compared to conventional ^{147}Sm-^{143}Nd ages.

Summary of Sm-Nd Ages: The conventional ^{147}Sm-^{143}Nd ages of these samples are similar to those Rb-Sr ages that haven't been reset, but are less variable. The most precisely determined values are ~4500 Ma (Figure 2). Thus, although the average value of all ages is 4524±54 Ma (1σ), the weighted average age is 4506±13 Ma (weighted 2σ). Samples with "old" (~4560 Ma) ages have high positive initial ε_{Nd} ~2.0 and low ^{39}Ar-^{40}Ar ages, as typified by the Y792510,65 clast [8]. Five samples lie along the 1:1 correlation line for equal ^{146}Sm-^{142}Nd ages and ^{147}Sm-^{143}Nd ages, but the correlation is poor. Previously reported ages for Ibitira are discordant, including a Pb-Pb model age of 4556±6 Ma [16] a ^{147}Sm-^{143}Nd age of 4460±20 Ma [17], and an ^{39}Ar-^{40}Ar age of 4495±15 Ma [18]. Discordant ^{147}Sm-^{143}Nd isochron ages for different Ibitira mineral combinations were attributed to post-crystallization metamorphism [20]. Considering those four eucrites with 2σ isochron uncertainties of ≤ 1% (Bholghati [13], EET87513,18E [19], EET90020[9], and A881394

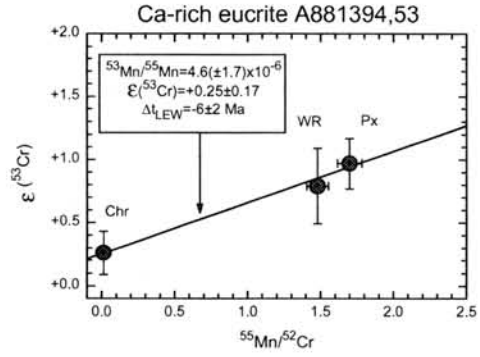

Figure 3. Mn-Cr isotopic data for Ca- raich eucrite A881394,53.

[15]) allows calculation of a simple average age of 4508±13 Ma (1σ), or a weighted average age of 4501±15 Ma (weighted 2σ). These results are compatible with one another, and the average values lie within the error limits of the individual samples, suggesting that these eucrites share a common ^{147}Sm-^{143}Nd age of ~4501 Ma.

Seven of the more precisely determined ^{146}Sm-^{142}Nd ages, calculated relative to $^{146}Sm/^{144}Sm$ = 0.0076 [21] and the Pb-Pb age of 4558 Ma [22] for LEW86010, range from 4484 to 4569 Ma. These ages show values that are both older and younger than the average ^{147}Sm-^{143}Nd age of ~4501 Ma. The precision of the ^{146}Sm-^{142}Nd chronometer decreases rapidly with decreasing ages.

Discussion: One of the oldest ^{146}Sm-^{142}Nd ages, 4554±26 Ma, was found for the Ca-rich eucrite, A881394. This result is expected to be robust, and indeed, Mn-Cr and Al-Mg isotopic data confirm an ancient age. A Mn-Cr isochron (Figure 3) determines initial $^{53}Mn/^{55}Mn$ = (4.6±1.7) x 10^{-6}, equal to the value reported by [23] for differentiation of the HEDPB. Thus, A881394 may have been produced during initial differentiation of its parent asteroid.

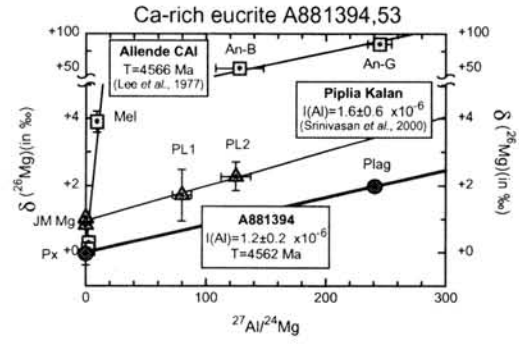

Figure 4. Al-Mg data for A881394 compared to that reported for eucrite Piplia Kalan [28], and Allende CAI [25].

To confirm the antiquity of A881394, we also measured the Mg isotopic composition of its plagioclase and pyroxene (Figure 4). Plagioclase contains a pronounced ^{26}Mg excess, $\delta^{26}Mg$ = 2 ‰, whereas $\delta^{26}Mg$ ~0 for pyroxene. These parameters correspond to initial $^{26}Al/^{27}Al$ = (1.2±0.2) x 10^{-6}, and an age T= 4562 Ma relative to T = 4566 Ma [24] for Allende CAI WA [25]. This absolute age is ~3 Ma less than the ~4565 Ma age given by [23] as corresponding to $^{53}Mn/^{55}Mn$ ~4.7 x 10^{-6} relative to an age of 4558 Ma for the LEW86010 angrite, suggesting some adjustment of the "absolute" ages of CAI and LEW86010 may be needed. An upward adjustment of the CAI age to ~4569 Ma would place it in the range 4568-4571 Ma previous estimated by [23] as the age of the solar system from Pb-Pb and Mn-Cr ages. The presence of ^{26}Mg and ^{53}Cr excesses in A881394 clearly establishes its antiquity in spite of

an apparently well-defined ^{147}Sm-^{143}Nd age of 4490±20 Ma.

Figure 5 illustrates how the ^{147}Sm-^{143}Nd age of A881394 could have been reset to a lower value. Post-crystallization, subsolidus partitioning of Sm and Nd among the minerals would not have affected the Sm/Nd ratio of the bulk rock. Thus, an isochron through the whole rock point corresponding to a crystallization age of 4562 Ma and initial ε_{Nd} = +0.13±0.45 reveals the direction of displacement of the Sm/Nd ratios of the various mineral phases during reequilibration. The pyroxene datum is not significantly displaced from the isochron, but plagioclase, tridymite, and a plagioclase leach are. Phases with relatively low REE abundances, could have acquired Nd from phosphate, which has a similarly low Sm/Nd ratio, thus similar $^{143}Nd/^{144}Nd$, and which contains the majority of the REE in most eucrites. Subsolidus partitioning of REE is likely to have increased the LREE in plagioclase relative to the HREE while increasing overall REE abundances in this phase, as indicated by ion probe analyses of plagioclase in EET90020, for example [9]. If phosphate data points are underrepresented when the data are regressed, the regression will return an "isochron" with a slope lower than that which corresponds to the primary crystallization age. The ^{146}Sm-^{142}Nd ages are more robust to this effect, since a few percent shift in the Sm/Nd ratio of the data make a negligible change in the age.

Conclusions: A881394 was classified as a cumulate eucrite based on its Mg-rich bulk composition [30]. However, cumulate texture is not preserved, and Takeda et al. [27] proposed metamorphic recrystallization followed by cooling at a rate comparable to that for cumulate eucrites. Apparently "young" ages of cumulate eucrites compared to the ~4566 Ma age of the solar system have been known for some time. The data presented here adds to evidence for "young" ages for non-cumulate as well as cumulate eucrites. We note Pb-Pb mineral isochron ages in the range ~4453-4521 Ma for non-cumulate eucrites Cachari, Nuevo Laredo, Bouvante, and Bereba [26]. The simplest interpretation of the radiometric data is that such ages arise from "late" volcanism on the HED PB. However, the presence of decay products of the short-lived nuclei ^{53}Mn and ^{26}Al in A881394 shows that igneous crystallization of this eucrite occurred earlier than indicated by the conventional Rb-Sr and Sm-Nd ages. Thus, at least some conventional radiometric ages based on long-lived radioactivities have been reset by one or more major thermal events on the HEDPB that post-dated the earliest volcanism, but predated the "cataclysmic" bombardment ~3.4-4.1 Ga ago. This is consistent with the interpretation that A881394 experienced metamorphism and slow cooling after initial crystallization during early crustal evolution of its parent body [27]. HED meteorites have been linked to the large impact basin near the south pole of 4 Vesta by [1] and [29]. Radiometric ages of ~4.50 Ga for EET90020 have been suggested to be linked to this basin by [9]. Perhaps this event affected eucrites more generally, and excavated cumulate eucrites from depth.

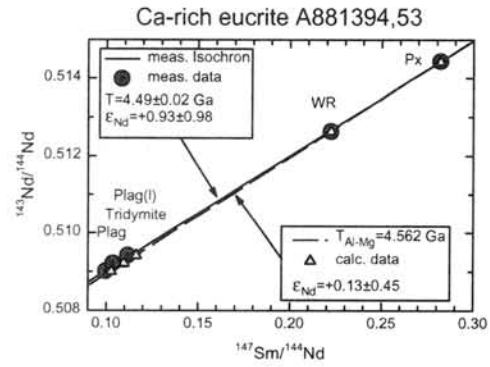

Figure 5. Effect of resetting of ^{147}Sm-^{143}Nd isochron by post-crystallization processes.

References: [1] Binzel R. P. (2001) *MAPS 36,* 481-499. [2] Birck J. L. and Allègre C. J. (1978) *EPSL 39,* 37-51. [3] Bogard D.D. (1995) *Meteoritics, 30,* 244-268. [4] Bogard D. D. and Garrison D. H. (2001) *LPSC 32,* #1138. [5] Nyquist L. E., et al. (1986) *JGR 91,* 8137-8150. [6] Takeda H., et al. (1994) *EPSL 122,* 183-194. [7] Takeda H. and Graham A. L. (1991) *Meteoritics 26,* 129-134. [8] Nyquist L. E., et al. (1997) *GCA 61,* 2119-2138. [9] Yamaguchi A., et al. (2001) *GCA*, in press. [10] Papanastassiou D. A. and Wasserburg G. J. (1969) *EPSL. 5,* 361-376. [11] Minster J.-F., et al. (1982) *Nature 300,* 414-419. [12] Begemann F., et al. (2000) *GCA 65,* 111-121. [13] Nyquist L. E., et al. (1990) *GCA 54,* 2195-2206. [14] Nyquist L. E., et al. (1994) *LPSC XXV,* 1015-1016. [15] Unpublished JSC data. [16] Chen J. H. and Wasserburg G. J. (1985) *LPS XVI,* 119-120. [17] Prinzhofer A., et al. (1992) *GCA 56,* 797-815. [18] Bogard D. D. and Garrison D. H. (1995) *GCA 59,* 4317-4322. [19] Nyquist L. E., et al. (1992) *LPSC XXIII,* 1009-1010. [20] Nyquist L. E., et al. (1999) *MAPS 34,* A87. [21] Nyquist L. E., et al. (1994) *Meteoritics 29,* 872-885. [22] Lugmair G. W. and Galer S. J. G. (1992) *GCA 56,* 1673-1694. [23] Lugmair G. W. and Shukolyukov A. (1998) *GCA 62,* 2863-2886. [24] Carlson R. W. and Lugmair G. W. (2000) In *Origin of Earth and Moon*, Univ. Ariz. [25] Lee T., et al. (1977) *Ap. J.* L107-110. [26] Tera F. et al. (1997) *GCA 61,* 1713-1731. [27] Takeda H., et al. (1997) *Antarct. Meteorite Res. 10,* 417-429. [28] Srinivasan G., et al. (2000) *LPSC 31,* #1795. [29] Drake M. J. (2001) *MAPS 36,* 501-513. [30] Cat. Antarctic Met. (1995), NIPR, Tokyo.

Microdistribution of noble gases in unequilibrated enstatite chondrites, Yamato 691 and Allan Hills 77295

R. Okazaki[1)], K. Nagao[1)], N. Takaoka[2)], and T. Nakamura[2)]
1) Laboratory for Earthquake Chemistry, Graduate School of Science, University of Tokyo, Hongo, Bunkyo-ku, Tokyo 113-0033, Japan
2) Department of Earth and Planetary Sciences, Faculty of Science, Kyushu University 33, Hakozaki, Fukuoka 812-8581, Japan

Introduction

Enstatite chondrites (ECs) are characterized by their highly reduced minerals and relative elemental abundances of noble gases trapped in them. Trapped noble gases in ECs are usually mixture between "subsolar" [Crabb and Anders, 1981] and Q-gas, which is trapped in a "phase-Q" [Huss et al., 1996]. These trapped noble gases are well discriminated by their $^{36}Ar/^{132}Xe$ and $^{84}Kr/^{132}Xe$ ratios; $(^{36}Ar/^{84}Kr/^{132}Xe)_{subsolar}$ = 2700/6/1 (for South Oman EC; Crabb and Anders, 1981), $(^{36}Ar/^{84}Kr/^{132}Xe)_{Q\text{-}gas}$ = 60/0.8/1 (for Murchison; Wieler et al., 1992).

Recently, we discovered that some *chondrules* in an enstatite chondrite Y-791790 (a high-Fe and type 4 EC: EH4) contained huge amounts of subsolar gas [Okazaki et al., 2001]. Our model to explain subsolar gas in chondrules is that solar-type noble gases from the young sun were implanted into the precursory materials of chondrules, and the elemental ratios of subsolar gas were produced by diffusive loss of the implanted gases during the chondrule formation. This hypothesis implies that subsolar gas should be contained in chondrules in every ECs. However, subsolar gas has never been found in unequilibrated ECs (UECs) [e.g., Patzer and Schultz, 2000], and only type 4-6 ECs show the subsolar signature.

To get more precise and extensive information on microdistribution of noble gases in ECs, we have investigated two UECs, Y-691 and ALH77295. Noble gases in individual components of these meteorites, such as chondrules, large opaque fragments (consisting of Fe-Ni metal, FeS, and several kinds of sulfide; e.g., Keil, 1968), and matrix portions, were extracted with a Nd-YAG laser with beam diameter of 30-70 μm [e.g., Nakamura et al., 1999]. Evolved noble gases were measured with a modified VG5400 mass spectrometer (MS-II) at University of Tokyo [e.g., Nagao *et al.*, 1999].

Results and discussion

a) Y-691

Y-691 contains clearly defined chondrules and does not show any sever shock feature [Kimura, 1988], indicative of its primitive nature. Microscopic observation revealed that matrices consisted mainly of FeS, and Fe-Ni metal, and several kinds of silicates (pyroxene, olivine, plagioclase, and silica mineral). Most chondrules are dominated by porphyritic pyroxene. Coarse opaque fragments are also seen.

Certain amounts of ^{84}Kr and ^{132}Xe (about 1×10^{-8} cm^3STP/g) are released from all matrix portions although ^{4}He, ^{20}Ne, and ^{36}Ar are rare. In contrast to the matrix portions, most of chondrules and opaque assemblages contain small amounts of trapped noble gases. As shown in Fig. 1, there is a good correlation between the $^{36}Ar/^{132}Xe$ ratio and ^{132}Xe concentration. The $^{36}Ar/^{132}Xe$ ratios of the matrix plot around that of Q-gas (shown as a dashed line), and $^{84}Kr/^{132}Xe$ ratios are confined within a range between 0.5 and 0.7. These signatures suggest that the heavy noble gases in the matrix materials are potentially Q-gas.

b) ALH77295

ALH77295 is paired with ALH77156, which is classified as a brecciated UEC [Wieler et al., 1985 and references listed there], which suggests that ALH77295 has experienced some shock events. Many chondrules are flattened, and their margins are not clear. Matrices contain small chondrule fragments, and are more enriched in silicates compared to matrix materials in Y-691.

High concentrations of ^{132}Xe (7×10^{-9} cm^3STP/g) were observed also in ALH77295 matrices (Fig. 1) , although it is a breccia. The $^{36}Ar/^{132}Xe$ ratios of the matrices are essentially identical to that of Q-gas (Fig. 1). Unlike Y691, some chondrules also show ^{132}Xe concentrations similar to those of matrices (Fig. 1). The Xe-rich chondrules are smaller than the other chondrules and the laser pits include surrounding matrix materials, which might be responsible for the high ^{132}Xe concentrations.

In addition to the Q-gas, there are abundant solar-type noble gases in matrices, in which high ^4He concentrations (up to 1×10^{-3} cm^3STP/g) and $^3He/^4He$ ratios close to those of solar wind (SW) or solar energetic particles (SEPs) were observed (Fig. 2). The small chondrules with high ^{132}Xe concentrations also exhibit the presence of solar He, which is also attributable to contamination of matrix materials. Noticeable amounts of ^{20}Ne (from 8×10^{-8} to 2×10^{-6} cm^3STP/g) are released only from matrices. As shown in Fig. 3, Ne-isotopes are indicative of large contribution of SEP Ne in matrices. These noble-gas signatures indicate that solar gases are located in fine-grained matrix materials.

The locality of solar He and Ne in fine-grained matrices of ALH77295 is consistent with the explanation for the solar-gas-rich brecciated meteorites: SW and SEPs have been implanted into the surface of fine grains during many impact events on the outermost layer of the EC parent bodies.

References: Crabb J. and Anders E. (1981) *GCA* **45**, 2443-2464; Huss G. R. et al. (1996) *GCA* **60**, 3311-3340; Wieler R. et al. (1992) *GCA* **56**, 2907-2921; Okazaki R. et al. (2001) submitted to *Nature*; Patzer A. and Schultz L. (2000) *Meteorit. Planet. Sci.* **35**, A125; Keil K. (1968) *JGR* **73**, 6945-6976; Nakamura T. et al. (1999) *GCA* **63**, 241-255; Nagao K. *et al.* (1999) *Antarct. Meteorite Res.* **12**, 81-93; Kimura M. (1988) *Proc. NIPR Symp. Antarct. Meteorites* **1**, 51-64; Wieler R. et al. (1985) *LPS* **XVI**, 902-903.

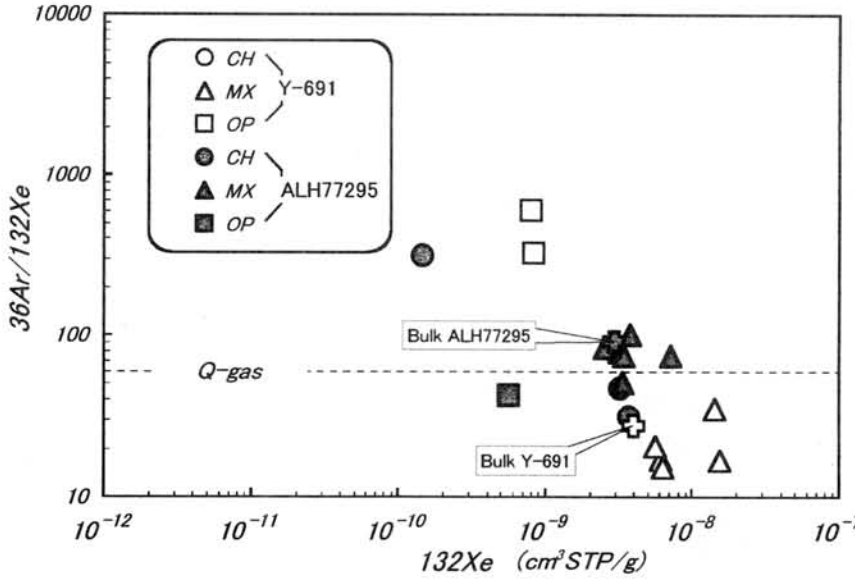

Fig. 1: Matrix portions in Y-691 and ALH77295 show high concentrations of ^{132}Xe and $^{36}Ar/^{132}Xe$ ratios similar to those of Q-gas. Abbreviations: CH, chondrule; MX, matrix portion; OP, coarse opaque grain

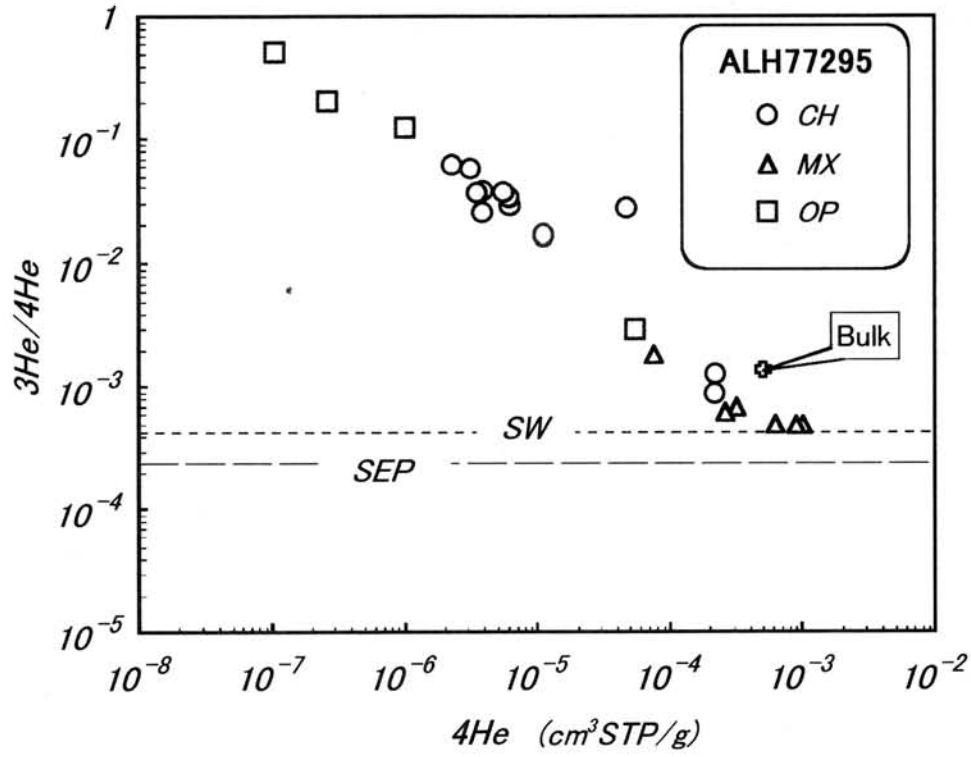

Fig. 2: Abundant solar He was observed in ALH77295 matrices. Abbreviations: SW, solar wind; SEP, solar energetic particle. The others are the same as those in Fig. 1.

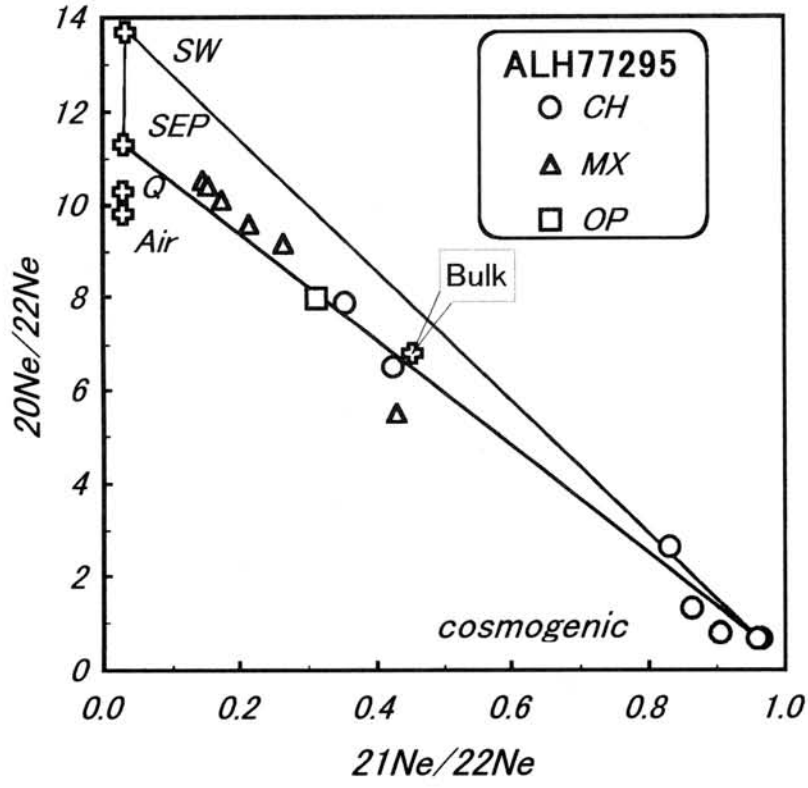

Fig. 3: Ne-three isotope plot shows that Ne in matrix materials of ALH77295 is more enriched in SEP Ne compared to other components. Abbreviations: See Fig. 2.

Characteristics of Antarctic Micrometeorites Collected by 39th JARE in Noble Gas Signature

Takahito OSAWA & Keisuke NAGAO

Laboratory for Earthquake Chemistry, Graduate School of Science,
The University of Tokyo, Hongo, Tokyo 113-0033, Japan

Introduction

From November 1998 to January 1999, the 39th Japanese Antarctic Research Expedition (JARE) performed large-scale collection of Antarctic Micrometeorites (AMMs) at three different localities (total 24 collection sites) around the Yamato Mountains in Antarctica [1,2]. In this study, we performed noble gas measurement for some AMMs. In our previous studies, extraterrestrial noble gases in Dome Fuji samples were detected. [3,4]. In the present work, 5 AMMs collected at Minami-Yamato section were selected to try to measure all noble gases for individual particles.

Samples

All samples are collected at the Meteorite Ice Field around the Yamato Mountains, Antarctica. They were identified as extraterrestrial dust particles with chondritic elemental compositions by SEM/EDS analysis, these data are published via World-Wide Web: URL is http://dust.cc.gakushuin.ac.jp/dust/. Measured 5 samples are comparatively large size AMMs weighting about 1 microgram.

Results

Concentrations of noble gases and isotopic compositions for individual AMMs are presented in Table 1 and Table 2. All data are corrected for blank and errors are one sigma. As in the case of Dome Fuji samples, all Minami-Yamato AMMs have solar He and Ne. Dome Fuji samples were collected from fallen snow around the Dome Fuji Station, they represent recent accretion of cosmic dust particles. On the hand, Minami-Yamato AMMs older accretion dusts. In spite of the difference between two AMMs series, the same SEP-like He and Ne are detected, which indicate terrestrial weathering during ice sealing may not affect depletion of solar noble gases in AMMs.

$^{40}Ar/^{36}Ar$ ratios were determined for 2 AMMs Y98K02KS275 and Y98K02KS261, while only upper limits can be decided for remaining 3 samples due to low amounts of released argon. The blank corrected $^{40}Ar/^{36}Ar$ ratios of the 2 AMMs are considerably low, which clearly show extraterrestrial origin. $^{36}Ar/^{36}Ar$ ratios of them are higher than that of atmosphere or Q-Ar though experimental ambiguities are large, which do not reflect cosmogenic ^{38}Ar but SEP-Ar because cosmogenic ^{21}Ne is not identified for the AMMs, and the production rate of ^{38}Ar is lower than that of ^{21}Ne. Albeit only Y98K02KS267 has high $^{21}Ne/^{22}Ne$ ratio that clearly indicates cosmogenic

^{21}Ne, its ^{36}Ar/^{36}Ar ratio is lower than those of Y98K02KS275 and Y98K02KS261.

High ^{129}Xe/^{132}Xe is detected in only Y98K02KS267, while other 4 AMMs have no excess ^{129}Xe. As only one AMM with excess ^{129}Xe had been discovered in our previous work [4], Y98K02KS267 is the second AMM with Xe anomaly. Krypton isotopic compositions are normal as in the case of previous study [3,4]. The 5 AMMs measured in the present work are similar to the Dome Fuji AMMs in total noble gas signature. One exception is the low concentrations of ^{40}Ar in these samples compared with the Dome Fuji samples, which shows that the atmospheric contamination is smaller in Minami-Yamato AMMs than in the Dome Fiji AMMs as shown in Figure 1.

Table 1 Concentrations of noble gases for AMMs

sample	weight(μg)	concentrations (ccSTP/g)					
		^{4}He	^{20}Ne	^{36}Ar	^{40}Ar	^{84}Kr	^{132}Xe
Y98K02KS275	1.2	3.72×10^{-5}	2.93×10^{-6}	1.03×10^{-6}	2.96×10^{-5}	3.68×10^{-9}	6.52×10^{-10}
Y98K02KS261	0.9	2.36×10^{-5}	5.15×10^{-5}	3.23×10^{-6}	2.89×10^{-5}	4.76×10^{-9}	1.14×10^{-9}
Y98K02KS048	0.8	6.69×10^{-5}	5.73×10^{-6}	9.34×10^{-7}	nd	3.47×10^{-9}	3.22×10^{-9}
Y98K02KS267	1.3	4.90×10^{-6}	1.68×10^{-6}	5.11×10^{-7}	1.48×10^{-5}	3.55×10^{-9}	1.20×10^{-9}
Y98K02KS268	1.1	1.92×10^{-5}	6.17×10^{-7}	2.45×10^{-7}	4.87×10^{-6}	4.04×10^{-9}	1.75×10^{-9}

Table 2 Noble gas isotopic compositions for AMMs

sample	^{3}He/^{4}He	^{20}Ne/^{22}Ne	^{21}Ne/^{22}Ne	^{40}Ar/^{36}Ar	^{38}Ar/^{36}Ar	84Kr=1			132Xe=1				
						82Kr	83Kr	86Kr	129Xe	130Xe	131Xe	134Xe	136Xe
Y98K02KS275	2.69×10^{-4} $\pm0.75\times10^{-4}$	11.1 ±1.4	0.033 ±0.023	28.1 ±25.6	0.202 ±0.022	0.19 ±0.04	0.20 ±0.11	0.34 ±0.09	1.12 ±0.12	0.20 ±0.11	0.80 ±0.19	0.37 ±0.12	0.35 ±0.14
Y98K02KS261	3.04×10^{-4} $\pm0.92\times10^{-4}$	10.5 ±0.3	0.034 ±0.007	8.7 ±11.2	0.203 ±0.013	0.27 ±0.09	0.18 ±0.08	0.35 ±0.18	1.02 ±0.38	0.18 ±0.11	1.11 ±0.74	0.61 ±0.42	0.28 ±0.16
Y98K02KS048	2.46×10^{-4} $\pm0.90\times10^{-4}$	11.9 ±1.0	0.031 ±0.010	<8.22	0.199 ±0.025	0.24 ±0.10	0.19 ±0.11	0.40 ±0.15	1.04 ±0.53	0.14 ±0.07	0.92 ±0.41	0.46 ±0.21	0.29 ±0.13
Y98K02KS267	3.23×10^{-4} $\pm2.59\times10^{-4}$	12.0 ±1.6	0.072 ±0.037	<75.9	0.193 ±0.034	0.27 ±0.14	0.24 ±0.16	0.25 ±0.08	1.53 ±0.47	0.20 ±0.12	1.28 ±0.54	0.49 ±0.17	0.17 ±0.07
Y98K02KS268	2.65×10^{-4} $\pm0.35\times10^{-4}$	15.4 ±3.7	0.016 ±0.023	<134	0.163 ±0.061	0.24 ±0.52	0.22 ±0.09	0.27 ±0.10	0.95 ±0.17	0.19 ±0.05	0.90 ±0.51	0.37 ±0.18	0.32 ±0.14

References

[1] Yada T. and Kojima H. (2000) *Antarct. Meteorite Res.* **13,** 9. [2] Terada et al. (2001) *Antarct. Meteorite Res.* **14,** 89. [3] Osawa T., Nagao K., Nakamura T. and Takaoka N. (2000) *Antarct. Meteorite Res.* 13, 322. [4] Osawa T. and Nagao K. (2001) in preparation.

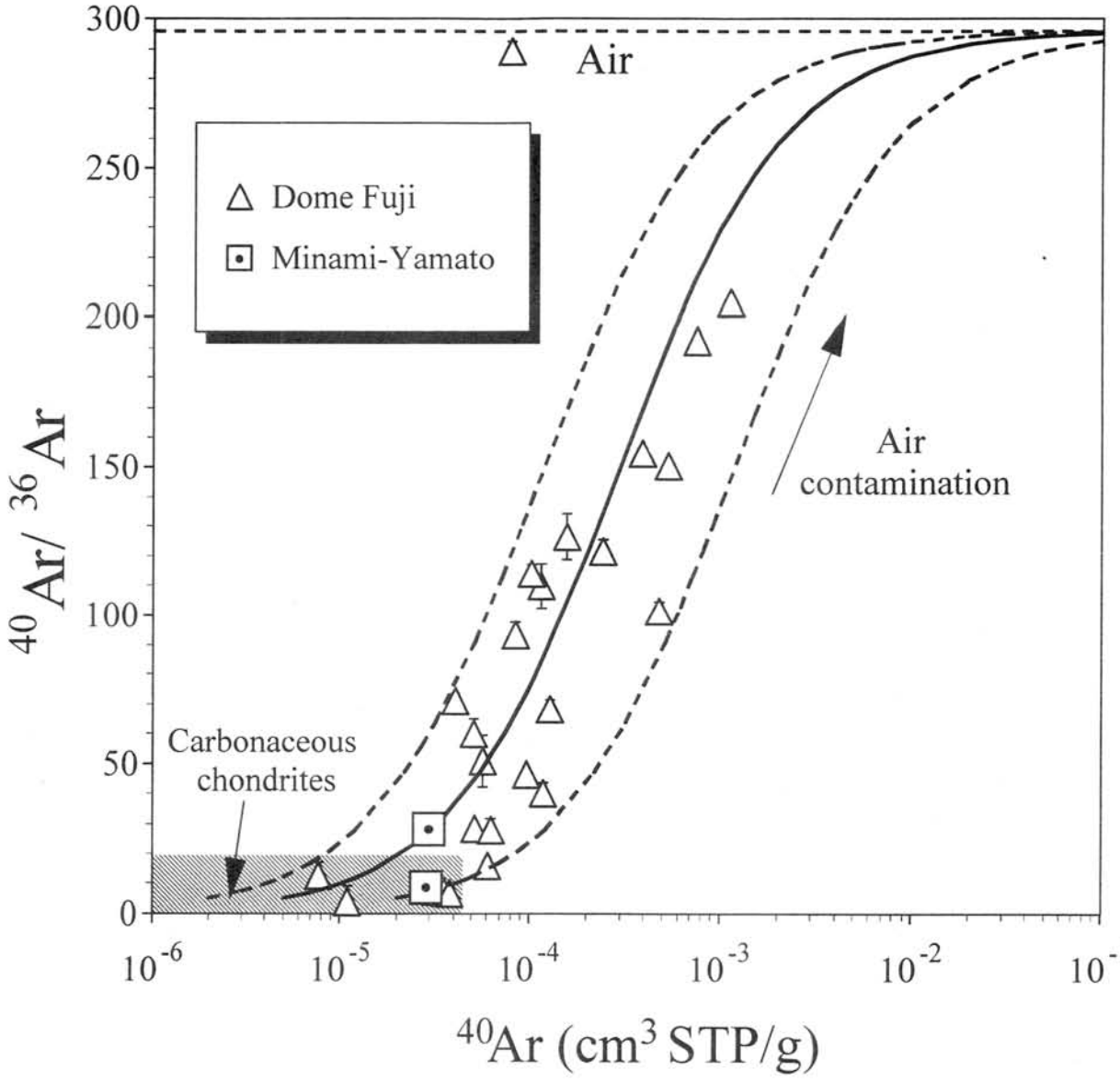

Figure 1 Argon isotopic ratios against concentrations of ^{40}Ar. Solid line and two dotted lines display mixing lines between primordial trapped component and terrestrial atmosphere. 40Ar/36Ar ratios of AMMs have a good correlation with concentrations of ^{40}Ar. Argon compositions of AMMs are affected by atmospheric ^{40}Ar generally. Two Minami-Yamato AMMs have lower $^{40}Ar/^{36}Ar$ ratios and lower 40Ar concentrations than those of general Dome Fuji AMMs, which indicate that the contribution of air contamination for argon is not dominant in these two AMMs. It is not clear whether this result is related to the difference of the collection sites or not. More data are necessary to confirm the conjecture.

Origin of ^{3}He in the Earth

Minoru Ozima

Department of Earth and Planetary Science, University of Tokyo, Bunkyo-Ku, Tokyo 113-0033; E-mail:EZZ03651@nifty.ne.jp

Persistent outgassing of ^{3}He from MOR (1) shows that primordial noble gases still are retained in the Earth's interior. It is then common to assume that this primordial noble gas was acquired during Earth accretion. Recently, this assumption was partly challenged by Anderson (2), who instead suggested that substantial fraction of mantle ^{3}He is due to cosmic dusts subducted with oceanic sediments. However, because of very poor retentivity of ^{3}He in cosmic dusts (3) and of much smaller observed fall-out rate of cosmic ^{3}He (e.g.4), the model failed to gain much support. On the other hand, an incoherent behavior of mantle ^{3}He with heavy noble gases has been pointed out by several authors (e.g., 5; 6; 7; 8). From extensive compilation of noble data on mantle-derived materials, Ozima and Igarashi (9) suggested that ^{3}He in the mantle is totally decoupled from heavy noble gases. The origin of terrestrial noble gas, especially of ^{3}He, still remains to be resolved. Recently our understanding of noble gases in the solar system greatly advanced through studies of extraterrestrial materials such as meteorites and lunar samples. We therefore decided to examine the nature of terrestrial ^{3}He in the light of newly obtained cosmochemical information as well as terrestrial data, since the question on such a fundamental issue as the origin of terrestrial noble gas is unlikely to fully be answered from terrestrial information alone.

Comparison of elemental ratios of the atmospheric noble gas (Ne, ^{36}Ar, Kr, Xe) with those of the solar noble gas (Fig.1) suggests that the former was derived by Rayleigh-type mass dependent fractionation from the latter component (10). Similar Rayleigh-type fractionation of noble gases, although not as clear as in the case of the Earth, is also seen among inner planets including primitive meteorites, suggesting that the fractionation process

was prevailing in the early solar nebula and was primarily responsible to the origin of primordial noble gases in terrestrial planetary objects.

However, the amount of primordial terrestrial ^{3}He expected from the fractionation process is too small to account for the observed terrestrial ^{3}He. For example, the amount of ^{3}He expected from the fractionation process is smaller than the amount of ^{3}He in the present atmosphere, an extreme minimum inventory in the Earth (note that He is not gravitationally bound to the Earth). Therefore, we conclude that ^{3}He in the present Earth was not derived from the solar nebula concomitantly with heavy noble gases. This distinct origin of ^{3}He is supported by the primitive isotopic ratio of mantle He, and is consistent with the empirical observation that ^{3}He in the mantle is totally decoupled from heavy noble gases (e.g. 11-14).

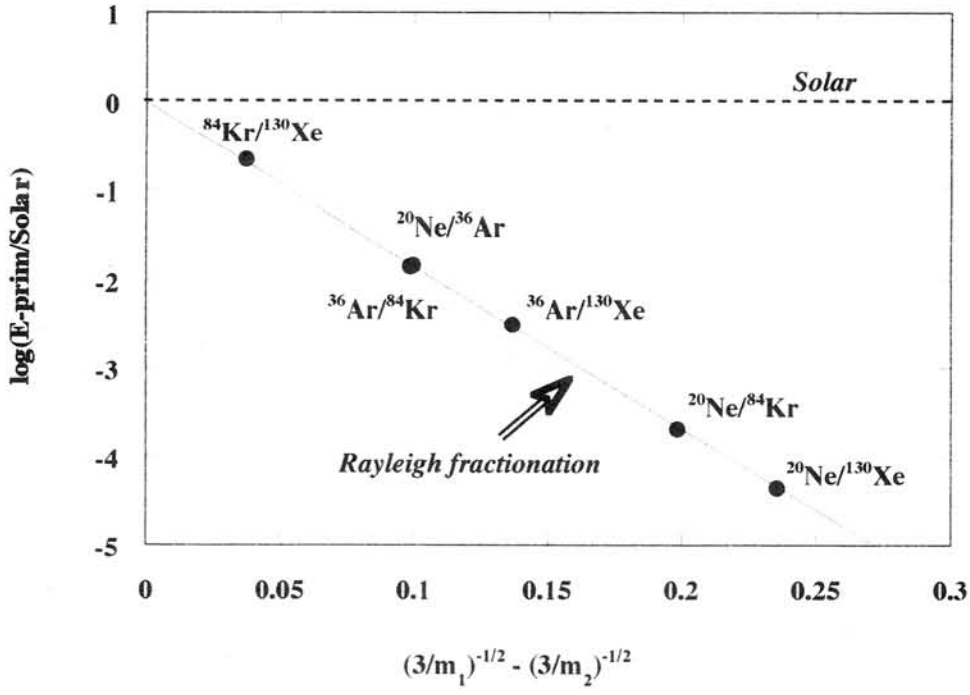

Fig.1 Ratios of elemental ratio of atmospheric noble gases (corrected for 90% missing Xe) are plotted in a Rayleigh fractionation diagram The slope of the linear line corresponds to a depletion factor of ^{3}He which is chosen as a common denominator for elemental ratios. After Ozima and Podosek (1999).

References.

1. H.Craig and J.E.Lupton, *Earth Planetary Science Letters*, **31**, 369 (1976). 2. D.L.Anderson, *Science*, **261**, 170 (1993). 3. H.Hiyagon, *Science*, **263**, 1257 (1994). 4. K.A.Farley, *Science*, **261**, 166 (1993). 5. M.Honda, I.McDougall, D.B.Patterson, A.Doulgeris and D.A.Clague, *Nature*, **349**,149 (1993). 6. J.Matsuda and B.Marty, *Geophysical Res. Lett.*, **22**, 1937 (1995). 7. D. L. Anderson, *Proc. Natl. Acad. Sci. U.S.A.* **95**, 4822 (1998). 8. D, Porcelli and A.N.Halliday, *Earth Planetary Sci. Lett.*, (in press). 9. M.Ozima and G.Igarashi, *Earth Planetary Sci. Lett.*, **176**, 219 (2000). 10. M.Ozima and F.A.Podosek, *J. Geophys. Res.* **104**, 25493 (1999). 11. M.Honda, I.McDougall, D.B.Patterson, A.Doulgeris and D.A.Clague, *Nature*, **349**,149 (1993). 12. J.Matsuda and B.Marty, *Geophysical Res. Lett.*, **22**, 1937 (1995). 13. D. L. Anderson, *Proc. Natl. Acad. Sci. U.S.A.* **95**, 4822 (1998). 14. D, Porcelli and A.N.Halliday, *Earth Planetary Sci. Lett.*, (in press).

Noble Gases in Towada H -Chondrite

Jisun Park[1)], Ryuji Okazaki[1)], Keisuke Nagao[1)] and Shigekazu Yoneda[2)]

[1)] *Laboratory for Earthquake Chemistry, Graduate School of Science, University of Tokyo, Hongo, Bunkyo-ku, Tokyo 113-0033, Japan*

[2)] *National Science Museum, Shinjuku-ku, Tokyo 169-0073, Japan*

Introduction

Towada meteorite, which weighed 53.5 gram, is found in Towada city, Aomori prefecture in 1999. It is considered that approximately ten years have been passed from the time of falling, by measuring gamma-ray spectra of cosmogenic ^{22}Na (half-life of 2.6 year), and according to the oxygen isotopic analysis, Towada meteorite is classified as H chondrite. (Yoneda and Kusakabe, personal. communication).

Because Towada meteorite is found only two years ago, there is no previous analysis and accurate information of it.

In the present paper, we report concentrations and isotopic ratios of noble gases. U/Th-He and K-Ar gas retention ages and the cosmic-ray exposure age of Towada meteorite were calculated. Furthermore, it is proved as the classification of H6 chondrite based on the heavy noble gas concentrations.

Experimental Method

Towada Meteorite sample was analyzed by using a mass spectrometric system, which is composed of an extraction oven, a purification system, a standard gas system, and a mass spectrometer (modified-VG5400/MS-II). The sample was weighed 0.0306g and wrapped by Al-foil. Then we put the sample into the glass sample holder, which was connected to extraction furnace. Noble gases were extracted at the temperature of 1800 ℃, then the gases were purified by using Ti, Zr getters. Four fractions of noble gases (He- Ne, Ar, Kr, and Xe) were measured separately; He, Ne and Ar were measured by using the Daly-multiplier system, and Kr and Xe by an ion counting system.

Results and Discussion

K-Ar and U/Th-He ages of the Towada meteorite were calculated as 1.3 b.y. and 0.38 b.y., respectively, by using radiogenic ^{40}Ar and ^{4}He concentrations and the average concentrations of U, Th and K reported for H-chondrites as listed in Table 1. Comparing the formation ages of 4.5 b.y. for chondrites, Towada meteorite would have experienced heating events about 1.3 b.y. ago.

Table 1. ***Concentrations of radiogenic ^{4}He and ^{40}Ar, and U/Th-He and K-Ar ages (T4 and T40, respectively).***

^{4}He 10^{-9} cc/g	^{40}Ar 10^{-9} cc/g	T4 m.y.	T40 m.y.	U * ppb	Th * ppb	K ** ppm	T4/T40
1027	6032	380	1340	12	42	782	0.28

*Ref [1] ** Ref [2]

Cosmic-ray exposure age of Towada was calculated as 31 m.y. (Table 2), based on cosmogenic ^{21}Ne concentration and production rate for ^{21}Ne by Eugster (1988) [3]. Towada meteorite belongs to the second peak of exposure age distribution for H-chondrites, which has two peaks at 7 and 33 m.y.. The exposure ages based on ^{3}He and ^{38}Ar are shorter than the 31 m.y., which may be due to diffusion loss of ^{3}He and ^{38}Ar. The ^{3}He loss is indicated in Fig 1, where Towada is plotted much lower than the correlation line for normal chondrites.

Table 2. ***Cosmogenic ^{3}He, ^{21}Ne, and ^{38}Ar concentrations and cosmic-ray exposure ages.***

^{3}He	^{21}Ne	^{38}Ar	$^{22}Ne/^{21}Ne$	P3	P21	P38	T3	T21	T38	$^{3}He/^{21}Ne$	T3/T21
10^{-9} cc/g				10^{-9} cc/g/m.y.			m.y.				
119	74.0	8.31	1.177	15.5	2.37	0.447	7.7	31.2	18.6	1.61	0.25

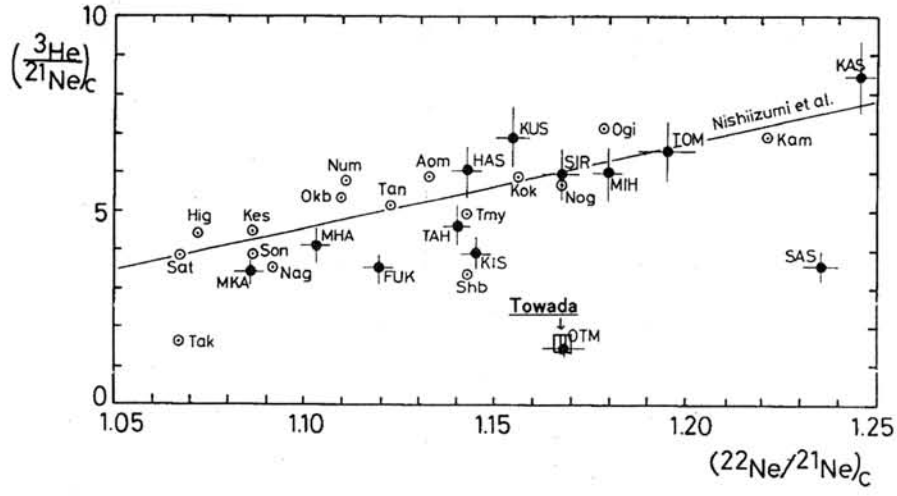

Fig.1. ***Plot of cosmogenic $^{3}He/^{21}Ne$ versus $^{22}Ne/^{21}Ne$ ratios of Towada meteorites. Other data are from [4] and [5].***

The plot for Towada meteorite in Fig 2 shows that the lighter isotopes ^{3}He and ^{4}He have been lost coherently from the meteorite. This helium loss would have occurred by solar heating

during orbital motion approaching to the Sun..

Trapped heavy noble gas concentrations of ^{36}Ar, ^{84}Kr and ^{132}Xe show clear correlation with the petrologic type of chondrites. As shown in Fig 3, Towada meteorite is plotted in the area for Type 6 chondrites, which suggests that the Towada meteorite is classified as H6 chondrite.

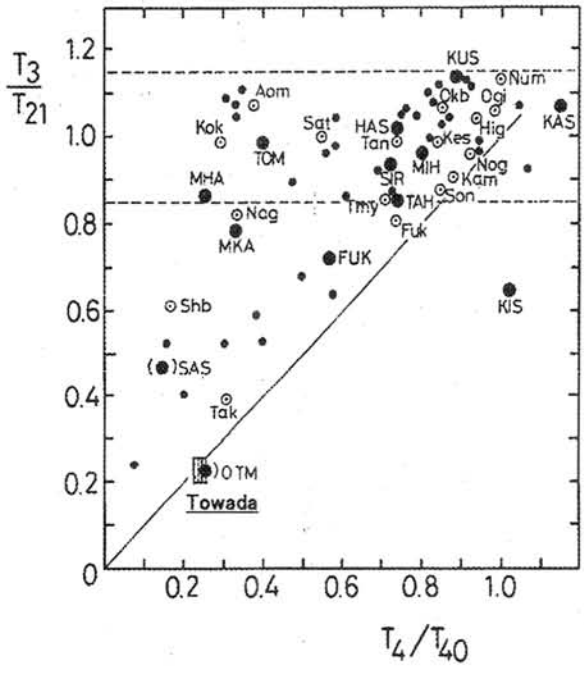

Fig. 2. ***Plot of T_3/T_{21} versus T_4/T_{40} ratios of Towada meteorite.***

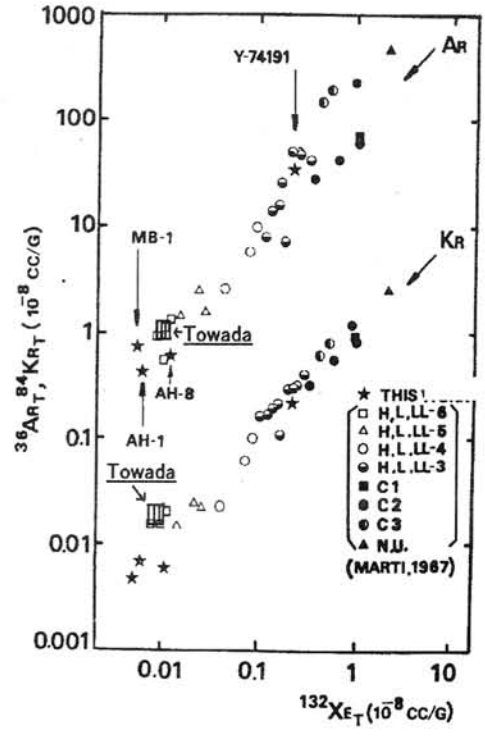

Fig 3. ***Correlation diagram of trapped ^{36}Ar, ^{84}Kr and ^{132}Xe. ★Ref. [6]***

References

[1] J. T. Wasson and G.W. Kallemeyn (1988) *Philos. Trans. R. Soc. London* **A325**, 535

[2] G.W. Kallemeyn, A.G. Rubin, D. Wang, and J. T. Wasson (1989) *Geochim. Cosmochim. Acta* **53**, 2747

[3] O. Eugster (1988) *Geochim. Cosmochim. Acta* **52**, 1649-1659.

[4] K. Nagao, Y. Miura and M.Shima (1993) *J. Mass Spectrom. Soc. Jpn.* **41**, 191-209

[5] K. Nishiizumi, S. Regnier, and K. Marti (1980) *Earth Planet. Sci. Lett.* **50**, 156

[6] K. Nagao, N. Takaoka (1979) *Memories of National Institute of Polar Research.* **12**, 207-222

The Irradiation History of Rumuruti-Chondrites

Ludolf Schultz and Hartwig W. Weber
Max-Planck-Institut für Chemie
D-55128 Mainz/Germany

Introduction: Rumuruti (R) chondrites are characterized by high contents of FeO-rich olivine and almost no metal. They form a distinct group with high $\Delta^{17}O$ in the standard three-isotope plot of oxygen. The first meteorite of this group - Carlisle Lakes - was discovered in the Nullarbor Plain, Australia (Binns and Pooley, 1979). Rubin and Kallemeyn (1989) noted the similarity of this meteorite with the Antarctic stone Allan Hills 85151. Weisberg *et al.* (1991) recognized their relationship to Yamato (Y) 75302 and termed these meteorites „Carlisle Lake-type" chondrites. Subsequently, additional members of this grouplet were found and described: Y 793575 (Yanai, 1992), Y 82002 (Nakamura et al., 1993), Acfer 217 (Bischoff et al., 1994), and two paired stones Pecora Escarpment 91002 and 91241 (Rubin and Kallemeyn, 1994). The first fall of this group - Rumuruti – has been described by Schulze et al. (1994) and its name adopted for this new chondrite group (Rumuruti chondrites or R-chondrites). Since then more R-chondrites have been detected. In hot deserts were found Dar al Gani 013 (Jäckel et al., 1996; Palme et al., 1996) and Dar al Gani 417, Hammadah al Hamra119, Hughes 030 (Bischoff et al., 1998), Sahara 98248 and three possibly paired stones Sahara 99527, 99531 and 99537 (A. Bischoff, priv. com.). From the Antarctic three new R-chondrites are described: Four paired stones, Mount Prestrud 95404, 95410, 95411 and 95412 (Rubin and Kallemeyn, 1994; Kallemeyn, 1998); Asuka 881988 and Yamato 791827 (Yanai and Kojima, 1995). The latter specimen is probably paired with Y75302 (Nagao et al., 1999). Recently, several other R-chondrites are reported from North West Africa: Ouzima, North West Africa 053, 753, and 755 (A. Bischoff, priv. com.). Kallemeyn et al. (1996) and Kojima et al. (1998) have summarized the mineralogical and chemical properties of R-chondrites.
More information on all R-chondrites is given in Tab.1. The Antarctic chondrite Elephant Moraine 96026 has been classified also as a R-chondrite (Ant. Meteorite Newsletter 21, Feb. 1998). however, oxygen isotope data do not confirm this finding (R.N. Clayton, priv. com.). This meteorite is thus not included in Tab.1.

Experimental: Noble gases have been measured in this laboratory in all R-chondrites, except those noted with (a) in Tab.1. Noble gases of R-chondrites are a mixture of different components. For the partitioning into the individual fractions (radiogenic, cosmogenic, solar, planetary) assumptions are made similar to those given in Weber and Schultz (1998). The calculation of cosmogenic $(^{22}Ne/^{21}Ne)_c$, the parameter used for shielding corrections of production rates, is difficult to obtain for solar gas containing samples; in this case a mean value of 1.11 is taken. For some of those meteorites, however, the $(^{22}Ne/^{21}Ne)_c$ was obtained from a fit through data of a stepwise heating experiment and an extrapolation to $(^{20}Ne/^{22}Ne)_c = 0.84$ (Fig.1).

Production rates for cosmogenic ^3He, ^{21}Ne, and ^{38}Ar were calculated from the mean chemical composition of R-chondrites (Palme et al. 1996) using procedures given by Eugster (1988). The exposure ages are listed in Tab.2. In some cases these ages are ^{21}Ne-exposure ages, otherwise the mean value of ^3He-, ^{21}Ne-, and ^{38}Ar-ages are given.

Tab.1: Rumuruti Chondrites: Find masses, classification and irradiation properties.

Meteorite	Mass [g]	Type	Shock stage	Weath. grade	Solar gas	$(^{22}Ne/^{21}Ne)_c$	Exposure age [Ma]	Ref.
Acfer 217	174	R3.8-5	S2	W5/6	Y	1.131	34.1 ± 1.0	
Allan Hills 85151	14	R3.6	S2	W2/3	Y	1.145	25.9 ± 0.4	
Asuka 881988	172	R4.0				1.228	19.5 ± 4.8	(a)
Carlisle Lakes	50	R3.8	S3	W3/4		1.077	6.3 ± 0.7	
Dar al Gani 013	205	R3.5-6	S1	W4		1.146	8.0 ± 1.0	
Dar al Gani 417	171	R3-4	S2	W3	Y	1.220	19.6 ± 3.1	
Hammadah 119	352	R4	S3	W4		1.121	2.4 ± 0.2	
Hughes 030	~100	R3-6				1.155	49.0 ± 5.8	
Mt. Prestrud 95404/ 410/411/412	40/42/ 44/15	R3			Y	(1.11)	17.0 ± 3.0	
Northwest Africa 053	390	R4	S2	W2		1.095	0.2 ± 0.1	
Northwest Africa 753	12000	R3.9	S2	W2				
Northwest Africa 755	352	R3.7	S2	W4				
Ouzima	642	R4	S2	W3-4		1.204	8.0 ± 0.4	
Pecora Escarpment 91002/91241	210/75	R3.8-6	S2	W2/3	Y	(1.11)	35.6 ± 7.1	
Rumuruti	67	R3.8-6	S2	W0/1	Y	1.141	16.7 ± 0.7	
Sahara 98248	39	R4	S2	W2		1.317	17.9 ± 0.1	
Sahara 99527+	19	R5	S2	W3		1.088	24.8 ± 2.7	
Sahara 99531+	31	R3-5	S3	W3/4	Y	(1.11)	27.9 ± 4.7	
Sahara 99537+	27	R3-6	S3	W3-4		(1.11)	31.4 ± 0.5	
Yamato 75302*	4	R3.8	S4	W3/4	Y	(1.11]	21.3 ± 0.2	(a)
Yamato 791827*	9	R4			Y	(1.11)	22.0 ± 1.8	(a)
Yamato 793575	25	R3.8	S2	W3/4		1.228	7.7 ± 0.5	
Yamato 82002	7	R3.9	S2	W4/5	Y	(1.11)	17.7 ±0.3	(a)

* or $^{+}$: possibly paired; (a) : Nagao et al. (1999)

Discussion: From find locations and petrographic observations several specimens of R-chondrites are considered to be paired. This is also confirmed by noble gas measurements. Meteorites where pairing is possible are identified in Tab.1.

Ten out of eighteen R-chondrites contain gases incorporated by the solar particle flux, these meteorites are therefore regolith breccias. Except for lunar meteorites, this is the highest percentage of regolith breccias within one meteorite group.

Fig.2 shows the so-called Bern-plot, which is used for shielding correction of production rates (e.g. Eugster, 1988). This plot also shows that the cosmogenic $^{22}Ne/^{21}Ne$ ratios of R-chondrites vary from about 1.06 to 1.30 indicating very high and very low shielding conditions of the samples measured. The meteorite with the highest value (Sahara 98248) is possibly influenced by solar cosmic rays (see Pätsch, 2000). Values below the Bern-Line are interpreted as a deficit of ^{3}He due to solar heating. This is the case for Hammadah al Hamra 119 and NWA 053.

The exposure ages of R-chondrites have a range from about 0.2 to 50 Ma with most having ages > 7 Ma. This is similar to exposure ages of ordinary chondrites, which are thought to have spent most of their exposure in the asteroid belt. After entering a resonance they are brought to Earth-crossing orbits relatively fast (Morbidelli and Gladman, 1998). However, the short exposure age of NWA 053 demonstrates that short transfer times from the asteroid belt to Earth are also possible for R-chondrites

(Patzer et al., 1999). Fig. 3 shows a comparison of the exposure age distribution of R- and L- chondrites.
Characteristic for many R-chondrites are rather high $^{129}Xe/^{132}Xe$ ratios. Most H-chondrite falls have values of 1.4 ± 0.2 independent from their amount of trapped Xe. This ratio is measured between 1.3 and 3.8 in R-chondrites.

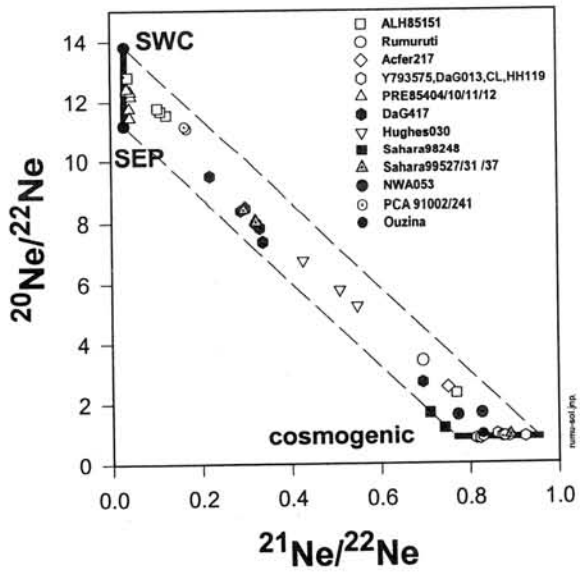

Fig.1: The neon isotopic composition of R-chondrites. Indicated are the solar compositions (SWC and SEP) as well as the range of cosmogenic neon.

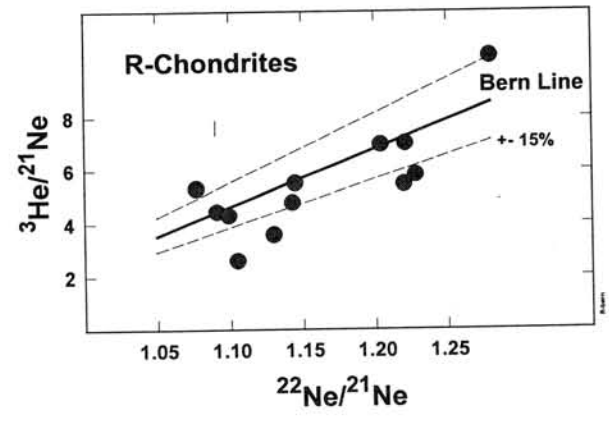

Fig.2: Cosmogenic $^{3}He/^{21}Ne$ vs. $^{22}Ne/^{21}Ne$ for R-chondrites. The two samples below the lines indicate diffusive loss of ^{3}He.

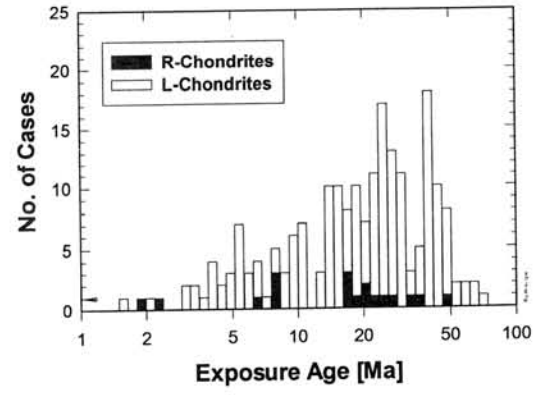

Fig.3: Comparison of exposure age distributions of L- and R-chondrites. The age scale is logarithmic with a resolution of 15% corresponding to estimated uncertainties.

References: Binns R.A. and Pooley G.D. (1979) *Meteoritics* 14, 349; Bischoff A. et al. (1994) *Meteoritics* 29, 264; Bischoff A. et al. (1998) *Meteorit. Planet. Sci.* 33, A15; Eugster O. (1988) *Geochim. Cosmochim. Acta* 52, 1649; Jäckel A. et al. (1996) *Lunar Planet. Sci.* 27, 595; Kallemeyn G.W. et al. (1996) *Geochim. Cosmochim. Acta* 60, 2243; Kallemeyn G.W. (1998) *Meteoritics Planet. Sci.* 33, A80; Kojima H. et al. (1998) *Antarctic Meteorites* **23,** ; Morbidelli A. and Gladman B.J. (1998) *Meteoritics Planet. Sci.* 33, 999 ; Nagao K. et al. (1999) *Ant. Met. Res.*12, 81; Nakamura T. et al. (1993) *Proc. NIPR Symp. Ant. Met.* 6, 171; Palme H.et al. (1996) *Lunar Planet. Sci.* 27, 991; Pätsch M. (2000) PhD-thesis, Univ. Mainz; Patzer A. et al (1999) *Lunar Planet. Sci.* 30, 1145; Rubin A.E. and Kallemeyn G.W. (1989) *Lunar Planet. Sci.* 20, 930; Rubin A.E., and Kallemeyn G.W. (1994) *Meteoritics* 29, 255; Schulze H. et al. (1994) *Meteoritics* 29, 275; Weber H.W. and Schultz L. (1998) *Lunar Planet. Sci.* 29, 1383; Weisberg M.K. et al. (1991) *Geochim. Cosmochim. Acta* 55, 2657; Yanai K. (1992) *Lunar Planet. Sci.* 23, 1559; Yanai K. et al. (1995) Catalog of the Antarctic Meteorites. Natl. Inst. Polar Res. (Tokyo), pp. 230.

Northwest Africa 766: A new ferroan ureilite with a variety of chromium-rich phases and associated Si,Al-rich glasses

Mathieu Sikirdji and Paul H. Warren
Institute of Geophysics, University of California, Los Angeles, CA 90095-1567, USA
(mat.sikirdji@wanadoo.fr, pwarren@ucla.edu)

We have studied the mineralogy of newly discovered ureilite NWA766. We only began analyzing this extraordinary meteorite in April, 2001, so this report must be considered very preliminary. The meteorite consists of ~80 vol% olivine, 20% pigeonitic pyroxene, several percent of interstitial black carbon phase(s), and slightly less than 1% Cr-spinel. The olivine is uncommonly ferroan, by ureilite standards, with cores averaging about $Fo_{76.3}$. As is typical of ferroan ureilites, the olivines are moderately CaO-rich (average 0.26 wt%). The average olivine (core) molar Fe/Mg, Fe/Mn and Fe/Cr ratios are 0.31, 49.1 and 52.7, respectively. More data are needed, but these ratios hint at possible deviations from the usual ureilite Fe/Mg-Fe/Mn-Fe/Cr systematics [*1*] in the same way, albeit less dramatically, as seen in the extremely ferroan sample LEW88774 [*1,2,3*]. The pyroxene clusters tightly around $En_{67.0}Wo_{14.5}$. The overall texture is typical ureilitic, with mafic grains averaging about 1 mm across (but up to 4 mm), curved intergranular boundaries, and abundant triple junctions. The rock has suffered moderate (W2 on Wlotzka's [*4*] scale) weathering.

The Cr-spinel is compositionally very similar to that of LEW88774 [*2*]. In addition, and generally in close proximity to Cr-spinel, there are traces of Cr-rich sulfides, and most interestingly, an association of slender masses of Al,Si-rich glass and a strange Cr-silicate phase. One of the NWA766 Cr-rich regions, believed to be fairly typical, is shown in Fig. 1. Average phase compositions (preliminary data) are shown in Table 1.

Table 1. Average phase compositions in NWA776: oxide wt%; atoms normalized to O = 24; and *mg* ratio (= molar Mg/(Mg+Fe)) in mol%.

element or oxide	olivine (cores) N=11	pyroxene N=9	Si,Al-glass N=9	Cr-rich silicate N=16	Cr-spinel N=6
SiO_2	37.88	53.56	79.52	38.76	0.08
MgO	38.42	22.84	0.19	14.15	18.43
Na_2O	0.01	0.48	1.62	0.26	0.00
Al_2O_3	0.03	1.89	13.46	2.12	17.12
FeO	21.23	11.26	0.53	4.26	4.63
MnO	0.43	0.44	0.04	0.65	0.74
Cr_2O_3	0.43	1.43	0.85	31.39	56.56
K_2O	0.01	0.00	0.48	0.01	0.00
CaO	0.26	6.87	2.39	7.22	0.06
TiO_2	0.02	0.13	0.32	0.52	0.82
sum	98.72	98.92	99.40	99.21	98.08
Si	5.98	7.84	10.07	6.11	0.014
Mg	9.04	4.98	0.037	3.30	5.05
Na	0.005	0.137	0.400	0.080	0.000
Al	0.006	0.325	2.014	0.395	3.70
Fe	2.803	1.378	0.056	0.567	0.721
Mn	0.058	0.055	0.004	0.087	0.116
Cr	0.054	0.166	0.086	3.93	8.25
K	0.001	0.000	0.078	0.002	0.000
Ca	0.044	1.078	0.324	1.203	0.011
Ti	0.003	0.015	0.031	0.061	0.113
O	24	24	24	24	24
mg	76.3	78.3	39.7	85.4	87.5

Similar glasses have been reported for a few other ureilites [e.g., *5*], but the associated Cr-rich silicate seems unprecedented. Analysis sums are consistently close to 99.2 wt%. They also show a consistent stoichiometry, with atomic Si/O ratio uniform at 0.2545±0.0026, even though the phase shows extensive heterogeneity in terms of its major cations (Fig. 2). For the average composition, a simplified chemical formula is $(Mg,Ca,Fe,Mn)_{2.5}(Cr,Al)_{2.1}(SiO_4)_3$. The minerals that most closely

match this composition, in terms of ideal chemical formula, are the knorringite-uvarovite varieties of garnet, whose formulas are $Mg_3Cr_2(SiO_4)_3$ and $Ca_3Cr_2(SiO_4)_3$, respectively. Shuiskite, $Ca_2(Mg,Al)(Cr,Al)_2(SiO_4)(Si_2O_7)(OH)_2 \cdot (H_2O)$, which would seem a more likely product of terrestrial aqueous alteration, can be ruled out because of the consistently good analysis sums. Krinovite, $NaMg_2CrSi_3O_{10}$, has a far higher Si/O ratio, higher Mg/Cr, and Na/Cr ~1. Further study will be necessary to ascertain whether this Cr-silicate is merely a terrestrial weathering product, or the product of some unusual mineralogical processing on a ureilite parent asteroid.

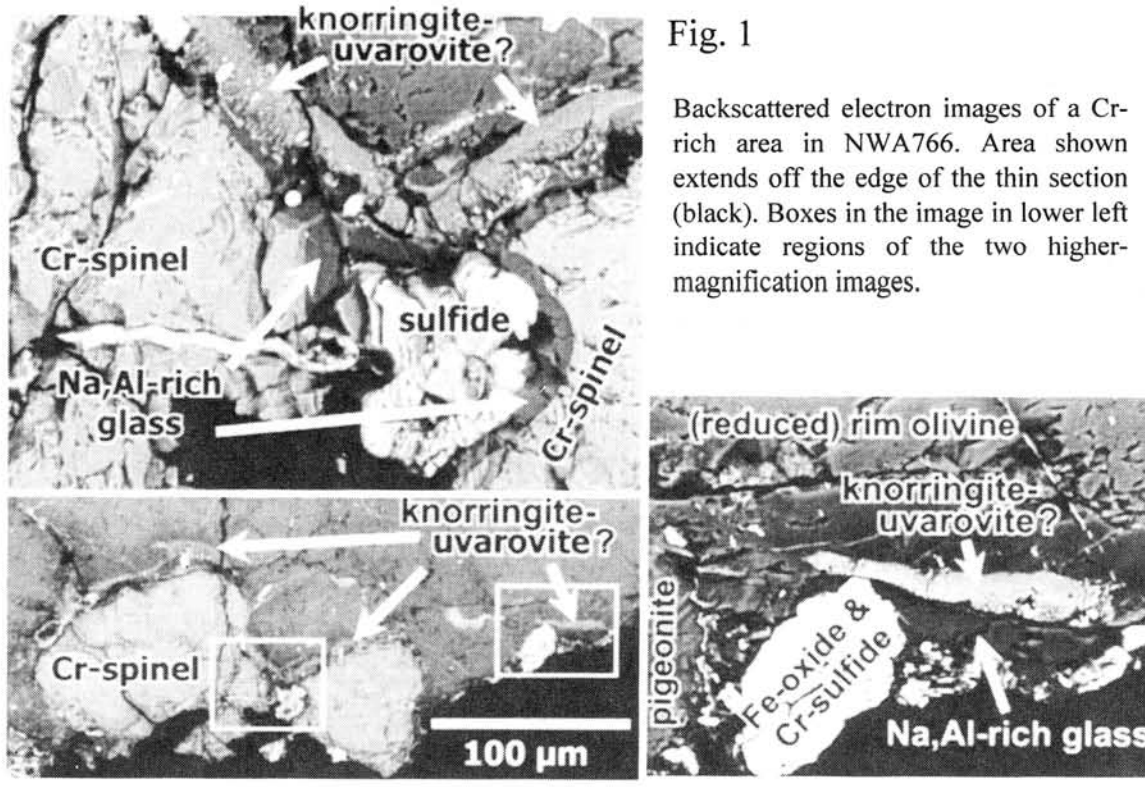

Fig. 1

Backscattered electron images of a Cr-rich area in NWA766. Area shown extends off the edge of the thin section (black). Boxes in the image in lower left indicate regions of the two higher-magnification images.

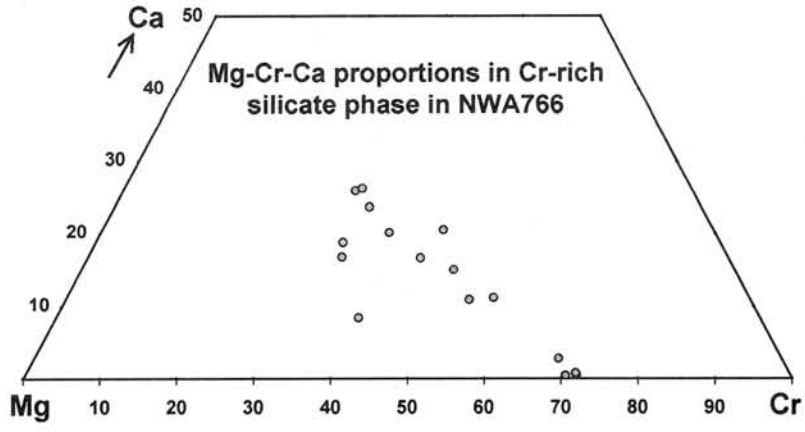

Fig. 2

References [1] Mittlefehldt D. W. et al. (1998) in *Planetary Materials*, Rev. Mineralogy 36, 4.1-4.195. [2] Warren P. H. & Kallemeyn G. W. (1994) *LPS* **XXV**, 1465-1466. [3] Prinz M. et al. (1994) *LPS* **XXV**, 1107-1108. [4] Wlotzka F. (1993) *Meteoritics* **28**, 460. [5] Ogata H. et al. (1991) *Meteoritics* **26**, 195-201.

Equilibration temperature of the Kobe meteorite

Yukiko Tachibana[1], Takao Hirajima[1], Masao Kitamura[1] and Noboru Nakamura[2]

1: Department of Geology and Mineralogy, Graduate School of Science, Kyoto University, Sakyo, Kyoto 606-8502, Japan

2: Department of Earth and Planetary Sciences, Kobe University, Kobe 657-8501, Japan

Introduction. The Kobe meteorite belongs to CK4 chondrite [1, 2]. Petrography and mineralogy of the Kobe meteorite already reported by the other members of the consortium [2] were also confirmed by the present study. Here, we report the estimation of the equilibration temperature of this metamorphosed carbonaceous chondrite.

Constituent Minerals. The thin section studied in the present work consists mainly of chondrules, 0.5-2 mm in size and matrix. Most of the chondrules are porphyritic olivine chondrules composed of olivine grains in euhedral shapes, spherical magnetite and mesostasis containing pyroxene and plagioclase in subhedral shapes. One barred olivine chondrule was found in the thin section. The matrix of the chondrite includes grains of olivine, orthopyroxene (Opx), clinopyroxene (Cpx), plagioclase, magnetite, pyrite and others. EDS (HITACHI S-3000) analysis was carried out for the representative minerals. Olivine grains in a bared olivine chondrule, porphyritic chondrules and matrix have a similar composition about $Fo_{69}Fa_{31}$. Opx in the thin section occurs in matrix. The sizes of the grains are 0.1-0.5mm. Opx grains are homogeneous and have the chemical composition about $En_{73}Fs_{26}Wo_1$. Cpx grains occur in both chondrules and matrix and are in subhedral shapes. The sizes of the grains are 0.1-0.5 mm. Cpx is homogeneous and has the chemical composition of $En_{44}Fs_{10}Wo_{46}$ (Fig.1). Plagioclase occurs both in chondrules and matrix and are in subhedral shape. The sizes of the grains are 0.1–0.5 mm. Plagioclase shows the wide range of the composition [2]. A compositional mapping of an area in the matrix show that two regions of plagioclase grains distinct in the anorthite component coexist. The compositions of the albite-rich and anorthite-rich regions are $\sim An_{40}$ and $\sim An_{60}$, respectively. No systematic distributions of these two parts were observed in the chondrite, differing from the observation of the reverse zoning with the albite-rich core and the anorthite-rich rim in a few CK chondrites [3]. Magnetite grains occur both in matrix and chondrules and are in spherical shapes. The sizes of the grains are 0.1-0.3 mm in diameter. Pyrite grains are in irregular shapes.

Equilibration temperature

No pair of grains of Opx and Cpx which contact directly with each other was found in the studied thin sections, since all observed Opx are surrounded by pyrite. Since the chemical compositions of two pyroxenes are constant within grains and also grain by grain, the equilibration between two pyroxenes can be assumed. Because of the homogeneity of the compositions, we use the averaged composition for each

pyroxene phase to evaluate the equilibration temperature. The equilibration temperatures estimated by using the phase diagram [4], the Wells's [5] and Brey & Köhler's [6] pyroxene geo-thermometers are about 800°C, 900°C and 850°C, respectively. The temperature of 800°C-900°C is almost similar to but slightly higher than those for the other CK chondrites estimated by an olivine-spinel thermometer, 750-850 °C, and much higher than those for the Maralinga meteorite estimated by 2px-thermometer, 650 °C [3]. In spite of the high temperature metamorphism, plagioclase shows the compositional heterogeneity. A phase relation of plagioclase feldspar [7] shows the miscibility gap between An_{40} and An_{60} above about 800°C. The compositional gap observed in the grains of plagioclase in the meteorite may correspond to this miscibility gap.

Acknowledgements: We thank Mr. Ryoichi Hirata for providing the Kobe meteorite sample.

References: [1] Nakamura, N. et al. (2000) Antarctic Meteorites XXV, 99. [2] Tomeoka, K. et al. (2000) Antarctic Meteorites XXV, 160. [3] Noguchi, T. (1933) Proc. NIPR Symp. Antarct. Meteorites, 6, 204-233. [4] Lindsley, D.H. (1983) Am. Mineral., 68, 477-493. [5] Wells, P.R.A. (1977) Contrib. Mineral. Petrol., 62, 129-139. [6] Brey, G.P. and Köhler, T. (1990) J. Petrol., 31, 1353-1378. [7] e.g., Spear, F.S. (1980) Contrib. Mineral. Petrol., 72, 33-41.

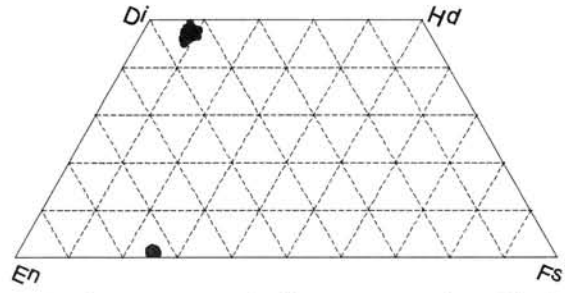

Fig 1. Chemical compositions of orthopyroxene and clinopyroxene plotted in the pyroxene quadrilateral

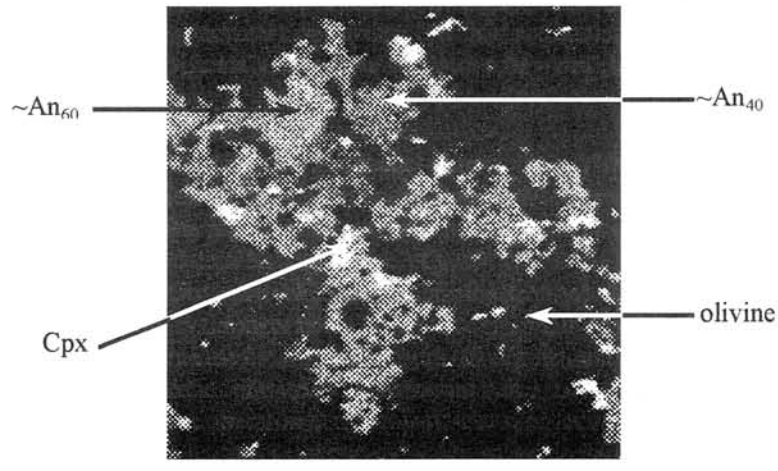

Fig 2. Compositional map of plagioclase.

Trace Element Chemistry of Minerals in Chemically Andesitic Material in the Caddo County IAB iron meteorite.

Hiroshi Takeda[1], Weibiao Hsu[2] and Hiromi Ogata[1].

[1]*Research Inst., Chiba Inst. of Technology, 2-17-1 Tsudanuma, Narashino City, Chiba 275-0016,*
[2]*Division of Geological and Planetary Science, Calif. Inst. of Tech., Pasadena, CA91125, U.S.A.*

Introduction

Only a few basalt types are known from asteroidal bodies. Eucrites are the most abundant basalts in our meteorite collections and were the major basalt group extruded on the surface of an asteroid, probably Vesta, in the early solar system [1]. Angrites are other asteroidal basalts known among the relicts of the early solar system, but their parent asteroid has not been even tentatively identified. In spite of extensive petrologic studies of the primitive achondrites [2-4], basalts representing their complementary partial melts are almost unknown. A plagioclase-enriched region was found in the lodranite/acapulcoite, EET84302 [4], and LEW 86220 [3]. Basalts representing a differentiated product for the iron meteorites have not been found in the meteorite collections or asteroids. Takeda *et al.* [4,5] found plagioclase-diopside-rich regions in a large slab of the Caddo County IAB iron. The compositions of IIAB and IIIAB irons can be modeled as arising during fractional crystallization of an asteroidal core, and these iron meteorite groups are collectively referred to as "magmatic" or "igneous" groups. Iron meteorite groups like the IAB group are referred to as "non-magmatic." However, Choi *et al.* [6] who have studied the IAB and IIICD iron meteorite groups, argue that these irons are really members of a single group, similar to that of some of the more poorly sampled magmatic iron groups [6]. In a terrestrial sense, the plag-diop-rich material may best be classified as a magnesian andesite, because the silica content of the Caddo County material is over 50 wt % [7]. The Na-Al-Ca-Si-rich melt that formed the andesitic material in Caddo County has been considered as a candidate for a partial melt of chondritic materials. The differences between such partial melts and eucritic materials have been discussed partly in connection with the origin of the HED meteorites [1].

Previous petrologic, chemical study of Caddo County by Palme *et al.*, [8] and chronological study by Stewart *et al.* [9] showed presence of silicate inclusions. The andesitic regions within a silicate inclusion were found on a 3.5 × 5.2 cm Caddo County slab [5]. Three polished thin sections (PTSs: 1A, 2A, 3A) parallel to this slab surface were made for this study. The andesitic material is not a clast within a breccia, but rather is a region located mainly at silicate-metal boundaries. The textures and mineralogy suggest that the andesitic material was formed by inhomogeneous segregation of partial melts from chondritic source materials. Compositional data on two samples (Chips 3Ba, 3Bb) of the andesitic material obtained by instrumental neutron activation analysis (INAA) [5] showed that the andesitic material is enriched in the incompatible lithophile elements Na, Ca, Sc, REE and Hf, consistent with a melt origin for the andesitic material. The older ^{39}Ar-^{40}Ar age (4.516 Ga to 4.523 Ga, with a few high temperature ages up to 4.54 Ga) could approximate the primary recrystallization age of silicates. Hsu *et al.* [9] made secondary-ion-mass-spectrometry (SIMS) of individual minerals in the andesitic materials in PTS 3A and 2A at Caltech. In the present study, based on the modal abundance of minerals of an andesitic region, we calculated bulk REE concentrations of the andesitic material. Our data are compared with those obtained by INAA [5] for a bulk silicate inclusion of Caddo County and clasts rich in alkali feldspar [10] found in IIE iron meteorites by Hsu *et al.* [9].

Samples and Experimental Techniques

PTS 2A and 3A contain the andesitic regions. The modal abundance of minerals of the selected area of the plagioclase-diopside-rich region was obtained using the mineral distribution map of 3A of Yugami *et al.* [11] using the Adobe Photoshop program. Chemical compositions of minerals analyzed by SIMS, were obtained by the JEOL 733 EPMA at Ocean Research Inst. of Univ. of Tokyo.

Rare-earth-element (REE) data for albite, diopside, orthopyroxene, Ca-phosphates and olivine were obtained with SIMS, a Cameca IMS 3f instrument at Caltech [9]. The method is the same as those used for the Colomera IIE irons by Hsu [9]. Samples were bombarded with primary O+ ions, using a current of 1-5 nA and an impact energy of 17 kV. The primary beam diameter on the samples was ~5-15 micrometer. The secondary ion mass spectrometer was operated at low mass resolving power and a 32V energy window. Secondary ions were energy filtered using a sample offset of 100V to suppress signals from complex molecular interferences and measured signals were deconvolved into REE and REE-oxide components following standard techniques [12, 13]. Absolute concentrations of each element we determined based on empirical relationships between measured peak/$^{30}Si+$ ratios, normalized to the SiO_2 content determined by prior EMP analysis. Standards were a synthetic Ti-pyroxene glass, NBS-612 glass, plagioclase glass, and Durango apatite.

Results

A mineralogical description of the andesitic material has been given by Takeda *et al.* [5]. Section 3A is an area adjacent to metal and consists of chromian diopside crystal set in plagioclase crystals. The modal abundances of silicate minerals in a rectangular area 7.5×5.5 mm in size adjacent to the blocky metal show the highest abundance of the andesitic material (Table 6 of [5]). Modal abundance of minerals in this andesitic region are: plagioclase (albite) 58.9 vol. %, diopside 27.7, olivine 8.1, orthopyroxene (Opx) 5.4, respectively. A curved vein of metal about 1 mm thick containing nickel-rich schreibersite is near one edge of the PTS 2A. A Ca-phosphate (apatite, Phos2-1) grain analyzed by SIMS is present adjacent to this metal vein (Table 3b in [5]). Crystals of diopside (Diop2-1), plagioclase (Plag2), and olivine (Oliv1) analyzed by SIMS are around this region. Data of another plagioclase and orthopyroxene (Opx5) are obtained for PTS 3A.

Fig. 1 shows CI-normalized rare earth element (REE) data for the Caddo County andesitic material. They are compared to the data of individual mineral separates of the bulk sample, determined by INAA by Palme *et al.* [8]. The bulk REE concentrations were calculated from the REE data of minerals measured by SIMS and modal abundance of the minerals. These calculated bulk values are in good agreement with those obtained by INAA (Chip 3Ba, 3Bb) of Mittlefehldt [5]. The Caddo County sample shows REE patterns broadly consistent with those expected of a melt derived from a chondritic precursor. They are enriched in all REE.

The mineral REE data reported by Palme *et al.* [8] are broadly similar to those of minerals analyzed by Hsu for the andisitic material. The light REE of apatite in PTS 2A (G1 of Table 3 in [5]) is little higher than that of the bulk silicate inclusions in Caddo County determined by INAA [8]. Whereas, the level of REE in diopside in the bulk silicate by INAA is little higher than that of the andesitic material. The REE of plagioclase in the andesitic material is higher than those by INAA. The REE of olivine were not determined by INAA. Both analytical data show positive Eu anomaly in plagioclase and negative anomaly trend in apatite, diopside and Opx.

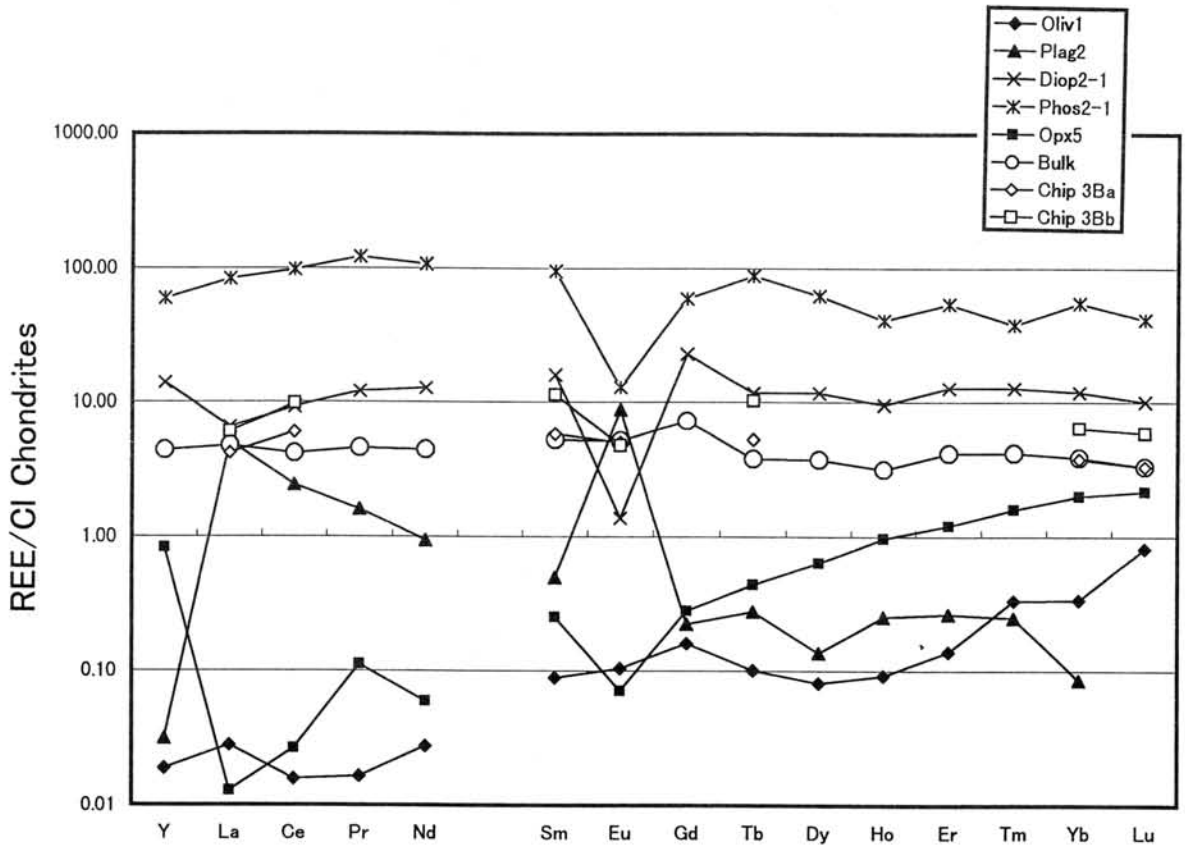

Figure 1: CI-normalized rare earth element (REE) data for the Caddo County andesitic material.

Discussion

The Caddo County andesitic material is distinct from the average IAB iron silicate inclusion in being enriched in refractory and moderately volatile lithophile elements relative to Cr (Fig. 7 of [5]). The process that made the metal-silicate assemblage in Caddo County is not fully known. The lithophile element pattern is broadly consistent with an igneous signature, in accord with the petrologic characteristics. The andesitic material rich in sodic plagioclase-diopside in Caddo County is thus a plausible product of partial melting of chondritic material such as winonaites. The andesitic material in Caddo County further suggests that there are other types of basaltic material in the asteroidal belt distinct from the Na-poor eucrites and angrites which contain Ca-rich plagioclase.

It is interesting to note that the abundances of REEs in the various phases of the Caddo County IAB iron are similar to those in acapulcoite by Floss [14] and the Colomera IIE iron reported before by Hsu *et al.* [9]. The trace-element data for Colomera, in general reveal that individual phases in different inclusions have similar trace-element abundances and patterns, despite large variations in textures, modes, and bulk compositions for the inclusions, except for the Colomera glasses. The mean REE concentrations of diopside in Colomera and Caddo County are nearly in the same range. The light REE of the Colomera diopside are lower than those of the Caddo County data. The mean REE of plagioclase and Ca phosphates are also nearly the same for the two groups, but the individual data of Colomera varies for different inclusions. The REE of Opx in Caddo County has steaper slope towards the heavy REE, while the data of Colomera is more flat and have higher concentration than those of Caddo County. The REE data of the Colomera glass vary considerably among different inclusions.

In conclusions, the bulk REE concentrations obtained in this study agree with those obtained previously by INAA. The Caddo County silicate inclusion we studied contains chemically andesitic material composed of coarse-grained Na-rich plagioclase and diopside. This material formed as a localized partial melt within a chondritic parent body. The material contains moderate concentrations of the incompatible elements (little less than ten times those of CI). The nearly flat REE pattern less than 10 % of the CI level suggests that this iron meteorite did not form as a product of a large scale differentiation involving gravitational separation and core formation. We propose that the andesitic material near metal in Caddo County was produced deep within the parent body by melting of a common, winonaitie-like parent material and by segregation of silicate partial melt and metal-sulfide melt.

Acknowledgments: We acknowledge Miner. Inst., Univ. of Tokyo for supplying us with the samples from the Planet. Materials Database Collections and Mr. J. Holder and Don Bogard of the NASA/JSC Curatorial Staff for making the large PTSs of the Caddo County samples. This work was supported in part by funds from the cooperative program (No. 84134), 2000 provided by Ocean Research Inst., Univ. of Tokyo, and by a Grant-in-Aid for Sci. Res. from the Japanese Ministry of Education, Sci. and Culture and is carried out as a part of "Ground Research Announcement for Space Utilization" promoted by Japan Space Forum. Additional support came from NASA grants to G. J. Wasserburg and to G. R. Huss. We acknowledge Mrs. M. Otsuki, M. Hatano and M. Okamoto, Mr. R. Osada, for their technical assistance and Drs. T. Ishii, K. Yugami, Mr. M. Tomobuchi, H. Kumada, and Dr. Don Bogard for their help in microanalysis and sample preparations. We are indebted to Profs. G. J. Wasserburg, G. Huss, Y. Ikeda, M. Miyamoto, Yuzo Kato, and to Drs. T. Arai, L. E. Nyquist, D. D. Bogard, K. Yugami, T. Mikouchi, R. Shinjo, H. Kojima for discussion and supports.

References: [1] TAKEDA H. (1997) *Meteoritics & Planet. Sci.* **32**, 841-853 (1997). [2] BENEDIX G. K., MCCOY T. J., KEIL K., BOGARD D. D. AND GARRISON D. H. (1998) *Geochim. Cosmochim. Acta* **62**, 2535-2553. [3] McCOY T. J., KEIL K., MUENOW D. W. and WILSON L. (1997) *Geochim. Cosmochim. Acta* **61**, 639-650. [4] TAKEDA H., MORI H., HIROI T. and SAITO J. (1994) *Meteoritics* **29**, 830-842. [5] TAKEDA H., BOGARD D. D., MITTLEFEHLDT D. W., GARRISON D. H. (2000) *Geochim. Cosmochim. Acta* **64**, 1311-1327. . [6] CHOI B.-G., OUYANG X. AND WASSON J.T. (1995) *Geochim. Cosmochim. Acta* **59**, 593-612. [7] TAKEDA H. and KATO Y. (1999) *Absr. Annual Meeting of Mineral. Soc. Japan*, p. 36, Mito. [8] PALME H., HUTCHEON I. D., KENNEDY A. K., SHENG Y. I. AND SPETTEL B. (1991) *Lunar Planet. Sci.* **XXII**, 1015-1016. [9] STEWART T. D., PAPANASTASSIOU D. A. and WASSERBURG G. J. (1996) *Earth Planet. Sci. Lett.* **143**, 1-12. [9] WASSERBURG G. J., SANZ H. G. and BENCE A. E. (1968) *Science* **161**, 684-687. [10] HSU W., TAKEDA H., HUSS G. R. and WASSERBURG G. J. (1997) *Meteoritics and Planet. Sci.* **32**, A61-62. [11] YUGAMI K., TAKEDA H., KOJIMA H. and MIYAMOTO M. (1998) *Antarct. Meteorite Res.* **11**, 49-70. [12] ZINNER E. AND CROZAZ G. (1986) *Int. J. Mass Spectrom. Ion Processes* **69**, 17-38. [13] FAHEY A. J., GOSWAMI J. N., MCKEEGAN K. D. and ZINNER E. (1987) *Geochim. Cosmochim. Acta* **51**, 329-350. [14] FLOSS C. (2000) *Geochim. Cosmochim. Acta* **35**, 1073-1085.

PRELIMINARY Rb-Sr ISOTOPIC AND REE ABUNDANCE STUDIES OF THE KOBE AND OTHER CK CHONDRITES.

Minako TAMAKI[1], Yusuke HIROTA[1], Noboru NAKAMURA[1,2],
Katsuyuki YAMASHITA[2], Hideyasu KOJIMA[3]
[1]Graduate School of Science and Technology, Kobe University; [2]Department of Earth & Planetary Science, Faculty of Science, Kobe University, Rokkoudai 1-1, Nada, Kobe, 657-8501 Japan; [3]Antarctic Meteorite Research Center, National Institute of Polar Research, 9-10, Kaga, Itabashi, Tokyo 173-8515,Japan

Introduction

The CK group, metamorphosed carbonaceous chondrites, consists of only two observed falls (Karoonda and Kobe) and more than 10 finds [1]. They have rarely been studied for Rb-Sr isotopic systematics, and therefore the thermal history of CK meteorite parent body have not been well understood. In addition, it is interesting that one of bulk Kobe samples shows an anomalous REE pattern indicative of nebular fractionations [2]. In order to obtain detailed chemical and isotopic characteristics, we have performed the Rb-Sr isotopic and isotope dilution analyses of lithophile elements for Kobe and some Antarctic CK group chondrites.

Sample and Analytical Procedures

Two aliquots from the bulk samples of Kobe (Kobe C, E), Karoonda (CK4) and Allende (CV3) were analyzed for Rb-Sr isotopes and lithophile elements. Small chips (30～80mg) of Antarctic CK chondrites (Y-693, Y-82102, Y-82191, A-882113) were also analyzed by isotope dilution. Alkaline elements were analyzed by direct loading IDMS, and REEs were analyzed by conventional IDMS. Rb-Sr isotopic analyses of Antarctic CK chondrites are now in progress.

Results and Discussion

Rb-Sr Systematics Results for Kobe whole rock samples (Kobe WR-C, C-3-2, E), mineral fragment (Kobe C-4-2pl) and Karoonda whole rock are shown in Fig. 1. It is pointed out that there exist relatively large variations up to three times in Rb/Sr ratio among the samples and that data points show roughly a linear array whose slope is about zero. Karoonda also plots on a similar trend. A close examination of the data points shows that data points are more or less scattered, indicating that Rb-Sr isotopic systems were disturbed by some young event(s). The slope of the line between two data points of Kobe meteorite (WR-C and E) corresponds to 230Myr. It is noted that the young Rb-Sr isotopic disturbance have been well documented for black hypersthene chondrites and that Rb-Sr data points of such chondrites tend to plot on the left side of 4.5 b.y. line in a ^{87}Rb-^{86}Sr evolution diagram [3]. Kobe meteorite has the weak shock stage of S2 that is assigned from the petrographical features [5]. In Fig. 1, data points (C-3, C-3-2 and Karoonda) plot on the right side of the 4.5 b.y. reference line, which is somewhat different from that of black hypersthene chondrites. Therefore, it is unlikely that the Rb-Sr disturbance of Kobe was due to the shock events but possibly to some unknown weak thermal events.

Major and Trace Element Abundances In Fig. 2, all the CK chondrites analyzed in this work show similarly flat REE patterns, though one sample (Y-82191) shows distinctly high absolute abundances. Moreover, it is worth noting that small negative anomalies of Ce and

Eu and variations of Yb are commonly found. It is suggested that Ce anormalies were produced in oxidizing environment. It is generally known that metamorphosed ordinary chondrites show REE patterns with more variable common REE but less variable Eu [6]. But such REE features are not seen in Fig 2. We, therefore, suggest that REE features of the CK chondrites originated in the nebular processes. Heterogeneous distributions of Alkali element (K, Rb) are also found in Fig 2.

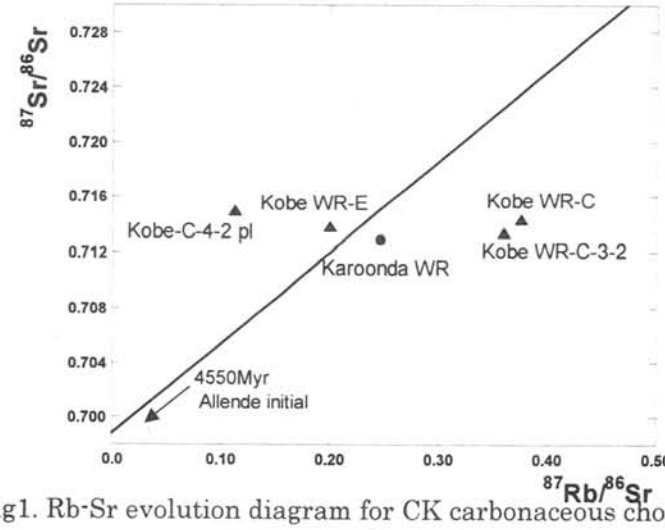

Fig1. Rb-Sr evolution diagram for CK carbonaceous chondrites.

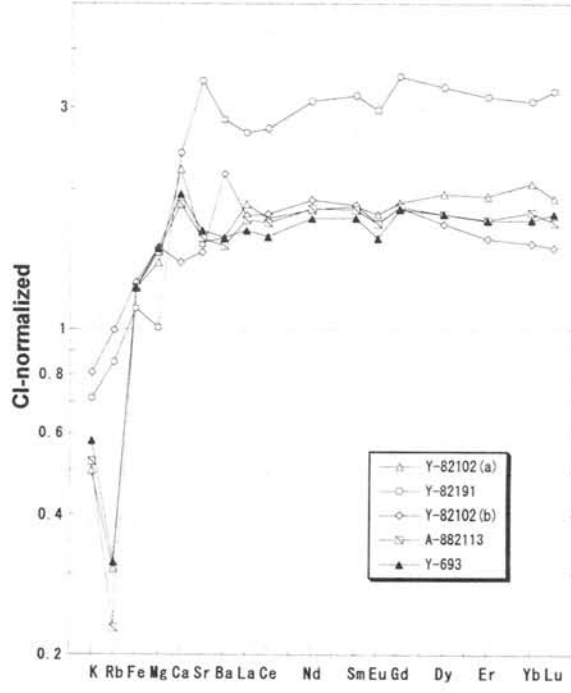

Fig2. CI-normalized lithophile element patterns for Kobe and other CK chondrites.

References:

[1] Kallemeyn G.W. et al. (1991) *GCA* 55,881-892 [2] Hirota Y. et al.(2000)*Proc. NIPR Symp. Antarct. Meteorites* 25,16-18. [3] Gopalin K. and Wetherill G.W. (1971) *J.G.R.* 76, 8484-8492. [4] Nakamura N. et al. (2000) *Lunar Planet.Sci.*31,1234. [5] Tomeoka K. et al. (2000) *Proc. NIPR Symp. Antarct. Meteorites* 25,160-162. [6] Nakamura N. (1974) *GCA* 38,757-775

WHAT CAUSES SILICATE DARKENING IN THE KOBE CK CHONDRITE?: IMPLICATIONS FOR SHOCK METAMORPHISM AT HIGH TEMPERATURE

Kazushige Tomeoka, Ichiro Ohnishi, Koji Kiriyama and Noboru Nakamura

Department of Earth and Planetary Sciences, Faculty of Science, Kobe University, Nada, Kobe 657-8501, Japan.

INTRODUCTION

The Kobe CK4 chondrite exhibits pronounced silicate darkening of matrix and chondrules, which is common to most of the metamorphosed CK chondrites [1,2]. Silicate darkening is also known from many metamorphosed ordinary chondrites [3,4]. It has been known that the silicate darkening in those chondrites is mainly caused by the dispersion of micron-to-submicron sized grains of opaque minerals such as Fe-Ni metal, Fe-Ni sulfides and magnetite within silicates. However, detailed features of those tiny opaque mineral grains have long remained unknown. Rubin [2], based on SEM observations, described curvilinear trails of tiny grains of opaque minerals in olivines in CK and ordinary chondrites and suggested that they are the principal cause of silicate darkening. Noguchi [5], based on TEM observations, described high densities of 100- to 300-Å sized grains of an Fe-rich mineral in olivines in some CK chondrites.

Most previous workers suggested that the silicate darkening resulted from shock metamorphism [e.g. 1-3]. It appears that Fe-Ni sulfide and metal were readily mobilized by shock-induced melting processes and injected into preexisting fractures of silicates [2]. However, this interpretation has been the subject of controversy. Scott et al. [6] argued that to produce melts from metal and sulfide, temperatures higher than 900-1000°C are required, and these temperatures are only reached in shock stage S4-S6, but olivines in most CK chondrites exhibit light shock effects that are consistent with shock stage S1-S2. Regarding this question, Rubin [2] suggested that the olivines in those chondrites have been annealed to remove strong shock effects by postshock heat during intense shock that produced the silicate darkening. However, Scott et al. [6] argued that erasing of shock features in olivine requires a high degree of thermal metamorphism that is characteristic of petrologic type 6, thus the suggestion of Rubin [2] is only valid for type 6 chondrites. In fact, there seems to be no strong correlation between degree of silicate darkening and shock stage among the CK chondrites [2,6] .

We present the results of detailed petrographic and scanning electron microscopic (SEM) observations of matrix and chondrules of Kobe. Our purposes are to clarify the mineralogical and textural characteristics that cause the silicate darkening and to determine the true origin of the silicate darkening.

PETROGRAPHY AND MINERALOGY

General Petrography: Silicate darkening in Kobe is observed in both chondrules and matrix, but it is less pronounced in chondrules than in matrix. In chondrules, olivine phenocrysts show a low but variable degree of darkening. Chondrule mesostases are distinctly more darkened than phenocrysts. Matrix is heterogeneously darkened, and in places, round to irregularly shaped highly dark patches of 50 to 300 μm in diameter occur. Darkened silicate phases include olivine, plagioclase and pyroxene, but olivine has a distinctly darker and dustier appearance than other silicates.

Many coarse olivine grains in matrix exhibit weak to moderate undulatory extinction, but olivine grains exhibiting planar fractures are rare. Many plagioclase grains also exhibit weak undulatory extinction. Based on these features of olivine, Kobe is assigned to be shock stage S2, which is comparable to the majority of known CK chondrites [2,6].

Matrix: Backscattered electron (BSE) images of highly dark regions in transmitted light reveal that they consist mainly of two types of fine-grained olivine. One forms subhedral to anhedral crystals that are typically 5-30 μm in diameter. The other is very irregular in shape; it commonly fills interstices of the subhedral to anhedral olivine crystals, exhibiting a complex network of veinlets that are typically 5-20 μm wide. The latter type of olivine has an unusual internal texture; it contains numerous tiny vesicles (<0.1-3 μm in diameter) and

spherical grains (<0.1-5 μm) of magnetite and pentlandite as well as anhedral grains (1-10 μm) of plagioclase, low-Ca pyroxene, diopside and chlorapatite. We hereafter call the former type of olivine nonvesicular olivine and the latter type of olivine vesicular olivine.

High-magnification BSE images of vesicular olivine, obtained using a field emission scanning electron microscope, reveal that both vesicles and mineral inclusions range down to 500 Å in diameter and those of 500-2000 Å in diameter occur pervasively at high densities. Vesicular olivine also occurs pervasively as a fine-scale intermixture with nonvesicular olivine throughout matrix. The volume proportion of these two types of olivine varies from region to region on scales of 50-300 μm. There is a tendency that a region having a higher volume proportion of vesicular olivine exhibits a darker and dustier appearance in transmitted light. Curvilinear trails of opaque mineral blebs are absent in vesicular olivine and rare in nonvesicular olivine.

Plagioclase also commonly contains tiny vesicles (0.2-2 μm in diameter) and spherical grains (0.2-5 μm) of magnetite and pentlandite as well as anhedral grains (1-20 μm) of olivine, diopside, low-Ca pyroxene and spinel. However, both vesicles and inclusions are much less abundant than in vesicular olivine, and those smaller than 0.2 μm are almost absent.

Chondrules: Tiny grains (0.5-2 μm in diameter) of magnetite and pentlandite fill grain boundaries and cracks in olivine phenocrysts, forming a network of curvilinear trails of the opaque mineral grains. However, such trails of opaque mineral grains do not occur in chondrule mesostases. Mesostases are commonly filled with vesicular olivine, plagioclase, both with tiny inclusions of magnetite (<0.2-5 μm in diameter), and minor amounts of low-Ca pyroxene and high-Ca pyroxene. The vesicular olivine and plagioclase in mesostases are almost identical in texture to those occurring in matrix. Curvilinear trails of opaque mineral grains in olivine phenocrysts are generally 30-100 μm apart, so the densities of opaque mineral grains in olivine phenocrysts are much lower than those in vesicular olivine in chondrule mesostases and matrix. This explains that chondrule phenocrysts exhibit a less dark appearance in transmitted light than chondrule mesostases and matrix.

***Chemical analyses of darkened olivine*:** Focused beam (~2 μm in diameter) chemical analyses were obtained from nonvesicular olivine and vesicular olivine in matrix. Nonvesicular olivine is very homogeneous in composition with an average Fa content of 31.1 mol%. It contains significant amounts of Ni (0.36 wt% NiO in average) and Mn (0.24 wt% MnO) but only trace amounts of Ca (0.05 wt% CaO). These features are almost identical to those of olivine phenocrysts in chondrules.

In contrast, analyses of vesicular olivine show several unusual features. They have significantly higher contents of S (0.50 vs. 0.01 wt% S), Ni (1.04 vs. 0.36 wt% NiO), Ca (0.18 vs. 0.05 wt% CaO) and P (0.05 vs. 0.03 wt% P_2O_5) than those of nonvesicular olivine. Sulfur, Ni, Ca and P are heterogeneous in distribution, but S and Ni are correlated, so are Ca and P. The enrichment and correlated distributions of these elements are also confirmed by X-ray chemical mapping analyses. From these analyses and the high-magnification BSE images described above, it is evident that most of S and Ni in the analyses occur as extremely tiny grains (<0.2 μm in diameter) of pentlandite, and Ca and P as phosphate at high densities. Analytical totals of vesicular olivine are consistently lower than 100 wt% (96.4 wt% in average), which is probably due to the abundant presence of tiny vesicles.

Analyses of vesicular olivine in chondrule mesostases are similar to those of vesicular olivine in matrix.

DISCUSSION

Our SEM observations of Kobe reveal that the curvilinear trails of opaque mineral blebs, which Rubin [2] suggested to be the main cause of the silicate darkening in the CK and ordinary chondrites that he studied, are rare in fine-grained olivines (<50 μm) in matrix and chondrule mesostases that show a relatively high degree of silicate darkening. However, instead, unusual inclusion-rich vesicular olivine occurs pervasively throughout matrix and chondrule mesostases, and it is particularly abundant in regions that exhibit a highest degree of darkening. The occurrence of curvilinear trails of opaque mineral blebs is mostly

restricted to olivine phenocrysts in chondrules and large olivine grains (>50 μm) in matrix that show a relatively low degree of darkening. Therefore, it is evident that the inclusion-rich vesicular olivine is the principal cause of the silicate darkening in Kobe.

The vesicular olivine is closely similar in internal texture to the shock-induced local melts observed in matrices of carbonaceous chondrites. The recent shock-recovery experiments of the Murchison CM chondrite [7] and the Allende CV chondrite [8] revealed that local melting occurs as veins and pockets in those meteorite matrices at equilibrium peak shock pressures of 20-30 GPa in Murchison and 25-40 GPa in Allende. The local melts produced in both experiments contain numerous tiny vesicles (<1-30 μm in diameter) and inclusions (0.5-3 μm) of Fe-Ni sulfides as well as fragmental grains of olivine and pyroxene (cf. Fig. 4b in ref. 7).

From these textural and compositional features, we suggest that the vesicular olivine in Kobe formed from melts that were produced from fine-grained olivine in the matrix by shock. The matrix of Kobe is only partially melted, and there still remains abundant unmelted nonvesicular olivine. This suggests that the matrix was heated heterogeneously and so temperature locally exceeded the melting point of the Fe-rich olivine. Both heating and cooling must have occurred instantaneously, thus the melted materials did not move in the distance and stayed locally. During melting, vesiculation occurred and numerous tiny vesicles were produced in the melts. Simultaneously the melts probably trapped numerous splashed droplets of melted magnetite and pentlandite as well as fragmented grains of other minerals.

We suggest that Kobe was probably shocked at the state where it was heated to a high temperature. Recently, Nakamura et al. [9,10] conducted shock-recovery experiments of Allende preheated to room temperature (20°C) and high temperatures (300 and 600°C) and found that the matrix of Allende shocked at 21 GPa and 600°C contain minor amounts of melted materials. The more recent results of shock-recovery experiments of Allende preheated to 800°C indicated that large amounts of vesicular melts are indeed produced in matrix at a peak pressure of 24 GPa [11]. Schmitt [13] also conducted a series of shock-recovery experiments of the Kervouvé H6 chondrite at pressures from 10 to 60 GPa and temperatures of 20°C and 647°C. He found that the shock experiments at high temperature (647°C) lead to the onset of melting at distinctly lower shock pressures and produced a much larger volume of melt at any given pressure than the shock experiments at low temperature (20°C). From these experimental results, we suggest that the vesicular olivine in Kobe was probably produced in a region of the parent body where it was heated to a temperature higher than 600°C and shocked at a pressure lower than 20 GPa. Therefore, mechanical effects on olivine such as fractures and deformation were relatively minor, but heating was strong enough to cause partial melting of matrix olivine.

REFERENCES

[1] Kallemeyn G.W., Rubin A.E. and Wasson J.T. (1991) *Geochim. Cosmochim. Acta* **55**, 881-892.

[2] Rubin A.E. (1992) *Geochim. Cosmochim. Acta* **56**, 1705-1714.

[3] Heymann D. (1967) *Icarus* **6**, 189-221.

[4] Kallemeyn G.W., Rubin A.E., Wang D. and Wasson J.T. (1989) *Geochim Cosmochim. Acta* **53**, 2747-2767.

[5] Noguchi T. (1995) *Papers presented to 20th NIPR Symp. Antarct. Meteorites*, 196-199 (abstr.).

[6] Scott E.R.D, Keil K. and Stöffler D. (1992) *Geochim. Cosmochim. Acta* **56**, 4281-4293.

[7] Tomeoka K., Yamahana Y. and Sekine T. (1999) *Geochim. Cosmochim. Acta* **63**, 3683-3703.

[8] Kiriyama K., Tomeoka K. and Sekine T. (2000) *Meteorit. Planet. Sci.* **35**, A88 (abstr.).

[9] Nakamura T., Tomeoka K., Sekine T. and Takeda H. (1995) *Meteoritics* **30**, 344-347.

[10] Nakamura T., Tomeoka K., Takaoka N., Sekine T. and Takeda H. (2000) *Icarus* **146**, 289-300.

[11] Kiriyama K., Tomeoka K. and Sekine T. (2001) *Papers presented to 26th NIPR Symp. Antarct. M*eteorites (this abstract volume).

[12] Schmitt R.T. (2000) *Meteorit. Planet. Sci.* **35**, 545-560.

A preliminary study on mechanism of high-pressure transition in $MgSiO_3$ pyroxene for shock metamorphism

Naotaka Tomioka[1,2], Kurt Leinenweber[1], Thomas G. Sharp[1]

[1,2]Department of Earth and Planetary Sciences, Faculty of Science, Kobe University, 657-8501, Japan

[2]Depertment of Geological Science, Arizona State University, Tempe, Arizona 85281, USA

Introduction

Phase transition mechanisms of silicate minerals under high pressure and high temperature is important to understand the fate of subducting slab in the deep Earth and the shock metamorphism in chondrites. Therefore, the high-pressure transition behavior in olivine, being the most abundant mineral in the Earth's upper mantle and chondrites, has been well investigated. Pyroxene, in this line, is the second major phase whose transition behavior should be also studies thoroughly. However, only one kinetic study on the high-pressure transition in $MgSiO_3$ pyroxene has been reported [1]. Recently, natural $(Mg,Fe)SiO_3$-ilmenite (akimotoite) and –perovskite, were found in shocked L-chondrites [2-3]. In the Tenham chondrite (L6), silicate ilmenite intergrown in clinoenstatite had topotaxial relationship [4]. This crystallographic feature shows preservation of the close-packed layers of oxygen in this phase transition and resembles the shear mechanism in olivine-spinel transition proposed by Poirier (1981) [5]. In this study, we experimentally investigated the high-pressure transition mechanism in $MgSiO_3$ pyroxene.

Experimental

High-pressure and high-temperature experiments were performed by a multianvil apparatus at Arizona State University, U.S.A. Tungsten carbide cubes with a truncated edge length of 3 mm were used as anvil material. An MgO octahedron was used as the pressure medium. Coarse crystals of $MgSiO_3$ enstatite synthesized by flux method (~200-500 μm), embedded in fine synthetic $MgSiO_3$ enstatite powder ($\lesssim$ 50 μm), were enclosed in a cylindrical rhenium heater. Specimen temperatures were monitored with a W26%Re-W5%Re thermocouple. The cell assembly used in this study is similar to that in Bertka and Fei (1996) [6]. Firstly, the specimens were held at pressure 12 GPa at 1300 °C for 3 hours to remove the elastic and the plastic strain in the samples formed during the compression at room temperature (hot-pressing stage). Only the run BB-73 (24 GPa, 1300 °C) was done without hot-pressing stage. Subsequently, specimens were hold at the pressure range of ~20-24 GPa and temperatures between 1250-1500 °C for 1-2 hours. The recovered specimens were investigated by optical microscopy and Raman spectroscopy and transmission electron microscopy.

Results and Discussion

Under the optical microscope, it is observed that large single crystals of enstatite in all specimens recrystallized into aggregates of finer grains (~10-100 μm) and those crystals orientated randomly. The Raman spectra from recovered specimens show ilmenite-phase formed

in all the specimens. In the specimens from lower than 22 GPa, original enstatite (inverted into clinoenstatite by compression) partially transformed into ilmenite, but the interface between relict enstatite and ilmenite was ambiguous. Whereas, in the specimen recovered from the highest pressure near the ilmenite-perovskite phase boundary (BB-79, 24 GPa, 1250 °C), part of former large crystal showed spectrum of ilmenite. Although the obtained Raman spectra from the other part of large crystal in the same specimen did not show obvious peaks, but electron diffraction pattern showed these were orthorhombic perovskite phase. In the specimen BB-73 (24 GPa, 1300 °C) without hot-pressing stage, there is no apparent difference in the reaction mode of enstatite.

In this study, single crystal of enstatite in all specimens partly or mostly transformed into randomly oriented polycrystalline aggregate of ultrahigh-pressure phases. Therefore, the transformation mechanism in $MgSiO_3$ is the interface-controlled nucleation and growth at the studied pressure-temperature conditions irrespective of P-T paths. Recently, it is reported that the clinopyroxene-ilmenite transition in $FeGeO_3$ is promoted by the shear mechanism at 13 GPa, even though the stability limit of clinopyroxene structure is ~1GPa, and it breaks down to spinel phase plus sthishovite [7]. Therefore, the shear mechanism in silicate pyroxene-ilmenite transition would occur at much high overstepping pressure.

In the Tenham chondrite, majorite is the dominant phase in the matrix of melt vein. According to the phase diagram of the Allende chondrite, majorite is a liquidus phase at 14-26 GPa and probably those majorites crystallized at this pressure range [8]. However, in the fragment in shock-vein, topotaxial intergrowth of ilmenite-phase in pyroxene formed in a solid-state reaction was observed. The results of this study suggest that much higher pressure than 24 GPa is required for this occurrence. Therefore, the peak pressure of shock event in Tenham is likely to be much higher than the crystallization pressure of the shock-induced melt. Further transformation experiments at higher pressure and lower temperature, where overstepping pressure is large but long-range atomic diffusion is hindered, are necessary to constrain the condition of shear mechanism and the peak pressure of shock event.

References

[1] Hogrefe et al. (1994), *Nature*, 372, 351-353.
[2] Sharp et al. (1997), *Science*, 277, 352-355.
[3] Tomioka N., and Fujino, K. (1997), *Science*, *277*, 1084-1086.
[4] Tomioka N., and Fujino, K., (1999), *Am. Mineral.*, *84*, 267-271.
[5] Poirier, J. P. (1981), In Anelasticity in the Earth., American Geophysical Union, pp.113-117.
[6] Bertka and Fei (1997), *J. Geophys. Res.*, 102, 5251-5264.
[7] Hattori et al. (2001), Phys. Chem. Minerals (in press).
[8] Agee et al. (1995), *J. Geophys. Res.*, 100, 17725-17740.

Chemical variations of chromites in L-chondrites.

T. Tomiyama[1], A. Yamaguchi[1,2], K. Misawa[1,2] and H. Kojima[1,2]

[1]*Department of Polar Science, School of Mathematical and Physical Science, Graduate University for Advanced Studies, 1-9-10 Kaga, Itabashi, Tokyo 173-8515, Japan.* [2]*Antarctic Meteorite Research Center, National Institute of Polar Research, 1-9-10 Kaga, Itabashi, Tokyo 173-8515, Japan.*

Introduction: Chromites are common minerals in ordinary chondrites and show wide chemical variations reflecting their histories of crystallization and metamorphism. In equilibrated ordinary chondrites (EOCs), chemistries of chromites systematically vary not only within chemical groups (H-L-LL) but also in petrologic types [1-4]. Relationships between chromite compositions and metamorphic grades of unequilibrated ordinary chondrites (UOCs) are not well known. Nehru et al. suggested that there is no correlation between chromite compositions and petrologic subtypes [5]. On the other hand, Kimura found that chromites in LL3 chondrites with higher petrologic subtypes are more enriched in Al and Mg [6]. In order to understand thermal histories of ordinary chondrite, we performed systematic survey of chondritic chromites. We present a possible relationship between chemical compositions of chromites and petrologic subtypes, and discuss thermal histories of L-chondrite parent bodies.

Samples and Experiments: Polished thin-sections of unbrecciated portions of L-chondrites were examined using an optical microscope, a scanning electric microscope (JEOL JSM-5900, equipped with Oxford LINK ISIS EDS system) and an electron probe microanalyzer (JEOL JXA-8800M) at National Institute of Polar Research. Electron probe analysis was carried out at accelerating voltage of 15 kV and beam current of 30 nA with 2 μm diameter. Counting time was 10-90 sec for each element. The classification of petrologic subtypes for UOCs is based on TL sensitivity and/or diversity of olivine compositions [7-10].

Results: Most chromites in UOCs occur as tiny grains (< 30 μm) and those in EOCs are generally coarser (> 100 μm). In many cases, chromites in chondrules from UOCs are euhedral, while those from EOCs are unhedral and associated with FeNi-metals and/or Fe-sulfides.

Cr# (=Cr/(Al+Cr)) ratios in chromites decrease with increasing metamorphic grade (Fig. 1). We classified our samples into four groups based on Cr#: i) Chromites show wide variation in Cr# from < 0.8 to 1.0 in A-9043 (L3.0-3.1), ALH-78041 (L3.4) and ALH-78119 (L3.5). Aluminum-free chromites are most abundant in these chondrites. ii) Chromites in Y-82055 (L3.6), Y-790770 (3.7), Y-86706 (L3.7-3.9) are less variable in Cr# than those in chondrites with lower petrologic subtypes. Most of the chromites have Cr# ~ 0.93. iii) Chromites in Y-8014 (L3.9) are Cr# ~ 0.89. iv) Chromites in EOCs (Y-8029 (L4), Y-87029 (L4), Y-86753 (L4), Y-791107 (L5), Y-74452 (L6)) have Cr# within the range of 0.84-0.87. Mg# (=Mg/(Mg+Fe)) ratios of chromites increase with decreasing Cr# (Fig. 2a). On a Mg# vs Cr# diagram, Mg# of chromites in most EOCs are plotted in a narrow region (Mg# = 0.08-0.14), whereas those in Y-86753 (Mg# = 0.12-0.18) are plotted in the upper end of, or higher than other EOCs'. Mn/Fe

vs Cr# plot shows chromites in L3.0-3.5 chondrites have lower Mn/Fe ratios (Mn/Fe = 0.01-0.02) than those in L3.6-6 chondrites (Mn/Fe = 0.02-0.03) (Fig. 2b).

Discussion: Iron-magnesium partition between spinel-group mineral and coexisting olivine-pyroxene is sensitive to the ambient temperature and Cr# of spinel. In general, Mg# of spinel increases with increasing temperature, and decreases with increasing Cr# of spinel [e.g., 11]. Because of the high diffusivity of Fe and Mg in chromite [12], Mg# of chromites are readily affected by thermal effects. Chromites in UOCs may have formed by condensation in the solar nebula [13] or by crystallization during chondrule formation [4]. Various crystallization conditions for individual chromites could have resulted in scattered initial Mg# of chromites. In contrast, our results show that most chromites in UOCs are homogenized in Mg# even in L3.0-3.5 chondrites. This indicates that all UOCs we examined have experienced mild reheating.

Except for Y-86753, EOCs show small variation in Mg# of chromites. On the basis of olivine-spinel Fe-Mg exchange geothermometer [14], we estimated equilibration temperatures for L4 at 520-610 °C, L5 at 570-660 °C, and L6 at 560-680 °C. This estimation is less sensitive to metamorphic grades compared with the approximate ranges of metamorphic temperatures of EOCs (estimated mainly from pyroxene mineralogy and chemistry; L4 at 600-700 °C, L5 at 700-750 °C, L6 at 750-950 °C) [15]. A possible explanation for this discrepancy is that chemical compositions of chromites in most EOCs have changed during cooling after they attained peak temperatures [4, 16]. Chromites in Y-86753 have relatively high Mg# compared with those in other EOCs. Equilibration temperature of Y-86753 estimated from olivine-spinel geothermometer is 640-740 °C. This high temperature signature suggests that Y-86753 cooled more rapidly than other EOCs, and further implies that Y-86753 was excavated from hot interior of the parent body.

The distribution patterns of Cr# of chromites in individual chondrites (Fig. 1) suggest that most chromites were equilibrated in different Cr# in relation to metamorphic grades. Chromites tend to be higher in Cr# under more oxidizing condition [17, 18]. We suggest that UOCs with lower petrologic subtypes were metamorphosed under more oxidizing conditions. It is consistent with the fact that chromites in L3.0-3.5 chondrites show relatively low Mn/Fe ratios.

References: [1]K. G. Snetsinger et al. (1967) *Amer. Min.* **52**, 1322-1331. [2]T. E. Bunch et al. (1967) *GCA* **31**, 1569-1582. [3]H. Yabuki et al. (1983) *Meteoritics* **18**, 426-428. [4]C. A. Johnson and M. Prinz (1991) *GCA* **55**, 893-904. [5]C. E. Nehru et al. (1997) *LPSC* **28**, #1651. [6]M. Kimura (2000) *LPSC* **31**, #1213. [7]J. N. Grossman (1994) *Meteoritics* **29**, 100-143. [8]K. Ninagawa et al. (1998) *Antarct. Meteor. Res.* **11**, 1-17. [9]K. Ninagawa et al. (2000) *Antarct. Meteor. Res.* **13**, 112-120. [10]M. Ohta et al. (2000) *Symp, Antarct. Meteor.* **25**, 120-121. [11]R. O. Sack and M. S. Ghiorso (1991) *Amer. Min.* **76**, 827-847. [12]R. Freer and W. O'reilly (1980) *Mineral. Mag.* **43**, 889-899. [13]S. Weinbruch et al. (1990) *Meteoritics* **25**, 115-125. [14]H. St. C. O'neill and V. J. Wall (1987) *Jour. Petrol.* **28**, 1169-1191. [15] R. T. Dodd (1981) *Meteorites*, Cambridge Univ. Press, Cambridge, p. 93. [16]F. Wlozka (1987) *Meteoritics* **22**, 529-530. [17]S. E. Haggerty (1972) *PLPSC* **3**, 305-332. [18]J. Akella et al. (1976) *PLPSC* **7**, 1179-1194.

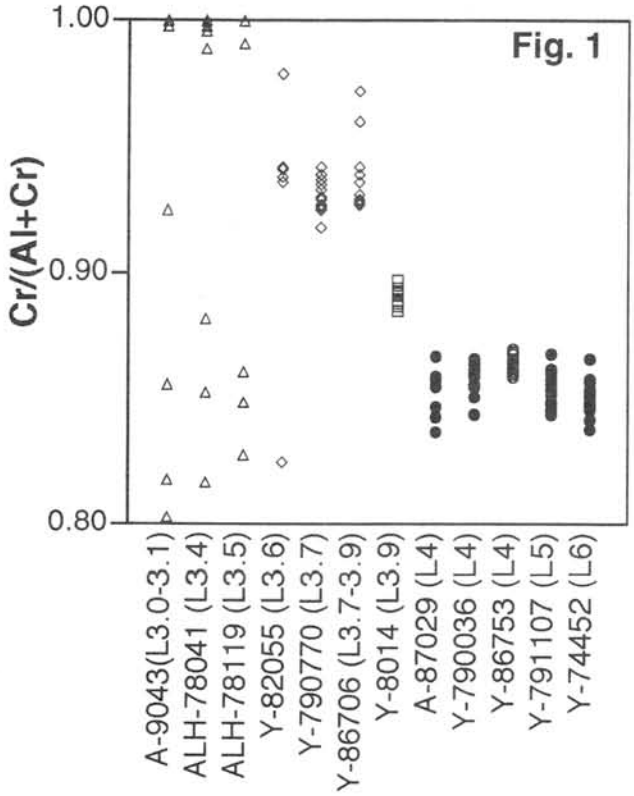

Fig. 1: Plots of molecular ratios of Cr/(Al+Cr) of chromites in individual chondrite.

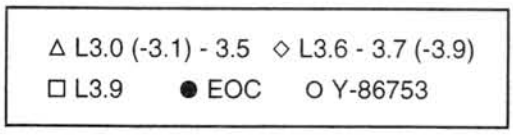

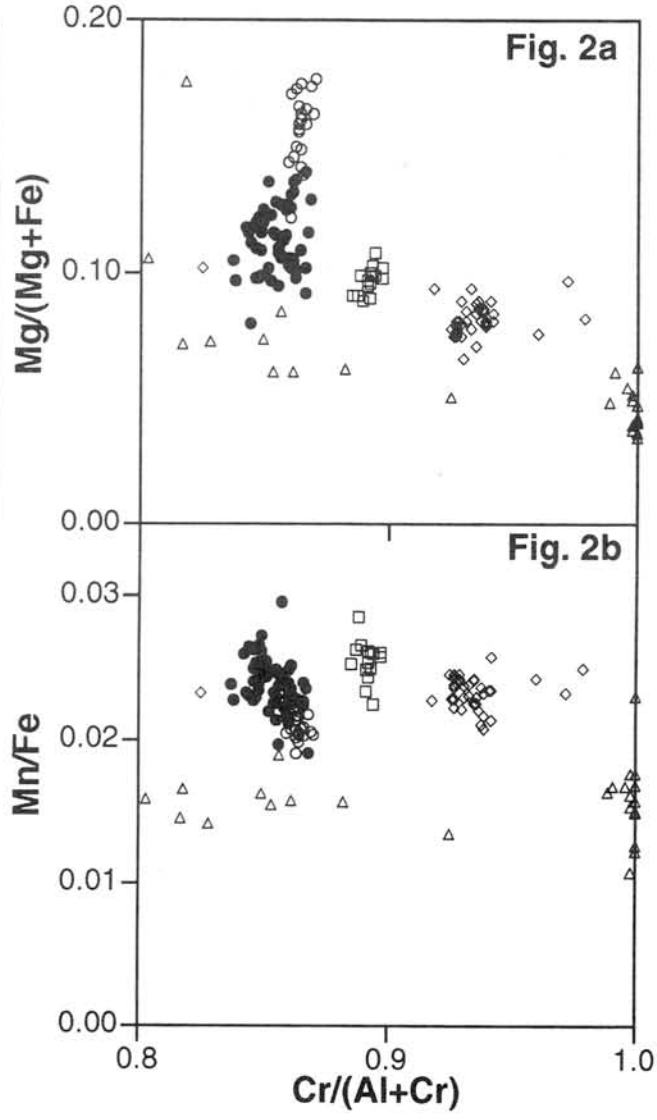

Fig. 2: Plots of **a)** Mg/(Mg+Fe), **b)** Mn/Fe ratios of chromites against Cr/(Al+Cr) ratios in the molecular unit.

PETROGRAPHY, MINERALOGY AND TRACE ELEMENT CHEMISTRY OF Y-86029, Y-793321 AND LEW 85332: AQUEOUS ALTERATION AND HEATING EVENTS

Eric Tonui[1], Mike Zolensky[1] and Michael Lipschutz[2]

[1]NASA Johnson Space Center, Mail Code SN2, Houston, Texas, 77058, USA
[2]Department of Chemistry, Purdue University, West Lafayette, Indiana 47907-1393, USA

Introduction

Recent petrographic and mobile trace element data on a number of Antarctic carbonaceous chondrites have revealed that they experienced both aqueous alteration and thermal metamorphic events in an asteroidal setting [e.g. 1,2,3]. These studies have provided the background upon which these events can be recognized in new carbonaceous chondrites. Trace element data based on radiochemical neutron activation analysis (or RNAA) of 15 thermally mobile elements suggests that Y-86029, LEW 85332 and Y-793321 were heated to various degrees in their parent bodies [1]. We hereby present mineralogical and petrological evidence of these events.

Descriptions

Y-86029 has CI affinities in that it is highly brecciated, contains a variety of clasts, no chondrules and abundant secondary minerals including coarse- and fine- grained phyllosilicates, Fe-Ni sulfides, carbonates and magnetite. Phyllosilicates within Y-86029 are present as fine-grained matrix or coarsely crystallized isolated clusters (30-300 μm). Ternary plots suggest a mixture of serpentine and saponite (Fig. 1) and high analytical totals (88.3-97.8%) consistent with extensive thermal metamorphism. Large periclase clasts (300-500 μm) with high Fe-Mn contents and minute grains of pyrrhotite are also present (Fig. 4) probably as a result of heating of carbonate. A few olivine aggregates have vesicular veins and polycrystalline aggregates and blebs of sulfides typical of shock induced melt recrystallization [4,5]. Sulfides are abundant and occur predominantly as pyrrhotite and rarely pentlandite. Magnetite is also abundant in different sizes and essentially all morphologies either individually or intergrown. Carbonates are present as individual crystals (rarely exceed 25 μm) or globular aggregates (10-15 μm) with high Mn contents (3-6%). The individual crystals have compositions ranging from dolomite to magnesite. The carbonate globules (Fig. 5) have inner Fe-rich cores (magnetite) with traces of S, while the rims are Ca-Fe rich (ankerite and siderite compositions). Interstitial spaces between the globules are Mg-rich (dolomite composition).

Y-793321 is a CM2 chondrite [6] that contains clasts exhibiting varying degrees of aqueous alteration. It consists of slightly altered chondrules, CAI's, tochilinite, carbonates, phyllosilicates, metal, opaques and glass. Most of the chondrules are olivine (average $Fo_{96\text{-}98.5}$) porphyritic types with no discernible rims. Barred olivine chondrules are also present. Fe-Ni metal (mainly kamacite) is sparse. Zoned olivine aggregates (average $Fo_{74.5\text{-}77.5}$) are quite common in the matrix often associated with the sulfides. Rounded CAI's typical of CM2 and CR2 [7] are present in Y-793321 and consists of a granular spinel core rimmed by a thin layer of Fe-rich serpentine and diopside (Fig. 6). Tochilinite is present within altered porphyritic chondrules or matrix. Opaque phases are mainly magnetite, pentlandite and less commonly pyrrhotite. Carbonates (mainly calcite) are abundant often intergrown with phyllosilicates or PCP's. Phyllosilicates occur as partial replacement of chondrules or as matrix. They are mostly serpentines (Fig. 2) with variable compositions and analytical totals ranging from 81.2-92.7%. Apart from few clasts that show high analyical totals between 88 and 92.7% there appears to be no other evidence of heating events in Y-793321.

LEW 85332 is a highly unequilibrated type-3.0-3.1 carbonaceous chondrite [8]. It is moderately-to-extensively weathered. Most of the matrix, chondrules, aggregates and metal

grains are stained or coated by iron oxides (Fig. 7). It consists mainly of chondrules, silicate aggregates, Fe-Ni metal, sulfides and matrix. Chondrules in LEW 85332 are olivine-rich (Fo_{94-97}) porphyritic or granular types, many of which contain blebs (5-40μm) and rims of Fe-Ni metal notably kamacite. Most of the silicate aggregates (10-150μm) are also olivine-rich (Fo_{75-77}) and range in shape from angular, subhedral to spherical forms. Fe-Ni metal grains of kamacite are highly abundant and occur within chondrules or matrix. Sulfides are also abundant and occur as troilite and rarely pyrrhotite often together with the Fe-Ni metal grains. Magnetite is rare while carbonates are absent. The phyllosilicates occur as a variety of clasts and matrix. Ternary plots suggest that the phyllosilicates are mixtures of saponite and serpentine (Fig. 3) with high analytical totals (83.1-94.4%) indicative of mild to moderate thermal metamorphism.

The labile trace element data (Table 1) shows loss of Cd in LEW 85332 and Cd, Tl, In and Bi in Y-86029. Y-793321 does not show any obvious loss suggesting absence of or very mild metamorphism.

Meteorite	Type	x±σ	Elements (No.)	Cd
Y-86029[$]	CI(?)	0.55±0.06	Cs→Zn (6)	0.115
LEW 85332[#]	CO3	0.26±0.04	Cs→Tl (8)	0.0026
Y-793321[#]	CM2	0.51±0.08	Cs→Cd (9)	0.50

Table 1: Mean atomic abundances (CI-normalized) for thermally mobile trace elements in Y-86029, LEW 85332 and Y-793321 [#1, $9].

Aqueous alteration and thermal histories

Y-86029 has unusual textures and shows the strongest evidence of heating events after aqueous alteration. The presence of periclase clasts, Ca-Mg-Fe carbonates with high Fe-Mn contents and sulfide rims around aggregates such as magnetite shows there was some sulfidization and extensive oxidation after aqueous alteration. The textures of the carbonate globules suggest that the inner magnetite-rich (with traces of S) core was originally siderite and pyrrhotite before heating, while the outer Ca-Fe rich cores would have predominantly been calcite. The lack of late stage aqueous alteration may explain the presence of coarse phyllosilicates. Thermal metamorphism in LEW 85332 and Y-793321 is only apparent in the composition of the phyllosilicates. This was more pervasive in LEW 85332, which shows homogeneity in phyllosilicate texture than in Y-793321 where heating appears to have been limited to very few clasts. The presence of tochilinite within the matrix and Ca-rich carbonates in Y-793321 also suggests absence of or very mild heating event. Phyllosilicate veins typical of CM and CI chondrites [10] are also present in Y-793321 suggesting that aqueous alteration occurred after brecciation. Probably, heating preceded brecciation and was obscured by later events although this may be difficult to demonstrate. LEW 85332 is highly brecciated and shows no clear evidence of alteration of chondrules or silicate aggregates. This suggests that the formation of hydrous phases and subsequent heating occurred prior to final accretion in parent body. This has hitherto not been demonstrated in studies of heated Antarctic meteorites. Based on these observations, the thermal histories of these meteorites compared to those of other heated Antarctic meteorites [1] can be ordered as:

Y-793321<A-881655=**LEW 85332**<B-7904=**Y-86029**<Y-82162<Y-86720.

References: [1] Lipschutz et al. (2000), *Antarct. Meteorite Res.* **12**, 57-80. [2] Wang, M and Lipschutz, M. (1998), *MAPS, 33, 1297-1302.* [3] Akai, J. (1990), *Antarct. Meteorites XV*, NIPR 86-87. [4] Bauer, J. (1979), *Proc. 10th LPSC*, 2573-2596. [5] Scott et al. (1992), *GCA*, **56**, 4281-4293 [6] Akai, J. and Sekine, T. (1994). *Antarctic Meteorites Res.* **7**, 101-109 [7] Weisberg et al., (1993), *GCA*, **57**, 1567-1586. [8] Brearly, A. (1997), *MAPS*, **32**, 377-388. [9] Tonui et al., (2001), *Proc. LPSC XXXII*, 1248-1249. [10] Browning et al., (1995). *LPSC XXVI*, 181-182.

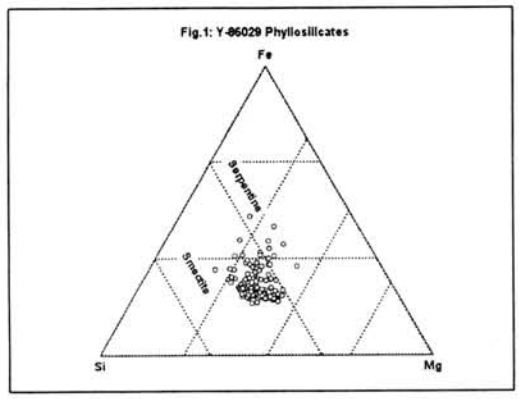

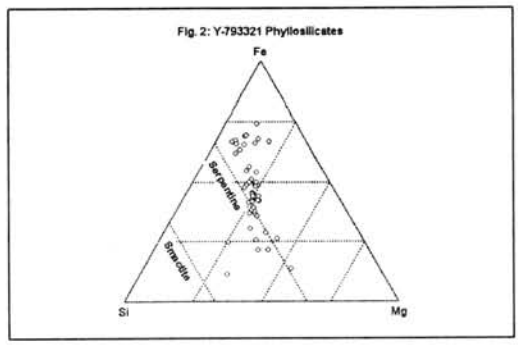

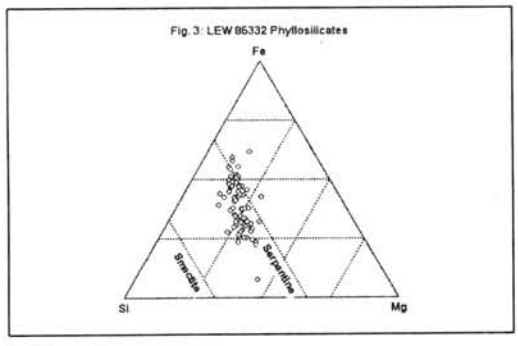

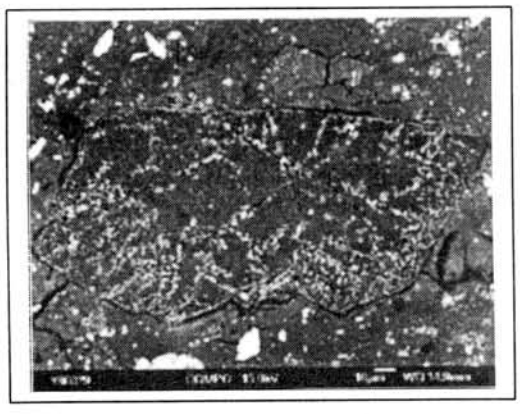

Fig. 4: Large periclase clast with minute sulfide grains within fractures in Y-86029

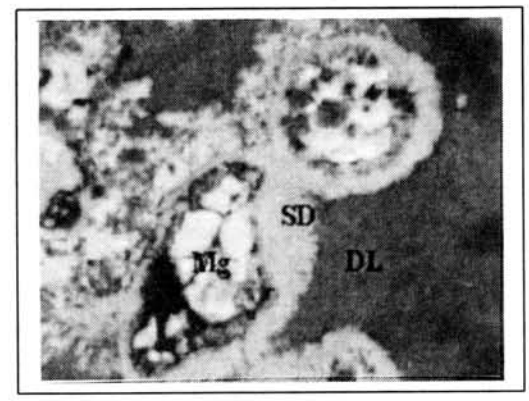

Fig. 5: Carbonate globules with magnetite (Mg) core, siderite (SD) rim and dolomite (DL) in Y-86029

Fig. 6: Granular spinel (Sp)with a thin inner rim of phyllosilicate and outer diopside rim in Y-793321

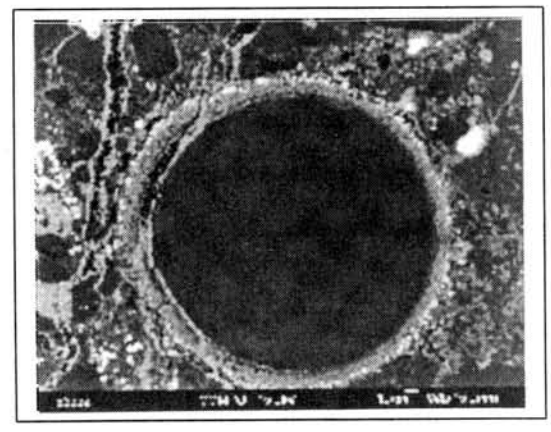

Fig. 7: Euhedral olivine grain rimmed by iron oxide and kamacite in LEW 85332

X-ray microtomography system using SR at SPring-8 for studies of three-dimensional microstructures of meteorites.

TSUCHIYAMA, Akira[1]*, UESUGI, Kentaro[2], NAKANO, Tsikasa[3], SUZUKI, Yoshio[2] and YAGI, Naoto[2].

*1) Department of Earth and Space Science, Osaka University, 1-1 Machikaneyama-cho, Toyonaka 560-0043, JAPAN, *akira@ess.sci.osaka-u.ac.jp. 2) Japan Synchrotron Radiation Research Institute, Mikazuki, 679-5198 JAPAN, 3) Institute of Geoscience, National Institute of Advanced Industrial Science and Technology, Tshukuba, 305-8567 JAPAN*

Introduction: X-ray CT (computed tomography) is a non-destructive method for investigation of materials by using X-ray attenuation. 3D internal structures can be obtained by constructing a number of successive cross-sectional CT images. This method has been applied to extra-terrestrial samples (e.g., [1,2]) as well as terrestrial samples (e.g., [3]). However, spatial resolution is not usually enough in the previous studies,

X-ray CT system using SR (synchrotron radiation) has been developed in material sciences [4]. High flux densities of X-ray beams give high S/N ratios of CT images. As monochromatic beams are easily obtained, beam-hardening artifacts are avoided and quantitative evaluation of CT values, which correspond to X-ray LAC (linear attenuation coefficient) of objects in CT images, is possible. In addition, highly collimated SR beams easily give 3D images with high spatial resolution. An X-ray microtomography system had been developed at Spring-8 of SR facility in Japan [5] and applied to geological samples including meteorites [6, 7]. The size of voxel, which is an imaging element in 3D images (c.f. pixel in 2D images), is 5.83 μm x 5.83 μm x 5.83 μm. This gives the spatial resolution of about 13 μm for samples with the diameters of <5 mm [5]. This resolution is sufficient for studying 3D structures of many samples. However, the resolution is still insufficient for some samples, especially meteorites having fine materials, such as chondrites and micrometeorites. Accordingly, we developed a new X-ray microtomography system with higher spatial resolution [8] and applied this system to mineral grains in chondrites and Antarctic micrometeorites (AMMs).

X-ray microtomography system in Spring-8: The new system consists of a double crystal monochrometer, a precise rotation stage for a sample and an X-ray detector. We used the beam lines, BL47XU, where monochromatic beams of 6-54 keV are available. Transmitted X-rays through a sample are converted to visual lights by a thin fluorescent screen of Ce-doped Lu_2SiO_5 single crystal. The visual lights are magnified by a rely-lens and imaged by a CCD camera with 1000 x 1018 pixels. Successive cross-sectional CT images (up to 1000x1000 pixels) are reconstructed by a convolution back projection method from transmitted images. The voxel size is 0.5 μm x 0.5 μm x 0.5 μm and this gives the spatial resolution of 1-1.5 μm [8]. For obtaining this spatial resolution, an air-bearing rotation stage is used to minimize a drift by rotation. The maximum sample diameter is about 0.4 mm. It takes about 1 to 6 hours for acquisition of transmitted images and a few to 24 hours for reconstruction of CT images.

In the X-ray CT systems using monochromatic beams, the CT value should equal to LAC. However, we found the relation that $CTvalue = \gamma \times LAC$ (γ=0.9) irrespective of the photon energy in the previous CT system. The factor γ may be due to power relation between X-ray intensities and X-ray counts in the X-ray detector. To obtain a value of γ in the new CT system cylindrical samples of different standard materials (Al. Ti and Fe) were imaged. Preliminary results show that the γ value is 0.9-0.95 at 10-25 keV. In the new CT system, however, this relation is disturbed in the periphery parts of samples (<10-100 μm depending on the material and photon energy) due to refraction of X-ray beams by the samples.

Applications: We have started to apply this system with co-investigators to mineral grains in carbonaceous chondrites (with Dr. M. Zolensky) and AMMs (with Drs. H. Yano and T. Noguchi). Two

mineral grains removed from the Orgueil meteorite (CI) were imaged at 8 and 10 keV to search aqueous inclusions reported by [9]. A mineral flake (100 μm x 100 μm x 25 μm) of probably calcite has small objects of a few μm with low LACs, which may be aqueous inclusions although we have not examined the sample yet.

Four AMMs of about 100 μm collected by JARE in 1998 [10] were imaged at 10 keV. One sample (Y98M03KS074) seems to contain coarse-grained crystals according to the SEM micrograph in the AMM catalog [11]. These "coarse-grained crystals" are imaged as grains of about 10 μm in size with rims (Fig.1a). These rims have bright contrast, which correspond to high LAC values. Grains with brighter contrasts (metal or iron sulfide) are also recognized. The other three samples (Y98M03KS036,

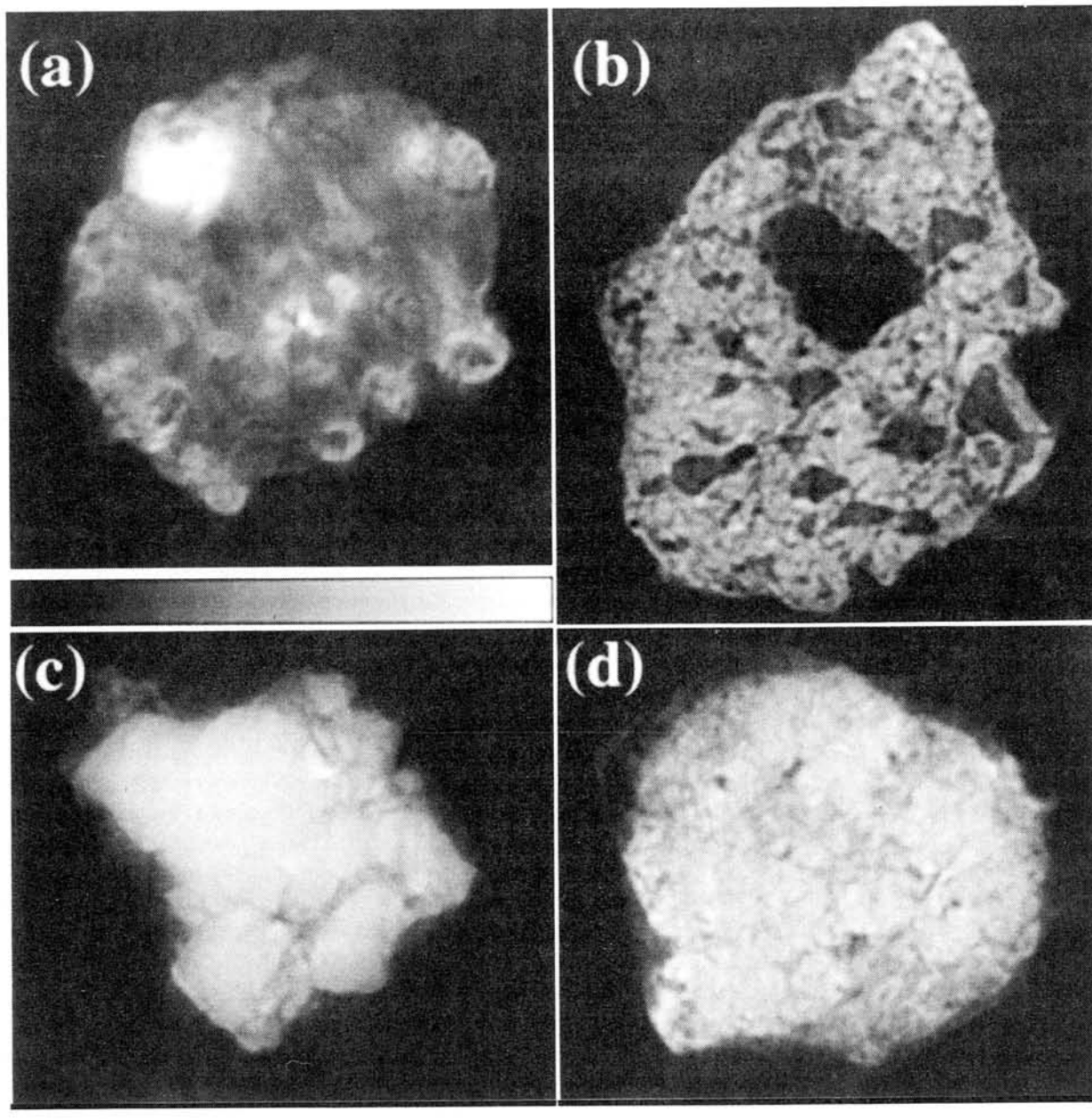

Figure 1. CT images of Antarctic micrometeorites (AMMs). (a) Y98M03KS074. (b) Y98M03KS036. (c) Y98M03KS068. (d) Y98M03KS094. The width of each image is 115 μm. Objects with bright contrasts have high LAC values. Slightly dark materials surrounding the micrometeorite grains are glycol phthalate for sticking the samples to glass rods.

Y98M03KS068 and Y98M03KS094) are vesiclated-scoriaceous ones according to the AMM catalog. In deed, one sample (Y98M03KS068) has many vesicles (Fig.1b), while the other two are not so vesiculated (Figs.1c and d). Some grains with different contrasts are also seen in the three samples. 3D images of these samples are shown in Fig.2. We are planning to examine these samples in more detail by SEM and TEM after cutting.

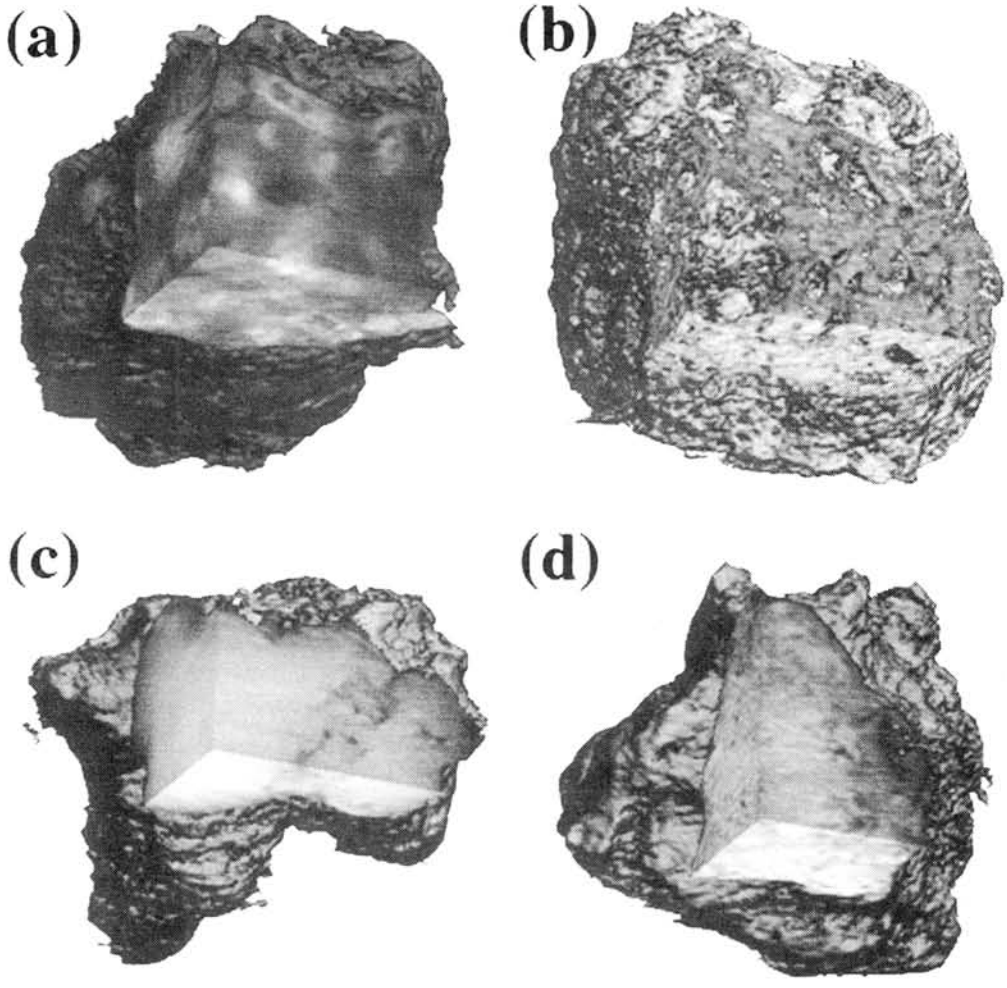

Figure 2. Three-dimensional images of the AMMs. (a) Y98M03KS074. (b) Y98M03KS036. (c) Y98M03KS068. (d) Y98M03KS094.

Acknowledgements: All the AMM samples presented here were collected by the 39th Japan Antarctic Research Expedition team in 1998 and kindly supplied by the National Institute of Polar Research through the open research proposal scheme for the Yamato 98 AMM sample allocation (PI: H. Yano, ISAS and Co-I: AT). We are also grateful to Drs. H. Yano and T. Noguchi for preparing the AMM samples and Dr. M. Zolensky for preparing the Orgueil samples.

References: [1] Arnold J. R. et al. (1982) *Science, 219,* 383-384. [2] Kondo M. et al. (1997) *Antarc. Meteor. Res., 10,* 437-447. [3] Denison C. et al. (1997) *J. Met. Geo., 15,* 29-44. [4] Bonse U. (1991) *J. Mater. Sci., 26,* 4076-4085. [5] Uesugi K. et al. (1999) *Proc. SPIE, 3772,* 214-221. [6] Kawabata et al. (1999) *Antarctic Meteor.* **XXIV**, 64-66. [7] Tsuchiyama A. et al. (2000) *LPS,* **XXXI**, 1566. [8] Uesugi K. et al. (2001) *Proc. Nucl. Instr. Methods. Ser.A, in press.* [9] Zolensky M. et al. (2000) *Antarctic Meteor.* **XXV**, 193-195. [10] Yada T. and Kojima H. (1999) *Antarctic Meteor.* **XXIV**, 190-191. [11] http://dust.cc.gakushuin.ac.jp/dust/

A correlation between erupted lava composition and degree of subsequent thermal metamorphism for HED-meteoritic basalts

Paul H. Warren and Gregory W. Kallemeyn
Institute of Geophysics, University of California, Los Angeles, CA 90095-1567, USA
(pwarren@ucla.edu, gregk@ucla.edu)

The heat source(s) for primordial asteroids has been much debated. Recently, fossil ^{26}Al was for the first time reported in a meteoritic basalt, the eucrite Piplia Kalan [*1*]. However, an earlier study of three eucrites found initial $^{26}Al/^{27}Al$ upper limits only 0.07-0.35 times as great as the initial $^{26}Al/^{27}Al$ reported for Piplia Kalan [*2*]. Eucrites are by far the largest group of basaltic meteorites, and the overwhelming majority of them have been thermally metamorphosed, with pyroxene compositions equilibrated at roughly 800-900°C [*3*]. In most cases, the basic texture (typically subophitic) survived metamorphism remarkably unscathed, and from these textures, cooling rates of 0.01-100°C/hour have been inferred [*4*]. At least initially, these rocks were emplaced as lavas or very shallow intrusives. Proposed mechanisms for thermal metamorphism include impact heating [*3,5*], burial metamorphism [*6*], and baking by rapidly sequential second lava flows [*3,7*].

Eucrite Bluewing 001 was found by Paul Gessler on 14 June 2000 as a single stone of 6.1 g, in Pershing County, Nevada. A 0.46 g sawn end piece was used to produce a 9×9 mm thin section, and a 0.174 g fragment was powdered for bulk analysis by INAA and fused bead electron-probe analysis. The texture is subophitic and fine-grained. Pyroxene lengths are up to 2 mm, but mostly under 1 mm. Plagioclase tends to be smaller by a factor of about one-half. The pyroxenes are extremely unequilibrated, with zoning as extensive as any yet discovered among HED meteorites (Figs. 1 and 2). Plagioclase is zoned from An_{89} to An_{75}, and averages An_{82}. Other phases include minor silica and ilmenite (MgO <0.2 wt%), and traces of apatite, fayalite (Fa_{97-99}), K-feldspar, felsic glass, merrillite, troilite, zircon, baddeleyite, Cr-spinel, and Fe-metal. Previous descriptions of fayalite among HED meteorites have been limited to scattered matrix grains [*8*] or tiny, poorly sampled clasts [*9*] within polymict breccias. In Bluewing 001, we can see that fayalite typically mantles ilmenite, or else occurs in symplectic intergrowths with various late-stage phases. The Fe-metal is almost pure iron. Five quantitatively analyzed grains have ~0.2 wt% Co and Ni below our electron microprobe detection limit of ~0.12 wt%. The absence of detectable Ni confirms that Bluewing 001 did not form as an impact melt. The meteorite is mildly weathered, with a trace of carbonate and some alteration of troilite, but its metals and phosphates appear unaltered. Apatites have 2-4 wt% F and <0.2-2 wt% chlorine. Concentrations of light rare-earth elements (LREE) are lower in the most chlorine-rich apatite (<1000 × CI chondrites) than in chlorine-poor grains (~4000 × CI). In the single merrillite analyzed, LREE are at ~50,000 × CI. For comparison, in a survey of eucrite phosphates, Delaney [*10*] found LREE levels of typically 500-1000 × CI for F-apatite, and 20,000-30,000 × CI for merrillite.

The nearest precedent among eucrites is the main lithology of the polymict eucrite Pasamonte [*4*]. Two additional unequilibrated samples have been found as HED breccia clasts: clast CF4 in the Kapoeta howardite [*11,12*] and a suite of clasts in the Y-75011 polymict eucrite [*3,13,14*]. In the metamorphic scale developed for eucrites by Takeda and Graham [*3*], Bluewing and Kapoeta-CF4 join the Y-75011 clast as only the second and third members of type 1. Results for diagnostic ratios such as Fe/Mn and Ga/Al (by weight, 35 and 0.04, respectively), confirm Bluewing's eucrite affinity. However, the rock is unusually enriched in incompatible elements such as Sm (3.7 μg/g) and Ti (6.0 mg/g). The collective data set for HED basalts manifests a remarkable correlation between degree of thermal metamorphism and incompatible-element composition.

The Kapoeta-CF4 and Y-75011 clast samples are small, and representativeness of the analyses is a concern. However, both are fine grained, and Smith [*12*] analyzed two separate pieces of Kapoeta-CF4 and obtained very similar results. The Y-75011 clast (2.8 cm across) has also been analyzed twice for REE, with very similar results [*5,14*]. In the case of Bluewing, mild weathering is also a concern. However, Ti compositional variations within the zoned pyroxenes confirm that Bluewing and Kapoeta-CF4 are truly products of incompatible-enriched melts.

Despite its high incompatible element contents, Bluewing 001 has a bulk *mg* of 40 mol%, slightly higher than average for noncumulate eucrites. Bluewing thus extends the "Stannern Trend" — the trend among the most incompatible-enriched eucrites to feature moderate-high *mg* ratio [*4*]. Bulk *mg* for the Y-75011 clast has not been directly measured, but is presumably also moderate-high, based on similarity between early pyroxene compositions for this clast [*13*] vs. both Kapoeta-CF4 and Bluewing (Fig. 1). Clearly, the metamorphism of eucrite lavas was far from random. The six samples that

exemplify the Stannern Trend (high incompatible element contents, high *mg* ratio) are metamorphic types 1-4. In contrast, all of the eucrites of undistinguished "Main Group" composition except Pasamonte are thoroughly equilibrated. It is tempting to invoke more than one parent asteroid. However, Kapoeta-CF4 is a clast in a patently HED polymict breccia. Nor does the composition-metamorphism correlation plausibly reflect depletion of incompatible elements during metamorphism, because ion microprobe data indicate that REE are not redistributed even within eucrite hand specimens, except in extraordinarily metamorphosed types such as EET90020 and Ibitira [*15*].

The composition-metamorphism correlation places important constraints on hypotheses for the thermal and magmatic evolution of HED asteroid. The burial hypothesis for eucrite metamorphism [*6*] postulates that the HED crust grew in a piecemeal way, by eruption of magmas formed by limited partial melting of the mantle. Gradual melting of the mantle would inevitably deplete its incompatible elements, so incompatible-enriched materials (the Stannern Trend, including Bluewing) would tend to be among the first lavas to erupt. If so, they should be among the most deeply buried and thus intensely metamorphosed, rather than extraordinarily unmetamorphosed. Impact heating [*3,5*] is not favored, because it would generally be scattered in both space and time, not compositionally and temporally systematic. The temporal aspect is mentioned because survival of fossil ^{26}Al in Piplia Kalan [*1*] suggests that this typically equilibrated eucrite has remained below ~700°C [*16*] since 4.55 Ga. Extinct ^{53}Mn ($t_{1/2}$ = 3.7 Ma) has also been found in several equilibrated eucrites, including the intensely metamorphosed Ibitira [*17*]. Conceivably, the Stannern Trend eucrites avoided major thermal metamorphism because they alone formed after the putative heat-generating impact(s) at ~4.55 Ga. However, the age of the Stannern Trend Y-75011 clast, by various interpretations of Rb-Sr and Sm-Nd data, is ~4.55 Ga [*5*]. The flow-to-flow baking model [*3,7*] has the advantage, vis-à-vis the fossil ^{26}Al and ^{53}Mn evidence, of implying metamorphism soon after extrusion of the lavas.

The earliest flows were presumably more prone to flow-to-flow baking (as well as burial) as the heat source presumably decayed during the epoch of eucrite magmatism. Thus, any relatively simple scenario implies that the unequilibrated, incompatible-rich Stannern Trend eucrites formed later than the equilibrated, compositionally undistinguished Main Group. We infer that Stannern Trend eucrites like Bluewing 001 may represent the complex final dregs of magmatism on the HED parent asteroid. Lunar KREEP basalts similarly feature an enigmatic combination of moderate-high *mg* with high incompatible concentrations, inferred to reflect mixing between primitive magmas uprising from the deep mantle and the urKREEP magma ocean residuum layer [*18*]. An analogous tendency toward mixing may have characterized the final stage of volcanism on the HED asteroid. In any event, the apparent correlation between composition and metamorphism represents a first-order constraint on the evolution of this asteroid.

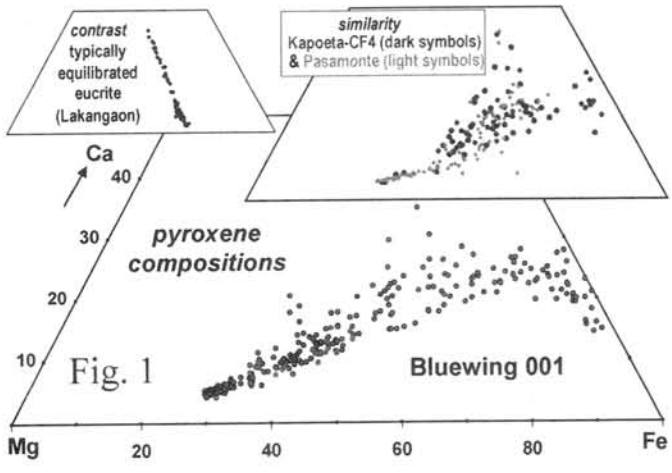

Fig. 1

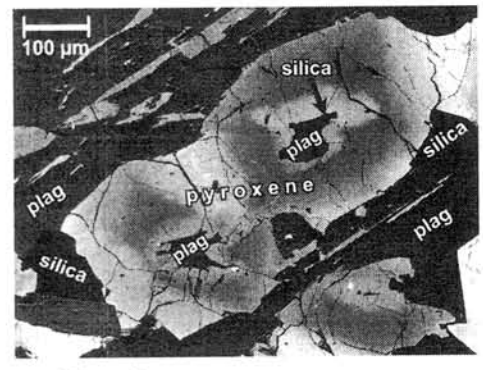

Fig. 2.
Backscattered electron image of complexly zoned pyroxene in Bluewing 001.

References [1] G. Srinivasan et al. (1999) *Science* **284**, 1348. [2] D. N. Schramm et al. (1970) *EPSL* **10**, 44. [3] H. Takeda & A. L. Graham (1991) *Meteoritics* **26**, 129. [4] BVSP (1981) *Basaltic Volcanism on the Terrestrial Planets*. [5] L. E. Nyquist et al. (1986) *JGR* **91**, 8137. [6] A. Yamaguchi et al. (1997) *JGR* **102**, 13381. [7] P. H. Warren (1997) *M&PS* **32**, 945. [8] J. S. Delaney et al. (1984) *PLPSC* **15**, C251. [9] A. H. Treiman & M. J. Drake (1985) *PLPSC* **15**, C619. [10] J. S. Delaney (1984) *LPS* **XV**, 208. [11] P. H. Warren & G. J. Taylor (1982) *Meteoritics* **17**, 293. [12] M. R. Smith (1982) Ph.D. Thesis, Oregon State Univ., Corvallis. [13] H. Takeda et al. (1994) *EPSL* **122**, 183. [14] H. Shimizu & A. Masuda (1986) *GCA* **50**, 2453. [15] C. Floss & G. Crozaz (1998) *M&PS* **32**, A41. [16] T. LaTourrette & G. J. Wasserburg (1998) *EPSL* **158**, 91. [17] G. W. Lugmair & A. Shukolyukov (1998) *GCA* **62**, 2863. [18] C. K. Shearer & J. J. Papike (1999) *Am. Mineral.* **84**, 1469-1494.

DISCOVERY OF THE HIGH-PRESSURE POLYMORPH OF WHITLOCKITE IN THE SHOCK MELT VEINS OF THE SUIZHOU METEORITE

Xiande XIE[1], M. E. MINITTI[2], Ming CHEN[1], Ho-kwang MAO[2], Deqiang WANG[1], Jinfu SHU[2] and Yingwei FEI[2]

[1]Guangzhou Institute of Geochemistry, Chinese Academy of Sciences, Guangzhou 510640, China
[2]Geophysical Laboratory, Carnegie Institution of Washington, Washington, DC 20015, USA

Introduction: The Suizhou meteorite, classified as an L6 chondrite, contains olivine, low-Ca pyroxene, plagioclase, Fe-Ni metal, troilite, whitlockite, chromite and ilmenite. Thin (0.02-0.09 mm) shock melt veins cut Suizhou and high-pressure phases, including coarse-grained $NaAlSi_3O_8$-hollandite, ringwoodite, majorite, and fine-grained liquidus majorite-pyrope$_{ss}$ are found within the veins.(Fig.1)[1-3]. The presence of these phases constrains the pressure and temperature experienced in the veins up to 23 GPa and 1900 °C - 2000 °C [3]. Also found within the shock veins is a previously unreported phosphate phase that shows the composition of whitlockite, but gives Raman spectrum distinctly different from that of whitlockite. The coexistence of this phosphate phase with several high-pressure phases in the shock veins suggests that the phosphate could be the high-pressure polymorph of $Ca_3(PO_4)_2$ discovered by [4] in laboratory experiments. The goal of this study is to determine the nature of the phosphate phase within the Suizhou shock melt veins and investigate possible links between the laboratory-produced high-pressure $Ca_3(PO_4)_2$ polymorph and the phosphate phase within the Suizhou shock melt veins. To accomplish this goal, we synthesized a high-pressure $Ca_3(PO_4)_2$ phase and obtained its Raman spectrum for comparison to the Raman spectra of the phosphate phases found both outside and inside the shock melt veins within Suizhou, and obtained the powder X-ray diffraction pattern of the synthesized high-pressure phase for comparison to that of whitlockite.

Analytical and experimental: Images of the Suizhou shock veins were obtained in the back-scattered electron mode of a Hitachi S-3500N scanning electron microscope at the Guangzhou Institute of Geochemistry. The chemical compositions of the phosphate phases inside and outside the Suizhou shock melt veins were also determined using a Cameca SX-51 electron microprobe at the Beijing Institute of Geology. Analytical conditions included a 15kV accelerating voltage and a 20 nA beam current. Raman spectroscopic analyses were conducted on the phosphate phases both inside and outside the Suizhou shock veins using a Renishaw RM-1000 laser Raman microscope at the Beijing Institute of Non-ferrous Metals.

The starting material for the high-pressure phase synthesis was $Ca_3(PO_4)_2$ powder stored in a drying oven at 100 °C prior to the experiment. To achieve pressure and temperature necessary to create the high-pressure $Ca_3(PO_4)_2$ polymorph, a multi-anvil apparatus was utilized following the method of [5]. The sample was housed in a 10/5 assembly containing a Re heater and a W_5Re-$W_{26}Re$ thermocouple was used to monitor sample temperature. The sample was first brought up to the final pressure of 14 GPa and then brought up to the final temperature of 1400 °C. The choice of the experimental pressure and temperature was guided by the findings of [4]. The sample was held for 24 hours at 14 GPa and 1400 °C, was quenched by shutting off the power to the heater and was then decompressed. For analysis of the experimentally produced high-pressure $Ca_3(PO_4)_2$ polymorph, the charge containing the experimental product was partially

ground away to reveal sample. Laser Raman spectroscopy and powder X-ray diffraction (XRD) analysis were conducted on the synthesized $Ca_3(PO_4)_2$ phase using a Raman spectrometer and an X-ray diffraction device at the Geophysical Laboratory.

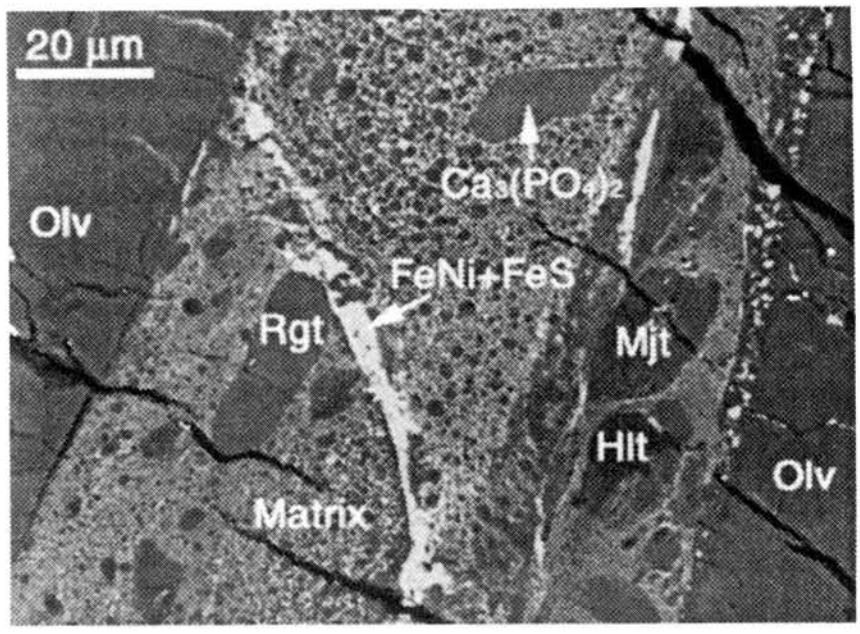

Figure 1 Back-scattered electron image of a shock melt vein in the Suizhou Meteorite. $Ca_3(PO_4)_2$ – high-pressure phase of whitlockite, Rgt – ringwoodite, Mjt – majorite, Hlt – hollandite, Olv – olivine.

Results and Discussion: The Raman spectra of the phosphate phases inside and outside the Suizhou shock veins reveal the shock-induced structural transformation of the phosphate. The transformation that occurred in the Suizhou shock veins was not simply caused by the disturbance of the phosphate crystal structure by shock as indicated by results of [6]. Comparison of the Raman spectra of shocked whitlockite measured by [6] and the spectrum of the Suizhou high-pressure phosphate phase reveals that distinct differences exist between the structures of these two phases. The differences in the Raman spectra of the shocked whitlockite and the high-pressure $Ca_3(PO_4)_2$ phase indicate that the degree of shock experienced in the Suizhou shock veins was sufficient to induce a fundamental structural change of the whitlockite. Comparison of the Raman spectra of the high-pressure $Ca_3(PO_4)_2$ phase in Suizhou and the synthesized high-pressure $Ca_3(PO_4)_2$ phase reveals excellent agreement between the two spectra and confirm the distinct structural character of the $Ca_3(PO_4)_2$ phase in the Suizhou shock veins. The XRD analysis of the synthesized high-pressure phase provides further evidence of such structure change. The electron microprobe analyses reveal little difference between chemical composition of the phosphate inside and outside the shock vein. This result indicates that the conversion of whitlockite to the high-pressure $Ca_3(PO_4)_2$ phase in Suizhou occurs without reaction of the whitlockite with surrounding phases and without decomposition of the whitlockite. Overall, the results imply that transient shock conditions within the Suizhou veins achieved

pressures and temperatures capable of forming the high-pressure phase synthesized in the laboratory. Because the high-pressure $Ca_3(PO_4)_2$ polymorph forms in laboratory experiments at 12-13 GPa at 1300 °C [2], its presence in the shock veins is consistent with the pressures and temperatures indicated by the presence of the other high-pressure phases in the shock veins. Thus, the Suizhou meteorites likely provides first naturally occurring example of the high-pressure $Ca_3(PO_4)_2$ polymorph.

The discovery of the high-pressure $Ca_3(PO_4)_2$ phase in natural samples is of important significance in understanding the mineralogy and geochemistry of the Earth's mantle. The mineral whitlockite has calcium sites with large coordination number and incorporates a large number of very large lithophile elements (VLLE), such as Sr and Ba, and rare earth elements (REE) in comparison with other rock-forming minerals [4, 7]. The behavior of whitlockite at high pressure and temperature (*P-T*) conditions has been of interest just because this mineral can accommodate VLLE and REE. It is known that the continental and oceanic crust can be subducted into Earth's upper and low mantle [8]. The phosphate mineral in the form of its high-pressure polymorph, being stable under relevant *P-T* conditions, would therefore acts as potential carrier of VLLE and REE from the Earth's surface down into the deep mantle during the subduction process.

Acknowledgements: This work was supported by the National Natural Science Foundation of China under grants 49672098 and 49825106. The authors are grateful to Professor Li Zhaohui for providing the Suizhou sample.

References: [1] Xie X., Chen M., El Goresy A. and Gillet P. (2000) *Antarctic Meteorites* **XXV**, 181-183. [2] Xie X., Chen M., and Wang D. (2000) *Antarctic Meteorites* **XXV**, 178-180. [3] Xie X., Chen M., Wang D. and El Goresy A. (2000) *Chinese Science Bulletin* **46** (6), 506-510. [4] Murayama J.K., Kato M., Nakai S., and Kumazawa M.(1986) *Phys. Earth Planet. Inter.* **44**, 293-303. [5] Bertka C.M. and Fei Y. (1997) *JGR* **102**, B3, 5251-5264. [6] Chen M., Wopenka B., Xie X. and El Goresy A. (1995) *LPSC* **XXVI**, 237-238. [7] Sugiyama S. and Tokonami M. (1987) *Phys. Chem. Miner.* **15**, 125-130. [8] Van der Hilst R. (1995) *Nature* **374,** 30-32.

Terrestrial accretion rates of micrometeorites in the last glacial period.

Toru Yada[1], Tomoki Nakamura[1], Nobuo Takaoka[1], Takaaki Noguchi[2], Kentaro Terada[3], Hajime Yano[4], and Hideyasu Kojima[5]

[1] Dept. Earth & Planet. Sci., Grad. School Sci., Kyushu University, Hakozaki Fukuoka 812-8581, Japan, [2] Dept. of Materials and Biological Science, Ibaraki University, Bunkyo 2-1-1, Mito, Ibaraki, 310-8512, Japan, [3] Dept. of Earth & Planetary Sciences, Hiroshima University, Higashi-Hiroshima, Hiroshima, 739-8526, Japan,[4] Planet. Sci. Div., The Institute of Space and Astronautical Science, 3-1-1 Yoshinodai, Sagamihara, Kanagawa, 229-8510, Japan, [5] National Institute of Polar Research, 1-9-10 Kaga, Itabashi, Tokyo, 173-8515, Japan.

Introduction Nowadays, about 40 thousand tons of micrometeoroids accrete on the Earth in a year [1]. They are supplied from their parent bodies intermittently by impact event between asteroids or comet spray due to ice sublimation, etc. On the contrary, they have been lost continuously by gradual descendent to the Sun due to the Poynting-Robertson effect and radial ejection outward the solar system from the Sun due to solar irradiation pressure. The abundance of micrometeoroids, therefore, should have been changing from the periods to the periods. The accretion rate of micrometeorites (MM) on the Earth reflects the change of the abundance of micrometeoroids. We have estimated the accretion rates of MMs in the last glacial periods from the concentration of Antarctic micrometeorites (AMMs) in glacier ice [2]. Here we report noble gas analyses for residues after handpicking in order to correct the accretion rates.

Samples and Methods The samples used in this study were collected from the bare ice around Yamato Mts. in Antarctica [3]. Among 24 collection points, five points (M03, K02, K11, J09 and J10) were selected for estimation of the accretion rates. Though the result of handpicking work for accretion rates has been reported before [2], the number of AMMs has revised and data of other collection points have added, as shown in Table 1. After handpicking, 20% to 70% portion of the residue particles were used to measure isotopic composition of He, Ne and Ar with a MM5400 mass spectrometer equipped with a Ta furnace and a stainless purification line at Kyushu University. Samples were wrapped in thin Al foil and heated in a sample holder at 110°C for a night to degas adsorbed atmospheric gases. They are heated in the Ta

furnace with 1700°C for 20 minutes to extract their included gas except for sample K02, which was heated stepwise at 700 and 1700°C. Details for noble gas measurements and data analysis are given in [4].

Results and Discussion The results of noble gas analyses of handpicked residues of 100~238μm fraction are summarized in Table 2. Isotopic compositions for He and Ne are nearly identical with those for solar energetic particles. This indicates that the residues contain extraterrestrial dust and atmospheric contamination is negligible for He and Ne. Ar isotopic ratios are approximately atmospheric, indicating that Ar is contaminated by air. With the assumption that all Ne in the samples is a mixture of solar and cosmogenic components, we calculated concentrations of solar ^{20}Ne. The content of solar ^{20}Ne in a single grain of AMM has been determined to be 4.1×10^{-6} ccSTP/g [5]. With this and Ne content determined in this work, the weights of AMMs left in the residues are estimated as found in Table 2. Adding these AMMs weight in the residues, the accretion rates displayed in Table 1 are revised as 10400 ton/a for M03, 8500 ton/a for K02, 5600 ton/a for K11, 2800 ton/a for J09 and 7500 ton/a for J10. With data for residue of 40~100μm fraction, we will finally conclude accretion rates of each collection point.

Reference: [1] Love and Brownlee (1993), Science, 262, 550-553. [2] Yada and Kojima (2000), Antarct. Meteorite Res., 13, 9-18. [3] Yada et al. (2000), Meteoritics Planet. Sci., 35, A173. [4] Nakamura et al. (2000), Antarct. Meteorite Res., 13, 311-321. [5] Osawa et al. (2000), Antarct. Meteorite Res., 13, 322-341.

Table 1. Handpicked AMMs from each collection point.

Sampling Point	M03	K02	K11	J09	J10	Total
Total AMMs	168	305	265	138	160	1036
unmelted AMMs	98	152	173	81	87	591
spherules	70	153	92	57	73	445
S-type spherules	21	44	45	33	40	183
G-type spherules	30	49	35	17	22	153
I-type spherules	19	10	12	7	11	59
Melted Ice (ton)	0.94	0.92	1.93	1.15	1.04	
Total AMMs (g)	2.58E-04	2.83E-04	3.77E-04	1.45E-04	2.82E-04	
Accretion rate (ton/a)	6100	6800	4300	2700	6000	

Table 2. He, Ne and Ar isotopic ratio of residue of handpicked Y98 samples.

	4He (ccSTP)	3He/4He	20Ne (ccSTP)	20Ne/22Ne	21Ne/22Ne	36Ar (ccSTP)	38Ar/36Ar	40Ar/36Ar	4He/20Ne	20Ne/40Ar	Solar 20Ne (ccSTP)	AMMs in residue (g)
M03,100~238um	1.234E-08	0.000242	2.40E-10	11.60	0.0339	8.08E-11	0.189	232.4	51.38	1.28E-02	2.40E-10	1.83E-04
	5.963E-11	0.000011	4.64E-12	0.39	0.0020	5.74E-13	0.003	1.5	1.02	2.76E-04		
K02,100~238um (700deg)	1.860E-09	0.000103	1.33E-11	11.19	0.0338	2.32E-11	0.180	306.6	140.34	1.86E-03	1.32E-11	6.98E-05
	1.303E-11	0.000057	1.23E-13	0.53	0.0110	3.24E-13	0.006	4.2	1.64	4.01E-05		
K02,100~238um (1700deg)	2.353E-09	0.000265	1.99E-10	12.07	0.0317	8.56E-11	0.186	188.9	11.85	1.23E-02	1.98E-10	
	1.344E-11	0.000042	1.33E-12	0.18	0.0018	7.43E-13	0.003	1.6	0.10	1.69E-04		
K11,100~238um	4.391E-09	0.000139	1.56E-10	11.34	0.0402	7.98E-11	0.197	302.4	28.23	6.45E-03	1.55E-10	1.09E-04
	3.093E-11	0.000016	8.53E-13	0.15	0.0023	2.59E-12	0.006	9.3	0.25	2.90E-04		
J09, 100~238um	8.375E-11	0.000478	2.83E-12	11.38	0.0285	4.70E-11	0.196	300.7	29.56	2.00E-04	2.83E-12	2.27E-06
	1.152E-12	0.000096	1.21E-13	1.55	0.0318	6.06E-13	0.005	3.9	1.33	9.32E-06		
J10,100~238um	1.058E-08	0.000453	8.33E-11	6.97	0.3892	2.89E-11	0.210	208.3	127.02	1.38E-02	6.75E-11	6.84E-05
	6.961E-11	0.000023	4.25E-13	0.08	0.0169	9.08E-13	0.005	1.8	1.06	4.56E-04		
Air		1.37E-06		9.78	0.0292		0.188	296.0		1.77E-02		
Solar Wind		0.000457		13.8	0.0328		0.182 -					
Solar Energetic Particle		0.000217		11.2	0.0295		0.205 -					

* Small numbers under each value are 1 sigma error.

Chemical analysis of Antarctic micrometeorites by an electron microprobe: Comparison with matrices of carbonaceous chondrites and interplanetary dust particles.

Toru Yada[1], Tomoki Nakamura[1], Nobuo Takaoka[1], Takehiko Setoyanagi[2], Takaaki Noguchi[3],and Hideyasu Kojima[4]

[1] Dept. Earth & Planet. Sci., Grad. School Sci., Kyushu University, Hakozaki Fukuoka 812-8581, Japan, [2] Grad. School Sci., Tokyo metropolitan Univ., Hachioji, Tokyo 192-0397, Japan. [3] Dept. of Materials and Biological Science, Ibaraki University, Bunkyo 2-1-1, Mito, Ibaraki, 310-8512, Japan, [4] National Institute of Polar Research, 1-9-10 Kaga, Itabashi, Tokyo, 173-8515, Japan.

Introduction

It has become clear recently that cosmic dust collected on the Earth is almost carbonaceous-chondrite-like material. Most of interplanetary dust particles (IDPs), cosmic dust of 10~50μm in size and collected at stratosphere, have chondritic chemical composition and higher content of carbon than carbonaceous (C) chondrite (Keller et al., 1994). Micrometeorite (MM), cosmic dust of 40~300μm in size and collected at polar region, are also reported as chondritic composition enriched in carbonaceous material (Engrand and Maurette, 1998). However, relationship between parent bodies of IDPs, MMs and C chondrite is not clear yet. Here we investigate chemical composition of Antarctic MMs (AMMs) to discuss about their origins.

Samples and Methods

Samples investigated in this study were collected from bare ice around Yamato Mts. in Antarctica (Yada and Kojima, 2000). One of 24 collection points, K02, is selected for this study. Ice age of this point is estimated as 30,000 years BP (Terada et al., 2001). In this point, about 300 of AMMs are handpicked in other study (Yada et al., this volume). About two thirds of them are mounted in epoxy resin and polished to observe their cross sections. Their cross sections are photographed and analyzed qualitatively by scanning electron microscope equipped with energy dispersive spectrometer JSM-5900LV at National Institute of Polar Research (NIPR) and then analyzed quantitatively by electron probe micro analyzer (EPMA) JXA-8800M at NIPR about fourteen elements. For analysis of bulk chemical composition, beam diameter is set to 5μm and three to eight points were analyzed in each AMM particle.

Results and discussion

Classification: From observation of the texture of cross sections of unmelted AMMs and silicate spherules, unmelted AMMs are classified into massive fine-grained, porous fine-grained, scoriaceous, coarse-grained type and spherules into glassy, cryptocrystalline, dendritic magnetite, barred olivine, porphyritic and relict grain type. The proportion of each type of texture is shown in Table 1. Unmelted AMMs are occupied about 90% by fine-grained type.

Difference in age: These AMMs are analyzed their bulk chemical composition by EPMA. Fig. 1 shows Si-Mg-Fe ternary plot of the measured bulk composition of unmelted AMMs of fine-grained type. French AMMs which were collected from ice of about 20,000 years BP and Dome Fuji AMMs which were collected from present snow (1950's) are displayed for comparison. Their distribution overlapped in principle but are a little different from each other, especially Y98K02 is different in lack of Fe-rich particle. This difference could indicate the change of interplanetary dust between 30,000 years BP, 10,000 years BP and present, although there remains a possibility that the difference result from alteration in glacier ice.

Implication for origin: Fig. 2 shows Al/Si to Ca/Si diagram of bulk composition of (a) fine-grained unmelted AMMs, silicate spherule measured in this work and (b) chondritic porous (CP) type and chondritic smooth (CS) type interplanetary dust particles (IDPs) from Schramm et al. (1989). Matrices of C chondrites are situated in the same region of the CS type IDPs (Zolensky et al., 1993). Depletion of Ca from the solar ratio in fine-grained type AMMs indicates that they experienced water alteration in their parent bodies same as matrices of C chondrites and CS type IDPs. On the contrary, more than half of silicate spherules are plotted on the solar ratio like CP type IDPs. This implies the same origin of some part of silicate spherules and CP type IDPs.

Reference: Engrand and Maurette (1998), Meteoritics Planet. Sci., 33, 565. Genge et al. (1997), Geochim. Cosmochim. Acta, 61, 5149. Keller et al. (1994), Analysis of interplanetary dust, ed. by Zolensky et al., p51. Schramm et al. (1989), Meteoritics, 25, 99. Terada et al. (2001), Antarct. Meteorite Res., 14, 89. Yada and Kojima (2000), Antarct. Meteorite Res., 13, 9. Zolensky et al. (1993), Geochim. Cosmochim. Acta, 57, 3123.

Table 1. The proportion of textural type of AMMs.

	Number	percentage
unmelted AMM	101	
massive fine-grainec	40	39.6%
porous fine-grained	32	31.7%
scoriaceous	16	15.8%
coarse-grained	13	12.9%
spherule	66	
glassy	13	19.7%
cryptocrystalline	11	16.7%
dendritic magnetite	5	7.6%
barred olivine	16	24.2%
porphyritic	7	10.6%
relict grain	14	21.2%

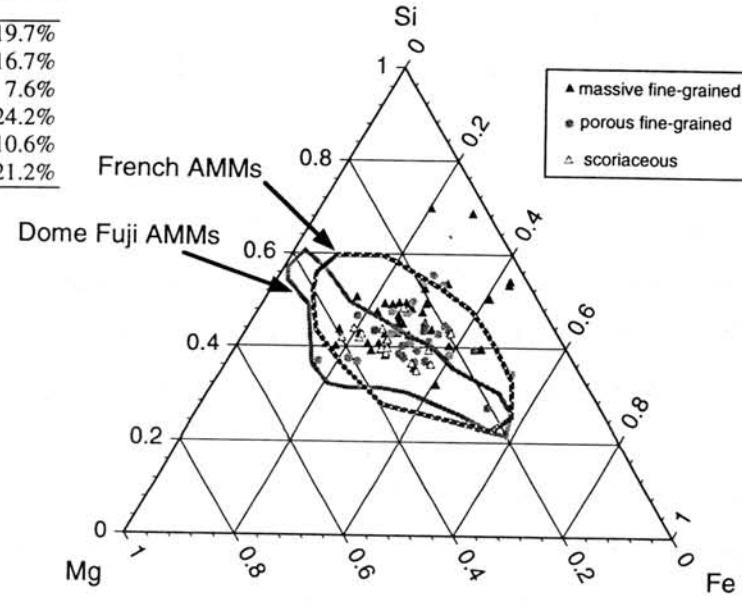

Fig. 1. A Si-Mg-Fe ternary plot of the AMMs of the previous study. French AMMs are after Genge et al. (1997) and Dome Fuji AMMs are Imae (1999, unpubl. data)

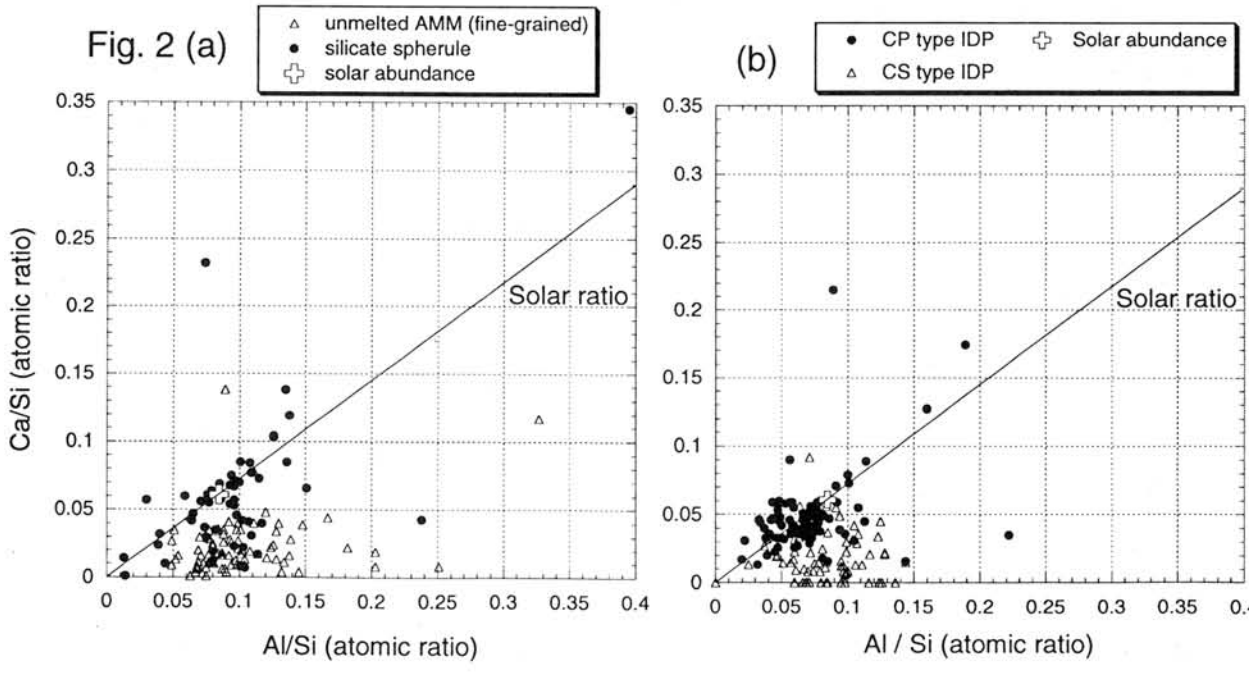

Fig. 2. Al/Si to Ca/Si diagram of bulk composition of (a) unmelted, fine-grained AMMs and silicate spherules and (b) CP and CS type of IDPs. Data of IDPs are from Schramm et al. (1989).

OCCURRENCE AND POSSIBLE ORIGIN OF ZIRCON IN BASALTIC EUCRITES

Akira Yamaguchi and Keiji Misawa
Antarctic Meteorite Research Center, National Institute of Polar Research
1-9-10 Kaga, Itabashi, Tokyo 173-8515 (yamaguch@nipr.ac.jp)

Introduction Zircon and baddeleyite are minor phases in basaltic eucrites. These minerals are extremely useful for determining U-Pb ages [e.g., 1,2]. Almost all basaltic eucrites are metamorphic rocks, and many of them are complicated breccias that experienced several stages of shock and thermal metamorphism. In such breccias, understanding the occurrence and origin of these Zr-bearing phases are very important for the interpretation of the U-Pb ages. We have examined 16 eucrites including basaltic clasts of the different degrees of equilibration from type 1 to type 6 [3], and metamorphosed breccias such as granulitic eucrites. The purposes of this study are to understand the origin of primary and metamorphic zircon and to relate to the U-Pb ages of these zircons that may date early volcanic and metamorphic events of the eucrite parent body, 4Vesta. We examined polished thin and thick sections of these eucrites optically and with a scanning electron microscope (SEM) equipped with both an energy despersive spectrometer (EDS) and a cathodoluminescence (CL) detector and an electron microprobe (EPMA).

Results and Discussion Zircons in unmetamorphosed clasts in Y-75011 and Y-74159 (type 1-2 eucrite, [3]) are typically located in silica-rich mesostasis, and are closely associated with ilmenite (Fig. 1). In most cases, zircon occurs as thin (<5-10 μm) veins and irregular inclusions in ilmenite, and/or thin rim (<5-10 μm) around ilmenite in contact with silica phases (Fig. 1). The fact suggests that they were formed at the final stage of crystallization from melt. Zircon was not found in the other type 1 clast in Y-75011, but it contains a few baddeleyites grains (<40 μm in size) in silica-glass. Bukovanska *et al.* [2] reported the presence of baddeleyites in Pasamonte, which is mostly composed of unequilibrated clasts.

Portions of Padvarninkai (type 5-6) and Y-792510 (type 6) roughly keep original basaltic texture although these eucrites experienced thermal annealing and shock metamorphism. In most cases, zircons occur in mesostasis and are associated with ilmenite (Fig. 2) as those observed in Y-75011 and Y-74159 (see above). The CL images of relatively large (> 20-30 μm) zircons show zoned textures or are composed of several domains (Fig. 2b). Y-86763, which is texturally basaltic but experienced partial melting during metamorphism [4], contains a zircon (~10 μm) between silica-phase and pyroxene.

A-881388 and A-881467 are granulitic eucrites, which almost totally lost original basaltic textures [5]. These eucrites experienced thermal metamorphism after brecciation. Zircon (<20 μm in size) in the granulitic eucrites most commonly occurs with ilmenite, and some of them occur alone in pyroxene grain (Fig. 3). These zircon grains typically shape rounded to subrounded. The CL-images show that these zircons are composed of several domains. Juvinas is a complicated rock, composed of three lithologies, basaltic portion, impact melt portion, and recrystallized clastic matrix [6]. Homogeneous Mg/Fe ratios in pyroxenes in those lithologies indicate that Juvinas is a metamorphosed impact melt breccia. In mesostasis in the basaltic portion, zircons are associated with ilmenite, and form rims or veins (<5-8 μm thick) as in those in type 1-2 eucrites. Most zircons in impact melt portions are also associated with ilmenite, but are not always related with silica-phases, probably. We found an elongated grain of baddeleyite (46 x 9 μm in size) in ilmenite in a granulitic pyroxene.

At the present, we did not find systematic chemical variations in zircons in the eucrites. HfO_2 contents of zircon in Y-75011 vary from 0.95-1.74 wt% in Y-75011 (type 1), but those in Y-792510 (type 6) have narrower range (1.35-1.69 wt%). One zircon in Y-75011 contains TiO_2 about 11.7 wt%. A baddeleyite found in Y75011 contains 1.26-1.63 wt% of HfO_2.

Several basaltic eucrites contain ~50-100 ppm of Zr [7], which corresponds to approximately ~0.002 vol% of zircon. This is consistent with the values estimated from modal abundance of zircons <0.02 vol% in the eucrites we examined. In unequilibrated eucrites and metamorphosed eucrites that kept basaltic textures, zircon is closely associated with ilmenite in silica-rich mesostasis, and often forms rims around ilmenites. The fact indicates that zircon was crystallized with ilmenite or after ilmenite crystallization. Zircon is likely to have been crystallized by the decrease of Zr solubility due to enrichment of SiO_2 [8] at the late stage of crystallization. Zircons in metamorphic breccias appear to be not always related to silica phase and ilmenite. This may be due to mechanical redistribution during metamorphism and brecciation. Floss et al. [4] inferred the redistribution of Zr from Zr-bearing phases during high temperature metamorphism. Zircon grains in metamorphosed eucrites shape subrounded possibly due to annealing. The CL-images of some zircons show complex internal textures in contrast to the simple morphology, indicating the overgrowth and recrystallization. Zircon is known to be chemically stable under a wide range of igneous and metamorphic conditions. Thus, these zircon may not be a entirely secondary product that formed during metamorphism. The presence of unreacted baddeleyites in silica-rich portion in Y-75011 clast is enigmatic. It could have been crystallized as a metastable phase during rapid crystallization from melts. It has been suggested that type 5-6 eucrites and granulitic eucrites experienced thermal metamorphism at ~800-1000 °C for a prolonged time [8,9]. The U-Pb ages of zircons in such eucrites would have been reset by the metamorphism. Comparison of U-Pb ages of zircons between unmetamorphosed and metamorphosed eucrites allows to determine the duration of eucrite metamorphism and volcanism of the eucrite parent body, 4Vesta. The results of U-Pb systematics of eucrite zircons are presented in the companion abstract [10].

References: [1] Ireland T.R. and Wlotzka F. (1992) *EPSL* **109,** 1-10. [2] Bukovanska M. and Ireland T.R. (1993) *Meteoritics* **28,** 333. [3] Takeda H. and Graham A.L. (1991) *Meteoritics* **26,** 129-134. [4] Floss C. et al. (2000) *AMR* **13,** 222-237. [5] Yamaguchi A. et al. (1997) *AMR* **10,** 431-453. [6] Takeda H. and Yamaguchi A. (1991) *Meteoritics* **26,** 400. [7] Warren P.H. and Jerde E. (1987) *GCA* **51,** 713-725. [8] Dickinson J.E. and Hess P.C. (1982) *EPSL* **57,** 336-344. [9] Miyamoto M. et al. (1985) *PLPSC* **15,** C629-C635. [10] Yamaguchi A. et al. (1997) *Icarus* **124,** 97-112. [11] Misawa K. and Yamaguchi A. (2001) *Antarctic Meteorites* **26,** this volume.

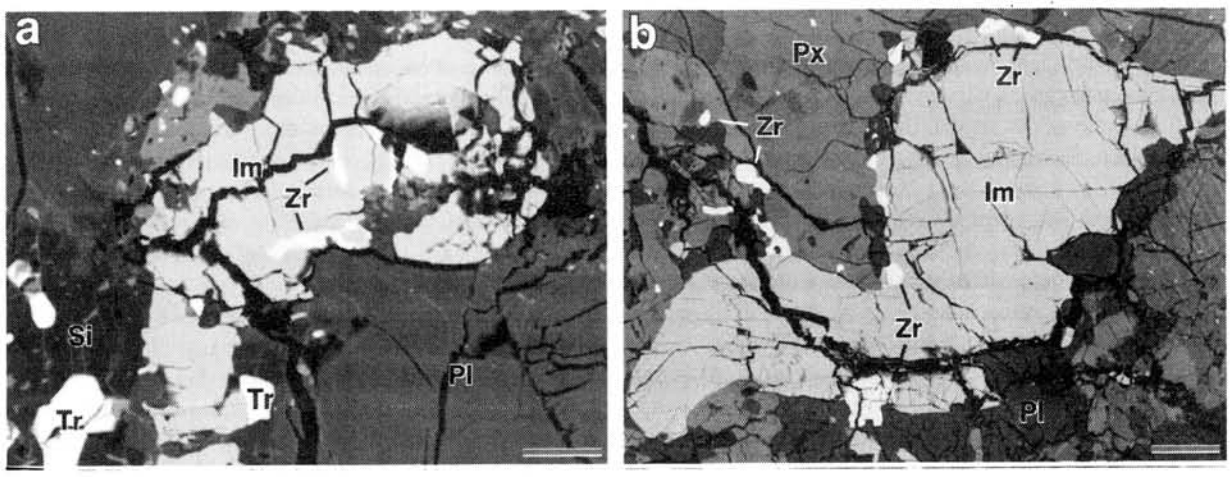

Fig. 1. Backscattered electron (BSE) images of zircons (Zr, white) in (a) Y-74159 (type 1-2) and in (b) Stannern (type 4). Zircons are closely associated with ilmenite, and often form vein and/or rim in ilmenite. Note that zircons in Stannern are subrounded due to thermal annealing. Im: ilmenite; Si: silica minerals; Pl: plagioclase; Px: pyroxene; Tr: troilite. Scale bars = 20 μm.

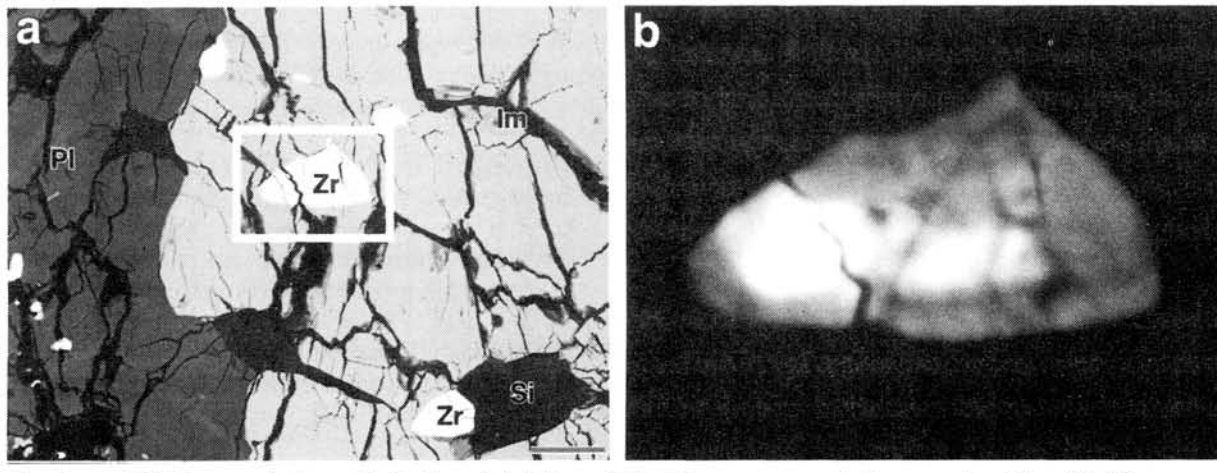

Fig. 2. (a) BSE image of zircons in Padvarninkai (type 5-6). There are several zircon grains (Zr, white) in ilmenite (Im, light grey). Zircon and ilmenite are fractured due to shock metamorphism. Scale bar = 20 μm. Si: silica minerals; Pl: plagioclase. (b) Cathodoluminescence (CL) image of bracketed area in (a), showing a luminescent cores surrounded by a weakly lminescent rim.

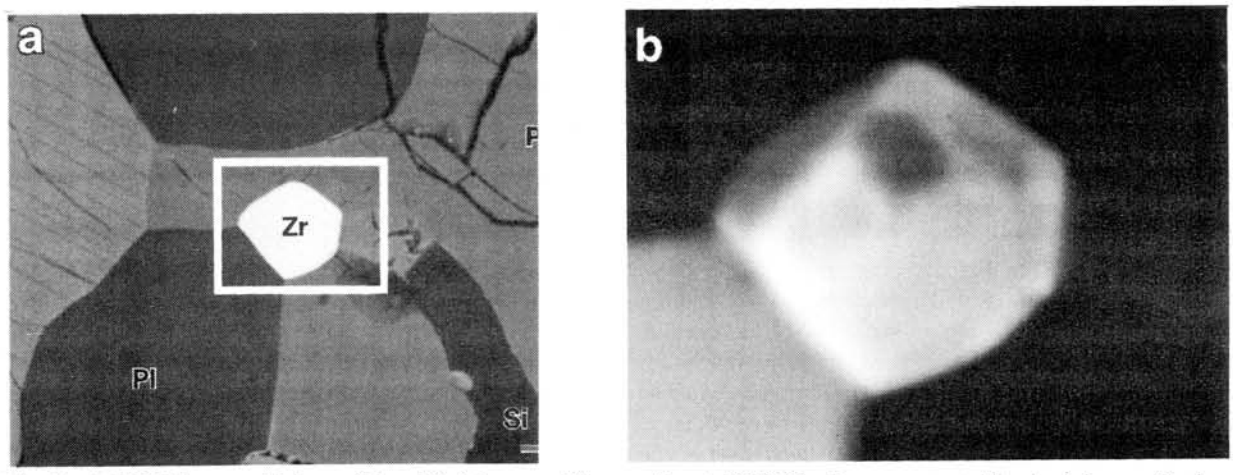

Fig. 3. (a) BSE image of zircon (Zr, white) in granulitic eucrite, A-881388. Px: pyroxene; Pl: plagiolcase. Scale bar = 20 μm. (b) CL image of bracketed portion in (a). Zircon may be composed of several domains.

On the evaporation mechanism of forsterite

Hayate Yamazaki and Akihiko Hashimoto

Hokkaido University, Department of Earth and Planetary Sciences, Sapporo 060, Japan

Forsterite is a most abundant silicate mineral that constitutes planetary bodies. Its evaporation mechanism has been a subject of debate since Hashimoto (1990) and Davis et al. (1990) suggested from their free evaporation and isotope mass fractionation experiments done on polycrystalline forsterite, that it evaporates via $Mg_2SiO_4(s) \rightarrow 2Mg(g) + SiO_2(g) + O_2$ (or 2O)(g). This is in apparent contradiction with the gas constituents in equilibrium with the solid and liquid forsterite: thermodynamics predicts SiO(g) rather than SiO_2(g). The authors suggested that SiO_2(g) generated first on the forsterite surface and then decomposed into stable species like SiO(g) + O(g) after its desorption. This idea explained the two characteristics of forsterite evaporation. In their experiments, the free evaporation of forsterite was about two orders of magnitude retarded compared to the equilibrium evaporation, which can be easily explained if the evaporation took place in the form of less abundant species like SiO_2 (which is about two orders of magnitude smaller than SiO in equilibrium vapor pressure). The magnitudes in isotope mass fractionation in Mg, Si, and O, determined by ion microprobe study on the residual forsterite, were best reproduced by Rayleigh Fractionation Theory involving Mg, SiO_2, and O_2 as gas species.

Nichols et al. (1998) has carried out a free evaporation - mass spectrometric analysis on a solid forsterite, and reported that a SiO(g) signal from the vapor phase was ~100 times more abundant than that of SiO_2(g). They argued from this observation that the actual vapor species emitted from the forsterite surface was SiO(g), in accordance with the thermodynamic prediction. In their experiments several dozens of forsterite grains were placed on a shallow crucible. This is not strictly a free evaporation condition as a portion of the generated vapor from forsterite strikes back on the forsteirte surface and recondense. None the less, their measurement in the evaporation rate of forsterite agreed well with Hashimoto (1990).

In order to resolve this apparent contradiction between the two parties, we have constructed a free evaporation-quadrupole mass spectrometric system in Hokkaido University and have carried out a preliminary experiment on a polycrystalline solid forsterite. The solid forsterite (a disk of 12 mm OD and 1.5 mm thickness: ~20% porosities) was synthesized from a mixture of 5N purity SiO_2 and MgO, sintered at 1700°C in air for 20 hours. A high vacuum chamber equipped with three turbo molecular pump and one oil-free roughing pump, and a quadrupole mass spectrometer (VG Elite-300H) enables its operation at ~10^{-7} Torr at room temperature and ~10^{-6} Torr at 1800°C. In the first experiment, the Q-mass was set in a differential pumping room separated by a five-fold stainless steel collimator (an 8 mm OD hole aligned through each plate) from the evaporation chamber. Although a good vacuum was guaranteed, a disadvantage was the distance from the evaporation source, ~330 mm. The signal

at 24 m/e (obviously from ^{24}Mg) was detected at 1800°C, but the mass range including 44 (SiO) and 60 (SiO_2) was swamped with background (residual?) gases. To improve the signal/background ratio, the Q-mass was installed near the evaporation source (~110 mm) without the collimator in the second experiment. The S/N ratio has improved; the signals at 24, 25 and 26 m/e, after subtration of the background (distinguished by on-off operation of a shutter placed in front of the ion source of Q-mass), appear to reproduce the terrestrial Mg isotope ratios. The signal height at 44 m/e, after correction of the background, is comparable to that of 24. We observed a peak at 60 m/e in one of the several spectrums obtained at 1800°C (it could be SiO_2 or CH_3COOH), but no peak at 60 in others. The spectrums obtained at temperatures as high as 1800°C were inconsistent with each other.

We observe that the background is still too high to obscure the genuine signals from the forsterite vapor. We are planning of baking the whole vacuum chamber at 150°C before the mass spectrometry to eliminate adsorbents. An extreme heat source when temperature is raised more than 1700°C appears to cause an erratic spectrum due perhaps to warming the tips of the quadrupoles. We are going to install a heavily insulating shutter in front of the ion source, and also collect a spectrum in a shorter duration.

Though it is not yet proved which evaporation mechanism is correct for forsterite, it is wise to consider a possible mechanism that explains the results of both Hashimoto(1990) + Davis et al.(1990) and Nichols et al.(1998). In 1998 Davis et al. has carried out an evaporation experiment of type B-like CAI liquid at 1500°C in a hydrogen flow (~$2x10^{-4}$ bar). The observed isotope mass fractionations in Mg and Si were very similar to those determined by Wang et al. (1994) in vacuum evaporation experiments of initially chondritic materials. On the other hand, the evaporation rate observed in the hydrogen experiment was ~1000 times more increased than that in vacuum. It is difficult to reconsile these data if the evaporation of Si-species occurred via SiO_2(g). A key to understand the obvious complexity might be found in yet unknown reactions occurring on the interface between solid and gas, viz. reactions on the solid surface. The isotope mass fractionation observed in residual solid is likely determined by the interaction between the host solid and the free molecules being detached from but temporarily adsorbed on the surface. On the other hand, the molecules directly observed with mass spectrometer are desorbed ones from the surface. It is not known whether the adsorbed and desorbed molecules must be the same.

The evaporation mechanism of forsterite will not be unambiguously identified even if the vapor speciation, such as from the present experiment, is revealed. However, the vapor speciation is one important step to the goal.

References

Hashimoto, A. (1990) *Nature* **347**, 53. Davis, A.M. et al. (1990) *Nature* **347**, 655. Nichols, R.H. et al. (1998) *Meteoritics & Planetary Science* **33**, A115. Wang, J. et al. (1994) *LPS* **XXV**, 1457. Davis, A.M. et al. (1998) *Meteoritics and Planetary Science* **33**, A39.

Effects of artificial aqueous alteration on noble gases in the Allende CV3 chondrite

Takehiro Yasuda, Eiji Nakasyo, Takuya Matsumoto and Jun-ichi Matsuda
Department of Earth and Space Science, Graduate School of Science, Osaka University, Toyonaka, Osaka 560-0043, Japan

Introduction

It is often the case that carbonaceous chondrites have experienced some degrees of aqueous alteration most likely in their parent bodies. Aqueous alteration had undoubtedly played an important role in increasing textual, mineralogical and compositional variations of chondrites. A reported inverse correlation between the degree of aqueous alteration and amounts of a primordial noble gas component in a series of CM chondrites exemplifies that the aqueous alteration is likely to affect the noble gas compositions of chondrites (Nakamura *et al.*, 1999). In order to understand the effect of the alteration on the noble gas compositions in chondrites, we have carried out an artificial hydrothermal alteration experiments on Allende and examined the changes in its noble gas compositions (Nakasyo *et al.*, 2000). Our results suggest that noble gas contents in Allende have decreased by ~30 % after exposing the matrix sample to 15 atms of water vapor for about a week. This implies that the alteration by water vapor certainly affects the noble gas compositions in chondritic materials. In addition, there was an indication that the retentivity of noble gases trapped in the phase Q could be different from that of the presolar diamond (= a carrier phase of a Xe-HL component). This observation, if confirmed, will have a great implication for better understandings of the distribution of primordial noble gas components in chondrites. Thus, in order to further understand the effects of the aqueous alteration on noble gases in chondrites, we have carried out a new set of experiments with an extended period of experimental time.

Sample and Experiment

We have prepared four samples for this study. The starting material for the artificial aqueous alteration was the matrix of the Allende chondrites separated by the freeze-thaw disaggregation method. This starting material (AC-2) was loaded into the pressure vessel with pure water and kept at 200 °C (with an estimated internal water vapor pressure of 15 atms) for 2, 3 and 4 weeks. Recovered samples after 2, 3 and 4 weeks of the treatments were named HM-2, HM-3 and HM-4, respectively, and were analyzed for noble gas elemental and isotopic compositions by the stepped heating gas extraction technique at 600, 1000, 1400, and 1600℃.

Result and Discussion

Because the starting material used for this study was the matrix of Allende, its noble gas compositions should be a mixture of several components with distinct isotopic signatures. In fact, isotopic compositions of xenon released during the stepwise heating (both on the starting materials and run products) suggest the presence of two types of primordial components (Xe-Q and Xe-HL), indicating that both the phase-Q and presolar diamonds are included in the samples. Thus, it is possible to estimate the amounts of these two components under some reasonable assumptions and examine the effect of

aqueous alterations onto each phase. Also, it is possible to trace the behavior of other various noble gas components in the silicate phases during the aqueous alteration (i.e., such as a cosmogenic ^{21}Ne, radiogenic ^{40}Ar and ^{129}Xe).

First, we will show here the behavior of two primordial noble gas components (Q and HL) by using the xenon isotopic compositions. In most of the present cases the observed xenon isotopic ratios (except for ^{129}Xe) can safely be regarded as a binary mixture of above two components. Thus, the contribution of each component in the sample was estimated by solving binary mixing equations. Only exception is the case of HM-3 in which the presence of air-Xe is obvious in addition to Q and HL components. Thus, we assumed three-component mixing to obtain the amount of Q- and HL-Xe for this sample. The results are shown in Fig. 1 where the amounts of Xe-Q and Xe-HL normalized to those in the starting material are plotted against the experimental time. It is clear from Fig. 1 that the Xe-Q had been lost from the samples with increasing the experimental time. After 4 weeks of treatments, roughly 40 % of Xe-Q appeared to be removed by aqueous alteration. In contrast, such a trend is not obvious for Xe-HL. Except for the result of HM-3 in which a different assumption had been applied, there is no significant difference in the concentration of Xe-HL in the starting material and the aqueously altered samples. Thus, the presolar diamonds, the carrier of Xe-HL, appears to be more resistant to gas loss by the aqueous alteration than the phase Q.

We have also examined the variations of the cosmogenic ^{21}Ne, radiogenic ^{40}Ar and ^{129}Xe components. The amounts of radiogenic ^{40}Ar and ^{129}Xe were estimated by using an excess over primordial components and air component. Because of the large contribution of radiogenic component, we regarded all ^{129}Xe as radiogenic component. On the other hand, neon isotopic ratios showed the existence of Air-Ne, Ne-A (the mixture of Q- and HL-Ne), and cosmogenic Ne. Therefore, the amount of cosmogenic ^{21}Ne was estimated by solving trinary mixing equations. The results are shown in Fig.2 where the amounts of radiogenic ^{40}Ar and ^{129}Xe and cosmogenic ^{21}Ne normalized to those in the starting material are plotted against the experimental time. It is clear from Fig.2 that the radiogenic and cosmogenic components had been lost from the samples with increasing the experimental time. After 4 weeks of treatments, roughly 40~80 % of these gases appeared to be removed by aqueous alteration. We will discuss the resistances to aqueous alteration in regard to noble gas retentivity for various phases.

Reference

Black D.C. and Pepin R.O. (1969) Earth and Planetary Science Letters 6, 395-405.

Nakasyo E., Maruoka T., Matsumoto T. and Matsuda J. (2000) Antarctic Meteorite Resarch, No.13, 135-144.

Huss G.R. and Lewis R.S. (1994) Meteoritics 29, 791-810.

Huss G.R., Lewis R.S. and Hemkin S. (1996) Geochim. Cosmochim. Acta. 60, 3311- 3340.

McSween Jr. H.Y. (1987) Geochim. Cosmochim. Acta. 51, 2469-2477.

Mazor E., Heymann D. and Anders E. (1970) Geochim. Cosmochim. Acta. 34, 781-824.

Nakamura T., Nagao K., Metzler K. and Takaoka N. (1999) Geochim. Cosmochim. Acta. 63, 257-273.

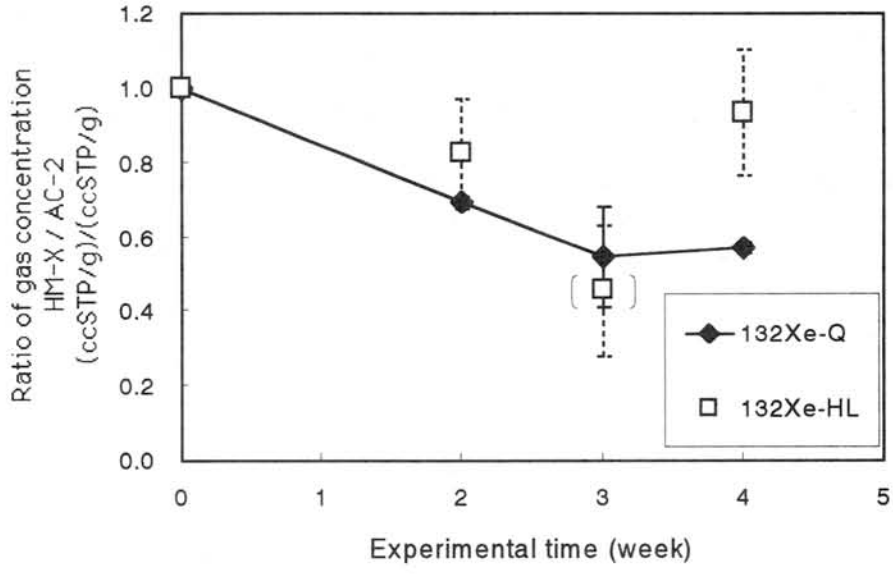

Fig.1. The variation of the concentrations of ^{132}Xe-Q and ^{132}Xe-HL. The values represent the concentration ratio to AC-2. The point of ^{132}Xe-HL at three weeks is marked in parentheses, because of the large contribution of air component.

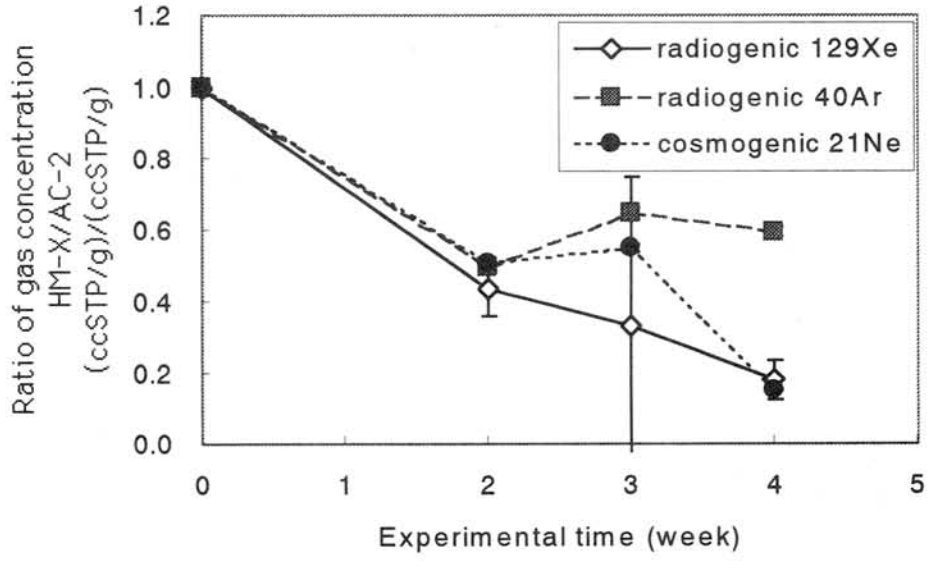

Fig.2. The variation of the concentrations of radiogenic ^{129}Xe, and ^{40}Ar, and cosmogenic ^{21}Ne. The values represent the concentration ratio to AC-2.

RECOVERY AND CLASSIFICATION OF TWO NEW JAPANESE METEORITES, SAYAMA CM AND TOWADA H CHONDRITES

S. Yoneda[1], M. Ebihara[2], Y. Oura[2], A.Okada[3], M. Kusakabe[4], T. Nakamura[5], K. Nagao[6], and H. Naraoka[2]

[1] *National Science Museum, Shinjuku, Tokyo 169-0073, Japan (s-yoneda@kahaku.go.jp)*
[2] *Graduate School of Science, Tokyo Metropolitan Univ, Hachioji, Tokyo 192-0397, Japan*
[3] *The Institute of Physical and Chemical Research (RIKEN), Wako, Saitama 351-0198, Japan*
[4] *Institute for Study of the Earth's Interior, Okayama Univ., Misasa, Tottori 682-0193, Japan*
[5] *Graduate School of Science, Kyushu Univ., Higashi, Fukuoka 812-8581, Japan*
[6] *Laboratory for Earthquake Chemistry, Univ. of Tokyo, Bunkyo, Tokyo 113-0033, Japan*

Introduction: Recently, two specimens were brought to the National Science Museum for investigation and subsequently recognized as meteorites. One of them is the Sayama meteorite, which name has been approved by the Nomenclature Committee of the Meteoritical Society and some of the preliminary results were already presented [e.g. 1, 2]. For the other meteorite, we propose the name Towada according to the city where it fell. Considering the circumstances of the recovery, both meteorites are recent falls. No fireballs, however, were observed for both meteorites and hence their date and time of the fall are uncertain. We here report the details of the recovery and classification of the meteorites.

CIRCUMSTANCES OF RECOVERY

Sayama meteorite (Fig. 1)**:** In the morning on or about April 29, 1986, a 430 gram stone was found near the entrance porch of the finder's house which is located in Sayama-city, Saitama-prefecture, Japan. He thought it could be a meteorite but didn't pick it up because the news of the accident at the Chernobyl nuclear reactor was just broadcast in Japan and he thought it might be a radioactive fragment of the reactor. He says it must have fallen during the daytime, one day before he found, otherwise someone in his family would have noticed the fall. No neighbors saw a fireball nor heard a sound, either. A few days later, it rained and the next-door neighbor found a leak in their roof facing the finder's house. Apparently, the meteorite first hit the roof of the next door and fell on the ground of the finder's house. At this point the finder decided to pick it up and he felt it was heavy because the meteorite had already soaked up the rainwater. When it became dry, the fusion crust became cracked. The meteorite was then brought to the local high school for examination and kept there in a polyethylene bag for 14 years.

Fig.1. Sayama meteorite (Size: 10cm x 9cm x 7cm)

Towada meteorite (Fig. 2)**:** The Towada meteorite fell in Towada-city Aomori-prefecture, Japan. One day of late April 1998, an employee of the finder found a hole at the eaves of the barn and informed the finder. The barn wasn't frequently used. The finder checked the hole and then turned his eyes onto the ground right beneath the hole. He noticed a small stone in a slight depression in the ground. There were neither snow nor weeds at that time. The 53.5 gram meteorite was already weathered and the color of the fusion crust is

partly brownish. Considering the circumstances, he had an impression that it had fallen within a few years from the date of find.

However, we measured the gamma-ray spectra and couldn't detect the cosmogenic Na-22 (half life: 2.6y) gamma-ray peak. The Na-22/Al-26 dpm/kg ratio is <1/10 (detection limit is two times the background). The ratio at the fall is normally between 1 and 2 for small ordinary chondrites. This implies that at least 8.6 years have passed since the fall assuming that the ratio at the fall is 1. If the ratio is 2, 11.2 years have passed.

Fig.2. Towada meteorite (Scale: cm)

CLASSIFICATIONS

Mineralogy and Chemical Compositions: The inside of the Sayama meteorite consists of black matrix and no large chondrules or inclusions are seen with the naked eye. We suspected Sayama might be CI, but the light element abundances (C: 1.99 wt%, H: 1.37 wt%, N: 0.08 wt% and S: 2.6 wt%) were close to CM compositions. Infrared spectroscopic study also show that Sayama doesn't exhibit the CI characteristic absorption band at 3685 cm^{-1} [3]. Instrumental Photon Activation Analysis (IPAA) subsequently confirmed that trace element abundances of Sayama most closely fit CM compositions except Na and K which were possibly mobilized at the aqueous alteration. Optical microscope and SEM studies show that chondrules in Sayama experienced extensive aqueous alteration and most of primary minerals in chondrules were replaced by phyllosilicates (mostly serpentine) like those in [4]. Yet, irregular-shaped relict olivine crystals (Fa0-23) are found in some chondrules and among matrix. Details are discussed in [2,5]. Since some chondrules contain relict olivine unlike CM1 defined by [4], the petrographic type 2 is assigned.

The Towada meteorite is an ordinary chondrite and apparently iron rich. SEM study show that the fayalite content in olivine is 19-20% and the ferrosilite content in low- ca pyroxene is 17-19%, which fits to the H chondrites. The CaO content in low-Ca pyroxene is 0.6-0.9% and plagioclase is well developed. Chondrite-matrix boundaries are obscured. Thus the most appropriate petrologic type is 6, but additional EPMA studies will be helpful. Trace element analyses are under way.

Noble gases and Oxygen Isotopes: From cosmogenic Ne-21, the exposure ages of Sayama and Towada are estimated to be 0.7 and 31 Myr, respectively. While Sayama contains abundant trapped noble gases, Towada contains quite low amounts, as low as other ordinary Type 6 chondrites, which is consistent with the mineralogical observation. Detailed results of noble gas measurements in Sayama and Towada are presented in [6] and [7], respectively.

The oxygen isotopic compositions are plotted in Fig. 3. The Sayama data fall on the O-16 poor end of the CM whole rock range [8]. As repetitive precision is about 0.1 permil, scattering of data indicates inhomogeneity of the sample. Towada is plotted in the region of H4-6 chondrites [9] quite well, and is also consistent with the mineralogical observation.

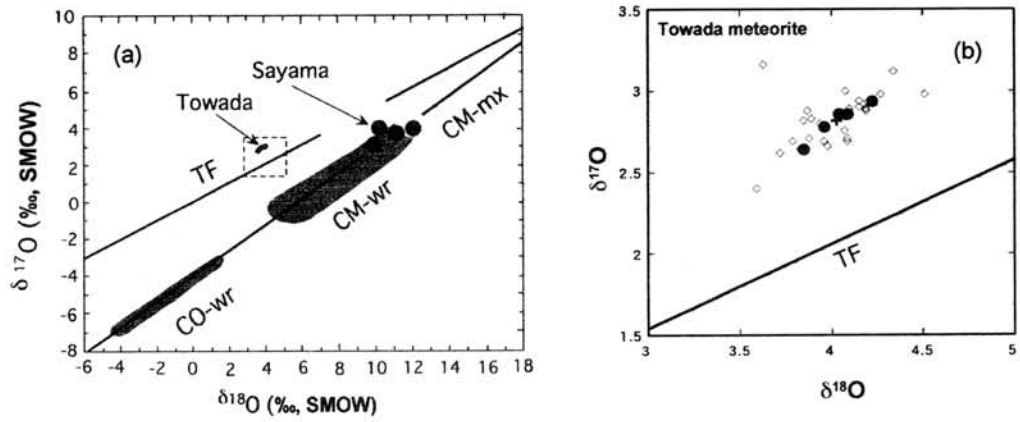

Fig. 3. Oxygen isotopic compositions. (a) Shaded areas for CM whole rock, matrix and CO whole rock are taken from [8]. (b) Expanded plot near Towada. The symbol + represents the average composition of Towada and open diamonds are H4-6 chondrites taken from [9].

Conclusion and Remarks: The Sayama meteorite is classified in a highly-hydrated CM2 chondrite, and is the second carbonaceous chondrite recognized in Japan after the Kobe CK4 chondrite which fell in 1999. The Towada meteorite is an ordinary H6 chondrite and the date of fall is quite uncertain, thus we must distinguish it from other known Japanese meteorites. The Aomori meteorite fell in 1984 at Aomori-city Aomori-prefecture, about 40 km from Towada-city, but it's a L6 chondrite. Although the Senboku H6 chondrite is recognized as a meteorite in 1992, which fell at Akita-prefecture, 100 km from Towada-city, the fall was observed by an ancestor of the possessor and the date is estimated more than 100 years ago. The closest meteorite fell in Japan within 50 years is the Tomiya H4-5 chondirte that also fell in 1984 at Miyagi-prefecture, and the distance from Towada-city is 200 km. Thus we conclude that Towada is a new meteorite.

References:

[1] Yoneda S. et al. (2001) *LPS XXXII* CD-ROM #2034
[2] Takaoka N. et al. (2001) *ibid.* #1645.
[3] Osawa T. et al. (2001) *ibid.* #1513.
[4] Zolensky M. E. et al. (1997) *GCA, 61*, 5099-5115.
[5] Nakamura T. et al. (2001) this volume.
[6] Ebisawa N. et al. (2000) *Abstracts of the 47th Annual Meeting of the Geochemical Society of Japan.*
[7] Park J. et al. (2001) this volume.
[8] Clayton R. N. and Mayeda T. K. (1999) *GCA, 63*, 2089-2104.
[9] Clayton R. N. et al. (1991) *GCA, 55*, 2317-2337.

Distributions of O isotopes in a type B2 CAI from the Vigarano meteorite

Miwa Yoshitake[1], Yoshiyuki Koide[2] and Hisayoshi Yurimoto[1]

[1]Department of Earth and Planetary Sciences, Tokyo Institute of Technology,

Meguro, Tokyo 152-8551, Japan.

[2]Kanagawa Prefectural Museum of Natural History, 499 Iriuda, Odawara, Kanagawa 250-0031, Japan

Introduction

Calcium-alminium-rich inclusions (CAIs) are known to have large O isotopic anomalies with $\delta^{17,\ 18}O$ ~-4% relative to the standard mean ocean water (SMOW) [1]. The O isotope anomalies are mainly established by the Allende meteorite. Allende meteorite belongs to oxided-CV3 and experienced fairly large aqueous metamorphism. On the other hand, reduced-type CV3 meteorites are less altered and more preserved original texture than the oxided-CV3 meteorites. Mineralogical and petrological studies of CAIs in reduced-CV3 have been performed [2,3,4,5]. However, reports of O isotopic composition for the individual mineral have not been enough to understand systematically [6,7,8].

We studied a type B2 CAI from Vigarano meteorite (reduced-CV3) in order to avoid aqueous metamorphism and to obtain more primary information of solar nebula. We report here the results of mineralogical studies and O isotope analyses for individual minerals in the type B2 CAI.

Experimental procedure

The sample used in this study was a polished thin section (TTV1) from the Vigarano meteorite (specimen name: NLM00012 [9]). The surface of the sample was coated with 20nm carbon film. The petrological and mineralogical studies were executed by scanning electron microscope, JEOL JSM-5310LV, equipped with energy depressive X-ray spectroscopy, Oxford LINK ISIS.

O isotopic composition of individual minerals has been measured by the TiTech CAMECA ims 1270 SIMS instrument. The primary ion beam was mass filtered positive $^{133}Cs^+$ ions accelerated to 20 keV and the beam spot size was ~3μm in diameter. Negative secondary ions of the ^{16}O-tail, ^{16}O, ^{17}O, ^{16}OH and ^{18}O were analyzed at a mass resolution power of ~6000, which is sufficient to completely eliminate hydride interference. In order to correct instrumental mass fractionation, a Russian spinel, SPU, with known O isotope ratios [10] was used for standardization.

Results and discussion

TTV1-01 is a fragment of type B2 CAI (3 x 2mm in size). Half of the CAI is rounded and surrounded by Wark-Lovering rim. Another side of the CAI is fragmented. From the roundness of W-L rim, original size of the CAI is estimated to over 5mm in diameter.

Major minerals in the CAI are spinel, melilite, fassaite, and anorthite. Spinel grain is relatively fine (~10μm). Spinel grains are often clustered as framboids and are usually dispersed in the all-major silicates. Some grains of the major minerals contain no spinel grains. Melilite and some anorthite grains

are lath shape. Fassaite and almost anorthite grains are blocky shapes. Melilite and fassaite grains are ~200μm or less. Anorthite grains are ~100μm or less.

Fig.1 shows O isotopic composition of individual minerals in TTV1-01. Terrestrial fractionation (TF) and carbonaceous chondrite anhydrous mineral (CCAM) lines are also shown in the figure. All plots are scattered along the CCAM line. O isotopic compositions of the minerals are clustered into two groups, i.e. ^{16}O-rich (-4‰) and ^{16}O-poor (close to terrestrial value). Spinel and fassaite belong to ^{16}O-rich group. Melilite is ^{16}O-poor. Anorthite grains belong to both the groups. Reports of ^{16}O-rich anorthite are rare in coarse-grained CAIs. Almost anorthite previously reported is ^{16}O-poor.

Fig.2 shows a texture around ^{16}O-rich anorthite. O isotope composition of adjacent of melilite is ^{16}O-poor, where as spinel and fassaite are ^{16}O-rich. Fig.3 shows a texture around ^{16}O-poor anorthite. Adjacent melilite is ^{16}O-poor. Fassaite and spinel are ^{16}O-rich. Since the mineral assemblage for both areas is similar, it is difficult to determine O isotope composition of anorthite by the texture. Compositions between ^{16}O-rich and ^{16}O-poor anorthite were the same within analytical error. At present we have not found any O isotope zoning in single anorthite grain. ^{16}O-rich and ^{16}O-poor anorthites consist of independent different grains.

Although, direct evidence of partial melting has not yet been observed in TTV1-01. However, similar partial melting process like an Allende CAI [11] can be applied to interpret the heterogeneous O isotope distribution among minerals in this study. ^{16}O-rich anorthite, fassaite and spinel grains are relicts and preserve original O isotope composition. Partial melting would cause exchange of O isotopes in CAI. O isotope of melilite and ^{16}O-poor anorthite was exchanged with ^{16}O-poor nebula gas. The partial melting model is not consistent with equilibrium phase relation of type B2 CAI. Kinetic melting may play an important role for the CAI formation.

References

[1] Clayton R. N. (1993) *Ann. Rev. Earth Planet. Sci. Let.* **21**, 115-49. [2] Wark D. N. and Lovering J. F. (1982) *Geochim. Cosmochim. Acta* **46**, 2581-2594. [3] Sylvester P. J., Grossman L. and MacPherson G. J. (1992) *Geochim. Cosmochim. Acta* **56**, 1343-1363. [4] Sylvester P. J., Simon S. B. and Grossman L. (1993) *Geochim. Cosmochim. Acta* **57**, 3763-3784. [5] Casanova I. and Grossman L. (1994) *Lunar & Planet. Sci.* **XXV**, 223-224. [6] McKeegan K. D., Leshin L. A. and MacPherson G. J. (1998) *Meteoritics &Planet. Sci.* **33**, A102-A103. [7] Cosarinsky M., Leshin L. A., MacPherson G. J. and Guan Y. (2001) *Lunar & Planet. Sci.* **XXXII**, abstract#1859. [8] Davis A. M., McKeegan K. D. and MacPherson G. J. (2000) *Meteoritics &Planet. Sci.* **35**, A47. [9] Koide Y. and Hirata D. (1996) *Catalogue of the Collection in the Kanagawa Prefectural Museum of Natural History* No.9, 3-72. [10] Yurimoto H. et al., (1994) *Earth and Planet. Sci. Let.* **128**, 47-53. [11] Yurimoto H., Ito M. and Nagasawa H. (1998) *Science* **282**, 1874-1877.

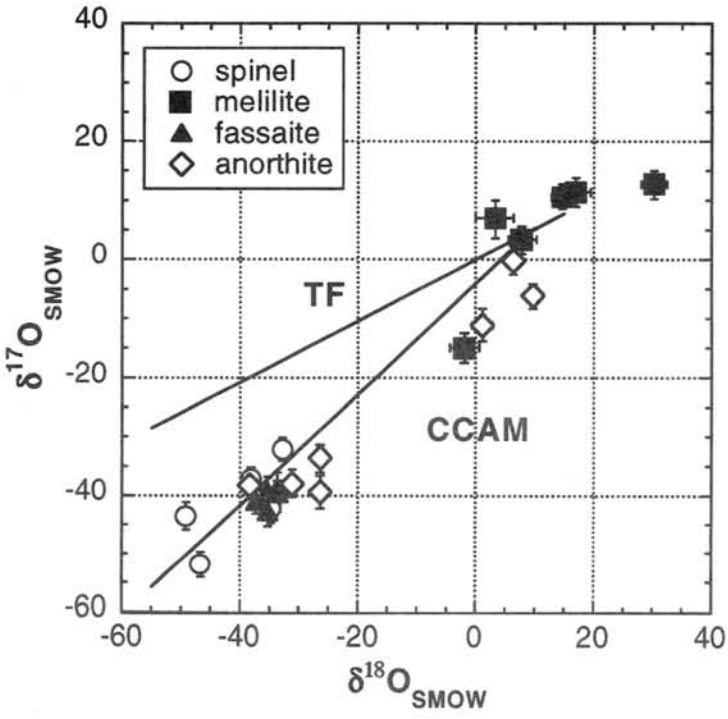

Fig.1: O-isotopic composition of individual minerals in Type B2 CAI (TTV1-01) from the Vigarano meteorite.

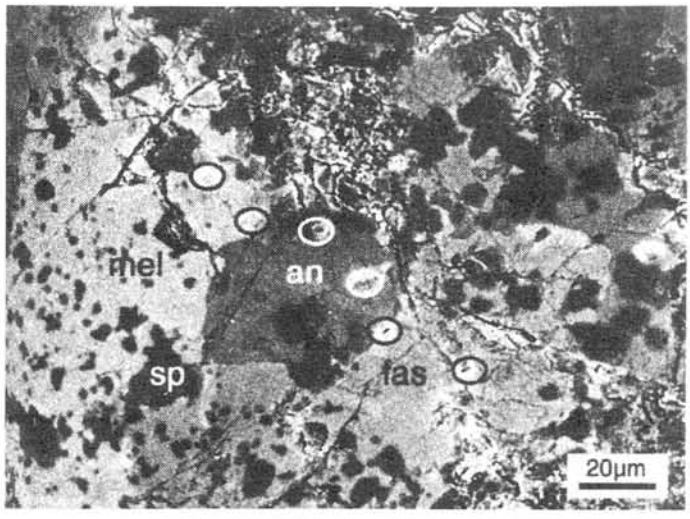

Fig.2: Back-scattered electron image around a ^{16}O-rich anorthite grain.
sp: spinel, mel: melilite,
fas: fassaite, an: anorthite.
Circles are sputtered craters by SIMS.

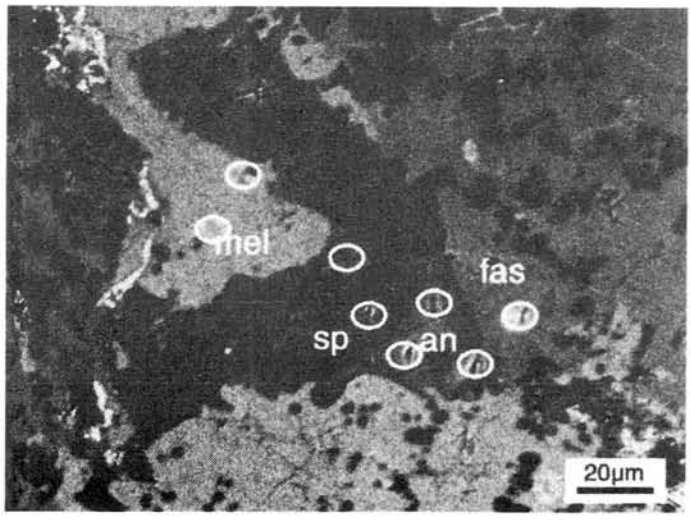

Fig.3: Back-scattered electron image around a ^{16}O-poor anorthite grain. Ablations are the same as Fig.2. Abbreviations are the same as Fig.2.

THE TAGISH LAKE METEORITE: NOT YOUR TYPICAL C2 CHONDRITE

M.E. Zolensky[1], K. Nakamura[2], E. Tonui[1], T. Mikouchi[3], M. Gounelle[4], A Hildebrand[5], and P. Brown[6]

[1]SN2, NASA Johnson Space Center, Houston, Texas 77058, USA. [2]Graduate School of Science and Technology, Kobe University, Kobe 657-8510, Japan. [3]Dept. Earth and Planetary Science, Graduate School of Science, University of Tokyo, 7-3-1 Hongo, Bunkyo-ku, Tokyo 113-0033, Japan. [4] Department of Mineralogy, Natural history Museum, London SW75BD, United Kingdom. [5]Dept. of Geosciences, University of Calgary, Calgary 2TN 1N4 Canada. [6]Los Alamos National Laboratory, Los Alamos, NM 87545 USA.

Introduction: Tagish Lake is an intriguing carbonaceous chondrite which bears numerous mineralogical and chemical similarities to CI1 and CM chondrite groups (Brown et al., 2000). However strong differences between Tagish Lake and these two chondrite groups suggest we are dealing with material from a different primitive asteroid. In fact Hiroi et al. (2001) suggest that Tagish Lake may be the first meteorite to originate from a D-class asteroid. Our measured density of Tagish Lake, 1.67+/1 0.05 g/cc., is by far the lowest of any meteorite, and is consistent with the suggestion that this is indeed unique meteoritic material. Here we present our further results on the mineralogy of Tagish Lake at the Scanning Electron Microscope and Electron Microprobe scale.

Results: We have studied 32 thin and thick sections of Tagish Lake, from 10 different individual stones, and identified three lithologies as being present: (1) a dominant carbonate-poor lithology which grades into (2) an-abundant carbonate-rich lithology, and (3) a less abundant, completely aqueously altered, carbonate-poor, sulfide-rich lithology.

Carbonate-poor lithology: This dominant lithology is a phyllosilicate-rich matrix-supported assemblage of fine-grained phyllosilicate-rich clasts, sparse chondrules, aggregates, sparse CAIs and a variety of loose grains of olivine, magnetite, Fe-Ni sulfides, Cr-Ni phosphides and Ca-Mg-Fe carbonates (uncommon). The mineralogy of the matrix is described Mikouchi et al. (2001), and consists mainly of saponite, serpentine and Fe-Ni sulfides. Matrix-supported clasts consist of fine-grained phyllosilicates with minor sulfides and/or magnetite. The majority of chondrule-like objects are partly to heavily aqueously-altered to coarse- and/or fine-grained phyllosilicates, but a few unaltered olivine (Fo_{99}) grains remain. Textures suggest that original chondrules were porphyritic and barred olivine chondrules. Magnetite and/or sulfides are common both inside and rimming chondrules. Most chondrules have fine-grained phyllosilicate-rich rims up to 200 μm thick. Aggregates have a mineralogy similar to that of porphyritic chondrules. We examined several altered CAIs (200-300 μm in size) having fine-grained phyllosilicate-rich rims. They consist of carbonates (dolomite and minor calcium carbonate), spinel and phyllosilicates (saponite and serpentine) homogeneous in composition. Rare perovskite grains are enclosed within dolomite. Olivine grains are common within chondrules, aggregates and isolated in the matrix. The composition of the olivine is mainly forsteritic (Fo_{99}) although a few iron-rich olivines (Fo_{60}) have been found in the matrix. Pyroxene is rarer than olivine and is iron- and calcium-poor ($En_{94-98}Wo_{1-5}$). Phyllosilicates are mostly confined to the fine-grained matrix but are also found as coarser grains associated with olivine, magnetite or carbonate. They consist of magnesium-rich serpentine and saponite in agreement with the TEM observations (Mikouchi et al., 2001). Magnetite is very abundant in the matrix but also in clasts, together with olivine, carbonates or phyllosilicates. Framboids are the most common morphologies. Most sulfides are pyrrhotite; pentlandite is much less common. Sulfides are typically fine-grained and display a wide variety of morphologies including rounded, elongated, irregular, and acicular. This latter morphology is otherwise only known from a Kaidun CM1 clast (Zolensky et al., 1996). Cr-Ni phosphide has been found as submicrometer plates within a coarse-grained phyllosilicate; an occurrence known otherwise only from another Kaidun clast (Ivanov et al., 2000). Calcium carbonate is by far the most abundant carbonate, occurring sparsely as very fine polycrystalline grains (<5 μm) scattered throughout the matrix, and forming associations with phyllosilicates and magnetite. It contains no detectable magnesium or manganese, though the iron content can be as high as 1.74 wt % FeO. Dolomite is the second most important carbonate. It is slightly coarser-grained (<10 μm) and usually embayed with phyl-

losilicates. It can contain up to 7.79 wt% FeO and up to 5.27 wt% MnO. Breunnerite is present only in one iron-rich aggregate. The CaO content is up to 3.46 wt% and the MnO content can reach 0.60 wt%. Other minerals include iron oxides, metal (in olivines), and schreibersite.

Carbonate-rich lithology: This lithology is similar to the previous one except that (1) fine-grained clasts and CAIs are almost absent (2) phyllosilicates are almost entirely saponite, and almost universally fine-grained, (3) andradite is present in association with phyllosilicates and magnetite, (4) magnetite is rare, and (5) Fe-Mg-Ca-Mn carbonates are **very** abundant, often rimming phyllosilicates. Calcium carbonate is rare. The MnO content of breunnerite can reach 2.91 wt% whereas the CaO content can reach 4.46 wt%. Calcium carbonate contains no detectable MgO or MnO. The iron content of calcium carbonate is below 0.34 wt% FeO. In general, this lithology is notably finer-grained than any other common lithology in carbonaceous chondrites, excepting the finest-grained CV3 dark inclusions (Krot et al., 1995).

Completely aqueously-altered, carbonate-poor, sulfide-rich lithology: This uncommon lithology (appearing in only two thin sections) appears as a rimmed clast. There are abundant completely-altered chondrules, sometimes crosscut by pyrrhotite or pentlandite veins. In fact, sulfides are very common in marked contrast to the bulk Tagish Lake. Magnetite is abundant. Olivine, pyroxene and carbonates are not present. The clast is rimmed by fine-grained, pyrrhotite-rich material. This clast appears identical to material in the Kaidun brecciated chondrite.

Discussion: Tagish Lake is undoubtedly a type 2 carbonaceous chondrite. Abundant phyllosilicates as well as chondrules (however sparse) and common olivine grains in the matrix preclude any other classification. The rarity of glass and chondrules, and the small size of the latter, distinguish it from CR2 chondrites (Weisberg et al., 1993), which actually have a similar matrix mineralogy. Altered chondrules and CAIs, olivine and spinel compositions, and the relative abundance of sulfides are reminiscent of CM2 carbonaceous chondrites. However, the relative abundance and extreme compositional range of carbonates (see Fig. 1), the composition of phyllosilicates, the presence of andradite and the absence of tochilinite are strong differences with the well known CM2 carbonaceous chondrites (Zolensky et al., 1993). Because anhydrous phyllosilicates are common in Tagish Lake and the oxygen isotopes are different from both CI1s and CMs (Brown et al., 2000) we propose that Tagish Lake represents a new kind of type 2 carbonaceous chondrite. This is supported by the bulk density of Tagish Lake (1.67 g/cc), which is far lower than CI or CM chondrites (2.2-2.3 and 2.6-2.9 g/cc, respectively), or any other meteorite for that matter (Wasson, 1974). We have noted similarities between Tagish Lake and some clasts within the enigmatic meteorite Kaidun; possibly there are genetic relationships here worth exploring. In fact the oxygen isotopic composition of the bulk Tagish Lake meteorite is identical to a previously-analyzed C1 clast in Kaidun (Robert Clayton, personal communication 2001). We are currently reassessing the nature of this Kaidun material. Hiroi et al. (2001) suggest that Tagish Lake may be the first meteorite to originate from a D-class asteroid. Perhaps Kaidun has already provided to us samples of this and other new asteroid classes.

References:

Brown P.G. et al. (2000) *Science* **290**, 320-325.
Engrand C. et al. al (2001) *LPSC* **XXXII**.
Ivanov A.V. et al (2000) *American Mineralogist* **85**, 1082-1086.
Krot A.N. et al. (1995) *Meteoritics* **30**, 748-775.
Mikouchi T. et al (2001) *LPSC* **XXXII.**
Wasson J.T. (1974) *Meteorites*, p. 175.
Weisberg M.K. et al (1993) *GCA* **57**, 1567-1586.
Zolensky M.E. et al. (1993) *GCA* **57**, 3123-3148.
Zolensky M.E. et al. (1996) *Meteoritics & Planet. Sci.* **31**, 484-493.
Zolensky M.E. et al. (1997) *GCA* **61**, 5099-5115.

Figure 1. Backscattered Electron (BSE) and five element maps of a carbonate aggregate grain from the carbonate-rich lothology. Mn-Fe-Mg rich carbonates have overgrown previous Ca-rich carbonates. Scale bar measures 5 microns.

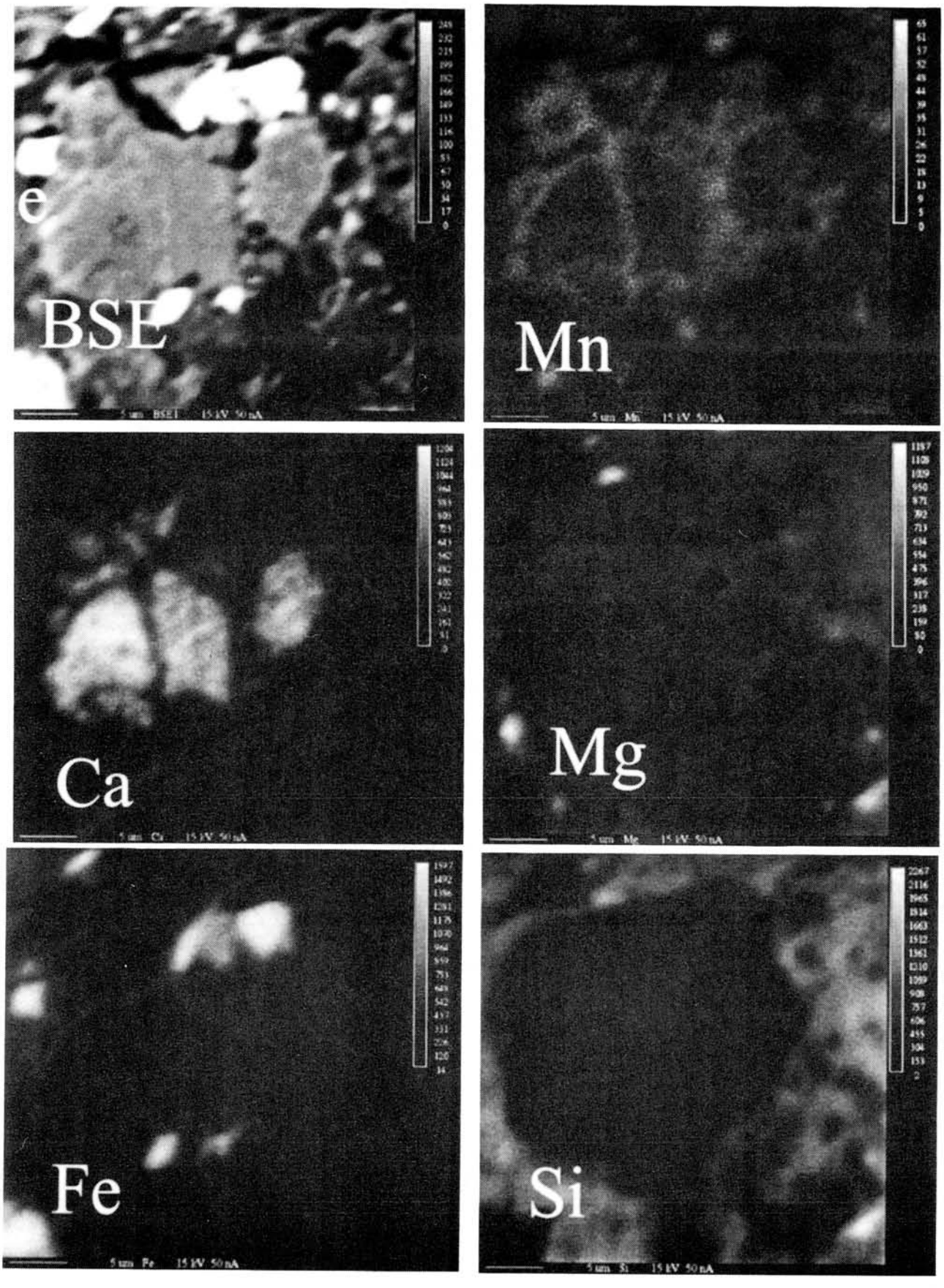

AUTHOR INDEX